# Brain regions and cell type specific Wnt signalling changes in Parkinson's disease mouse models

Si Hang Lei

Thesis submitted for the degree of Doctor of Philosophy

University College London

Department of Pharmacology,

UCL School of Pharmacy,

29-39 Brunswick Square

London, WC1N 1AX

I, Si Hang Lei confirm that the work presented in this thesis is my own. Where information is derived from other sources, I confirm that this has been indicated in the thesis.

# Abstract

Parkinson's disease (PD) is a late onset neurodegenerative disease characterised by the loss of dopaminergic neurons with motor and cognitive symptoms. Different mutations have been identified as a risk factor or direct cause of the disease. *LRRK2* gene mutation is a major cause of sporadic and inherited Parkinson's disease (PD), but the exact mechanism of how *LRRK2* mutation causes PD remains to be revealed. LRRK2 is a huge complex protein with both GTPase and Kinase domains. G2019S is the most common LRRK2 mutation on the kinase domain. There is accumulate evidence showing LRRK2 as a scaffolding protein interacts with canonical and non-canonical Wnt signalling pathways. These pathways play an important role on immune responses, nerves system development as well as neuronal maintenance.

This project aims to study how LRRK2 influence Wnt signalling pathways activities, we used LRRK2 wild type (WT), LRRK2 knock-out (KO) and G2019S knock-in (KI) mouse models in the project. We identified the brain regions with Wnt and NFAT signalling activities by applying biosensor system via lentiviral construct transduction into the brain at P0 and investigated the signalling activation by immunohistochemistry at 6 months old. We discovered LRRK2 KO and G2019S KI alter Wnt signalling activity in several brain regions including the PD important striatum. mRNA and protein expression level analysis in selected brain regions showed a region specific dysregulation of Wnt signalling cascade components, the dysregulation was differed between male and female mice.

We discovered Wnt and NFAT signalling activity might be higher in glial cells than neurons in primary culture experiment, which lead us to put our focus on astrocytes. LRRK2 KO and G2019S mutation caused changes in Wnt and NFAT signalling activities in astrocytes under basal and stimulated conditions. These differences were reflected in mRNA expression levels of signalling mediators.

Taken together, these data suggest astrocytes might hold a key insight towards a better understanding of the correlation between Wnt signalling dysregulation and PD progression.

# Impact statement

LRRK2 mutation is one of the most common mutations in Parkinson's disease patients. G2019S as the most common mutation site on LRRK2. The interactions of LRRK2 and Wnt signalling activities draw attention in discovering PD development before symptoms appear in patients.

The work presented in this thesis has contributed to understanding how LRRK2 mutations interfere Wnt signalling activities in different brain areas. I present LRRK2 affects mRNA and protein expression changes in different brain areas. Furthermore, I demonstrate Wnt and NFAT signalling is more predominant in astrocytes than neurons. LRRK2 KO and G2019S KI have a similar effect on Wnt signalling activities in astrocytes under different stimulations, and both mutations distort astrocyte morphology.

# Acknowledgements

I would like to thank Professor Kirsten Harvey for providing this excellent opportunity to work under her supervision, and for her support and guidance during this journey. I would also like to thank Professor Ahad Rahim's group for providing the lentivirus constructs widely used in this study. Thank you, Dr Andrea Wetzel, Mr Tiansheng Liu and Ms Yunan Peng, for their input in this study. A special thanks to the staffs in the biological unit for looking after my mice colonies, especially during the pandemic. A big shout out to every single person I have met at UCL to make my time at the School of Pharmacy unique and unforgettable.

I would also like to thank my friends for all the fantastic times. Special thanks to my brother Wesley, my cousin Howard, and my girlfriend Suki for their support during my ups and downs in this journey.

A very special thanks to my grandparents who encouraged me to study aboard and to pursue a career in science.

At last, I would also like to express my love to my parents for their unconditional support and loves for getting me to where I am today.

# Table of Contents

# List of Tables

# List of Figures

# Abbreviations

| Name | Abbreviations |
|---|---|
| Alzheimer’s disease | AD |
| Autosomal dominant | AD |
| Adenomatosis polyposis coli | APC |
| Activator protein-1 | AP1 |
| Autosomal recessive | AR |
| Ankyrin repeats | ANK |
| Armadillo repeats | ARM |
| Autophagy-related genes | Atg |
| Axis inhibition protein 2 | Axin2 |
| Blood-Brain-Barrier | BBB |
| Brain-derived neurotrophic factor | Bdnf |
| $Ca^{2+}$ calmodulin-dependent kinase | CaMK |
| cAMP-response element binding protein | Creb |
| Catechol O-methyltransferase | COMT |
| Chaperone-mediated autophagy | CMA |
| Dopamine | DA |
| Deoxyribonucleic acid | DNA |
| Dishevelled | Dvl |
| Dickkopf | Dkk |
| Glyceraldehyde 3-phosphate dehydrogenase | GAPDH |

| | |
|---|---|
| Glycogen synthase kinase 3β | Gsk3β |
| Genome-Wide Association Study | GWAS |
| Heat shock 70 kDa protein 8 | Hsc70 |
| Hydrochloric acid | Hcl |
| Hypoxanthine guanine phosphoribosyl transferase | HPRT |
| Intracerebroventricular | ICV |
| Integration 1 | Int1 |
| Interleukin | IL |
| Idiopathic Parkinson's disease | IPD |
| Levodopa | L-DOPA |
| LDL receptor related proteins | LRP |
| Leucine-rich repeats | LRR |
| Lewy body | LB |
| Lipopolysaccharide | LPS |
| Mammalian target of rapamycin | mTOR |
| Monoamine oxidase B | MAO-B |
| Microtubule-associated protein 1 light chain 3 | LC3-I |
| Non-coding RNA repressor of NFAT | NRON |
| Nuclear factor activation T-cells | NFAT |
| Nuclear factor kappa-B | NFκB |
| Olfactory bulb | OB |
| Polymerase chain reaction | PCR |
| Planar cell polarity | PCP |
| Parkinson's disease | PD |

| | |
|---|---|
| Protein kinase C | PKC |
| Ribonucleic acid | RNA |
| Substantia nigra pars compacta | SNc |
| Toll-like receptor 4 | TLR4 |
| T-cells factor and lymphoid enhancer factor | TCF/LEF |
| Unc-51-like kinase 1 | Ulk1 |
| Wingless2 | Wg2 |
| α-synuclein | SNCA |
| β-catenin destruction complex | BDC |
| 1-methy-4-phenyl-4-propionoxy-piperidine | MPPP |
| 1-methyl-1-phenyl-tetrahdropyridine | MPTP |

# 1 Introduction

## 1.1 Parkinson’s Disease

Parkinson’s disease (PD) is the world's second most common neurodegenerative disease. It was first described as a “shaking palsy” two centuries ago by a British doctor, James Parkinson. He described 6 different case studies of patients’ symptoms and disease progression (Parkinson, 2002). Mr. Parkinson suggested that the disease progresses slowly, and continuous observation of the same patient is required to understand the disease better. Shaking Palsy was later renamed Parkinson’s disease by Jean-Martin Charcot, a French neurologist in 1872(Goetz, 2011), who later on differentiated PD from other tremorous disorders and added bradykinesia as an additional feature of the illness.

In the modern world, PD is the second most common neurodegenerative disease after Alzheimer’s disease (AD). PD affects 1% of patients over 60 years old and about 4% of patients at the age 85 or above (de Lau and Breteler, 2006). PD is a chronic and progressive disease in which patients experience difficulties in daily life as the disease progresses. Both genetics and environmental factors can cause PD. Continuous pesticide exposure has been reported to be a risk factor that causes PD. Serval types of pesticides may cause PD by different mechanisms, such as mitochondrial dysfunction, oxidative stress, and protein aggregation but the exact type of pesticide

that causes PD is still unclear *(Dick, 2006).* However, ageing has been suggested to be the most significant risk factor that causes PD (Reeve et al., 2014). A Genome-Wide Association Study (GWAS) has been carried out by Simon *et al.,* showing that genetic factors contribute to familial and sporadic PD. Interestingly, some of these identified genetic risk variants colocalise with known familial PD genes. Overall, findings have suggested a strong correlation between PD and genetic variation/mutation (Gandhi and Wood, 2005, Simon-Sanchez et al., 2009).

Although there are numerous studies on PD, the exact causes of PD remain to be identified. To date, there are no cures for PD available. With advanced technologies, a better understanding of PD and related gene mutations can be achieved, hopefully revealing the PD's mystery and leading to the development of a disease-modifying cure.

## 1.1.2 PD Epidemiology

Approximately 1 in 1000 of the population is affected by PD. The affected population is mainly 60 years old or above. However, there are also reported cases of patients starting to experience motor symptoms around an average age of 45, which is considered a young-onset PD (Tysnes and Storstein, 2017). A study carried out by Parkinson's UK has projected the prevalence and incidence of PD in 2018 and beyond. About 1 in every 37 people in the UK will be diagnosed with PD. The estimated prevalence and incidence of PD are expected to grow due to the ageing population; the number of patients is expected to double by 2065 (**https://www.parkinsons.org.uk/professionals/resources/incidence-and-prevalence-parkinsons-uk-report**). By 2065, the prevalence and incidence rate for age above 80 would be 0.22% and 0.04%, respectively, among the population in the UK. Although the chances are extremely low, populations between 20 to 40 years old also have a chance to develop PD (**Fig 2**). The report has also shown that the prevalence of PD is 1.5-fold higher in men than in women 50-85 years old. Approximately 32 in 10,000 males will develop PD in their lifetime, whereas about 22 in 10,000 females will develop the disease. The information above is in line with previous studies that have suggested age and gender may have a crucial role in PD pathogenesis (Gillies et al., 2014, Moisan et al., 2016).

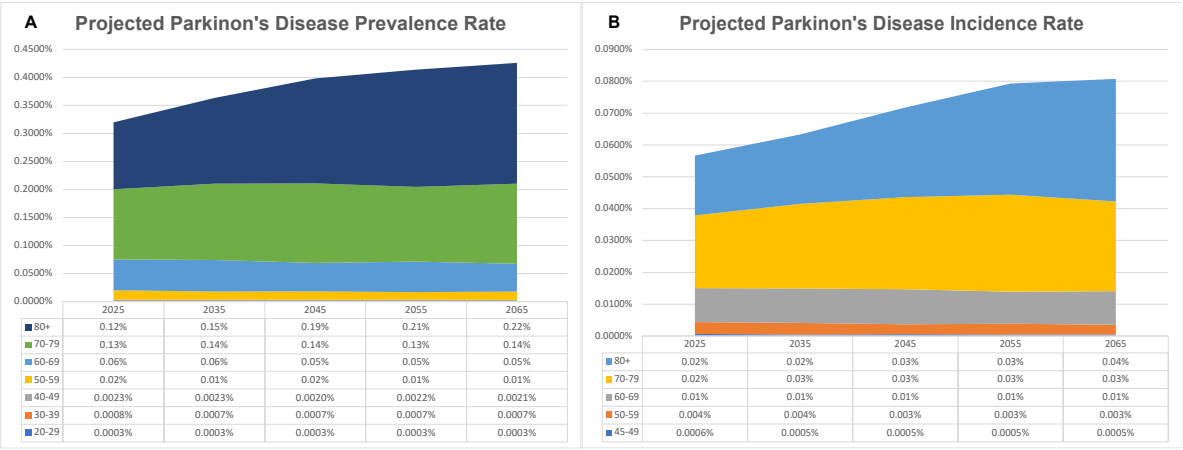


**Figure 1.1: Projected PD prevalence and incidence rate in the UK in a 10-year interval.**

Left: Projected PD prevalence rate in the UK up till 2065. Right: Projected PD incidence rate in the UK up till 2065. Data sourced from PD UK report 2018 **(**https://www.parkinsons.org.uk/professionals/resources/incidence-and-prevalence-parkinsons-uk-report**)**

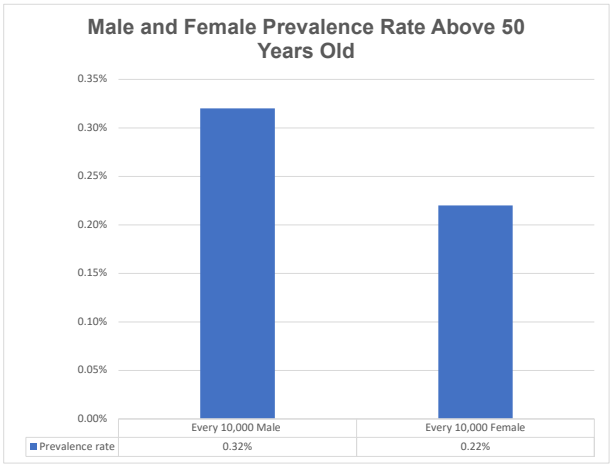


**Figure 1.2: Estimated male and female prevalence rate ratio above 50 years old**

32 males in every 10,000 males will develop PD, 22 females in every 10,000 females will develop PD in the age group of above 50 years old.

## 1.1.3 PD Pathology

Pathophysiologically, PD is classified by the loss of dopaminergic neurons in the substantia nigra pars compacta (SNc) in the basal ganglia and protein aggregation in Lewy bodies (LB). Dopaminergic neurons are specialised for the synthesis of dopamine (DA). DA is a catecholamine neurotransmitter which regulates the excitability of striatal neurons to control the balance of body movement and reward-motivation behaviours (Berridge et al., 2009). In PD patients, the degeneration of DAergic neurones diminishes dopamine levels in the striatum, with most patients only experiencing motor symptoms after 60-80% loss of dopaminergic neurons in the SNc (Surmeier, 2018).

Another pathological hallmark of PD is protein aggregation in Lewy bodies. They were first described in 1912 by the German neurologist Fritz Heinrich Jakob Lewy, who discovered these inclusion bodies in certain neurons in the brain, which he thought could be related to PD (Engelhardt and Gomes, 2017). A year later, Lewy's findings were first acknowledged by Gonzalo Rodriguez Lafora. In 1919, Konstantin Nikolaevich Tretiakoff confirmed these protein inclusion bodies in the substantia nigra (Engelhardt, 2017, Holdorff et al., 2013) and named them Lewy bodies. Although the findings have been underestimated for a long time, the discovery of Lewy bodies in the SNc became one of the most important, clinically and for basic PD research.

Lewy bodies are a composition of aggregated proteins with misfolded α-synuclein (SNCA) as its main constituent. Mutations in *SNCA*, encoding α-SN, result in

misfolding of the α-SN protein, leading to the formation of a β-sheet-like protein structure. The misfolded α-SN deposits as oligomers, proto-fibrils, and fibrils have been suggested to form pores in the cell membranes. The process leads to neuronal death via oxidative stress, excitotoxicity, and neuroinflammation (Michel et al., 2016).

Braak staging is used to classify the stage of PD post-mortem, from stage one to six, in an ascending order to characterise disease progression. The first stage is the appearance of Lewy neurites within the olfactory bulb and medulla oblongata. As the disease progresses to the midbrain, Lewy bodies begin to form in the SNc, and severe DA cell destruction begins. As the disease progresses, it will eventually invade the neocortex. At this stage, it has been suggested that patients start to experience cognitive symptoms(Braak et al., 2003, Dickson et al., 2010).

### 1.1.4 PD Clinical Diagnosis and Treatments

PD is classified as a late-onset neurodegenerative disease and is diagnosed clinically by motor symptoms: resting tremor, rigidity, bradykinesia, and postural instability. As the disease progresses, patients may experience non-motor symptoms, such as depression, anxiety, and dementia (Sveinbjornsdottir, 2016). Depression, anxiety and anosmia are also considered prodromal PD symptoms. Current treatments are only symptomatic to maintain the patient's quality of life, but not yet an effective treatment to stop the progression of the disease. However, the effect of the medication is temporary and diminishes over time.

Patients commonly experience side effects such as dyskinesias after about 5 years of dopaminergic replacement therapy. The side effects are probably due to the significant reduction of DA neurons and hypersensitivity of the DA receptors (Hinz et al., 2011, Wolf et al., 2006, Porras et al., 2014). This is probably due to the reduction of the DA neurons (Dorszewska et al., 2014). The most common PD treatment is Levodopa (L-DOPA) which is always taken with carbidopa to prevent the conversion of L-DOPA into DA outside the Blood-Brain-Barrier (BBB). Monoamine oxidase B (MAO-B) and Catechol O-methyltransferase (COMT) inhibitors are also used with L-DOPA to inhibit peripheral L-DOPA metabolism (Kostrzewa et al., 2005, Jankovic and Stacy, 2007). Nevertheless, this medication is only symptomatic. As the disease progresses, deep brain stimulation of the subthalamic nucleus to improve motor function and reduce the use of drugs can be considered to maintain symptom and side effect control (Groiss et al., 2009).

## 1.1.5 Environmental factors

Environmental factor was first linked to PD in 1983 by William Langston and Phillip Ballard. They have documented 4 drug users who self-administrated 1-methyl-4-phenyl-4-propionoxy-piperidine (MPPP), a synthetic opioid, via intravenous injection. It was reported that during synthesis, MPPP could be contaminated with another compound, 1-methyl-1-phenyl-tetrahdropyridine (MPTP). MPTP could be metabolised into MPP+, which inhibits the activity of complex 1 in the metabolic chain reaction. The four patients displayed irreversible Parkinsonism even after stopping the administration of the MPPP. A followed-up study was performed on squirrel monkeys to confirm the toxicity of MPTP, which metabolised to MPP+. The studies objects displayed dopaminergic neuronal loss in the substantial nigra pars compacta and motor symptoms. To date, MPP+ is known as a neurotoxin which causes depletion of ATP and leads to rapid cell death. MPP+ can pass through the blood-brain-barrier and causes dopaminergic neuronal loss (Langston et al., 1983, Langston et al., 1984, Przedborski et al., 2000). Later, more environmental agents were identified as a risk factor for causing Parkinsonism. Pesticides rotenone was identified as a selective inhibitor of complex I activities, whereas paraquat induces oxidative stress. Researchers have applied these compounds to rodents and are able to replicate features of PD pathogenesis, such as motor deficits and dopaminergic neuron loss (Goldman, 2014, Sherer et al., 2007)

Dick et al. have performed a national study with 959 PD patients and 1989 controls. They surveyed each individual on whether they have been exposed to chemicals,

heavy metals, or pesticides, and if they had any head trauma, as well as their occupation. The authors reported that individuals exposed to pesticides and head injuries that resulted in the loss of consciousness had a significantly higher risk of developing PD in their lifetime. It was later reported by Bellou *et al* that repeated head trauma has a positive correlation with an increased incidence of PD (Dick et al., 2007, Bellou et al., 2016)

## 1.1.6 Genetics factor

Most PD cases are sporadic, with approximately 10-15% of patients reported to have a family history (Thomas and Beal, 2007). Several gene mutations were reported to link to PD with advanced technologies. To date, 23 PARK loci have been identified as PD-related, including 19 disease-causing genes and 4 genetic risk factors (**Table 1.1**). The disease-causing genes can further be characterised as autosomal dominant genes; PARK1/SNCA (a-synuclein); PARK8/LRRK2 (leucine-rich repeat kinase 2); PARK17/VPS35 (vacuolar protein sorting-associated protein 35) and autosomal recessive genes; PARK2 (Parkin); PARK6 (PINK1); PARK7 (DJ-1); PARK9 (ATP13A2) (Deng et al., 2018).

Genome-wide association studies (GWAS) were used to identify gene loci associated with PD. A small scale of GWAS was performed with 5074 PD patients and 8551 healthy controls of European ancestry and found out the gene encoded SNCA and MAPT are strongly associated with PD (Simon-Sanchez et al., 2009). To date, a large scale of PD GWAS assayed 7.8 million single nucleotide polymorphisms (SNPs) in 37,688 PD cases, 18,618 UK Biobank proxy cases and 1.4 million controls. The study has identified 90 risk signals across 78 genomic regions. The 90 variants accounted for 16-36% of the heritable (Nalls et al., 2019). Loci associated with PD were named PARK, followed by a number according to the order in which they were discovered.

**Table 1.1: Genetic mutations related to Parkinson's disease pathology**

Autosomal dominant (AD); Autosomal recessive (AR). The table is adapted from (Deng et al., 2018)

| Locus | Location | Gene | Full Gene Name | Inheritance |
|---|---|---|---|---|
| PARK1 | 4q22.1 | *SNCA* | α-synuclein | AD |
| PARK2 | 6q26 | *PRKN* | parkin RBR E3 ubiquitin protein ligase | AR |
| PARK3 | 2q13 | *PARK3* | Parkinson disease 3 | AD |
| PARK4 | 4q22.1 | *SNCA* | α-synuclein | AD |
| PARK5 | 4p13 | *UCHL1* | ubiquitin C-terminal hydrolase L1 | AD |
| PARK6 | 1p36 | *PINK1* | PTEN induced putative kinase 1 | AR |
| PARK7 | 1p36.23 | *DJ-1* | parkinsonism associated deglycase | AR |
| PARK8 | 12q12 | *LRRK2* | leucine-rich repeat kinase 2 | AD |
| PARK9 | 1p36.23 | *ATP13A2* | ATPase 13A2 | AR |
| PARK10 | 1p32 | *PARK10* | Parkinson disease 10 | Unclear |
| PARK11 | 2q37.1 | *GIGYF2* | GRB10 interacting GYF protein 2 | AD |
| PARK12 | Xq21-q25 | *PARK12* | Parkinson disease 12 | X-linked inheritance |
| PARK13 | 2p13.1 | *HTRA2* | Htra serine peptidase 2 | AD |
| PARK14 | 22q13.1 | *PLA2G6* | phospholipase A2 group VI | AR |
| PARK15 | 22q12.3 | *FBX07* | F-box protein 7 | AR |
| PARK16 | 1q32 | *PARK16* | Parkinson disease 16 | Unclear |
| PARK17 | 16q11.2 | *VPS35* | VPS35 retromer complex component | AD |
| PARK18 | 3q27.1 | *EIF4G1* | eukaryotic translation initiation factor 4 Gama 1 | AD |
| PARK19 | 1p31.3 | *DNAJC6* | DnaJ heat shock protein family | AR |
| PARK20 | 21q22.1 | *SYNJ1* | synaptojanin 1 | AR |
| PARK21 | 20p13 | *TMEM230* | transmembrane protein 230 | AD |
| PARK22 | 7p11.2 | *CHCHD2* | coiled-coil-helix-coiled-coil-helix domain containing 2 | AD |
| PARK23 | 15q22.2 | *VPS13C* | vascuolar protein sorting 13 homology C | AR |
| | 11p15.4 | *RIC3* | RIC3 acetylcholine receptor chaperone | AD |

## 1.2 Leucine-Rich Repeat Kinase 2

### 1.2.1 LRRK2 mutations

The *PARK8* locus was first mapped at 12p11.2q13.1 by Funayama *et. al* in a genome-wide linkage analysis on a large Japanese family with autosomal dominant parkinsonism (Funayama et al., 2002). After the discovery by Funayama, two independent groups have reported mutations at this locus within the gene leucine-rich repeat kinase 2 (*LRRK2*) in autosomal-dominant late-onset parkinsonism patients. Zimprich *et al* discovered two individuals from different families had brainstem dopaminergic degeneration and a-synuclein positive inclusion bodies. Each individual carried a different LRRK2 mutation; one at the codon 1699 with tyrosine to cysteine substitution (Y1699C), and the other had a mutation at position 1441 with arginine to cysteine substitution (R1441C). Paisan *et al* examined four families, three from Spain and one from the UK. The Spanish families suffered from the substitution of arginine to glycine mutation (R1441G) and the British family was suffered from Y1699C mutation (Paisan-Ruiz et al., 2004, Zimprich et al., 2004). In 2014, Martin *et. al* reported mutations in LRRK2 in sporadic PD patients (Martin et al., 2014). These findings suggested that LRRK2 mutations may have an essential role in neurodegeneration in familial and sporadic PD.

To date, many variants of *LRRK2* have been identified. However, only seven mutations have been reported to be pathogenic. These were discovered in different populations (Rubio et al., 2012, Aasly et al., 2010). p.Asn1437His (N1437H) was discovered in a Norwegian family (F04) (Aasly et al., 2010). p.Arg1441Cys (R1441C), p.Arg1441Gly (R1441G) and p.Arg1441His (R1441H) were identified in Western Nebraska families, Spain families and European/Taiwanese families, respectively (Paisan-Ruiz et al., 2004, Zimprich et al., 2004, Lin et al., 2008, Huang et al., 2007). Both mutation locations (N1437H, R1441C/G/H) are harboured in the ROC domain. A UK family cohort also carried a mutation at p.Tyr1699Cys (Y1699C) (Khan et al., 2005) located in the COR domain. Both p.Ile2020Thr (I2020T), which was identified in a study carried out within the original Japanese family cohort (Funayama et al., 2005) , and p.Gly2019Ser (G2019S) identified in European, and Latin America families (Kachergus et al., 2005) are in the kinase domain.

The G2019S mutation is the most known familial PD mutation. It contributes to 1% of sporadic and 4% of familial PD cases globally, and the incidence of PD in G2019S mutant carriers increases from 28% at 59 years to 51% at 69 years and 74% at 79 years (Healy et al., 2008). The mutation frequency is highest in Northern Africa and Ashkenazi Jews populations, contributing 30-40% and 10-30% of PD, respectively (Lesage et al., 2010, Benamer and de Silva, 2010).

Although patients with LRRK2 mutations are usually heterogeneous and clinically indistinguishable from sporadic PD, some studies report that LRRK2-related PD patients tend to have more atypical features, such as hallucination, dementia and

orthostatic hypotension. Interestingly, a majority of the investigated Lewy body positive cases were from patients with the G2019S mutation (Kett and Dauer, 2012).

## 1.2.2 LRRK2 protein

LRRK2 is a huge multidomain protein belonging to the ROCO protein family with GTP hydrolysing (GTPase) and kinase activity. The protein consists of 2527 amino acids and has a molecular weight of 286kDa (Kumari and Tan, 2010). The ROCO proteins are characterised by the combination of a Roc (Ras of complex protein) domain and a COR (C-terminal of Roc) domain (Civiero et al., 2012). Starting from the N-terminus, LRRK2 contains 13 armadillo repeats (ARM), 7 ankyrin repeats (ANK) and 14 leucine-rich repeats (LRR), followed by the RoCOR bi-domain, a kinase domain and 7 WD40 repeats. Both ARM, ANK, LRR and WD40 domains are protein-protein interaction domains (**Fig 1.3**) (Wauters et al., 2019). The RocCOR domain was described to interact with 14-3-3 proteins and tubulins, whereas the important protein interactions site was sitting between the ANK and LRR domains (Law et al., 2014, Mills et al., 2014).

LRRK2 is widely expressed in the brain, especially in the striatum, hippocampus, cortex, olfactory bulb, midbrain, cerebellum, and brain stem. It has been detected in striatal and cortical neurons and immune cells such as macrophages and microglia (Lee et al., 2017, Kang and Marto, 2017, Maas et al., 2017, Popugaeva and Bezprozvanny, 2014). LRRK2 is also highly expressed in peripheral organs such as kidneys, heart, liver, spleen, and intestine. Interestingly, although LRRK2 has been

related to PD pathology, there are relatively low expression levels of LRRK2 in human dopaminergic cells. The finding suggested that LRRK2 related neurodegeneration may not be related to the LRRK2 expression level (Galter et al., 2006, Giasson et al., 2006)

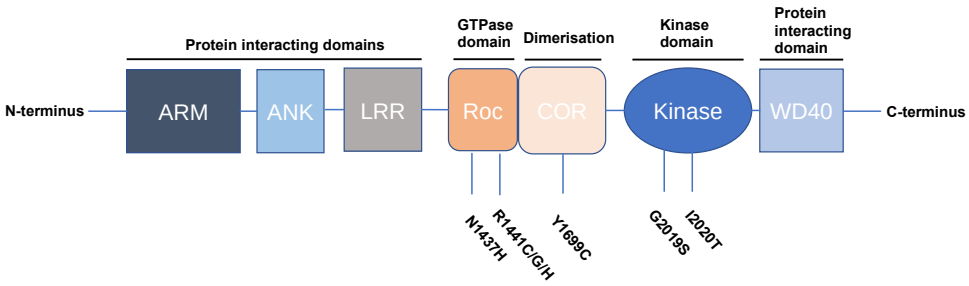


**Figure 1.3: Diagram of LRRK2**

LRRK2 protein composition with RocCOR and kinase domains as a central enzymatic region along with other protein-protein interaction domains: ARM, ANK, LRR and WD40. Point mutations are indicated below each of the specific domains.

## 1.2.3 LRRK2 kinase activity

The G2019S mutation is found within the kinase domain of LRRK2. Studies have found that this mutation increases LRRK2 kinase activity by approximately 2-fold and suggested a relationship between LRRK2 kinase activity and the formation of inclusion bodies and neurodegeneration (West et al., 2005, Greggio et al., 2006). The LRR repeats have been demonstrated to be phosphorylated at the position Ser860, 910, 935, 955 and 973, where Ser 910 and 935 have been shown to be important for interacting with 14-3-3 proteins (Nichols et al., 2010). Protein phosphatase 1 has been proposed to be responsible for the LRRK2 dephosphorylation (Lobbestael et al., 2013). Interestingly, *in vitro* work has suggested that ARM, ANK, and LRR domains are not involved in the intrinsic phosphotransferase activity of LRRK2, whereas the WD40 domain seems to be essential for the intrinsic phosphotransferase activity (Jaleel et al., 2007, Kamikawaji et al., 2009). Inhibition of LRRK2 kinase activity or knockout of LRRK2 showed to reduce toxicity and have a protective effect *in vivo* and *in vitro* (Lee et al., 2010). The hypothesis that LRRK2 mutation is a gain of function has led to the development of LRRK2 inhibitors. To date, different LRRK2 inhibitors are developed and in clinical trials. Denali has developed the first oral LRRK2 kinase inhibitor drug, passing the phase I clinical trial and entering phase IIb trial in 2022 (Kingwell, 2022).

The kinase activity was reported to regulate by autophosphorylation in *in vitro* and *in vivo* experiments. The positions are at T1410 and T1503 in the Roc domain and S1292 in the LRR domain. Pathogenic LRRK2 was reported to facilitate autophosphorylation at S1292. However, the phosphorylation could be dephosphorylated by phosphatases

PP1 and PP2 (West, 2017, De Wit et al., 2018). A group of small GTPases were identified as heterologous substrates of LRRK2 (Rab3A/B/C, Rab8A/B, Rab10, Rab12, Rab29, Rab35 and Rab43), which have a role in membrane trafficking and synaptic vesicle recycling. However, the exact mechanism of Rab phosphorylation remains to be revealed. The hypothesis is that when the phosphorylated Rab proteins become inactivated and remain in the intracellular membrane (Steger et al., 2017, Steger et al., 2016). An unbiased screen for LRRK2 binding proteins study has revealed that Rab29 tends to increase LRRK2 kinase activity. A potential negative feedback mechanism has also been reported that Rab29-LRRK2 interactions weaken its ability to facilitate LRRK2 kinase activity (Purlyte et al., 2019, Liu et al., 2018). The overall findings make Rab29 an interesting target to study in future studies.

### 1.2.4 LRRK2 GTPase activity

The LRRK2 RocCOR domain carries out the hydrolysis of GTP to GDP. The Roc domain shows a similar structure to Rab-proteins, and the COR domain enables the dimerisation of LRRK2. Deyaert *et. al.* demonstrated that Roco proteins undergo monomerisation when GTP is bound and dimerised after hydrolysing GTP into GDP. The process is dependent on the GDP concentration (Deyaert et al., 2017). Research has been mainly focused on the LRRK2 kinase domain, but pathogenic mutations on the RocCOR domain should not be ignored. Pathogenic mutations (R1441C/G/H, Y1699C, N1437H) were reported to decrease GTP hydrolysis rates, increase GTP's affinity, or have both effects. However, the R1398H mutation works as a protective

variant against PD and Crohn's disease (CD) by weakening GTP binding and enhancing the GTP hydrolysis (Nixon-Abell et al., 2016, Berwick and Harvey, 2014).

LRRK2 kinase domain and GTPase domain have a complex counterplay between each other. Mutation of LRRK2 may alter kinase activity and GTPase activity. However, the exact role of LRRK2 in neurodegenerative disease is still unclear. LRRK2 mutations were suggested to either result in a gain of function or a loss of protein function. Recent studies have gathered evidence that LRRK2 mutations are more likely confer a gain of function. However, the specific cell biological target of LRRK2 mutant gain of function is yet to be discovered.

## 1.2.5 LRRK2 signalling

The LRRK2 mediated signalling was reviewed by Harvey *et* al. LRRK2 is involved in different signalling pathways, including MAPK, Rac/PAK, Akt, PKA, canonical Wnt signalling pathways and non-canonical Wnt signalling pathways. The related pathways mediate various biological functions, including neuronal development, haemostasis, synaptic transmission, immune response, autophagy, and endocytosis. However, pathogenic LRRK2 mutations have been related to the change of kinase and GTPase activity. LRRK2 has been described as a scaffolding protein that interacting with protein complexes and facilitates phosphorylation in specific pathways (Berwick and Harvey, 2011, Berwick et al., 2017, Sancho et al., 2009, Chen et al., 2012, Chuang et al., 2014, Civiero et al., 2015, Greggio et al., 2017).

P21-activated kinase 6 (PAK6) is a serine/threonine protein kinase pathway involved in actin cytoskeleton and synaptic formation. It was reported to interact with the LRRK2 GTPase domain. In the *in vivo* study, PAK6 was identified as a positive regulator that affects neurite outgrowth, neurite length was decreased when LRRK2 was knock-out. In the same study, idiopathic and G2019S carriers in post-mortem brain tissue increased phosphorylation of PAK6. LRRK2 was also shown to affect the activation status of PAK6 and its downstream regulator LIM domain kinase 1 (LIMK1) as part of the scaffolding complex. In contrast, the activation status decreased when LRRK2 was knock-out (Civiero et al., 2015). Mitogen-activated protein kinase (MAPK) signalling is important for physiological and pathophysiological cell responses. MAPK-JNK (c-jun-terminal kinase) signalling pathways mediate neuronal function. Chen *et al* have

demonstrated in their study that when G2019S mutation is overly expressed, it increases phosphorylation of MKK4 and JNK and upregulated target gene *Bim* and *FasL* transcription. Activation of the pathway also induced dopaminergic neuron degenerations in G2019S mice (Chen et al., 2012). Another study showed a reduction of dopaminergic neuron damage by inhibiting JNK (Pan et al., 2009).

The nuclear factor-keppa-B (NF-κB) signalling pathway is a well-studied pathway which involves innate and adaptive immune responses, and the pathway regulates gene transcriptions of inflammatory cytokines. Kim *et al* demonstrated a reduction of NF-κB signalling activity in LRRK2 knock-out microglia culture. Similar results were observed in Russo *et al* study. They have treated the primary microglia culture with lipopolysaccharides (LPS) on LRRK2 knock-out sample or sample treated with a kinase inhibitor. The results showed a reduction of NF-κB signalling activity and a decrease in proinflammatory cytokines (Russo et al., 2015, Kim et al., 2012). Russo *et al* later on suggested that LRRK2 works as a negative regulator of PKA signalling and hence affects NF-κB signalling activity. This was caused by inhibiting phosphodiesterase 4 (PDE4) activity. As a result, it interrupts cAMP degradation. The authors also treated G2019S primary microglia a-synuclein pre-formed fibrils and found that G2019S mutations downregulated PKA activation and resulted in decreased of PKA mediated NF-κB signalling activity (Russo et al., 2018).

## 1.2.6 LRRK2 autophagy

PD is common with accumulating misfolded proteins such as α-synuclein, which has failed to be removed because of impaired autophagy. Autophagy is known for removing any cellular wastes, such as damaged or misfolded proteins or organelles. Autophagy has been categorised into macroautophagy, microautophagy, and chaperone-mediated autophagy (CMA) (**Fig 1.4**) (Albanese et al., 2019). Microautophagy is the least characterised among the other 2 types, and it involves the direct engulfment of contents into the lysosomes through the invagination of the lysosome membrane (Li et al., 2012). Whereas the substrates of CMA carry a specific sequence called the KFERA motif, which is recognised by the cytosolic heat shock 70 kDa protein 8 (hsc70). Upon binding of the substrate and hsc70 leads to the formation of a chaperone complex and, subsequently, trafficked across the lysosomal membrane by the interactions with the LAMP2A receptor (Tekirdag and Cuervo, 2018, Kaushik and Cuervo, 2018). Macroautophagy requires a more complex mechanism. The process is initiated by the inhibition of the mammalian target of rapamycin (mTOR), which leads to the dephosphorylation of Unc-51-like kinase 1 (Ulk1) and transcriptions of the autophagy-related genes (Atg). The Atgs and Ulk1 complex forms the phagophores, which engulf cellular contents and lead to the formation of autophagosomes. The microtubule-associated protein 1 light chain 3 (LC3-I) is cleaved to become LC3-II and covers the autophagosome membrane. The level of LC3-II is a common marker for autophagy. The other marker is the adaptor protein, autophagic cargo receptor sequestosome 1 (p62), which binds the LC3II and enters the autophagosome for degradation. The autophagosome fuses with the lysosomal

membrane and releases the cargo, and the lysosome's hydrolytic inner core degrades the autophagosome's contents (Lipton and Sahin, 2014, Roosen and Cookson, 2016).

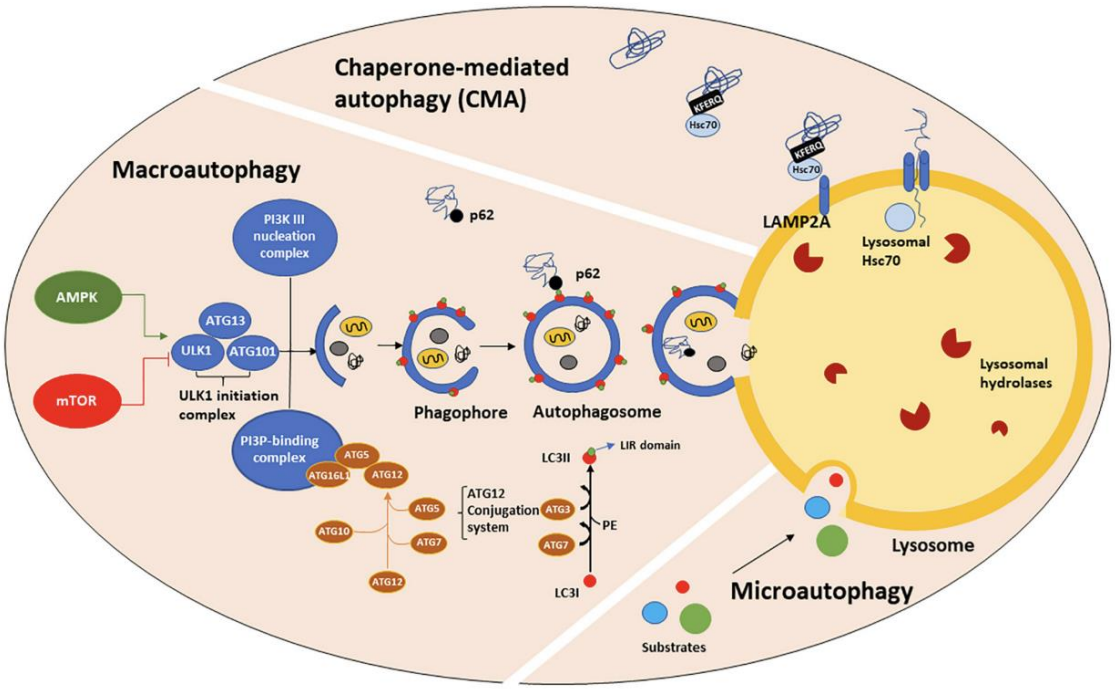


**Fig 1.4 Illustration of 3 major types of autophagy**

Chaperone-mediated autophagy (CMA), macroautophagy and microautophagy (figure adapted from Albanese *et al.*) (Albanese et al., 2019)

Orenstein *et al* have identified LRRK2 as a substrate of CMA. Inhibition of lysosome activity in both SH-SY5Y cell line and mice brains increased in intracellular LRRK2 level. In addition, they also discovered that G2019S mutation inhibits CMA. The increased LRRK2 level upregulated LAMP-2A, which was observed in post-mortem G2019S carrier patients' brain samples (Orenstein et al., 2013). CMA was also indicated as an essential pathway for $\alpha$-synuclein clearance. Inhibiting the CMA resulted in accumulating the high molecular weight and insoluble $\alpha$-synuclein (Vogiatzi et al., 2008). Dysfunction of CMA by LRRK2 mutation may suggest the lead to $\alpha$-synuclein pathology in PD patients.

# 1.3 Wnt Signalling Pathways

Wnt signalling pathways are a group of signal transduction pathways with essential roles in embryonic development and adult homeostasis. The term WNT is a combination of the homologous genes *wingless2* (*Wg2)* and *integration1* (*Int1)*. *Int1*, also known as *WNT1* was first identified as a proto-oncogene that encodes a secreted cysteine-rich protein, whereas the *Drosophila gene Wg2* was reported to play a role in controlling segment polarity during larval development (Nusslein-Volhard and Wieschaus, 1980, Nusse and Varmus, 1982, Rijsewijk et al., 1987). Wnt signalling pathways can be divided into three branches: canonical (Wnt/β -catenin), planar cell polarity (PCP) and non-canonical Wnt/Ca2+-signalling pathways. Both canonical and non-canonical pathways begin with the binding of a Wnt protein to the extracellular frizzled (FZD) receptor. Wnt ligands have a molecular weight of about 40kDa and belong to the family of secreted lipid-modified signalling glycoproteins. Glycosylation and palmitoylation are essential for Wnt secretion, allowing the protein to bind to receptors. To date, 19 genes have been reported to encode Wnt proteins in humans. Wnt signalling has been suggested to be important for neurogenesis and plays a crucial role in neuron maturation. Research has demonstrated that Wnt signalling facilitates not just transcriptional regulation but also supports pre and post-synaptic assembly (Zhang et al., 2011, Maguschak and Ressler, 2012, Bamji et al., 2003). Hence, dysfunction of Wnt signalling pathways is suggested to contribute to neurodegenerative diseases. In the past decade, LRRK2 has been suggested to be a

candidate that dysregulates Wnt signalling pathways. Previously, *PRKN* knock-out was shown to increase the level of β-catenin and lead to the death of dopaminergic neurons (Rawal et al., 2009). The evidence of Wnt signalling to play an important role in dopaminergic cell development and cell maintenance suggested a potential correlation between dysregulation of Wnt signalling and Parkinson's disease. (Schulte et al., 2005, Surmeier, 2018).

### 1.3.1 Canonical Wnt signalling and Planar Cell Polarity pathways

Under the basal condition, when no Wnt ligands bind to the Frizzled (Fz) receptors. β-catenin binds to an inhibitory cytosolic complex known as β-catenin destruction complex (BDC). The complex is formed by Axin, adenomatosis polyposis coli (APC), CK1α/β and glycogen synthase kinase 3β (GSK3β). β-catenin is phosphorylated by GSK3β and CK1 within the destruction complex, subsequently ubiquitinated and degraded by the proteasome. Hence, no β-catenin will be accumulated, preventing translocation into the nucleus to promote gene transcriptions (Rao and Kuhl, 2010).

Upon binding of the Wnt ligand to the FzD receptor and low-density lipoprotein receptor-related protein (LRP5/6) co-receptor recruits dishevelled (Dvl) protein to the plasma membrane. Dvl protein mediates translocation of the β-catenin destruction complex to the plasma membrane forming a larger complex, the so-called Wnt signalosome (Gammons et al., 2016), which contains the extracellular Wnt ligand, the

transmembrane receptors, and the intracellular protein complex. As a result, β-catenin cannot be phosphorylated and degraded by the proteasome. β-catenin accumulates in the cytosol, translocates into the nucleus and interacts with the T-cells factor and lymphoid enhancer factor (TCF/LEF) transcriptional factor to activate the transcription (MacDonald et al., 2009)

Planar Cell Polarity (PCP) pathway does not involve β-catenin, instead the downstream signalling of Dvl proteins is transduce by small GTPases Rac1 and RhoA, transmit the signal to c-Jun N-terminal kinase (JNK) to activate activator protein 1 (AP1) dependent transcription. PCP pathway is linked to cell polarity, actin cytoskeleton rearrangement, and dysregulation of PCP pathway has also been related to cancer development and metastasis.

## 1.3.2 NFAT/$Ca^{2+}$ signalling pathway

NFAT signalling pathway is another β-catenin independent pathway. Activation of the Wnt/$Ca^{2+}$ signalling pathway increases the intracellular $Ca^{2+}$ level. The increase in $Ca^{2+}$ levels results in the activation of protein kinase C (PKC), calcineurin, $Ca^{2+}$ calmodulin-dependent kinase II (CaMKII), which further activates NF-κB, cAMP-response element binding protein (CREB) and nuclear factor activation T-cells (NFAT) dependent transcription (Sugimura and Li, 2010, Katoh, 2005). Under the basal condition, NFAT is subsequently phosphorylated by a non-coding RNA repressor of the NFAT (NRON) complex. The activation of calcineurin facilitates the

dephosphorylation of NFAT, mediates localisation into the nucleus, and promotes gene transcription.

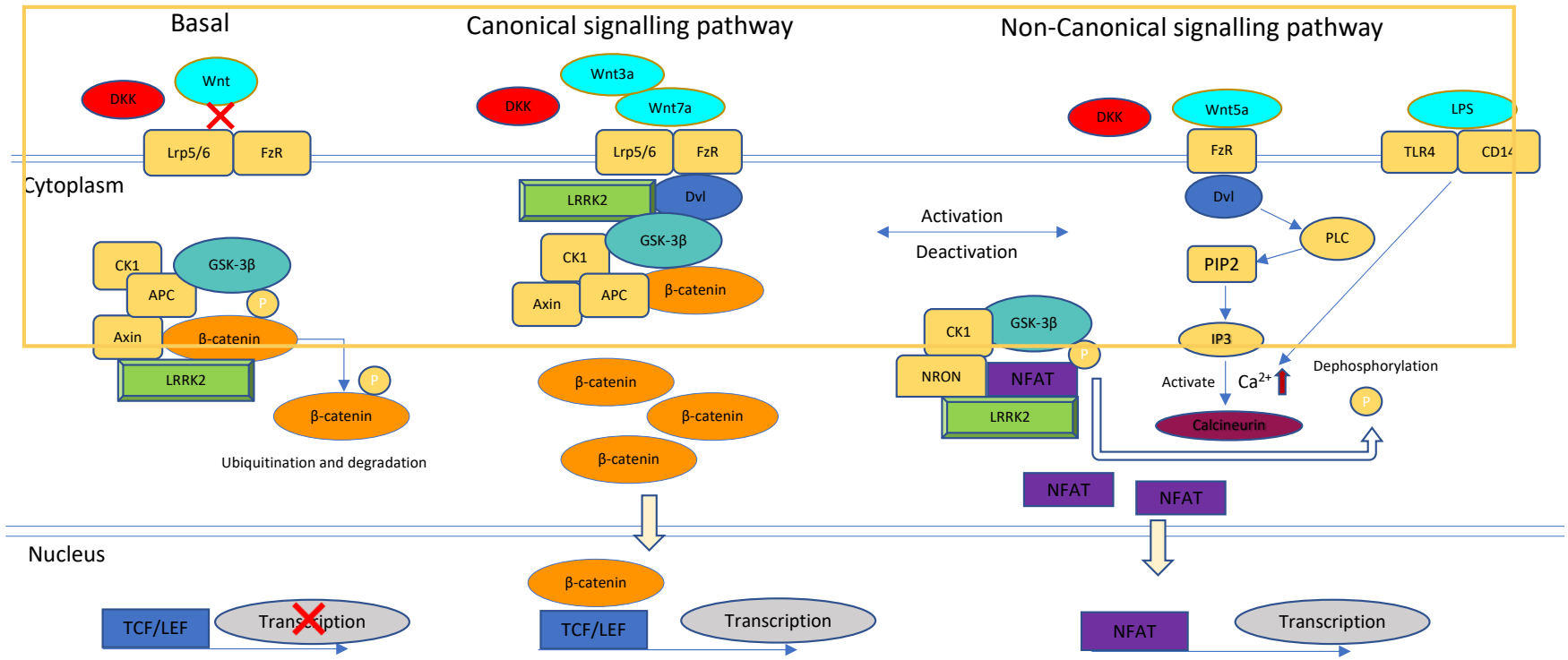


**Figure 1.5: Canonical and non-canonical Wnt signalling pathways**

Presentation of Wnt signalling pathways under basal condition; β-catenin dependent (Canonical Wnt signalling pathway); β-catenin independent (Non-canonical Wnt signalling pathway – NFAT/$Ca^{2+}$ signalling pathway

## 1.3.3 LRRK2 as a scaffolding protein in canonical and non-canonical Wnt signalling pathways

Overall, Wnt signalling regulates cell division, growth, and homeostasis. Growing evidence shows that LRRK2 plays a role as a scaffold protein in the pathway. Sancho *et al*. first described the interaction between Dvl and the LRRK2 RocCOR domain. The pathogenic mutations in LRRK2 strengthened the interaction with Dvl proteins (Sancho et al., 2009). Dvl protein functions as a central regulator in both canonical and non-canonical Wnt signalling pathways, suggesting that LRRK2 plays a role in both pathways. It was reported that LRRK2 also interacts with the canonical Wnt co-receptor Lrp6 and β-catenin destruction complex components. The authors have demonstrated that a protective LRRK2 variant R1398H increases canonical Wnt signalling, whereas all LRRK2 mutants and pathogenic variants decrease canonical Wnt signalling. This indicates an inverse correlation between Parkinson's disease risk and canonical Wnt signalling for LRRK2 variant carriers. However, it should be noted that inhibiting wild-type LRRK2 kinase decreased Wnt signalling. This could potentially be caused by affecting protein-protein interaction through reducing LRRK2 autophosphorylation. ((Berwick and Harvey, 2012, Berwick et al., 2017)

LRRK2 acts as a signalling scaffolding protein in the BDC, facilitating phosphorylation of β-catenin by CK1 and GSK3β under basal conditions. But upon activating the signalling pathway, LRRK2 acts as an enhancer, increasing Wnt signalling. It has been reported that LRRK2 works as a connector between the membrane and cytosolic

components, such as Dvl proteins and Lrp6. The authors have suggested that reducing LRRK2-Lrp6 interaction decreases Wnt signalling at the membrane (Berwick et al., 2017, Berwick and Harvey, 2012). However, without stimulation, LRRK2 may work as a stabiliser for the BDC, potentially explaining why LRRK2 KO models show a higher canonical WNT signalling activity under basal conditions. Interestingly, the canonical Wnt signalling pathway and PCP pathway work antagonistically against each other, and LRRK2 was reported to switch interactions between both pathways LRRK2 enhances Wnt signalling activity by forming an interaction with Dvl and BDC. However, the interaction could be influenced by binding with a PCP pathway component PRICKLE1. Hence, it suppresses the (Niehrs, 2012)canonical Wnt signalling activity (Sato et al., 2010, Niehrs, 2012).

NFAT signalling is essential for innate immune responses and neuronal development (Moore and Goldberg, 2011). It was first described to link to LRRK2 in a study using LRRK2 knock-out mice in a Crohn's disease model, showing increased NFAT signalling in immune cells. Mice also showed an increased level of interleukin-2 (IL-2) and interleukin-6 (IL-6) (Wong et al., 2018, Liu et al., 2011). Liu *et al.* has demonstrated that LRRK2 interacts with the non-coding RNA repressor of NFAT (NRON) complex that inhibits NFAT activity by preventing nuclear translocation due to phosphorylation of NFAT by GSK3$\beta$ (Liu et al., 2011). Interestingly, when the $Ca^{2+}$ level increases through extracellular receptor activation, it activates calcineurin phosphatase, which dephosphorylates the phosphorylated NFAT, allows NFAT to translocate into the nucleus, and promotes the gene transcription (Sharma et al., 2011). A hypothesis has suggested that NFAT signalling pathways crosstalk with the Wnt signalling pathway

by interactions between NFAT and Dvl proteins. NFAT works as a competitor to bind with Dvl proteins, which influences the interactions between β-catenin and Dvl, which affects Wnt signalling activity (Huang et al., 2011)

## 1.3.4 Wnt signalling and neurodegeneration

Wnt signalling has been linked to neurodegenerative disease such as schizophrenia, bipolar disorder, and AD. A substantial amount of hypothesis has been made on AD and dysregulated Wnt signalling cascades. It was reported that canonical and non-canonical Wnt signalling pathways were dysregulated at an early stage of the disease. A study on post-mortem AD patients' brains showed an elevated level of GSK3β and phosphorylated β-catenin. Interestingly, the authors have also observed an increased level of Wnt signalling antagonist Dkk1 (Dickkopf-1) (Inestrosa and Arenas, 2010, Caricasole et al., 2004). The increased level of Dkk1 suggested an inhibitory effort of the Wnt signalling pathway, which facilitates GSK3β activity and enhances the phosphorylation of β-catenin. Similar results were observed in PD studies, *β-catenin* gene expression was significantly downregulated in post-mortem PD patients' brains compared to controls. Another group also reported that in an MPTP-treated PD mice model, FzD and β-catenin were downregulated, and they suggested that β-catenin signalling is essential for dopaminergic neuron repairs (Cantuti-Castelvetri et al., 2007, L'Episcopo et al., 2014).

As discussed above, a shed of strong evidence shows that LRRK2 interferes with canonical and non-canonical Wnt signalling pathways. Nuur1, a transcriptional factor

for β-catenin was linked with PD pathogenesis. Knock-out of Nuur1 resulted in dopaminergic neuron function impairments; a reduced level of Nuur1 was also found in PD midbrain neurons with α-synuclein positive Lewy bodies (Jankovic et al., 2005).

## 1.4 Hypothesis

PD is more prevalent in men than women. LRRK2 has been linked to familial and idiopathic PD, and to cell signalling including Wnt and NFAT signalling pathways. Expression levels of LRRK2 were found to be tissue and cell type specific, resulting for example in different LRRK2 expression levels between brain regions. Although LRRK2 has been identified as a signalling scaffold protein, the exact mechanism on how LRRK2 mutations affect the pathway activity remains unclear. I hypothesised that *Lrrk2* mutations dysregulate Wnt and NFAT signalling activity differently in different brain regions and cells in male and female mice.

## 1.5 Aims and objectives

The aim of this project is to identify how LRRK2 mutations affect Wnt and NFAT signalling in different brain regions and cells under basal and stimulated condition.

**Objective 1**: Investigate canonical Wnt and NFAT signalling activity in male and female LRRK2 mutant and wild type mouse brain.

**Objective 2**: Investigate mRNA and protein expression levels of signalling components in male and female LRRK2 mutant and wild type mouse brain.

**Objective 3**: Investigate mRNA expression and morphological changes in mutant and wild type primary astrocyte cultures.

# 2 Methods and Materials

## 2.1 Buffers and materials

**1.5% agarose gels** were made by adding 1.5g of UltraPure agarose (Life Technologies, USA) into 100ml of 1X Tris-acetate-ethylenediaminetetraacetic acid (TAE) buffer. The mixture was heated until boiled to dissolve the powders. Molten agarose solution was cooled to room temperature, and 8μl of SybrSafe was subsequently added to allow nucleic acid visualization. The solution was poured into a cast to let it set, and a comb was used to create wells in the gel.

**50X TAE buffer** was made by mixing 242g of Tris (Sigma-Aldrich, USA), 57.1ml of Acetic acid (Thermofisher Scientific, USA) and 100ml of 0.5M Ethylenediamine tetraacetic acid (EDTA) (Sigma-Aldrich, USA) and $dH_2O$ to make up a final volume of 600ml in a 1L media bottle. The mixture was placed on a magnetic stirrer, a stir bar was placed in the bottle to help the dissolution. $dH_2O$ was used to dilute 50X TAE into 1X TAE.

**10X TBS** was prepared in 2 separate containers. One bottle contained 302g of Trizma base (Sigma-Aldrich) dissolved in 1.5L $dH_2O$. Another bottle contained 425g of NaCl

(Sigma-Aldrich) dissolved in 1.5L of $dH_2O$. Both solutions were mixed, and 160ml of concentrated 1M HCL (Sigma-Aldrich) was added to the mixture under a fume hood. The solution pH was adjusted to pH 7.6 with 1M HCL and made up to the final volume of 5L with $dH_2O$. $dH_2O$ was used to dilute 10X TBS into 1X TBS.

**TBSAF** was made by mixing 545ml of 1X TBS, 5ml of sodium azide 10%, 300ml ethylene glycol, 150g of sucrose and $dH_2O$ to make up to the final volume of 1L. The mixture was placed on a magnetic stirrer with a stir bar inside the bottle to help with the dissolution.

**4% Paraformaldehyde (PFA)** was prepared by adding 40g of paraformaldehyde powder into 800ml of 1X PBS, which was preheated to approximately 60 °C in a glass beaker on a stir plate in a ventilated hood. The powder was dissolved by slowly adding 1M NaOH dropwise until the solution turned clear. The solution was then cooled and filtered, and the volume was adjusted to 1L with 1X PSB. Diluted HCL was used to adjust the final pH to approximately pH6.9. The solution was aliquoted and frozen at -20°C.

**Dissection medium** was prepared by mixing 500ml Hank's Balanced Salt Solution (HBSS, no calcium, no magnesium) (Life Technologies) with 10μl of β-mercaptoethanol ().

**Plating medium** was prepared by adding 100μl of β-mercaptoethanol (), with 0.5% penicillin/streptomycin (P/S, Life Technologies), 10% glutamax (Life Technologies),

1% glucose (Sigma Alrich) and 1X B27 supplement. Neurobasal medium (Life Technologies) was used to mix up the final volume to 500ml.

**Astrocyte culture medium** was prepared by adding 1% of P/S (Life Technologies) along with 10% Fetal Bovine Serum (FBS, Life Technologies) and Dulbecco's Modified Eagle Medium (DMEM, Life Technologies) to make a total volume of 500ml.

Both Maintenance medium and astrocyte culture medium were pre-warmed at 37°C before application.

## 2.2 Animals

All animal studies were approved by the UCL Ethics Committee and UK Home office for the conduct of regulated procedures under license (Animal Scientific Procedures Act, 1986) and according to the ARRIVE guidelines and recommendations. LRRK2-KO (Knock-out), LRRK2-WT (Wild-Type) and LRRK2-G2019S mice were used in this study. *LRRK2*-KO and *LRRK2*-G2019S mice were purchased from the Jackson Laboratories, and *LRRK2*-WT mice were purchased from Charles River. All mice were bred at the UCL School of Pharmacy animal house on a C57BL/6J background.

# 2.3 Genotyping

## 2.3.1 DNA Isolation

DNA was extracted from a fraction of the ear, which was collected from the mice. Each collected ear clip was cooked in 35ml (0.2mM EDTA+25mM NaOH) at 98°C for 1 hour. After 1 hour, the samples were cooled to room temperature for approximately 15 minutes. 35ml of 40mM Tris-Hcl at pH5.5 was added to each sample, followed by centrifugation at 9000rpm/min. The extracted DNA was stored at -20°C before use.

All RNA and DNA concentrations (ng/ml) were quantified using a Nanodrop spectrophotometer.

## 2.3.2 Polymerase Chain Reaction (PCR)

PCR identified the mouse genotypes before any further experiments were conducted. Each set of PCR reactions contained 1μl of the sample DNA, 12.5μl of Pfx master mix (Invitrogen) and 1.5μl of the desired primer mixes to make up a total volume of 15μl. The primer mix was prepared by a 1:10 dilution of the forward and reverse primers with $dH_2O$ (deionized $H_2O$). LRRK2 and G2019S primers (**Table 2.1**) were used to identify knock-out and knock-in mice, respectively. All PCR reactions were carried out in a SimpliAmp Thermal Cycler (Life Technologies).

The PCR reaction was started at 95°C for 5 minutes at the initiation stage, followed by 33 cycles of the annealing stage with initial denaturation at 95°C for 5 minutes. The reaction temperature was then lowered to 60°C for 30 seconds to allow the primers to anneal to the single-stranded DNA (ssDNA), and each cycle was finished with an elongation step at 68°C for 1 minute. The PCR reaction was finished with a final extension stage at 68°C for 5 minutes and a final hold at 4°C for an indefinite time. All PCR products were subsequently analysed by Agarose gel electrophoresis to confirm the size of the final product.

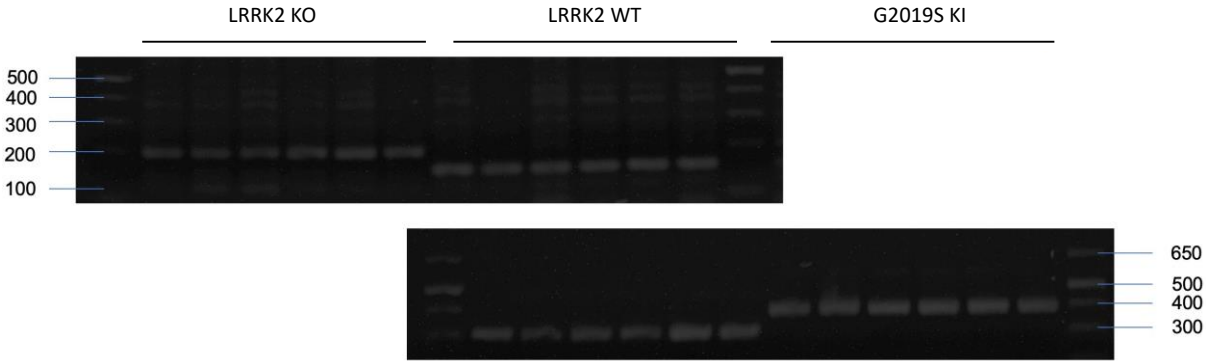


**Figure 2.1: Agarose electrophoresis confirmation of the LRRK2 genotypes**

1kb DNA ladder was loaded on both ends of the gel. The gel on top represents PCR products amplified by LRRK2 KO primers; the gel below represents PCR products amplified by G2019S primers. Each of the genotypes has an n=6 with three males and three females.

### 2.3.3 Agarose gel electrophoresis

All PCR samples were analyzed by agarose gel electrophoresis. 3.3ml of nucleic acid sample loading buffer (BIO-RAD) was added to each sample and loaded into the gel with GeneRuler 1kb Plus DNA ladder (Thermo Scientific) as a molecular weight ladder. The gel was run at 130V for 30 – 50 minutes. Depending on the size of the gel and visualised under an ultraviolet transilluminator.

**Table 2.1. Primers used in genotyping study. KO: Knock-out; KI: Knock-In**

| PCR Product | Forward Primer | Reverse Primer |
|---|---|---|
| **LRRK2 KO allele** | 5' CTCTGAGAGCAGGAGCCGT 3' | 5' TGCCTTCCTGGACATTATTCAGCC 3' |
| **G2019S KI allele** | 5' CAGGTAGGAGAACAAGTTTAC 3' | 5' GGGAAAGCATTTAGTCTGAC 3' |

## 2.4 mRNA expression analysis

### 2.4.1 RNA isolation and reverse transcription

Desired brain regions were collected from sacrificed 6 months old mice. 25mg of each selected brain region was used to isolate the RNA by using the RNAse kit (QIAGEN,). Instructions were followed as per the provided protocol. To produce cDNA, each RNA sample was diluted to 200ng/ul by using the water provided in the SuperScript III Reverse Transcriptase kit (ThermoFisher) to make up a total volume of 7ml. To each diluted RNA sample, 2ml of dNTPs, 1ml of RNaseOUT and 1ml of random hexamer

were added. The mixed solution was incubated at 65°C for 5 minutes and cooled down on the ice. After placing it shortly on ice, 2ml of 10xRT buffer, 2ml of DTT and 4ml of MgCL (25mM) were added to each reactions. The mixture was incubated at 37°C for 5 minutes followed by adding 1ml of SSIII to each of the reactions. Both reactions were incubated at 37°C for 2 hours followed by 70°C incubation for 10 minutes. The cDNA samples were diluted with EB-BSA in a 1:10 dilution. EB-BSA was prepared by mixing 1 volume of BSA with 9 volumes of EB buffer.

### 2.4.2 Real-Time PCR (qPCR)

To optimise our qPCR reaction, we have followed specific rules upon designing the primers to maximise the primers' efficiency as well as accuracy. First, we ensured that the primer size was around 18-22bp and the primer melting temperature was approximately 58-63 °C. The primers must be intron (exon-exon junction) spanning to avoid genomic DNA contamination. The GC content should be approximately 50-60% to maximise the stability of our primers. Lastly, the primers should not be self-complementary to minimise the formation of primer-dimers which also affects the efficiency (Bustin and Huggett, 2017). Most of our primers showed an efficiency within the range of 90%-110%. A master mix control was used to ensure there was no contamination for each of run. The melt curve and amplification curve further helped to check the purity of each of the reactions.

qPCR results are commonly analysed by the equation, assuming the primer efficiency is optimal and that both target gene and reference gene primers have 100% efficiency.

However, our studies found that not all of our primers have 100% efficiency. Therefore, we have applied the relative expression equation, which considers primer efficiency. (Pfaffl, 2001).

$$\textbf{Relative expression} = \frac{\mathbf{E_{TARGET}}^{\Delta \mathbf{CP_{TARGET}(Control-Sample)}}}{\mathbf{E_{REF}}^{\Delta \mathbf{CP_{REF}}}(\mathbf{Control - Sample})}$$

The qPCR reaction mixture contained 10ml of iTaq universal SYBR green supermix (BIO-RAD), 1.5ml of forward primer (Eurofins), 1.5ml of reverse primer (Eurofins), 5ml of nuclease-free H2O (Fisher Scientific) and 2ml of cDNA. Primers (**Table 2.2**) were diluted in 1:10 dilution with dH2O prior to use. Each sample mixture was loaded in triplicate/duplicate subject to cDNA availability into a PCR 96-well plate. The qPCR reaction was carried out in a StepOne Real-Time PCR system. The reaction was initiated at 95°C for 20 seconds at the holding stage, followed by 40 cycles of the cycling stage. Each cycle was initiated at 95°C for 3 seconds and lowered to 60°C for 30 seconds. After the cycling stage was completed, the melt curve stage started at 95°C for 15 seconds, followed by 60°C for 1 minute. The temperature was gradually increased by 0.3°C every 15 seconds until 95°C reached the completion of the whole reaction. All the data was recorded by the StepOne software.

A melt curve was performed for each qPCR run to identify any primer dimer formations or mRNA contamination in the primer mixture. Non-overlapped peaks indicated the purity of our working solution. A single peak also indicated that a single product was formed during the reaction (**Fig 2.2**), which increased the reliability of our result.

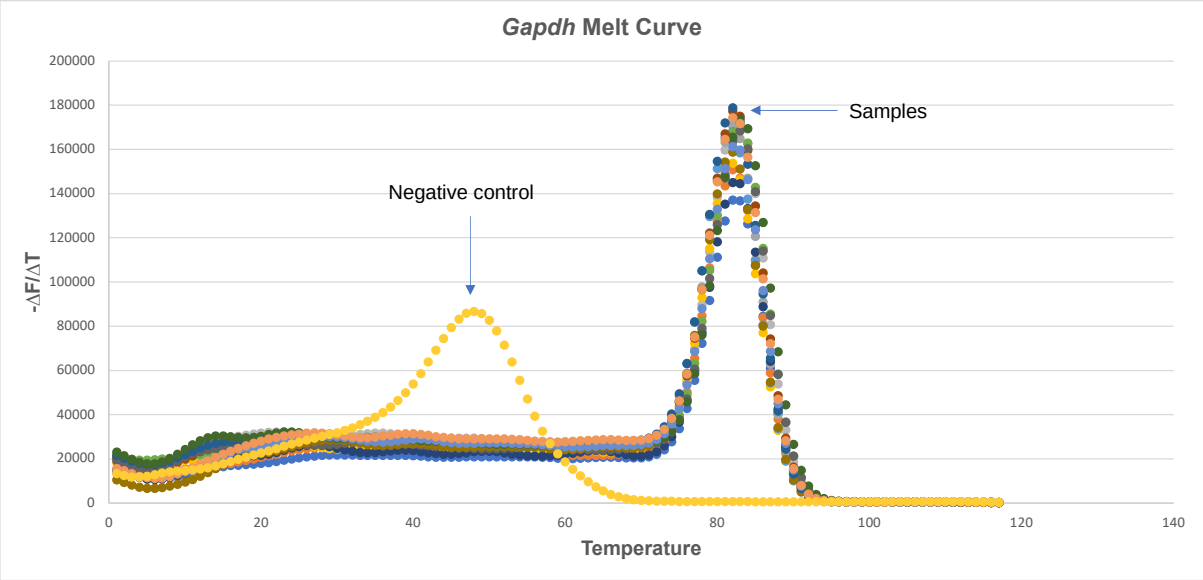


**Figure 2.2: Illustration of melt curve for qPCR analysis**

Negative control: Consisted of SYBR green, primer mix and water.

Samples: Consisted of SYBR green, primer mix, water, and cDNA

**Table 2.2: List of primers used for qPCR in this study**

*Wls* was adopted from (**https://www.origene.com/catalog/gene-expression/qpcr-primer-pairs/mp205119/wls-mouse-qpcr-primer-pair-nm_026582**); *Lrp5* was adopted from (Shin et al., 2014). Other primers were designed or provided in the Harvey's laboratory.

| Target Gene | Forward Primer 5'-3' | Reverse Primer 5'-3' | Efficiency | Slop |
|---|---|---|---|---|
| *Gapdh* | GCCCAGAACATCATCCCT | GTCCTCAGTGTAGCCCAAGA | 102% | -3.262 |
| *Hprt* | AGTCCCAGCGTCGTGATTAG | GGGCCACAATGTGATG | 103% | -3.167 |
| *Wls* | TTGCTGTTGGCTCCTTCTGCC T | GGCAGATACCTGCCACAATGATG | 68.58% | -4.409 |
| *Lrp5* | CTGAGGAACGTCAAAGCCAT CAACTATG | TACTGGCTGTACGATGT TGGCATCTTC | 100% | -3.302 |
| *Wnt5a* | GTGCCATGTCTTCCAAGTTC | TGCCTGTCTTCGCACCTT | 99.56% | -3.332 |
| *Wnt7a* | CGCCAAGGTCTTCGTG | AGCCTAAGCTCTCGGAACTGT | 105% | -3.198 |
| *Dkk3* | GCAAGCTTACCTCCCAACTA | GGCTGGCAGGTGTACTTGAA | 101% | -3.285 |
| *Dvl1* | TCTACCACATGGACGAGGAG | GGCAACTTGGCATTGTCATC | 113% | -3.037 |
| *Dvl2* | GGTGTAGGCGAGACGAAGGT | TAGGCGGGCATTGTCA | 87.95% | -3.649 |
| *Dvl3* | CCACCACCTCCGCATCCCTAC | TCTGACTCGCTGCCGCTA C | 99.28% | -3.339 |
| *β-catenin* | CATTGGTGCCCAGGGAGA | GATCAGGCAGCCCATCAACT | 106% | -3.176 |
| *Gsk3β* | TTGGACAAAGGTCTTCCGGC | AAGAGTGCAGGTGTGTCTCG | 108.83% | -3.127 |
| *Tcf1* | ATCTGCTCATGCCCTACCCA | GCGGCCTGTGAACTCCT | 107% | -3.146 |
| *Nfatc1* | CGGGAAGAAGATGGTGCT | CTGGTTGCGGAAAGGTGGTA | 112% | -3.062 |
| *Creb* | GAAGCAGCACGGAAGAGAG | CTGATTTGTGGCAGTAAAGG | 93.75% | -3.481 |
| *NFκB* | GGGCATTCTTTCAGAAGC | TGGGTAGTTCGGTTCCACAC | 100% | -3.309 |
| *Bdnf* | CGGGACGGTCACAGTC | CCGAACATACGATTGGGTAG | 95.95% | -3.422 |
| *Cyclin-D1* | CCTTGACTGCCGAGAAGTTG | TTGCGGATGGTCTGCTTGT | 107% | -3.150 |
| *Cox2* | GGGCAGGAAGTCTTTGGTCT | TGAAGTGGTAACCGCTCAG | 97.47% | -3.384 |
| *Axin2* | GCCGACCTCAAGTGCAAACT | GCCGGAACCTACGTGATAA | 99.84% | -3.326 |

# 2.5 Protein expression analysis

## 2.5.1 Tissue protein extraction and Western blotting

Brain tissues were dissected from mice and stored under -80°C. Upon protein extraction, tissues were thawed on ice. Lysis buffer was added to the tissues and subsequently homogenised by a glass rod or electronic homogeniser tissue grinder (Dixon Science). Homogenised tissues were centrifuged at maximum speed at 4°C. The supernatant was then transferred to a fresh collection tube.

Dr Andrea Wetzel performed the western blot experiments, and I collected and analysed the raw data.

Protein concentration was determined by Bicinchoninic acid (BCA) assay (Fisher Scientific). Sample protein concentrations were normalised to 1mg/ml to the standard loading samples. Protein lysate was mixed with 4X NuPAGE LDS sample buffer (Fisher Scientific) and 10X NuPAGE reducing agent (Fisher Scientific, USA) and heated under 95°C for 10 minutes to denature proteins. 10-30mg of proteins were loaded into each well on a 4-12% Bis-Tris plus gels (LifeTechnologies) with 10ml of molecular weight rainbow markers (Fisher Scientific, USA) to confirm the molecular weight of the visualised bands. Protein fragments were separated by Sodium Dodecyl Sulphate (SDS) polyacrylamide gel electrophoresis (PAGE) with 1X bolt MES running

buffer (Fisher Scientific) at 120V for approximately 2 hours until bands reached almost the bottom of the gel.

The gel with protein bands was transferred to a polyvinylidene fluoride (PDVF) membrane (Bio-rad), which was activated by soaking in methanol. 2 stacks of filter paper (Bio-rad) were soaked in 1X transfer buffer (Bio-rad). Filter paper and activated membrane were placed on a semi-dry transfer rack with the gel on top and an additional stack of filter paper on top before placing into the trans-blot turbo transfer system. The semi-dry transfer was run at 400mA for 45minutes. After the proteins were successfully transferred onto the membrane, it was blocked with 5% normal serum (Sigma-Alrich) in 5% skimmed milk in Tris-buffered saline with 0.1% Tween (TBST) for 1 hour.

The membrane was incubated overnight with the target primary antibody at 4°C. All primary antibodies were diluted into desired concentration with a blocking buffer. The next day, the membrane was washed three times for 5 minutes with PBS, followed by 2 hours of incubation with horseradish peroxidase (HRP)-conjugated secondary antibody (**Table 2.3**). The membrane was washed three times for 5 minutes with TBST after incubation before imaging.

**Table 2.3: List of antibodies used for Western Blot in this study**

| Primary antibody | Host | Source | Dilution |
|---|---|---|---|
| **Anti-ß-actin** | Mouse | Sigma (A2228) | 1:5000 |
| **Anti-LRRK2** | Rabbit | Abcam (ab133474) | 1:1000 |
| **Anti-Wnt3a** | Rabbit | Abcam (ab198220) | 1:200 |
| **Anti-Wnt5a** | Rabbit | Abcam (ab174963) | 1:100-500 |
| **Anti-pLRP6** | Rabbit | Cell Signalling Tech (CST2568) | 1:1000 |
| **Anti-LRP6** | Rabbit | Cell Signalling Tech (CST3395) | 1:1000 |
| **Anti-pGSK3ß** | Mouse | Cell Signalling Tech (CST612313) | 1:1000 |
| **Anti-GSK3ß** | Rabbit | Cell Signalling Tech (CST9315) | 1:2000 |
| **Anti-Active- ß-catenin** | Mouse | Sigma (SKU05-665) | 1:1000 |
| **Anti-ß-catenin** | Rabbit | New England BioLabs (NEB9587) | 1:2000 |
| **TCF/LEF family antibody sampler kit** | Rabbit | New England BioLabs (NEB9383) | 1:1000 |
| **Anti-NFAT** | Rabbit | New England BioLabs (NEW5861) | 1:1000 |
| **Anti-BDNF** | Rabbit | Abcam (ab226843) | 1:1000 |
| **Anti-Cyclin-D1** | Rabbit | Abcam (ab134175) | 1:10000 |
| **Anti-Cox2** | Rabbit | ProteinTech (12375-1-AP) | 1:500 |
| **Anti-TNF** | Rabbit | New England BioLabs (NEB3703) | 1:1000 |
| **Anti-IL-6** | Rabbit | New England BioLabs (NEB12912) | 1:1000 |

| Secondary Antibody | Host | Source | Dilution |
|---|---|---|---|
| **Anti-mouse IgG** | Goat | Stratech Sci. (115-035-003-JIR) | 1:5000 |
| **Anti-Rabbit IgG** | Goat | Stratech Sci. (111-035-003-JIR) | 1：5000 |

### 2.5.2 Western blot imaging and quantification

The membrane was developed using the SuperSignal West Pico/Femto Chemiluminescent Substrate system (Pierce). The procedure was followed as per the manufacturer's protocol. The membrane was imaged under GeneGenome XRQ Chemilluminescence imager (Syngene). The intensity of each protein band was measured by the GeneSnap software.

## 2.6 Localisation of Wnt signalling activity *in vivo*

### 2.6.1 Perfusion

P1 neonatal pups were first injected with 5ml of lentiviral vector containing an expression cassette of TCF/LEF-Luc-eGFP or NFAT-Luc-eGFP (provided by Dr. A. Rahim laboratory and designed by Dr Simon Waddington and Prof Tristan Mckay) via intracerebroventricular (ICV) injection targeting anterior horn of the lateral ventricle by Dr. A. Wetzel, the procedure is illustrated in **section 3.2.1**. Mice were sacrificed at 7 months old via transcardial perfusion with PBS under isoflurane-induced anaesthesia. An incision was made through the skin and abdominal wall below the rib cage. The sternum was lifted, and the thoracic cavity was cut open to access the heart. A small incision was made on the right atrium, followed by a slow injection of 10-20ml of PBS

into the left ventricle with a 24-gauge needle. Muscle contraction and liver blanching were indications of successful perfusion. The perfused brains were subsequently fixed in 1X PBS with 4% PFA in individual 50ml tubes. The skull was removed after 24 hours, and the brain was placed back into PFA for another 24 hours. After 48 hours of fixation, brains were transferred into 1X PBS with 30% sucrose for cryoprotection.

### 2.6.2 Chrome gelatine coating of slides

All microscope slides (VWR) were double-coated with gelatine to increase tissue adhesion to the surface during the staining and washing steps. 2.5g of gelatine powder (VWR) was gradually dissolved with constant stirring in 500ml of dH2O at 45°C. 0.25g of chromium (III) potassium sulphate 12-hydrate (VWR) was added to dissolve in the solution. Slides were loaded into suitable racks and immersed into the solution, and left to dry overnight at 56°C. The process was repeated after 24 hours to produce double-coated microscope slides, which were used in our study.

### 2.6.3 Immunohistochemistry (IHC)

Coronal sections of the perfused mice brains were cryosectioned into 40μm at -20°C using a Leica CM3050 cryostat. The collected slices were stored at 4°C in TBSAF in a 96-well plate. Representative sections were chosen from the 96-well plates and placed into a 6-well plate with 1-well per brain. 3ml of 1X TBS was added to each well to wash the brain sections. 1% $H_2O_2$ in 1X TBS was used as a blocking agent to block the endogenous peroxidase activity for 30 minutes, followed by three washes in 1X

TBS with agitation for 5 minutes. The washed sections were incubated in 15% normal goat serum in 1X TBS for 30 minutes to block any non-specific binding sites. Sections were then incubated at 4°C overnight with 10% normal serum in TBS-T with an anti-eGFP primary antibody.

After three 5-minute washing steps with 1X TBS, sections were incubated in 10% normal serum in TBS-T with biotinylated anti-rabbit secondary antibodies at room temperature for 2 hours (**Table 2**.**4**). After the three 5-minutes washing steps after the 2$^{nd}$ incubation, sections were incubated with Vectastain avidin-biotin solution for 2 hours (ABC, Vector Laboratories, UK). The solution contained a mixture of reagents A and B diluted 1:1,000 in 1X TBS. Sections were washed as described before, followed by incubation with 0.05% DAB solution (Sigma-Aldrich) and 30% $H_2O_2$ in 1X TBS for approximately 15-30 minutes. The 6-well plates were covered with foil to limit light exposure.

After DAB incubation, the DAB solution was removed from the wells, followed by the addition of ice-cold 1X TBS to stop the reaction. Sections were washed three times for 5 minutes per wash in 1X TBS. The stained sections were then mounted onto the double gelatine-coated slides and dried overnight. Slides with mounted sections were placed into a rack and immersed in 100% ethanol for 30 seconds. The racks were shaken, drained on paper, and immediately emerged into Histo-Clear (National Diagnostics) for 15 minutes. The racks were shaken to discard any impurities and immersed for another 15 minutes. Mounting agent DPX (VWR, UK) was applied onto the slide and coverslips (VWR) were then placed on top and left to dry for 1-2 days.

**Table 2.4: List of antibodies used for IHC in this study**

| Primary antibody | Host | Source | Dilution |
|---|---|---|---|
| **Anti-eGFP** | Rabbit | Abcam(ab290) | 1:10,000 |

| Secondary Antibody | Host | Source | Dilution |
|---|---|---|---|
| **Biotinylated Anti-Rabbit IgG** | Goat | Vector Lab Inc (BA-1000) | 1:1000 |

### 2.6.4 Immunohistochemical image capture and analysis

Quantitative thresholding images of the brain sections were analysed using a Nikon Eclipse E600 light microscope (Nikon). Light intensity was set constant while images were taken. Approximately 30-40 non-overlapping x40 magnification images were taken for each region of interest with a Nikon DS-Fil camera (Nikon). Non-overlapped Images were analysed using Image-Pro Premier (Media-Cybernetics). ImageJ was used to measure individual eGFP positive cell intensity level for each region of interest image. Data was presented as light intensity ± standard error of the mean (SEM) for each region. A maximum of 50 cells were randomly selected for each of the sex in each genotype groups.

# 2.7 Primary culture

6-wells and 24 wells plates were used for the culture. All the wells were coated with Poly-L Lysine (PLL, Sigma) 24 hours before cell culture. On the day of the experiment, plates were washed with PBS twice. 10μl of the cell suspension was used to estimate the cell density by hemocytometer under a light microscope before plating.

## 2.7.1 Primary neuronal culture

WT, LRRK2 and G2019S KI brains were collected from postnatal (P0-1) mice. The instruments were sterilised with 70% ethanol. A 60-mm Petri dish with a dissection medium was prepared to collect 6-8 hippocampus and cortex from each genotype. 10ml of dissection medium was added to the tissues and waited until the tissues settled to the bottom of the tube. The medium was aspirated and repeated this process twice. Tissues were resuspended in a 4.5ml dissection medium with 0.5ml of 2.5% trypsin solution and incubated at 37 ºC for 20 minutes. The medium was aspirated and washed tissues with 10 ml of dissection medium twice, followed by washing with 10ml of plating medium twice. Tissues were resuspended in a 2.5ml plating medium and carefully homogenised by a glass pipette to obtain cell suspension. The same number of cells were plated into individual wells with 500ml plating medium and stored at 37 ºC in a cell culture incubator. An additional 200ml of plating medium was added 24 hours (DIV1) later, and 5mM of cytarabine was added to eliminate the growth of glial cells.

## 2.7.2 Primary astrocyte culture

A similar protocol is described in **section 2.6.1**. 6-8 whole brains were collected from P0-3 postnatal mice. Dissection was performed on a 60mm Petri dish with a dissection medium. Meninges were carefully removed from the brains. The brains were halved and transferred into a 50ml falcon tube with 22.5ml dissection medium. The tissues were gently aspirated up and down approximately 5-10 times with a 5ml plastic pipette to obtain smaller pieces. 2.5ml of 2.5% trypsin was subsequently added to the tube, mixed, and incubated at 37 ºC for 30 minutes. Gently shake the tube every 10 minutes to mix the medium and the tissues. Tubes were centrifuged at 300rpm for 5 minutes, and the supernatant was carefully discarded. Tissues were dissociated into cell suspension by adding 10ml astrocyte culture medium and pipetted using a 10ml plastic pipette until tissue pieces were homogenised and adjusted the total volume to 20ml with the plating medium. The cell suspension was then transferred to a T75 uncoated flask and stored at 37 ºC under a cell culture incubator. The medium was changed 2 days after and changed every 3days.

Glial cell culture usually reaches approximately 90% confluency after 7 or 8 days. At this stage, microglia and oligodendrocyte were sitting on top of the astrocyte. These unwanted glia cells were removed by directly hitting each side of the flask with the palm 20-30 times on each side. The medium was aspirated and washed with PBS twice. 5ml of 0.25% trypsin EDTA (Life Technologies) was added to the flask and incubated at 37 ºC for 5 minutes until astrocytes were detached from the flask. 5ml of plating medium was added to the astrocyte-contained medium and centrifuged at

180rpm for 5 minutes. Carefully discarded the supernatant and resuspended the pellet with a 40ml plating medium. The cell suspension was split into half and platted in 2 T75 flasks with 20ml each.

14-21 days after the first split, astrocytes were ready to either plate in appropriate cell concentration for experiments or freeze down with a freezing medium. Astrocytes were platted in PLL-coated 6 wells or 24 wells plates 24 hours prior experiment. 10,0000 cells were seeded on 6 wells plates for qPCR analysis. 5000 and 20,000 cells were seeded on 24 wells plates for immunofluorescence study and stimulations study, respectively.

### 2.7.3 Lentivirus transduction and stimulations

2 days after plating the primary neuronal or astrocyte culture, half of the culture medium was replaced with a medium containing lentivirus. Cells were transduced with lentivirus, which contained either TCF/LEF or NFAT-secNanoLuc transcriptional factor together with control lentivirus with spleen focus-forming virus (SFFV)-secVluc with a multiplicity of infection (MOI) of 1 for 72 hours. The cells secreted luciferase when the transcriptional factor was activated.

$$Volume\ (\mu l) = \frac{(Plaque\ Forming\ unit\ (\frac{vp}{\mu l}) * MOI\ )}{Cell\ density}$$

The complete medium was changed with a fresh culture medium after viral transduction. Different stimuli were added to the culture with appropriate concentration

along with the fresh culture medium. Stimuli were prepared as instructed on the production information. Lipopolysaccharide (Sigma) was dissolved in a culture medium, Wnt3a (R and D system) was dissolved in 0.1% BSA, ionomycin (Sigma-Aldrich) was dissolved in DMSO and LiCl was dissolved in PBS.

10ml of the luciferase-contained medium was transferred to a 96-well plate for NLuc measurement. NLuc was measured by adding 10ml of Furimazine (Nano-Glo Luciferase Assay, Promega) and 80 of dH2O; Furimazine was diluted as instructed as per the protocol provided. To detect VLuc, Vargulin (Prolume) was diluted to 5nM with luciferase assay buffer. 20ml of 5nM vargulin was added to 20ml of luciferase-contained medium and 60ml of luciferase assay buffer. Bioluminescence was recorded by IVIS spectrum *In Vivo* Imaging system (PerkinElmer) with 5 minutes absorption time. VLuc reading was normalised to NLuc reading per biological repeat.

### 2.7.4 Immunofluorescence

Immunofluorescence was used to analyse the morphology of astrocytes. 5000 cells were seeded on PLL-coated coverslips in a 24-wells plate. 4% PFA was added to each well without removing the medium and incubated for 15 minutes at room temperature. Coverslips were washed with PBS for 5 minutes for 5 times and stored in PBS with 0.02% Sodium Azide at 4°C.

The working medium was prepared as follows, 0.1% Triton-X was added to PBS to make 0.1% PBS-T. Wells were washed with PBS for 10 minutes, followed by blocking with 10% goat serum in 0.1% PBS-T for an hour at room temperature. The primary

antibody was diluted in 10% serum PBS-T, added to each well, and incubated overnight at 4°C, followed by 3 times 5 minutes of washing the other day. Wells were incubated with secondary antibody was diluted in 10% serum PBS-T for 2 hours in a light limited condition. Alexa Fluor 635 phalloidin (Invitrogen A34054) was dissolved in 1.5ml methanol to prepare a 40X methanol stock solution. 5ml of the 40X methanol stock solution was added into the well containing 200ml of secondary antibody solution 1 hour after secondary incubation (**Table 2.5**). Three times 5 minutes, washed with PBS and counterstained with 4',6'-diamidino-2phenylindole (DAPI, Sigma-Aldrich) for nuclear visualisation. 1mg/1ml stock solution of DAPI was diluted in 1:10,000 with PBS and applied to each of the wells for a 5-minute incubation.

Coverslips were mounted on SuperFrost Plus slides (ThermoScientific) with anti-fade Fluoromount G and sealed with clear nail polish. Slides were left to dry and stored at 4°C. Samples were visualised with Zeiss 980 Airyscan 2 (Carl Zeiss AG). Images were processed by ZenBlue 3 and analysed by ImageJ.

**Table 2.5: List of antibodies used for immunofluorescence in this study**

| Primary antibody | Host | Source | Dilution |
|---|---|---|---|
| **Anti-GFAP** | Rabbit | Abcam (ab7260) | 1:1000 |

| Secondary Antibody | Host | Source | Dilution |
|---|---|---|---|
| **Alexa Fluor 488 Anti-Rabbit IgG H&L** | Goat | Abcam (ab150077) | 1:400 |

## 2.8 Statistical analysis

All statistical analyses were carried out with GraphPad Prism (version 9.0) program. Student T-test was performed for two sample comparisons with Welch's correction. Multiple groups were analysed by either ONE-WAY ANOVA or TWO-WAY ANOVA followed by Tukey's honest significant difference post-hoc test. All graphs are presented as mean ± standard error of the mean (SEM). Differences between groups were considered as statistically significant when $p<0.05$, which are presented as $p>0.05$ = ns (non-significant), $p<0.05$ = *, $p<0.01$ = **, $p<0.001$ = ***, $p<0,0001$=**** on the graphs.

# 3 *In vivo* Wnt and NFAT signalling activity analysis in the brain

## 3.1 Introduction

PD patients experience motor and non-motor symptoms as the disease progresses, which suggests that although PD is characterised by dopaminergic neuronal loss in the substantial nigra pars compacta, the disease might start to develop much earlier in other brain regions.

As described in **Chapter 1**, LRRK2 expression was reported in different brain regions and peripheral organs by several investigators (West et al., 2014, Taymans et al., 2006). Growing evidence shows that LRRK2 plays a role in several signalling pathways, including Wnt and NFAT signalling, whereas mutant LRRK2 was reported to cause signalling dysregulation. LRRK2, as a part of signalling scaffolds, has been reported to regulate canonical Wnt signalling activity and to be a negative regulator of

NFAT signalling (Berwick et al., 2017, Berwick and Harvey, 2012). Given the important role of Wnt and NFAT signalling pathways in adult brain maintenance and inflammatory response, disruption of these pathways might lead to synaptic dysfunction, neuronal loss, or inflammation.

LRRK2 mutations, including the G2019S mutant, are generally considered gain of function mutations. However, to understand in more detail how wild type and mutant LRRK2 regulates Wnt and NFAT signaling in different brain regions, we injected male and female LRRK2 wild type, knockout and G2019S mutant mice with lentiviral biosensors (Buckley et al., 2015). Signalling activity was recorded as eGPF expression and quantified in the olfactory bulb, striatum, lateral ventricles, hippocampus, and cortex. We will compare the signalling activity between the different genotypes and the sexes. This might help identify where signalling dysregulation starts in the brain and shed light on PD pathogenesis, informing disease prevention or treatment. This chapter also reviews the pros and cons of the application of lentivirus biosensors *in vivo.*

# 3.2 Results

## 3.2.1 Wnt and NFAT signalling activities in different brain regions

P0/1 neonatal mice were injected with the lentiviral constructs containing an expression cassette with the Wnt canonical pathway transcriptional factor TCF/LEF or transcriptional factor NFAT, along with a luciferase primary reporter gene and eGFP as a secondary downstream reporter gene (**Fig 3.1 A**). Lentiviral vectors were administrated directly into the left lateral ventricle (**Fig 3.1 B**) When the pathway is activated, ß-catenin or NFAT will translocate into the nucleus and bind to the corresponding transcriptional factor to activate Wnt or NFAT pathways, respectively. The activation of the pathway induces the expression of eGFP in the cells (**Fig 3.1 C**). Both injected and non-injected mice were sacrificed at the age of 6 months, and brains were collected for anti-eGFP immunohistochemistry analysis. Representative images were captured for each brain region with positive eGFP expressing cells.

Brain slices were screened for areas with eGFP expression regardless of the genotype, which gave us a general idea of where Wnt and NFAT signalling pathways are activated in the brain. Stained sections were analysed and imaged via light microscopy. We have detected eGFP expression in the olfactory bulb, cortex, striatum, hippocampus, lateral ventricle, and midbrain areas such as the thalamus and

hypothalamus, as well as superior colliculus and inferior colliculus (**Fig 3.2**). We also observed similar eGFP expression in NFAT cohorts' brain regions. However, no eGFP positive cells were observed in the striatum within the NFAT studying group (**Fig 3.3**). eGFP positive cells were not observed in substantia nigra pars compacta in both Wnt and NFAT signalling study groups. No eGFP expressing cells were observed in non-injected control mice. As expected, eGFP was not only expressed within the nucleus but all over the cell body, including axons and dendrites. Extensive eGFP staining was observed in olfactory bulbs, whereas other regions showed fewer or no eGFP expressing cells.

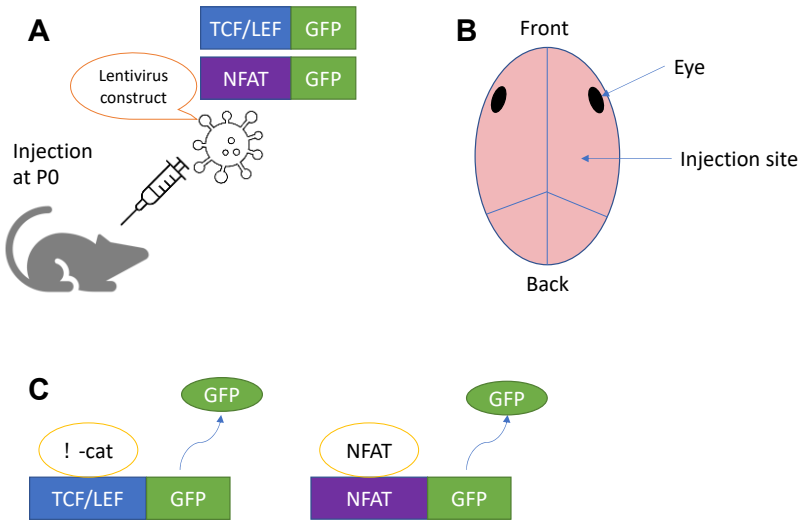


**Figure 3.1: Lentiviral vector administration procedure**

(A) Illustration of different lentiviral vectors injected at the age of P0/1

(B) Illustration of injection site used for P0/1 neonatal lateral ICV administration

(C) Illustration of eGFP gene transcription upon the binding of transducer onto transcriptional factor for both Wnt and NFAT signalling pathways.

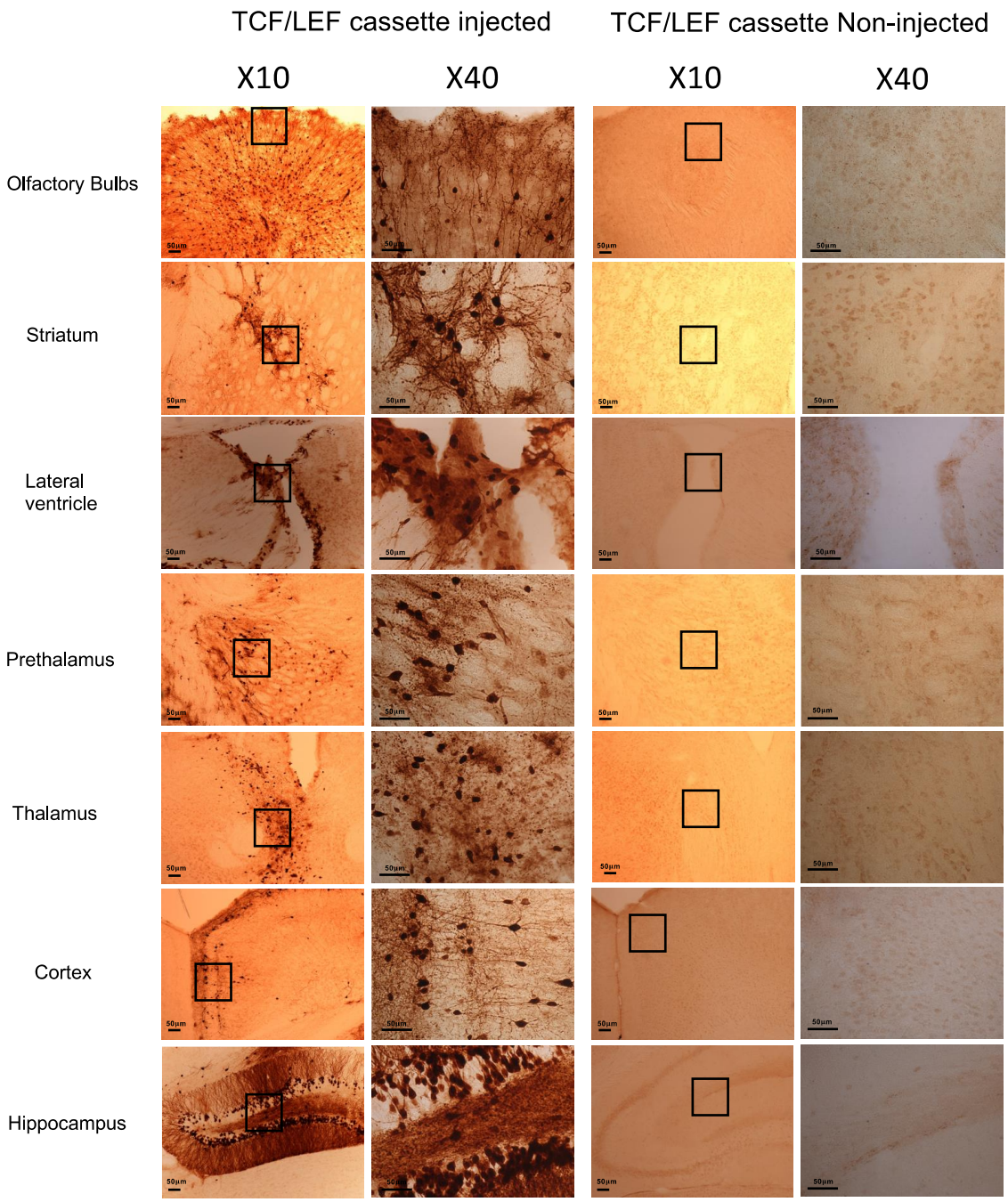
TCF/LEF cassette injected
TCF/LEF cassette Non-injected
X10
X40
X10
X40
Olfactory Bulbs
Striatum
Lateral ventricle
Prethalamus
Thalamus
Cortex
Hippocampus

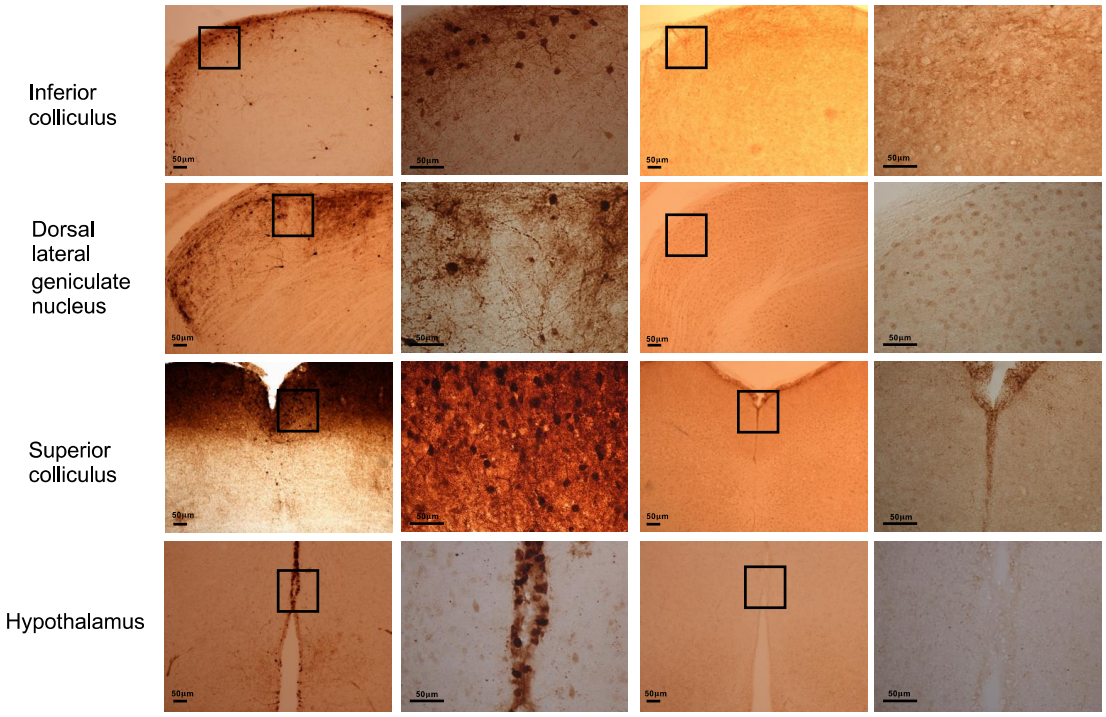


**Figure 3.2: eGFP expression in different brain regions as a result of Wnt signalling activation**

Coronal sections showing canonical Wnt signalling activation as eGFP expressing brain regions from 6 months old mice. Representative images of pLNT.TCF/LEF.FLuc.2A.eGFP.WPRE injected mice and non-injected negative controls. Images are presented in two magnification X10, magnification scale bar: 50µm; X40, magnification scale bar: 50µm.

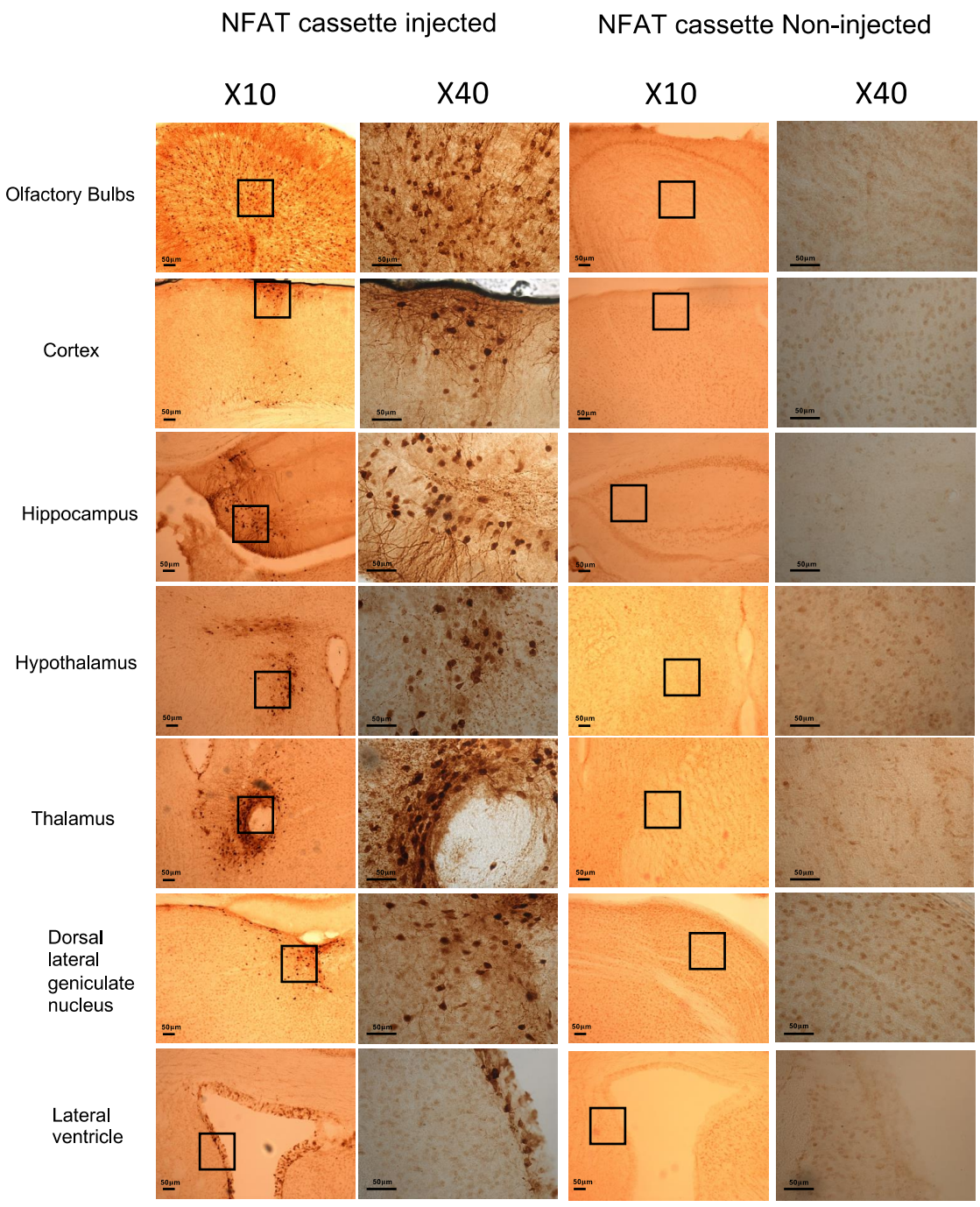
NFAT cassette injected
NFAT cassette Non-injected
X10
X40
X10
X40
Olfactory Bulbs
Cortex
Hippocampus
Hypothalamus
Thalamus
Dorsal lateral geniculate nucleus
Lateral ventricle

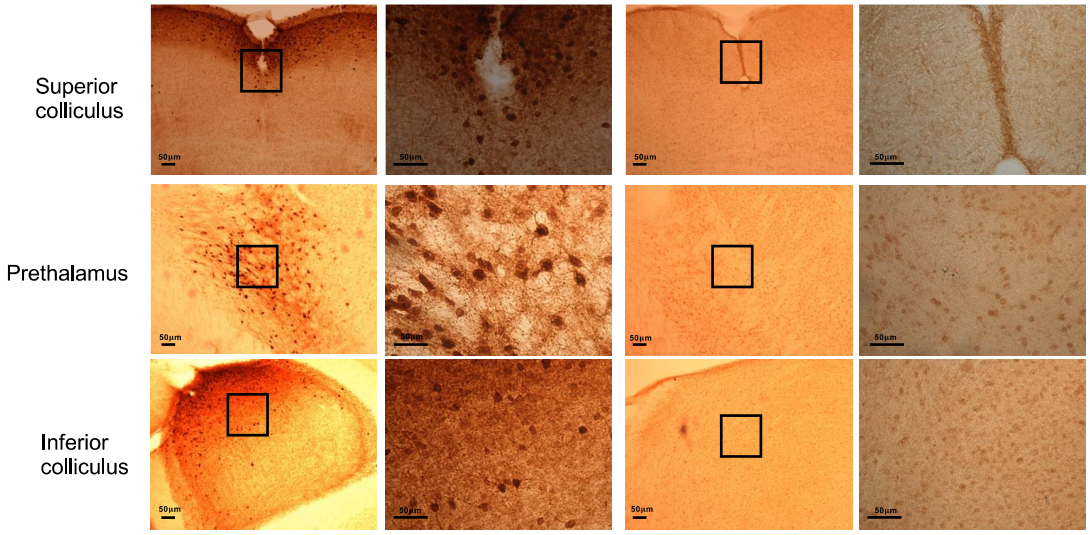


**Figure 3.3: eGFP expression in different brain regions as a result of NFAT signalling activation**

Coronal sections showing NFAT signalling activation as eGFP expressing brain regions from 6 months old mice. Representative images of pLNT.NFAT.FLuc.2A.eGFP.WPRE injected mice and non-injected negative controls. Images are presented in two magnifications X10, magnification scale bar: 50µm; X40, magnification scale bar: 50µm.

### 3.2.2 Effects of sex on Wnt signalling activity in different brain regions

After identifying the signalling activities in various brain regions, we focused on studying the Wnt signalling activities. Several brain regions have showed consistently eGFP expressing cells. We have chosen the brain regions that have the most consistent signals in both sexes and genotypes for further analysis of differences between genotypes and sexes: olfactory bulbs, cortex, striatum, lateral ventricle, and hippocampus. Study groups consisted of LRRK2 WT (n=5/sex), LRRK2 KO (n=5/sex) and G2019S KI (n=5/sex). We have randomly selected a maximum of 50 cells per gender per genotype overall from X40 magnification images to perform the analysis for each of the brain regions. Light transmission intensity of the individual cells was measured for the analysis.

We analysed the activity difference between biological sexes for each of the genotypes. We have compared the female Wnt signalling activity level to male in selected brain regions. We observed that male and female Wnt signalling activity level differences were not only found in different brain regions but differ in genotypes. Female's olfactory bulbs and cortex Wnt signalling activity level were similar to male signalling activity level in both WT and G20192S KI (**Fig 3.4 A, C**). However, the activity levels showed a significant sex difference in the LRRK2 KO cohort. Female's signalling activity was decreased by about 30% ($p<0.0001$) in olfactory bulbs and increased by approximately 10% ($p<0.05$) in cortex when compared to males (**Fig 3.4 B**). Female signalling activity level in striatum was similar to male's level in both WT and LRRK2

KO samples (**Fig 3.4 A, B**), but the signalling activity was significantly decreased ($p<0.001$) in G2019S KI in comparison to males (**Fig 3.4 C**). Signalling activity in lateral ventricle was decrease ($p<0.05$) in female WT (**Fig 3.4 A**), but slightly increased ($p<0.05$) in female LRRK2 KO (**Fig 3.4 B**), and activity level was similar when compared to males in G2019S KI (**Fig 3.4 C**). Signalling activity level changes in female hippocampus were non-significant when compared to male in both LRRK2 KO and G2019S KI samples, but it was significantly decreased by 20% ($p<0.0001$) in WT.

The overall data suggested that sex influences signalling activity differently in different genotypes and between the brain regions within the same genotype.

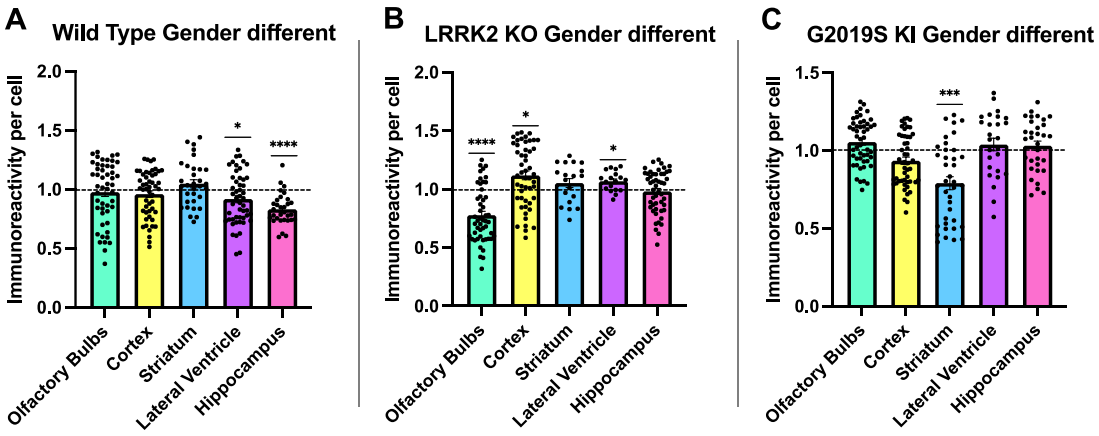


**Figure 3.4: Brain regions specific male and female Wnt signalling activity difference in different genotypes**

eGFP intensity was measured from individual cells. Male Wnt signalling activity level was set as one for each of the brain regions and presented as a line on the graphs. Bar charts represented female (F) Wnt signalling activity level in olfactory bulb, cortex, striatum, lateral ventricle, and hippocampus when compared to the matched region's signalling activity level in male (M). Data presented as mean ± S.E.M., compared by unpaired t-test with Welch's correction for sex difference, $p<0.05$ = *, $p<0.01$ = **, $p<0.001$ = ***, $p<0.0001$ = ****

**A)** LRRK2 WT male and female Wnt signalling activity level differences

**B)** LRRK2 KO male and female Wnt signalling activity level differences

**C)** G2019S KI male and female Wnt signalling activity level differences

**Wild type** (Olfactory bulb M: n=50; F: n=50, cortex M: n=50; F: n=50, striatum M: n=50; F: n=32, lateral ventricle M: n=50; F: n=50 hippocampus M: n=45; F: n=31)

**LRRK2 KO** (Olfactory bulb M: n=50; F: n=50, cortex M: n=50; F: n=50, striatum M: n=44; F: n=19, lateral ventricle M: n=50; F: n=18 hippocampus M: n=43; F: n=50)

**G2019S KI** (Olfactory bulb M: n=50; F: n=50, cortex M: n=45; F: n=50, striatum M: n=50; F: n=38, lateral ventricle M: n=50; F: n=26 hippocampus M: n=28; F: n=32)

### 3.2.3 Effect of LRRK2 genotypes on Wnt signalling activity in different brain regions

After we have established the gender differences in the selected brain regions. We would like to know how LRRK2 interferes with Wnt signalling activity in different genotypes. We have used WT as a baseline to compare with LRRK2 KO and G2019S KI signalling activity. We presented the data separated by gender, as well as combined gender together to observe how much gender influences Wnt signalling activity. As samples reacted differently to DAB staining, it was important to use control samples as a background reading for more accurate measurement of immunoreactivity.

**Olfactory Bulbs**

eGPF positive cells were observed all over the olfactory bulbs (**Fig 3.5 A, B**). G2019S KI mice olfactory bulbs showed an increase of signalling activity level when compared to WT ($p<0.001$) and LRRK2 KO ($p<0.0001$) in female cohorts (Fig. 3.5 C). In the male cohort, both the LRRK2 G2019S ($p<0.05$) and KO ($p<0.01$) showed a higher signalling activity when compared to WT (**Fig 3.5 D**). When we combined both male and female data, G2019S showed a significant increase of signalling activity when compared to WT ($p<0.0001$) and LRRK2 KO ($p<0.001$) (**Fig 3.5 E**). The overall data showed G2019S KI increased Wnt signalling activity in olfactory bulbs. The effect of LRRK2 KO on the other hand was significantly influenced by gender (**Fig 3.4 B**).

**Cortex**

eGFP positive cells were mainly observed in the outer layers of the cortex (**Fig 3.6 A, B**) at M1 and M2 areas. In females, we observed a slight increase of signalling activity in LRRK2 KO when compared to WT, but it was statistically non-significant ($p=0.23$). G2019S showed significantly lower activity than LRRK2 KO ($p<0.05$) **(Fig 3.6 C**). Male LRRK2 KO and G2019S showed a lower activity level when compared to WT but with no significant differences ($p>0.1$) (**Fig 3.6 D**). The overall combined data showed no significant differences, which suggested the signalling activity reduction in LRRK2 G2019S in comparison to WT cortex observed in females might be sex dependent (**Fig 3.6 E**).

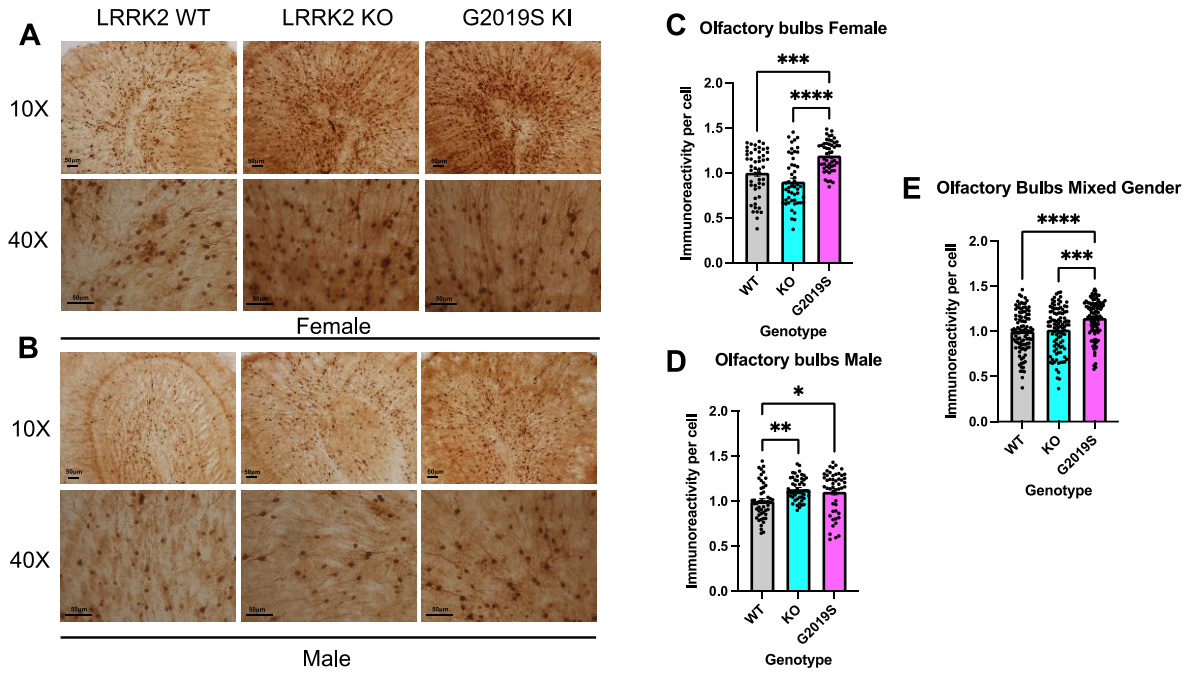


**Figure 3.5: Wnt signalling activity analysis in olfactory bulbs**

TCF/LEF lentiviral vectors were administration in P0/1 WT, LRRK2 KO and G2019S KI mice via ICV injection. Brains were harvested and stained with anti-eGFP for IHC analysis. Each dot on the bar chart represented the single cell immunoreactivity intensity level and was measured and analysed by One-Way ANOVA with Tukey post hoc test. An overall maximum of n=50 cells were measured from each of the sex per genotype group. Data presented as mean ± S.E.M., $p<0.05$ = *, $p<0.01$ = **, $p<0.001$ = ***, $p<0.0001$ = ****

**A)** Representative images of female olfactory bulbs under two different magnification 10X and 40X; Scale bar: 50μm for both magnifications

**B)** Representative images of male olfactory bulbs under two different magnification 10 X and 40X; Scale bar: 50μm for both magnifications

**C)** Quantification of positive eGFP expressing cells in female samples (WT n=50, LRRK2 KO n=50, G2019S KI n=50)

**D)** Quantification of positive eGFP expressing cells in male samples (WT n=50, LRRK2 KO n=50, G2019S KI n=50)

**E)** Quantification of positive eGFP expressing cells in combined gender (WT n=100, LRRK2 KO n=100, G2019S KI n=100)

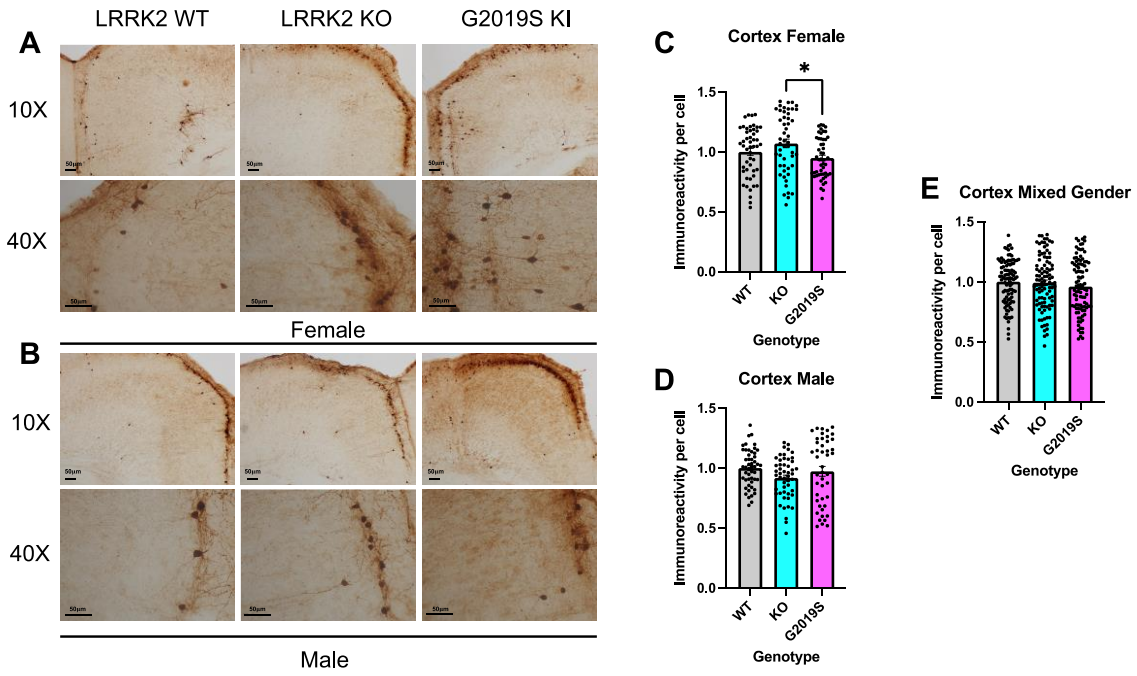


**Figure 3.6: Wnt signalling activity analysis in cortex**

TCF/LEF lentiviral vectors were administration in P0/1 WT, LRRK2 KO and G2019S KI mice via ICV injection. Brains were harvested and stained with anti-eGFP for IHC analysis. Each dot on the bar chart represented the single cell immunoreactivity intensity level and was measured and analysed by One-Way ANOVA with Tukey post hoc test. An overall maximum of n=50 cells were measured from each of the sex per genotype group. Data presented as mean ± S.E.M., $p<0.05$ = *, $p<0.01$ = **, $p<0.001$ = ***, $p<0.0001$ = ****

**A)** Representative images of female olfactory bulbs under two different magnification 10X and 40X; Scale bar: 50μm for both magnifications

**B)** Representative images of male olfactory bulbs under two different magnification 10 X and 40X; Scale bar: 50μm for both magnifications

**C)** Quantification of positive eGFP expressing cells in female samples (WT n=50, LRRK2 KO n=50, G2019S KI n=50)

**D)** Quantification of positive eGFP expressing cells in male samples (WT n=50, LRRK2 KO n=50, G2019S KI n=45)

**E)** Quantification of positive eGFP expressing cells in combined gender (WT n=100, LRRK2 KO n=100, G2019S KI n=95)

**Striatum**

Although eGFP positive cells were also observed in the striatum of both genotypes and genders, in comparison to olfactory bulbs and cortex, eGFP positive cells were observed in smaller numbers. Less eGFP expressing cells were observed in male samples in WT in comparison to LRRK2 KO, but less eGPF expressing cells were found in female G2019S samples in comparison to WT and KO samples(**Fig 3.7 A, B**). LRRK2 KO showed a trend towards higher signalling activity when compared to WT in female ($p<0.053$) and, was significantly higher in male ($p<0.01$). Male G2019S signalling activity level was slightly lower than LRRK2 KO but higher than WT, although there were no significant differences ($p>0.1$). Female G2019S KI mice showed significantly lower Wnt signalling activity in the striatum in comparison to female LRRK2 KO ($p<0.0001$) and WT ($p<0.01$) mouse cohorts (**Fig 3.7 C-D**). When combining the data together, LRRK2 KO showed a significant increase in signalling activity when compared to WT ($p<0.01$) and G2019S KI ($p<0.0001$). Although G2019S KI samples showed a decrease of signalling activity when compared to WT and LRRK2 KO but there were no significant differences ($p>0.1$) (**Fig 3.7 E**). This showed the importance of taking the data separated by gender, since different gender displayed a different signalling activity profile.

**Lateral Ventricle**

eGFP positive cells were observed in lateral subventricular zone in both genders and genotypes (**Fig 3.8 A, B**). LRRK2 KO and G2019S KI had a higher signalling activity level when compared to WT in both female and male study groups. The effect was more pronounced in the female cohort. LRRK2 KO and G2019S KI Wnt signalling

activity levels were significantly higher than WT in females ($p<0.0001$), LRRK2 KO had the highest signalling activity level and showed a trend towards increased activity in comparison to G2019S KI samples ($p=0.06$) (**Fig 3.8 C**). Both mutated LRRK2 study groups showed a less significant increase of Wnt signalling activity when compared to WT in the male cohort, LRRK2 KO signalling activity level was slightly higher than WT ($p<0.05$) and G2019S KI ($p=0.08$) (**Fig 3.8 D**). When combining the gender data together, both LRRK2 KO and G2019S KI showed a highly significant increase of Wnt signalling activity when compared to WT, ($p<0.0001$) and ($p<0.01$), respectively. Wnt signalling activity in LRRK2 KO was also higher than G2019S KI ($p<0.05$) (**Fig 3.8 E**).

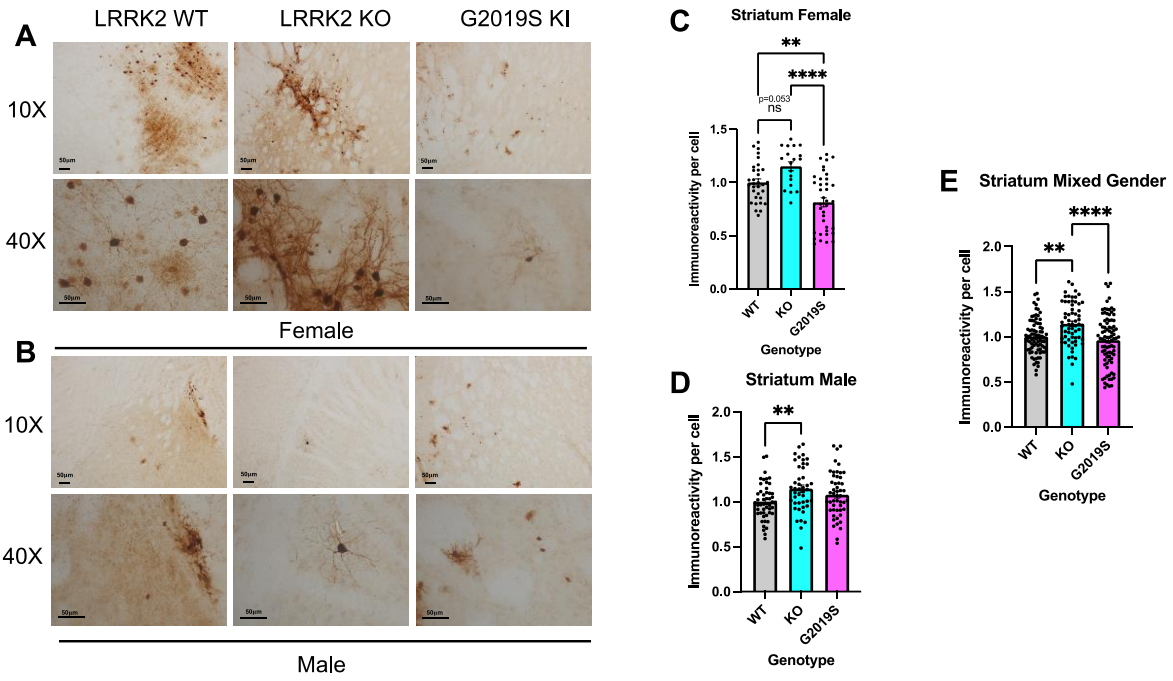


**Figure 3.7: Wnt signalling activity analysis in striatum**

TCF/LEF lentiviral vectors were administration in P0/1 WT, LRRK2 KO and G2019S KI mice via ICV injection. Brains were harvested and stained with anti-eGFP for IHC analysis. Each dot on the bar chart represented the single cell immunoreactivity intensity level and was measured and analysed by One-Way ANOVA with Tukey post hoc test. An overall maximum of n=50 cells were measured from each of the sex per genotype group. Data presented as mean ± S.E.M., $p<0.05$ = *, $p<0.01$ = **, $p<0.001$ = ***, $p<0.0001$ = ****

**A)** Representative images of female olfactory bulbs under two different magnification 10X and 40X; Scale bar: 50μm for both magnifications

**B)** Representative images of male olfactory bulbs under two different magnification 10 X and 40X; Scale bar: 50μm for both magnifications

**C)** Quantification of positive eGFP expressing cells in female samples (WT n=32, LRRK2 KO n=19, G2019S KI n=38)

**D)** Quantification of positive eGFP expressing cells in male samples (WT n=50, LRRK2 KO n=44, G2019S KI n=50)

**E)** Quantification of positive eGFP expressing cells in combined gender (WT n=82, LRRK2 KO n=63, G2019S KI n=88)

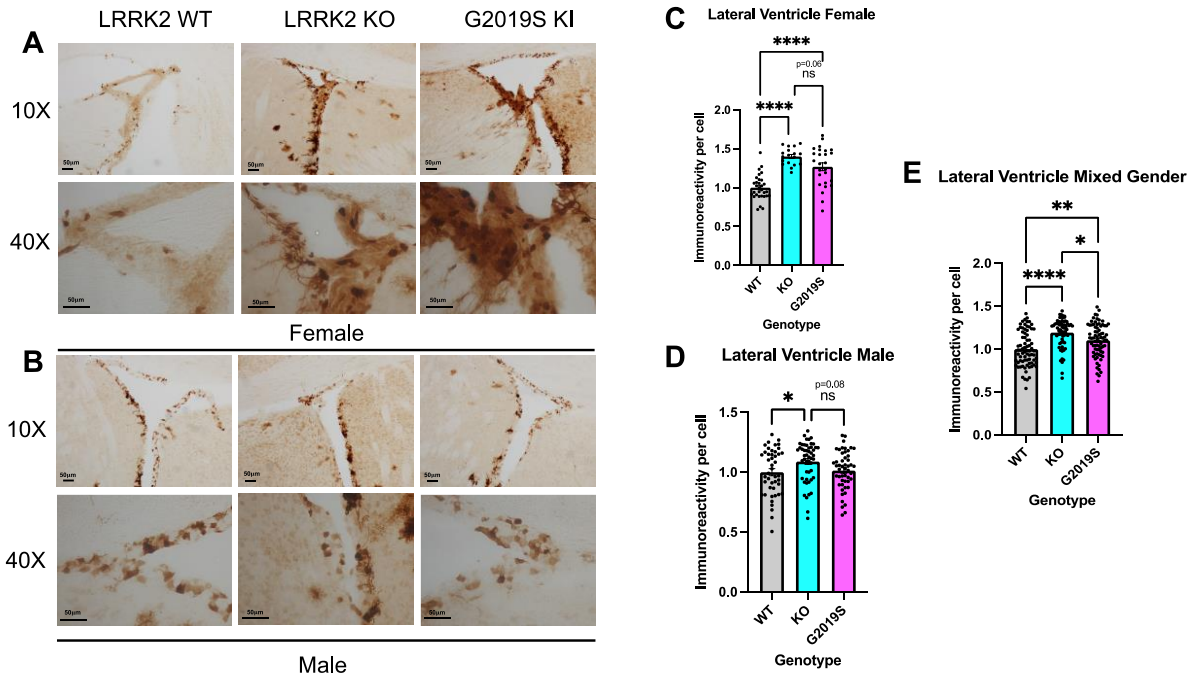


**Figure 3.8: Wnt signalling activity analysis in lateral ventricle**

TCF/LEF lentiviral vectors were administration in P0/1 WT, LRRK2 KO and G2019S KI mice via ICV injection. Brains were harvested and stained with anti-eGFP for IHC analysis. Each dot on the bar chart represented the single cell immunoreactivity intensity level and was measured and analysed by One-Way ANOVA with Tukey post hoc test. An overall maximum of n=50 cells were measured from each of the sex per genotype group. Data presented as mean ± S.E.M., $p<0.05$ = *, $p<0.01$ = **, $p<0.001$ = ***, $p<0.0001$ = ****

**A)** Representative images of female olfactory bulbs under two different magnification 10X and 40X; Scale bar: 50μm for both magnifications

**B)** Representative images of male olfactory bulbs under two different magnification 10 X and 40X; Scale bar: 50μm for both magnifications

**C)** Quantification of positive eGFP expressing cells in female samples (WT n=31, LRRK2 KO n=18, G2019S KI n=26)

**D)** Quantification of positive eGFP expressing cells in male samples (WT n=45, LRRK2 KO n=50, G2019S KI n=50)

**E)** Quantification of positive eGFP expressing cells in combined gender (WT n=76, LRRK2 KO n=68, G2019S KI n=76)

**Hippocampus**

Similar to what we have visually observed in striatum, overall less eGFP positive cells were also stained observed in male hippocampus for all genotypes than in females. Most of the eGFP expressing cells were observed in the dentate gyrus area (**Fig 3.9 A, B**). Since we were measuring individual cell's immunoreactivity intensity level, the limited number of eGFP expressing cells was not a limiting factor. Female G2019S KI hippocampi showed a trend towards a higher signalling activity level than WT ($p=0.08$). LRRK2 KO also showed a slightly increased of signalling activity level than WT with no statistically significant difference ($p>0.1$) (**Fig 3.9 C**). There were no significant differences in male and combined gender data; all genotypes showed a similar signalling activity level, which was closed to 1 (**Fig 3.9 D, E**).

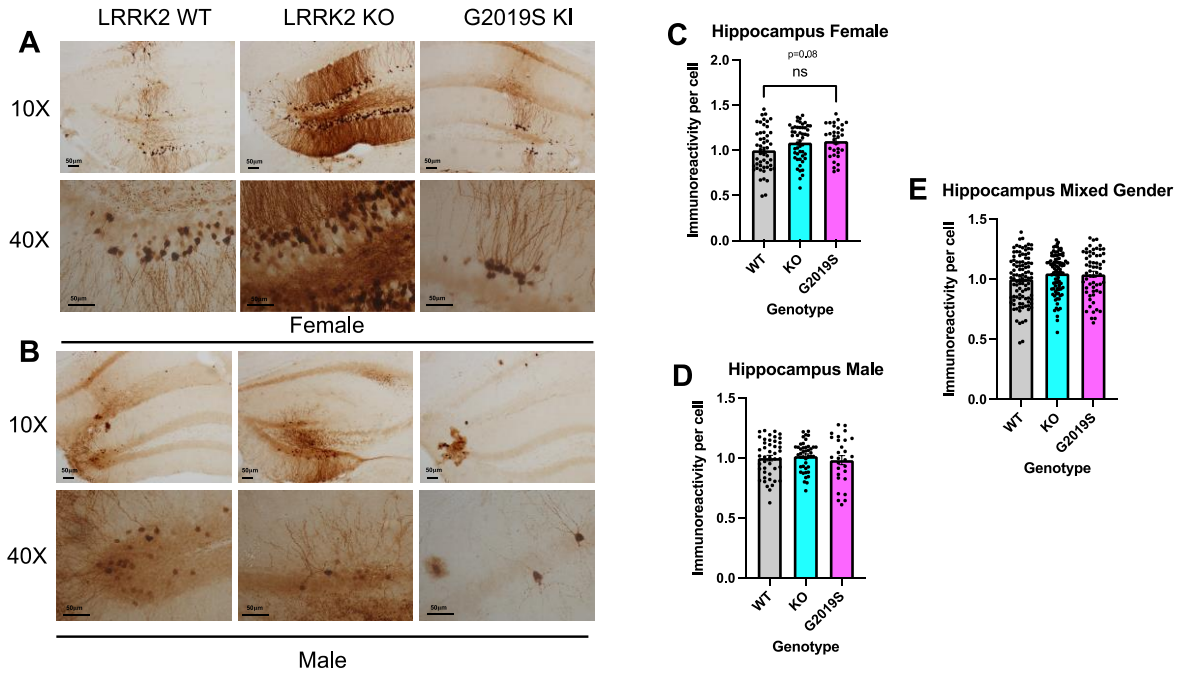


**Figure 3.9: Wnt signalling activity analysis in hippocampus**

TCF/LEF lentiviral vectors were administration in P0/1 WT, LRRK2 KO and G2019S KI mice via ICV injection. Brains were harvested and stained with anti-eGFP for IHC analysis. Each dot on the bar chart represented the single cell immunoreactivity intensity level and was measured and analysed by One-Way ANOVA with Tukey post hoc test. An overall maximum of n=50 cells were measured from each of the sex per genotype group. Data presented as mean ± S.E.M., $p<0.05$ = *, $p<0.01$ = **, $p<0.001$ = ***, $p<0.0001$ = ****

**A)** Representative images of female olfactory bulbs under two different magnification 10X and 40X; Scale bar: 50μm for both magnifications

**B)** Representative images of male olfactory bulbs under two different magnification 10 X and 40X; Scale bar: 50μm for both magnifications

**C)** Quantification of positive eGFP expressing cells in female samples (WT n=50, LRRK2 KO n=50, G2019S KI n=32)

**D)** Quantification of positive eGFP expressing cells in male samples (WT n=45, LRRK2 KO n=43, G2019S KI n=28)

**E)** Quantification of positive eGFP expressing cells in combined gender (WT n=100, LRRK2 KO n=93, G2019S KI n=60)

# 3.3 Discussion

Following lentiviral biosensor transduction into mice, we detected brain region specific WNT and NFAT signalling activation by measuring the optical density of eGFP positive cells (Buckley et al., 2015). We have observed eGFP expressing cells in striatum, cortex, hippocampus, olfactory bulbs, lateral ventricle, and the thalamic area. The stained cells could be neurons and/or glial cells. However, lentiviruses are more likely to transduce neurons and the observed staining pattern speaks for the detection of mostly neurons. However, it is difficult to distinguish the exact cell type without further neuronal or glial cell marker staining. Importantly, eGFP positive canonical Wnt and NFAT signalling active cells were observed in striatum, cortex, hippocampus, thalamus, and olfactory bulbs. These are the areas in which LRRK2 has previously been found to also be expressed. For example, Taymans *et al.* described that LRRK2 is highly expressed in striatum, cortex and hippocampus, and expressed at relatively lower levels in olfactory bulbs, hypothalamus and substantia nigra (Taymans et al., 2006), whereas other research groups found LRRK2 to be highly expressed in substantia nigra in mice but not in rat (West et al., 2014). In addition, *LRRK2* was also reported to be expressed in human brain, including astrocytes and microglia (Miklossy et al., 2006). Therefore, our findings consolidated our hypothesis that Wnt and NFAT signalling pathways are active in brain areas expressing LRRK2 and that this signalling pathway activation might impact on PD pathogenesis.

Although the biosensor system provided a reliable method to visualise and quantify Wnt signalling activity between mutant and WT mice, we have experienced a limited expression of eGFP in certain brain areas. This might be partially due to the distance from the virus injection site, the virus preferentially following different neuronal tracts from the injection site, and potentially loss of biosensor expression over time. It should also be considered that our mouse models were in a healthy state and Wnt and NFAT signalling activity would therefore be expected at a basal state, which might have also limited the activation of the signalling pathways and thereby expression of eGFP.

Further technical limitations are that the lentiviral vector might not be injected into the exact same area in each of the mice at P0/1, which might cause an unequal distribution of viral transduction at an early stage. However, this error would be expected to be similar between genotypes. Lentiviral vectors were administrated via ICV injection targeting the lateral ventricle where the rostral migratory stream (RMS) is located. The RMS is situated in the subventricular zone (SVZ) at the outer layer of the lateral ventricle and provides a route for neural progenitor cells to travel towards the direction of the olfactory bulbs (Pencea et al., 2001). These progenitor cells, known as neuroblasts, eventually migrate and differentiate into neurons in the olfactory bulbs. The mechanism of cell migrations has been reviewed by different groups; these cells can also migrate to the injury site of the brain to play a role in regeneration. (Capilla-Gonzalez et al., 2015, Lim and Alvarez-Buylla, 2016). The above taken together with the fact that Wnt signalling is crucial during neurogenesis might explain why we observed more eGFP positive cells in the olfactory bulbs than in any other brain region.

The higher number of stained cells also had the advantage of providing a more confident result in our analysis.

We focused in more detail on canonical Wnt signalling activation in different brain regions of male and female mice with different LRRK2 genotypes. The mice in this study were hosted in a controlled environment, which minimized the potential exposure of environmental risk factors, allowing a focus on genetic and sex effects.

In line with our results, it has previously been reported that in human bone marrow stromal cells, Wnt ligands gene expression differs at different ages and between sexes. *Wnt7a* and *Wnt14* gene expression was higher in samples from younger participants and declined with increasing age. The authors also indicated that Wnt4, Wnt7b, Wnt13, Wnt14, and Wnt17 expression was sex dependent in hMSC samples (Shen et al., 2009). The findings suggest that Wnt signalling declines with age and is affected by the biological sex of participants. Our study shows that LRRK2 genotype seems to have an additional effect on Wnt signalling activity than sex alone. Our data showed more brain region specific sex differences in LRRK2 KO mice than WT or G2019S KI mice, with females showing only lower Wnt signalling activity than males in the G2019S KI study group. Higher Wnt signalling activity could facilitate higher neurogenesis activity, and vice versa for lower Wnt signalling activity. Although we observed a different Wnt signalling activity profile in male and female study groups, the effect diminished when the data were combined. The finding suggests that LRRK2 genotype might play a more prominent role in regulating Wnt signalling activity in one

sex than the other and shows the importance of analyzing data not just by genotype and brain regions but also by sex.

PD patients experience non-motor symptoms such as depression, anxiety and hyposmia, which are related to hippocampus and olfactory bulbs. It has been reported that hyposmia is less frequent in G2019S PD patients than idiopathic PD patients, whereas the neuropsychiatric symptom occurrence rate is similar between idiopathic PD patients and G2019S carriers (Gaig et al., 2014).

Wnt signalling is highly active during neurogenesis, and dysregulation of neurogenesis might occur an early stage of PD development (Marchetti et al., 2020). Therefore, the significant observed Wnt signalling activity increase in LRRK2 KO and G2019S KI mice in the lateral ventricles and olfactory bulbs might suggest our mutant mice were undergoing increased neurogenesis. Of particular interest, in the PD G2019S KI mice, the increase in Wnt signaling activity in comparison to KO and WT might have been a reaction to potentially higher neuronal loss or damage, and hence, required a higher neurogenesis activity when compared to WT and LRRK2 KO.

The striatum is a component of the basal ganglia, which has the function of controlling voluntary movements. It has been reported that the LRRK2 level rises after birth and is highest in the striatum. The authors further suggested that LRRK2 mutations alter excitatory synaptic activity and change the shape of postsynaptic structures in the striatum (Matikainen-Ankney et al., 2016). Other groups also reported that G2019S KI mice showed a reduced striatal glutamatergic current when dopamine D2 receptors are stimulated by quinpirole(Tozzi et al., 2018). Wnt signalling activity was significantly

lower in female G2019S compared to WT and LRRK2 KO mice but showed no differences in the male cohort. Fewer eGFP expressing cells visually observed in the striatum of the female cohort might further suggest that Wnt signalling activity is lower in general in all genotypes in the female than male striatum. As the striatum is one of the most affected regions in the brain in PD patients, we hypothesise that neurogenesis might be more dysregulated in G2019S females than males.

The cortex is a huge area that contributes to functions such as motor function and memory, awareness, and consciousness. Much research has been done on the cortex and showed G2019S mutation carriers are affected similarly to sporadic PD patients with cognitive impairment (Gomez and Ferrer, 2010, Poulopoulos et al., 2012). It was reported that decreased or increased Wnt signalling pathways could lead to the death of post-mitotic neurons (Rawal et al., 2009). Our data showed a significantly higher Wnt signalling activity in female KO compared to G2019S KI, but no further observations were made in the male and combined gender analysis groups. The decreased or increased Wnt signalling activity could potentially lead to the interruption of neurogenesis, and/or a decrease in synapse function leading to neurodegeneration (**Fig 3.6**).

Our data suggest that LRRK2 mediates canonical Wnt signalling in the selected brain regions investigated in a sex and LRRK2 genotype dependent manner. PD progression is described thoroughly in the Braak staging system. The disease first starts at the brainstem and olfactory system and migrates towards the midbrain and frontal neocortex, affecting motor and sensory areas in the brain. Our data

demonstrated an increase in signalling activities in the olfactory bulb and lateral ventricles (**Fig 3.5, 3.8**). As these are potentially the first areas affected in PD, this might indicate that changes in Wnt signalling precede other pathogenic changes in LRRK2 mutant PD. It is not surprising that we did not observe a Wnt signalling activity difference between the genotypes in the hippocampus as this is an area affected at a later stage of the disease (Braak et al., 2003). We also observed an overall higher eGFP signal for canonical Wnt signalling in LRRK2 KO samples compared to the WT cohort, which is in line with previous research (Berwick et al., 2017). LRRK2 KO and G2019S KI seemed to increase Wnt signalling activity in a similar manner in most of the studied brain regions, whereas G2019S KI, on the other hand, decreased Wnt signalling significantly in the female striatum when compared to WT. This suggests that Wnt signalling activity is regulated differently in the female striatum in LRRK2 PD than in the male striatum. Overall, more changes were observed in the female cohort, which suggested gender may influence the effect of LRRK2 genotypes on canonical Wnt signalling pathways.

The PD prevalence and incidence rates differ in males and females. It was reported that oestrogen has a beneficial role in the dopaminergic neurons, which might explain the higher striatal dopamine level and slower PD symptoms development in females (Haaxma et al., 2007, Lee et al., 2019). Research has also shown that male PD patients had more cognitive impairment than females, sex also has a stronger effect on cognitive performance than motor symptoms (Cholerton et al., 2018, Reekes et al., 2020). Given the prevalence rate difference in idiopathic PD and G2019S *LRRK2* carries, San *et al* reported that idiopathic PD (IPD) men had more severe symptoms

than women. However, IPD women tended to have better olfaction but more therapy complications. Interestingly, LRRK2 PD patients showed better olfaction than IPD patients. In the meta-analysis conducted by Shu *et al*, LRRK2 G2019S cases were higher in females and mostly had a family history of PD. Nevertheless, G2019S carriers tended to show a better response to L-DOPA treatment and better quality of life than non-carriers (San Luciano et al., 2017, Shu et al., 2018). We observed a higher Wnt signalling activity in G2019S KI olfactory bulb samples, which might indicate Wnt signalling has a protective effect at early stages in G2019S mutation carriers (**Fig 3.5**). Moreover, apart from the striatum, our data demonstrated the male and female mice showed a similar trend of Wnt signalling activity when compared to WT. This could also explain why more brain regions showed a sex difference in WT and LRRK2 KO but not in G20192S KI mice (**Fig 3.4**). These preliminary data suggested a close relationship between LRRK2 and Wnt signalling pathways. The mice might have a different physiological development during their lifetime; hence, a higher n number is needed to eliminate the biological effect. An appreciate number of animals will be needed to identify in future studies. A power calculation would be beneficial to calculate an ideal sample size for future studies on a larger scale to generate significant yet accurate results (Jones et al., 2003, Charan and Kantharia, 2013, Festing and Altman, 2002).

Overall, LRRK2 might be a key Wnt signalling mediator, and LRRK2 mutations might affect Wnt signalling activity and Wnt signalling component level. To address this further, we performed mRNA and protein expression level analysis of various Wnt and NFAT signalling components in selected brain regions in the next chapter.

# 4 mRNA and protein expression level analysis in different brain regions

## 4.1 Introduction

In the previous chapter, we have established the effect of sex and genotypes on Wnt signalling activity. To investigate how LRRK2 interferes with Wnt and NFAT signalling activity on transcriptional and proteomic levels, we have performed real-time PCR and western blot to measure the mRNA and protein expression level changes between the genotypes and sex under basal conditions. As described in the introduction chapter, LRRK2 works as a scaffolding protein in Wnt and NFAT signalling pathways. It is most likely to interact with the β-catenin destruction complex and NRON complex to play a role in the phosphorylation of beta-catenin and NFAT respectively. Our group had previously reported that Wnt signalling activity was significantly increased when LRRK2 was knocked down, and the G2019S mutation caused an opposite effect in *in vitro* data (Berwick et al., 2017). Other groups also reported that LRRK2 knockout

would increase the expression level of inflammatory cytokines (Liu et al., 2011). Gathering the previous data together, LRRK2 as a scaffolding protein affects both signalling pathways in its physiological form. However, how exactly LRRK2 affects the signalling pathways' activities remains unclear.

In **Chapter 3**, we have identified Wnt signalling activity dysregulation in different brain regions, and we aimed to provide more information on how LRRK2 WT, LRRK2 KO and G2019S KI change the mRNA and protein expression level of the components of the Wnt and NFAT signalling pathway cascades under basal condition. 6 months old mice were used to compare with the data from **Chapter 3**. Based on the finding in the previous chapter, olfactory bulbs, hippocampus, cortex and striatum were selected for further investigation. PD patients might experience anomia and cognitive disorders during their disease progression, which made olfactory bulbs and the hippocampus an exciting target to study. The cortex and striatum are essential areas for movement regulation and it would be critical to know if Wnt signalling is dysregulated at an early age with G2019S KI mutation. The half brain provides an overview picture of Wnt signalling activities across the brain in the LRRK2 mouse models. Primers and antibodies were tested on WT mice samples and used as a baseline of our study. In this chapter, we observed different gene or protein expression level in different brain areas, which suggested different Wnt signalling activities across the brain. We revealed the expression changes of the Wnt signalling mediators, from co-receptor Lrp6, Wnt ligands: Wnt3a, Wnt5a and Wnt7a; beta-catenin destruction complex components: GSK-3β, Axin2; canonical Wnt signalling transcriptional factor: β-catenin,

TCF and LEF; target genes such as BDNF, Cyclin-D1, Cox2; and also that of the transcriptional factor: NFAT.

# 4.2 Results

## 4.2.1 Effect of sex on mRNA and protein expression level

We first checked mRNA and protein expression level differences between males and females. Hippocampus and olfactory bulbs showed the least differences in WT, LRRK2 and G2019S KI. We described the data from the region with the least expression differences to the most in this section. Representative Western blot images were attached to figures in **section 4.2.2-4.2.6**.

**Expression level in WT**

When comparing female WT mice mRNA and protein expression levels of our genes of interest to that of male WT mice we observed no significant differences in the hippocampus and olfactory bulb. However, the Wnt ligand *Wnt7a* expression level showed a trend of increase compared to males (p=0.05) (Fig.4.1D). Co-receptor LRP6 also showed a trend towards a decrease (p=0.06) in protein level (Fig.4.2D). Female olfactory bulbs showed a slightly increased *Gsk3β* mRNA level (p=0.06). In protein level analysis, Wnt3a showed a trend of decrease (p=0.07), and NFAT a trend of increase (p=0.06) compared to males (**Fig 4.1E, 4.2 E**). Overall, female olfactory bulbs and hippocampus showed minimal mRNA and protein levels differences when compared to male.

We hypothesised that half brain demonstrates an overall view of signalling component's mRNA and protein levels changes among different brain regions. We observed a significantly higher mRNA level of transcriptional factor *Tcf1* ($p<0.05$) and target gene *Cyclin-D1* ($p<0.05$), but no sex differences were observed on protein levels in half brain samples (**Fig 4.1-4.2 A**).

Interestingly, there were more albeit not always significant sex gene and protein expression level differences in WT cortex and striatum. Wnt antagonist *Dkk3* ($p=0.09$), signal transducer *β-catenin* ($p=0.08$), target genes *Bdnf* ($p=0.08$) and *Cox2* ($p=0.06$) were decreased on mRNA level in female cortex compared to the male counterpart. When looking at protein levels, the female cortex had a significantly higher LPR6 protein level ($p<0.05$), whereas phosphorylated GSK3β (pGSK3β at Y216) and GSK3β trended towards a decrease ($p=0.06$) compared to males (**Fig 4.1-4.2 B**).

WT female striatum showed the most genes of interest with significant mRNA expression level differences compared to male among the selected brain regions. *Wnt7a* ($p<0.01$), *β-catenin* ($p<0.05$), *Tcf1* ($p<0.05$), and *Nfat* ($p<0.01$) had a higher mRNA level in female. However, this was not reflected in protein levels. Only pGSK3β ($p=0.05$) and Cox2 ($p=0.06$) showed a trend towards increase in samples from females compared to males (**Fig 4.1-4.2 C**).

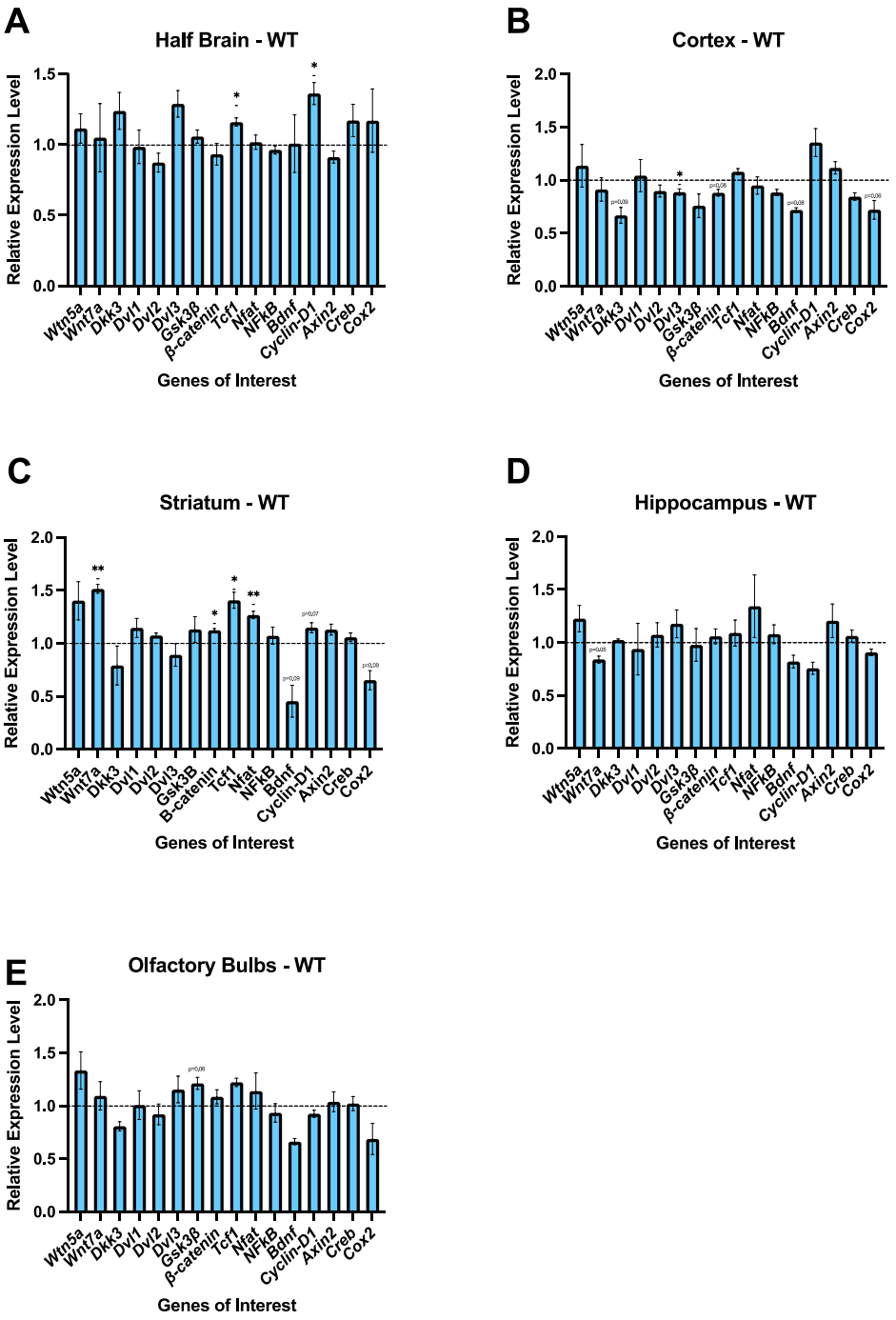


**Figure 4.1: Wild type female mRNA expression level against male**

Each of the genes of interest was compared to the corresponding male's value. Male was set as 1 and presented in a line.

**Wnt ligands:** *Wnt5a*, *Wnt7a*; **Antagonist**: *Dkk3*; **Cytoplasmic components**: *Dvl1-3*; **β-catenin destruction complex**: *Gsk3β*, *β-catenin*, *Axin2*; **Transcriptional factors**: *Nfat*, *Nfκb*, *Tc1*; **Downstream targets**: *Cyclin-d1*, *Bdnf*, *Creb*, *Cox2*.

Data presented as mean ± S.E.M., compared by unpaired t-test with Welch's correction for sex difference, $p<0.05$ = *, $p<0.01$ = **, $p<0.001$ = ***, $p<0.0001$ = ****; n=3 per sex.

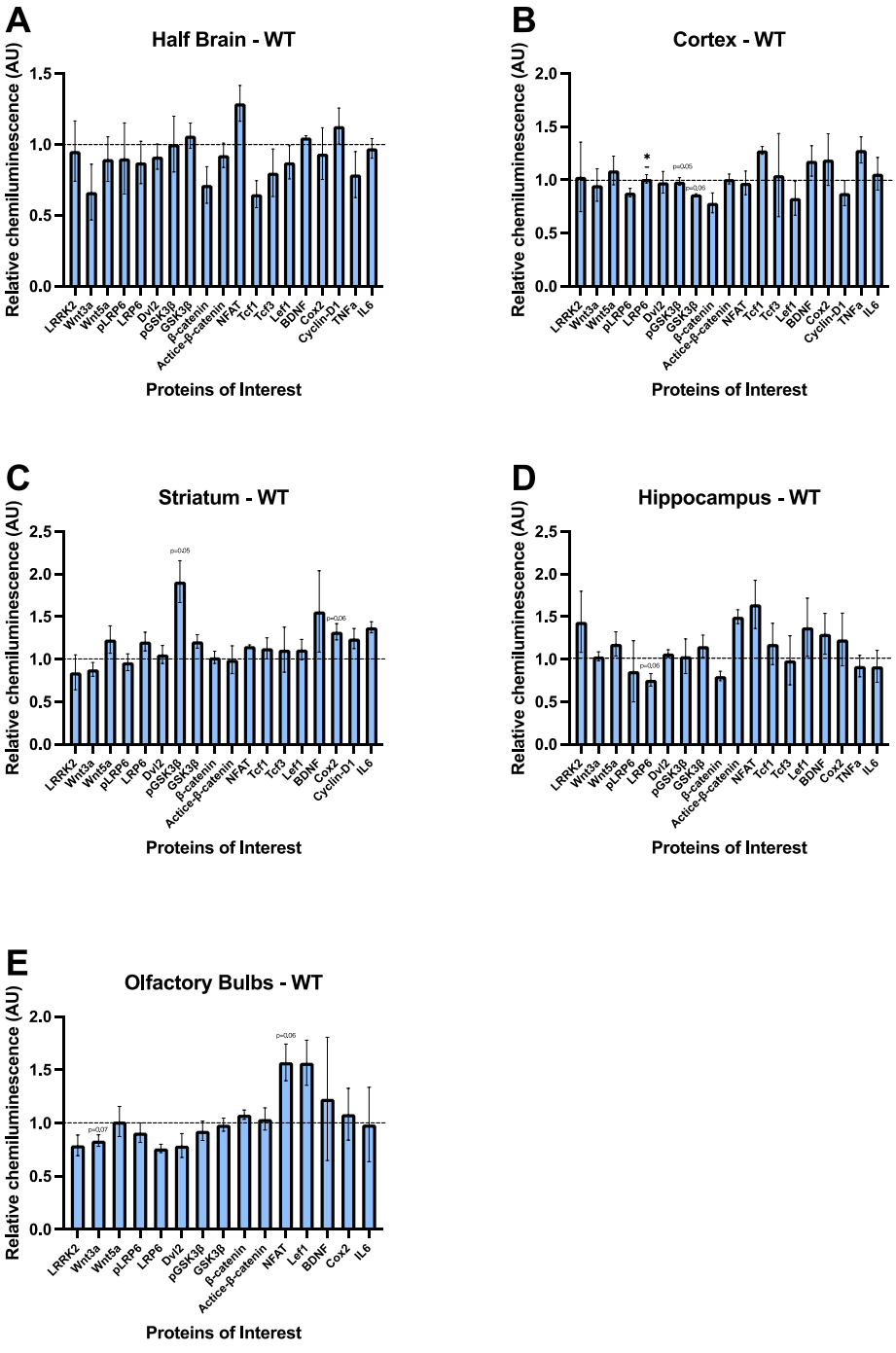


**Figure 4.2: Wild-type female protein expression level against male**

Each of the proteins of interest was compared to the corresponding male's value. Male was set as 1 and presented in a line.

**Wnt ligands:** *Wnt5a*, *Wnt7a*; **Antagonist**: *Dkk3*; **Cytoplasmic components**: *Dvl1-3*; **β-catenin destruction complex**: *Gsk3β*, *β-catenin*, *Axin2*; **Transcriptional factors**: *Nfat*, *Nfκb*, *Tc1*; **Downstream targets**: *Cyclin-d1*, *Bdnf*, *Creb*, *Cox2*.

Data presented as mean ± S.E.M., compared by unpaired t-test with Welch's correction for sex difference, $p<0.05$ = *, $p<0.01$ = **, $p<0.001$ = ***, $p<0.0001$ = ****; n=3 per sex.

**Expression level in LRRK2 KO**

In comparison to the differences observed in WT mice, a different expression level profile was observed in LRRK2 KO cohorts. In the female hippocampus we only observed a trend towards a lower *Wnt5a* mRNA level (p=0.09), and no statistical differences compared to males. Unlike WT samples, more protein expression sex differences were observed in LRRK2 KO mice. Wnt3a and Wnt5a showed a significantly higher protein level in females ($p<0.05$), and a trend of increase in BDNF (p=0.05) and TNF$\alpha$ (p=0.09) protein levels compared to males (**Fig 4.3-4.4 D**).

Female olfactory bulbs showed a significantly lower *Gsk3*$\beta$ ($p<0.05$) and a trend of decrease of *Tcf1* (p=0.07) mRNA levels. The Wnt target gene *Cox2* showed a substantially higher mRNA level in females. However, this was not a statistically significant difference due to a large error bar. Protein levels was similar in male and female, and no statistical difference was observed (**Fig 4.3-4.4 E**).

Female half brain and striatum mRNA levels showed no statistical differences compared to male mice. More protein level differences have been observed in these two brain regions. In half brain canonical Wnt signalling pathway ligand Wnt3a showed a significantly lower protein level in female ($p<0.05$), whereas, interestingly, active-$\beta$-catenin protein level was significantly higher in female than male ($p<0.05$). However, none of the target proteins showed any down or upregulations. In addition, the NFAT signalling pathway transcriptional factor NFAT showed a tendency towards a decrease in female (p=0.07). (**Fig 4.3-4.4 A**). In the female striatum, Wnt5a (p=0.07) and NFAT (p=0.06) protein levels showed a trend towards higher expression levels than male.

Co-receptor LRP6 protein level was significantly higher in female than male ($p<0.05$). GSK3β and β-catenin protein levels were also higher in female than male ($p<0.05$).

A statistically lower *Dvl1* mRNA level ($p<0.05$) was detected in female cortex, and a trend towards downregulations of *NFκB* ($p=0.07$), *Bdnf* ($p=0.09$) and *Creb* ($p=0.09$) compared to males. Phosphorylated LRP6 (pLRP6, at S1490), GSK3β and LEF1 had a significantly higher protein level ($p<0.05$) in female cortex. An increase in pLRP6 and LEF1 protein levels, should indicate an activation state of Wnt signalling pathways. However, active-β-catenin was significantly lower ($p<0.01$). The total β-catenin protein level showed a trend towards an increase in females ($p=0.06$) (**Fig 4.3-4.4 B**).

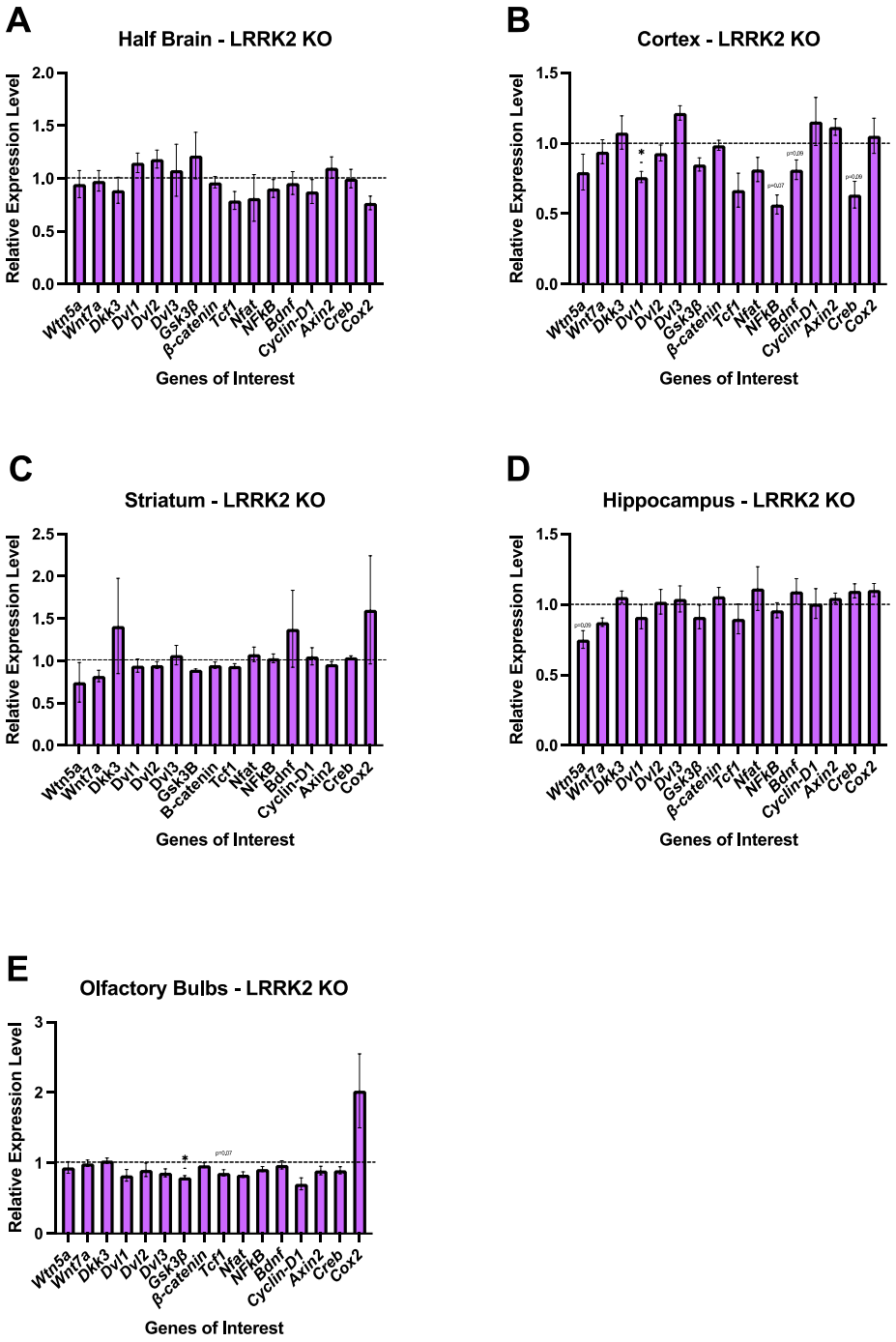


**Figure 4.3: LRRK2 KO female mRNA expression level against male**

Each of the genes of interest was compared to the corresponding male's value. Male was set as 1 and presented in a line.

**Wnt ligands:** *Wnt5a*, *Wnt7a*; **Antagonist**: *Dkk3*; **Cytoplasmic components**: *Dvl1-3*; **β-catenin destruction complex**: *Gsk3β*, *β-catenin*, *Axin2*; **Transcriptional factors**: *Nfat*, *Nfκb*, *Tc1*; **Downstream targets**: *Cyclin-d1*, *Bdnf*, *Creb*, *Cox2*.

Data presented as mean ± S.E.M., compared by unpaired t-test with Welch's correction for sex difference, $p<0.05$ = *, $p<0.01$ = **, $p<0.001$ = ***, $p<0.0001$ = ****; n=3 per sex.

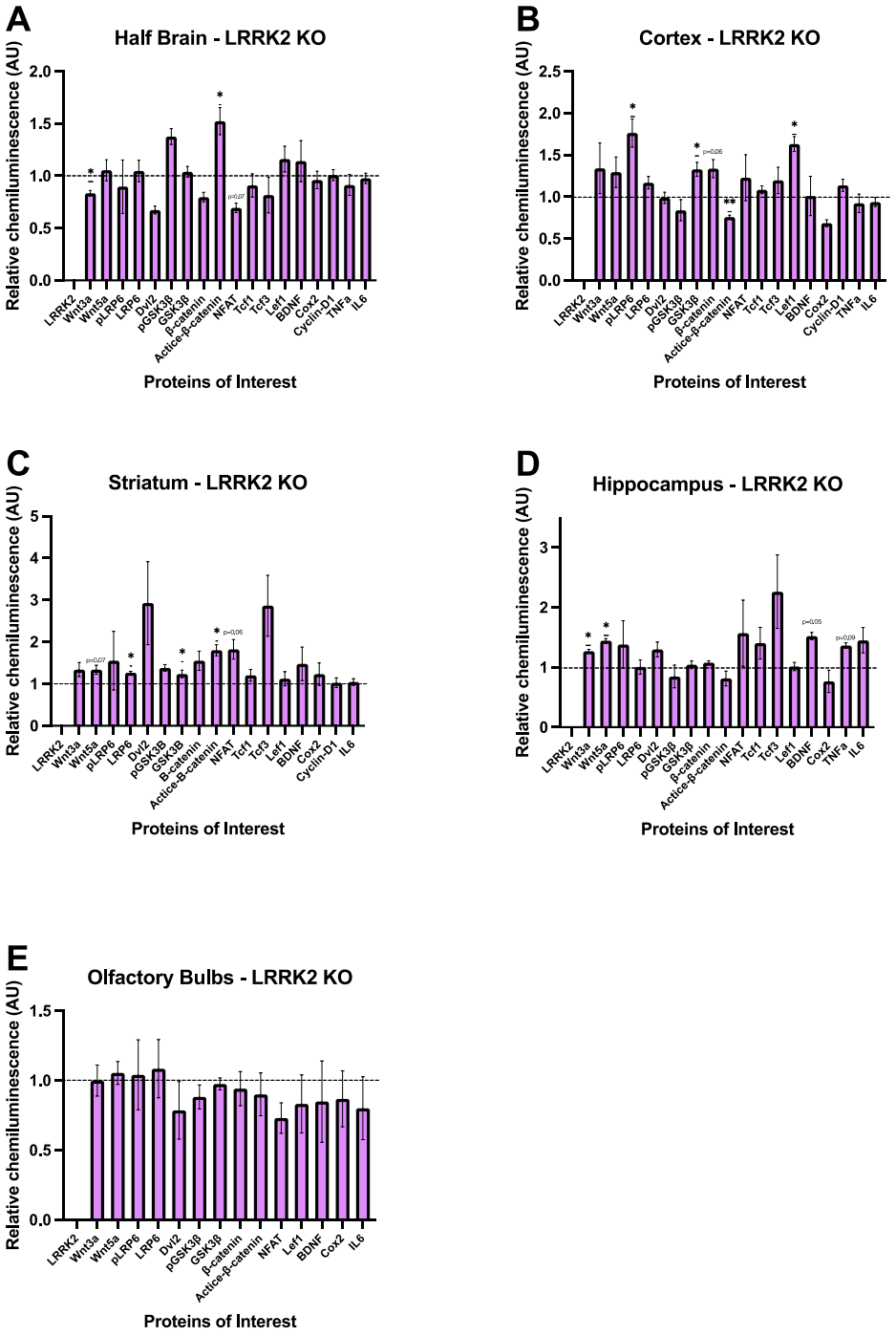


**Figure 4.4: LRRK KO female protein expression level against male**

Each of the proteins of interest was compared to the corresponding male's value. Male was set as 1 and presented in a line.

**Wnt ligands:** *Wnt5a*, *Wnt7a*; **Antagonist**: *Dkk3*; **Cytoplasmic components**: *Dvl1-3*; **β-catenin destruction complex**: *Gsk3β*, *β-catenin*, *Axin2*; **Transcriptional factors**: *Nfat*, *Nfκb*, *Tc1*; **Downstream targets**: *Cyclin-d1*, *Bdnf*, *Creb*, *Cox2*.

Data presented as mean ± S.E.M., compared by unpaired t-test with Welch's correction for sex difference, $p<0.05$ = *, $p<0.01$ = **, $p<0.001$ = ***, $p<0.0001$ = ****; n=3 per sex.

**Expression level in G2019S KI**

In the PD G2019S mice we observed more significant sex dependent mRNA and protein expression level changes than in LRRK2 WT and KO mice. Female hippocampus had a significant lower *Bdnf* ($p<0.01$) and *Cox2* ($p<0.01$) mRNA level than male. Surprisingly, these results were not reflected in β-destruction complex components *Gsk3β* ($p=0.08$), *β-catenin* ($p=0.09$), and *Axin2* ($p=0.07$) mRNA levels. These genes showed a tendency towards downregulations in mRNA levels in female compared to male. Interestingly, there was a higher canonical Wnt signalling pathway ligand Wnt3a protein level ($p=0.08$). TNFα on the other hand, showed less protein expression in females than males ($p=0.07$) (**Fig 4.5-4.6 D**).

Female olfactory bulbs showed a significantly lower *Gsk3β* mRNA level ($p<0.001$), which was reflected in the slight increase of *β-catenin* ($p=0.09$) and target gene *Bdnf* ($p=0.07$). pLRP6 protein level was higher in females ($p<0.05$) and a lower β-catenin ($p<0.05$) protein level was observed in female olfactory bulbs (**Fig 4.5-4.6 E**).

In half brain, only *Gsk3β* showed a male and female expression difference in mRNA level, females had a lower *Gsk3β* expression level ($p<0.05$) compared to males. Co-receptor LRP6 ($p=0.06$) and transcriptional factor TCF3 ($p<0.05$) had a lower protein expression in females than males. There was a significantly higher pGSK3β protein level ($p<0.05$) in female mice (**Fig 4.5-4.6 A**).

Female cortex had a lower mRNA level than male in most of the investigated genes. Female Wnt ligand *Wnt7a* ($p<0.05$); β-catenin destruction complex *Gsk3β* ($p<0.05$), *β-catenin* ($p<0.05$); target genes *Bdnf* ($p<0.05$) and *Cyclin-d1* ($p<0.01$) mRNA levels were significantly lower than in males. Regulator *Dvl2* ($p=0.06$) and transcriptional factor *Creb* ($p=0.07$) both showed a trend towards decrease in female mice, as well. However, the male and female differences were less in protein levels. Active-β-*catenin* ($p<0.01$) was significantly lower in females than males, inflammatory cytokines TNFα ($p<0.05$) was also lower in female, whereas IL-6 was significantly higher in female mice ($P<0.05$) (**Fig 4.5-4.6 B**).

*Dvl2* ($p<0.05$), *Gsk3β* ($p<0.01$) and *Axin2* ($p<0.05$) mRNA levels were significantly lower in the female striatum than male. Non-canonical ligand *Wnt5a* ($p=0.06$) also showed a trend towards decreased in female striatum. When we investigated protein levels, LRP6 ($p<0.01$), Dvl2 ($p<0.001$), β-catenin ($p<0.001$), NFAT ($p<0.05$) and Tcf1($p<0.01$) were significantly higher in female striatum then male. Wnt5a ($p=0.09$), BDNF ($p=0.07$) and IL-6 ($p=0.09$) also showed a trend towards a slightly higher protein expression level in female (**Fig 4.5-4.6 C**).

**Overview**

We have established the mRNA and protein expression differences in different brain regions. The effect of sex had an apparent effect on both mRNA and protein expression levels, and it also differed in different genotypes. The significant mRNA expression level sex differences were most pronounced in G2019S mice in comparison to KO and WT mice with 12 significant changes in the G2019S in

comparison to WT with 7 and KO mice with 2 significant sex dependent changes. On protein level we observed only 1 significant sex dependent change in WT mice in comparison to 11 in KO mice and 12 in KI mice. Most sex differences in WT mice were observed on mRNA level in the striatum, whereas most sex differences in LRRK2 KO mice were observed on protein level in the cortex and striatum. In the G2019S mice most sex differences were observed in mRNA and protein level in the cortex and striatum. Therefore, in all genotypes the sex differences are most significant in the cortex and striatum. The genes of interest most affected overall by sex differences in these two brain regions were GSK3β, Lrp6 and β-catenin.

In the next section, we investigated Wnt signalling mediators mRNA and protein expression differences in G2019S KI and LRRK2 KO compared to WT. Male and female data were compared separately. We also combined both sex groups for analysis to increase the n number.

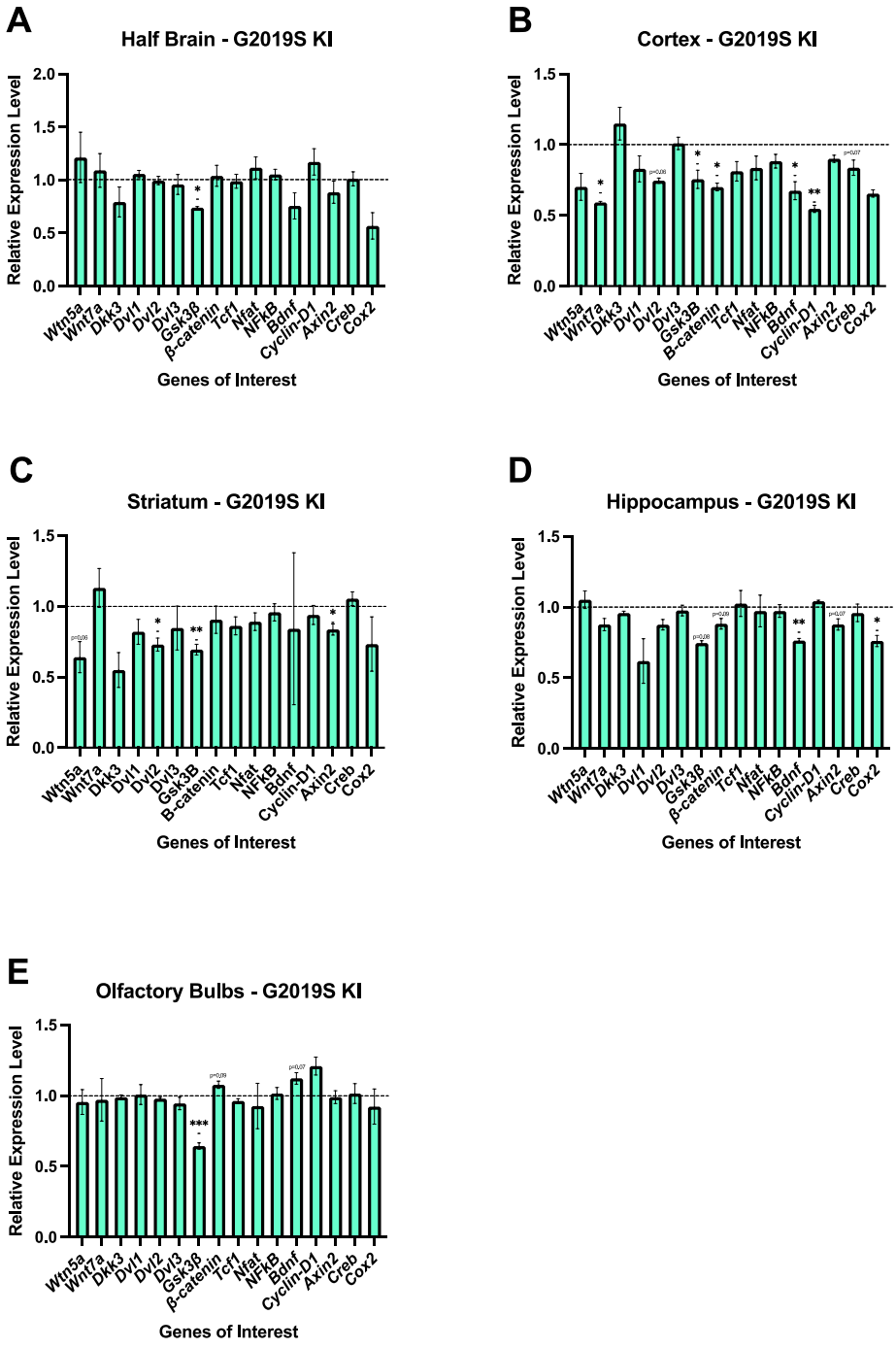


**Figure 4.5: G2019S KI female mRNA expression level against male**

Each of the genes of interest was compared to the corresponding male's value. Male was set as 1 and presented in a line.

**Wnt ligands:** *Wnt5a*, *Wnt7a*; **Antagonist**: *Dkk3*; **Cytoplasmic components**: *Dvl1-3*; **β-catenin destruction complex**: *Gsk3β*, *β-catenin*, *Axin2*; **Transcriptional factors**: *Nfat*, *Nfκb*, *Tc1*; **Downstream targets**: *Cyclin-d1*, *Bdnf*, *Creb*, *Cox2*.

Data presented as mean ± S.E.M., compared by unpaired t-test with Welch's correction for sex difference, $p<0.05$ = *, $p<0.01$ = **, $p<0.001$ = ***, $p<0.0001$ = ****; n=3 per sex.

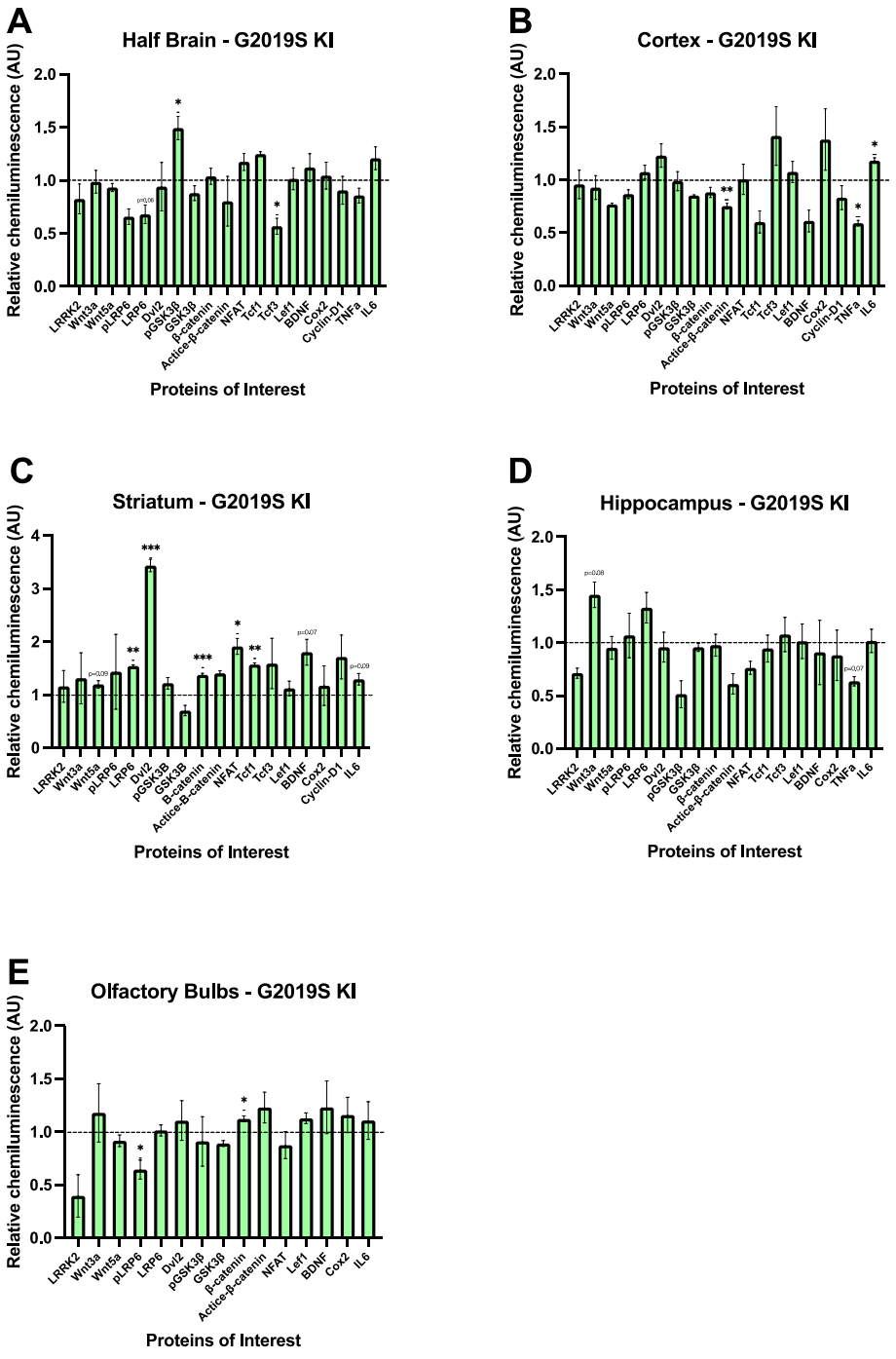


**Figure 4.6: G2019S KI female protein expression level against male**

Each of the proteins of interest was compared to the corresponding male's value. Male was set as 1 and presented in a line.

**Wnt ligands:** *Wnt5a*, *Wnt7a*; **Antagonist**: *Dkk3*; **Cytoplasmic components**: *Dvl1-3*; **β-catenin destruction complex**: *Gsk3β*, *β-catenin*, *Axin2*; **Transcriptional factors**: *Nfat*, *Nfκb*, *Tc1*; **Downstream targets**: *Cyclin-d1*, *Bdnf*, *Creb*, *Cox2*.

Data presented as mean ± S.E.M., compared by unpaired t-test with Welch's correction for sex difference, $p<0.05$ = *, $p<0.01$ = **, $p<0.001$ = ***, $p<0.0001$ = ****; n=3 per sex.

### 4.2.2 mRNA and protein expression level differences in half brain

We first compared Wnt ligand mRNA and protein expression differences in LRRK2 KO and G2019S KI to WT mouse half brain. In combined sex analysis, the non-canonical Wnt signalling pathway ligand *Wnt5a* mRNA level was significantly lower in LRRK2 KO ($p<0.05$) and showed a trend towards decrease in G2019S KI ($p=0.06$) compared to WT. G2019S KI had a higher canonical Wnt ligand *Wnt7a* mRNA level when compared to LRRK2 KO and WT ($p<0.05$). An increase in *Wnt7a* mRNA level between G2019S KI and LRRK2 KO was also observed in the male study group ($p<0.05$) (**Fig 4.7 A-C**). In line with observed mRNA changes in LRRK2 KO, Wnt5a ($p=0.07$) protein level showed a trend towards decrease when compared to WT in the combined sex group (**Fig 4.8C**). However, in the G2019S half brain the Wnt5a ligand ($p<0.01$) protein level showed a significant decrease in comparison to WT (**Fig 4.8D**). When we separated the sex groups, male LRRK2 KO mice showed more protein level differences in comparison to WT than the female mice. Wnt3a ($p<0.05$) and Wnt5a ($p<0.05$) had a significantly lower protein expression level in male LRRK2 KO than WT mice (**Fig 4.8 E)**

Co-receptor LRP6 protein level showed a trend towards increased ($p=0.08$) in the G2019S KI combined sex group (**Fig 4.8 D**), and higher expression level in male G2019S KI ($p<0.05$) (**Fig 4.8 F**). pLRP6 (S1490) and pLRP6 in relation to total LRP6

protein levels were significantly lower in G2019S combined sex group ($p<0.001$) and male study group ($p<0.05$), similar results were observed in female study group, pLRP6 ($p<0.01$) and pLRP6 in relation total LRP6 ($p<0.05$) (**Fig 4.8 D, F, H).**

Wnt signalling enhancer *Dvl2* mRNA level was higher in LRRK2 KO than WT ($p<0.05$) and G2019S KI ($p=0.06$). Both *Dvl1* ($p<0.05$) and *Dvl2* ($p=0.05$) mRNA levels were also higher in female LRRK2 KO when compared to WT (**Fig 4.7 A-C**).

*Gsk3β* mRNA level was lower in LRRK2 KO than WT ($p<0.01$) and G2019S KI ($p<0.01$). A similar observation was made in the female study group. LRRK2 KO had a lower *Gsk3β* ($p<0.05$) mRNA level than WT. *Gsk3β* was significantly lower than both male WT ($p<0.05$) and G2019S KI ($p<0.01$), and the mRNA level in G2019S KI was higher than WT ($p<0.05$) **(Fig 4.7 A-C**). pGSK3β ($p=0.09$) protein level trended to decrease in LRRK KO when compared to WT in the combined sex group (**Fig 4.8 C**). pGSK3β ($p<0.05$) protein level was significantly lower in male G2019S KI than in WT (**Fig 4.8 F**). The other β-catenin destruction complex components, *β-catenin* ($p<0.05$) *and Axin2* ($p<0.05$) mRNA levels were lower in LRRK2 KO when compared to WT in the combined sex study group (**Fig 4.7 A**). There were no expression differences when we separated the sex groups.

Transcriptional factor *Tcf1* ($p=0.05$) mRNA expression was slightly lower in female LRRK2 KO than WT **(Fig 4.7 C**). LRRK2 KO Tcf1 protein level ($p=0.06$) showed a

trend towards decrease when compared to WT in the combined sex group (**Fig 4.8 C**). Tcf1 protein level (p=0.07) was slightly higher in female LRRK2 KO when compared to WT (**Fig 4.8 G**). Tcf1 protein level was higher in combined sex group (p<0.05) with a higher significance in female but no change observed in male in G2019S KI mice (p<0.001) (**Fig 4.8 D, H**), whereas male G2019S KI showed higher (p<0.05) Tcf3 protein expression than WT (**Fig 4.8 F**). Another transcriptional factor component LEF1 (p<0.05) had a lower protein expression level in male LRRK2 KO when compared to WT (**Fig 4.8 E**). The signalling transcriptional factor *NFκB* showed a trend towards a lower mRNA expression level in LRRK2 KO than G2019S KI (p=0.07) **(Fig 4.7 A**). In female LRRK2 KO, NFAT (p<0.05) protein level was significantly lower compared to WT (**Fig 4.8 G**).

The downstream targets *Cyclin-D1* (p<0.05) mRNA expression was higher in male LRRK2 KO than in WT **(Fig 4.7 B**). LRRK2 KO Cyclin-D1 (p=0.07) showed a trend towards decrease when compared to WT in the combined sex group. The target protein BDNF (p<0.05) were slightly higher in LRRK2 KO than WT (**Fig 4.8 C**), whereas BDNF protein level was higher (p<0.05) in male LRRK2 KO. Cyclin-D1 (p<0.01) protein level was significantly lower in G2019S KI combined sex group (**Fig 4.8 D**), and the protein level (p<0.05) was also significantly lower in G2019S male mice while it showed a trend towards decrease in females (p=0.08) (**Fig 4.8 F, H**). BDNF (p<0.001) protein level was significantly lower in G2019S KI combined sex group (**Fig 4.8 D**), and the protein levels (p<0.05) were also lower in G2019S male and in female mice (**Fig 4.8 F, H**). G2019S mice had a higher inflammatory cytokine Cox2 (p<0.01)

protein level compared to WT. IL-6 protein level on the other hand, was lower in G2019S KI combined data ($p<0.05$) (**Fig 4.8 D**), as well as in male study group ($p=0.09$) (**Fig 4.8 F**).

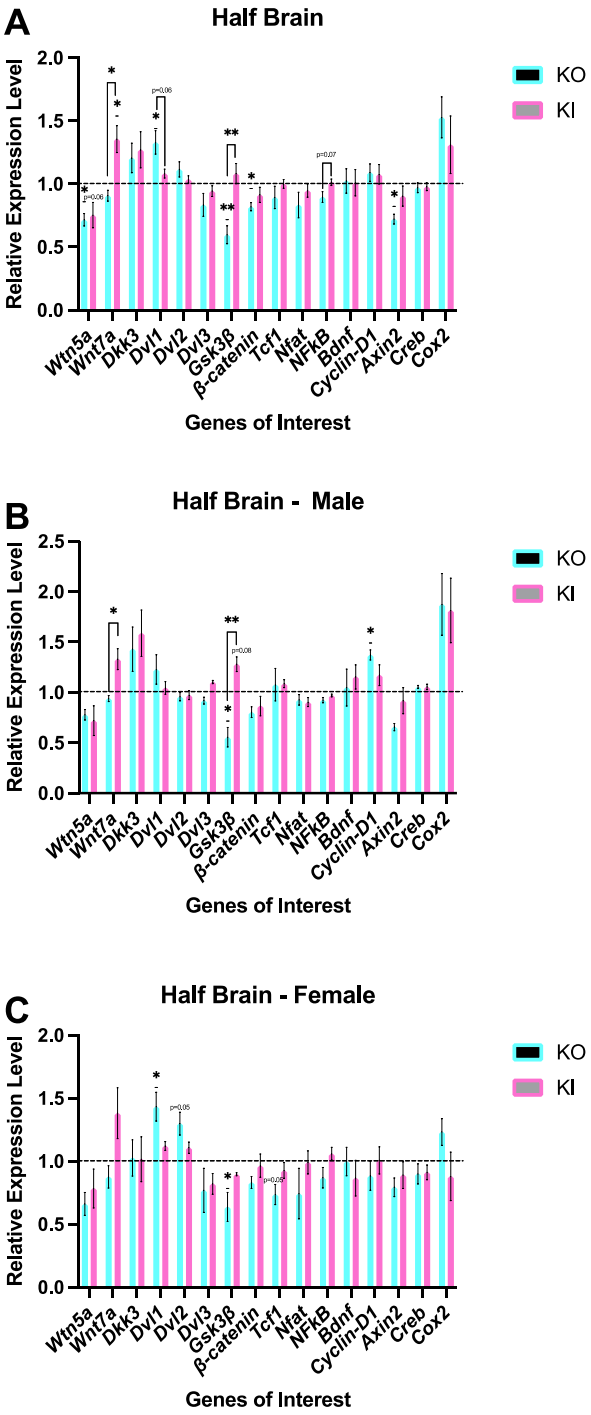


**Figure 4.7: mRNA expression level analysis against wild type in half brain**

Each of the genes of interest was compared to the corresponding WT's value. WT was set as 1 and presented in a line.

**Wnt ligands:** *Wnt5a*, *Wnt7a*; **Antagonist**: *Dkk3*; **Cytoplasmic components**: *Dvl1-3*; **β-catenin destruction complex**: *Gsk3β*, *β-catenin*, *Axin2*; **Transcriptional factors**: *Nfat*, *Nfκb*, *Tc1*; **Downstream targets**: *Cyclin-d1*, *Bdnf*, *Creb*, *Cox2*.

Data presented as mean ± S.E.M., compared by ONE-WAY ANOVA followed by Tukey's post hoc test, $p<0.05$ = *, $p<0.01$ = **, $p<0.001$ = ***, $p<0.0001$ = ****; n=3 per sex per genotype.

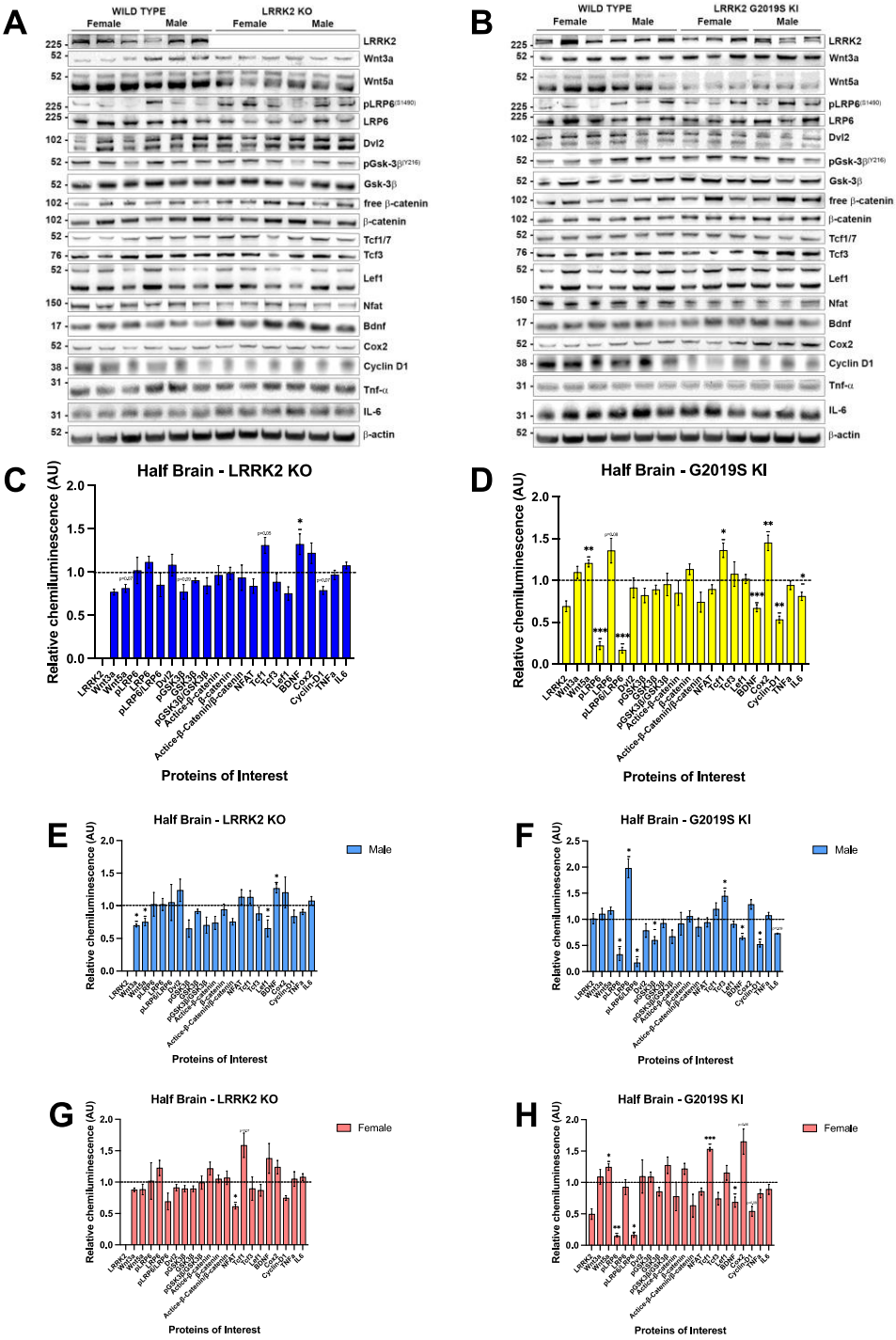


**Figure 4.8: Protein expression level analysis against wild type in half brain**

Each of the proteins of interest was compared to the corresponding WT's value. WT was set as 1 and presented in a line.

**Genotype:** LRRK2; **Wnt ligands:** Wnt3a, Wnt5a; **Co-receptors**: pLRP6, LRP6; **Cytoplasmic components**: Dvl2; **β-catenin destruction complex**: pGsk3β, Gsk3β,

β-catenin, active-β-catenin; **Transcriptional factors**: NFAT, NFκB, Tc1, Tcf3, Lef1; **Downstream targets**: Cyclin-D1, BDNF, Cox2, TNFα, IL-6.

Data presented as mean ± S.E.M., compared by unpaired t-test with Welch's correction, $p<0.05$ = *, $p<0.01$ = **, $p<0.001$ = ***, $p<0.0001$ = ****; n=3 per sex per genotype.

### 4.2.3 mRNA and protein expression level differences in cortex

Fewer expression differences were observed in cortex combined sex analysis. NFAT signalling ligand *Wnt5a* mRNA level was lower in LRRK2 KO ($p<0.05$), and the expression was also lower in the female LRRK2 KO group ($p<0.05$) when compared to WT (**Fig 4.9 A, C**). Canonical Wnt ligand Wnt3a protein level was significantly lower in LRRK2 KO than WT in mixed gender analysis as well as in the male study group ($p<0.05$) (**Fig 4.10 C, E**). Wnt3a ($p<0.05$) protein level was higher in G2019S KI when compared to WT in mixed gender analysis (**Fig 4.10 D**). In G2019S KI female group, Wnt3a was slightly higher ($p=0.09$) than WT, and NFAT signalling ligand Wnt5a ($p<0.01$) was significantly lower than WT (**Fig 4.10 H**).

LRRK2 KO phosphorylated co-receptor LRP6 (S1490) ($p<0.05$) and pLRP6 in relation to LRP6 ($p<0.05$) protein level was also lower in LRRK2 KO mixed gender group when compared to WT (**Fig 4.10 C, E, G**). Total LRP6 protein level was significantly lower in G2019S KI mixed gender group ($p<0.05$), male group ($p<0.05$) and female group ($p<0.01$) when compared to WT. pLRP6 (S1490) protein level was also significantly lower ($p<0.01$) in G2019S KI than WT in the female group. As a result, the pLRP6 (S1490) in relation to total LRP6 protein level was significantly higher in the G2019S mixed gender ($p<0.05$) as well as female study group ($p<0.01$) (**Fig 4.10 D, F, H**).

Male LRRK2 KO *Dvl1* mRNA level was significantly higher than WT ($p<0.01$) (**Fig 4.9 B**). Female LRRK2 KO *Dvl2* mRNA level was slightly higher than G2019S ($p=0.08$),

and *Dvl3* mRNA level was also higher ($p<0.05$) in LRRK2 KO when compared to WT. Male G2019S KI had a higher *β-catenin* mRNA level ($p<0.01$) than LRRK2 KO (**Fig 4.9 B)**. LRRK2 KO active-β-catenin protein level ($p=0.08$) was slightly higher than WT in mixed gender analysis (**Fig 4.10 C**). The protein level of active-β-catenin level in relation to total β-catenin ($p=0.08$) was higher in LRRK2 KO male group when compared to WT (**Fig 4.10 E**). LRRK2 KO females had a significantly higher total β-catenin ($p<0.05$) protein level when compared to WT (**Fig 4.10 G**).

In the male LRRK2 KO study group, protein levels of phosphorylated GSK-3β (Y216) ($p=0.09$) were slightly higher, total GSK-3β protein level ($p<0.05$) was significantly lower, which made the pGSK-3β (Y216) in relation to total GSK3β protein level ($p<0.05$) also higher when compared to WT. The protein expression level profile was different in LRRK2 KO female, pGSK3β (Y216) protein level ($p=0.06$) was lower than WT; total GSK3β ($p<0.05$) was significantly higher compared to WT (**Fig 4.10 G**). G2019S KI pGSK3β (Y216) protein level was significantly lower in G2019S KI mixed gender ($p<0.001$), also slightly lower in male ($p=0.05$) and female ($p<0.05$) G2019S KI groups when compared to WT. pGSK3β (Y216) in relation to total GSK3β protein level ($p=0.06$) also showed a tendency towards a decrease in G2019S KI mixed gender group (**Fig 4.10 D, F, H**).

Transcriptional factors *Tcf1* mRNA level ($p=0.05$) trended to increase in male LRRK2 KO than in WT (**Fig 4.9 B**). When compared to WT, the transcriptional factor, LEF1 protein level ($p<0.05$) was lower in G2019S KI mixed gender samples, whereas the

protein level was slightly higher (p=0.07) in female G2019S KI group (**Fig 4.10 F, H**). NFAT signalling pathways transcriptional factor NFAT protein level was lower in LRRK2 KO mixed gender (p=0.06), male (p<0.05) when compared to WT, but not in the female study group (**Fig 4.10 C, E, G**).

Downstream target *Bdnf* was lower in both LRRK2 KO (p<0.05) and G2019S KI (p<0.05) when compared to WT (**Fig 4.9 A**). LRRK2 KO BDNF protein level (p=0.05) showed a tendency towards increase compared to WT in mixed gender analysis. BDNF protein level was also higher in male LRRK2 KO than in WT (p<0.05) (**Fig 4.10 C, E**). Male G2019S KI *Cyclin-D1* mRNA level was significantly higher than both LRRK2 KO (p<0.01) and WT (p<0.01). The protein level of Cyclin-D1 (p=0.05) trended to increase in LRRK2 KO compared to WT in mixed gender analysis (**Fig 4.10 C**). *Cox2* (p=0.07) mRNA level in male LRRK2 KO was slightly lower than WT (**Fig 4.9 B**).

Other downstream targets, such as IL-6 protein level, were significantly lower (p<0.01) in LRRK2 KO mixed gender group, as well as in the male study group (p<0.05) and slightly lower expression level in the female study group (p=0.07) (**Fig 4.10 C, E, G**). IL-6 was significantly lower in G2019S KI in both mixed gender (p<0.001), male (p<0.01) and female (p<0.05) when compared to WT (**Fig 4.10 H**). In addition, the TNF$\alpha$ protein level (p<0.001) was also lower than WT in the female G0219S KI group (**Fig 4.10 H**).

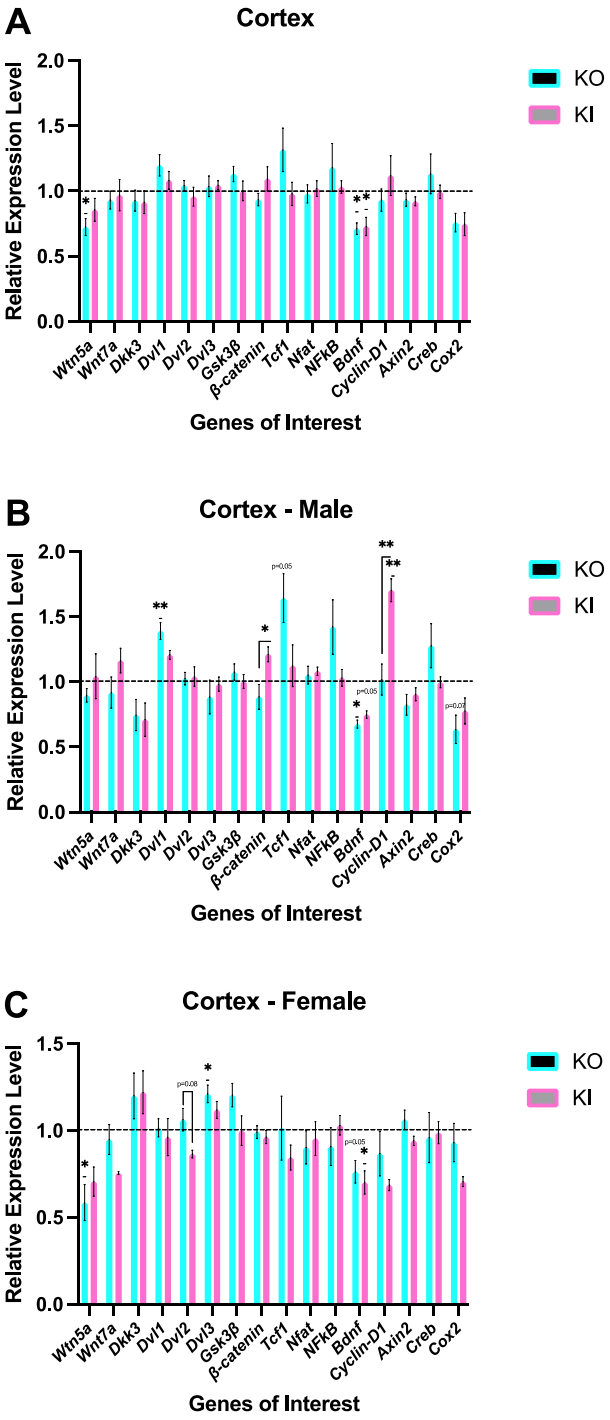


**Figure 4.9: mRNA expression level analysis against wild type in cortex**

Each of the gene of interest was compared to the corresponding WT's value. WT was set as 1 and presented in a line.

**Wnt ligands:** *Wnt5a*, *Wnt7a*; **Antagonist**: *Dkk3*; **Cytoplasmic components**: *Dvl1-3*; **β-catenin destruction complex**: *Gsk3β*, *β-catenin*, *Axin2*; **Transcriptional factors**: *Nfat*, *Nfκb*, *Tc1*; **Downstream targets**: *Cyclin-d1*, *Bdnf*, *Creb*, *Cox2*.

Data presented as mean ± S.E.M., compared by ONE-WAY ANOVA followed by Tukey's post hoc test, $p<0.05$ = *, $p<0.01$ = **, $p<0.001$ = ***, $p<0.0001$ = ****; n=3 per sex per genotype.

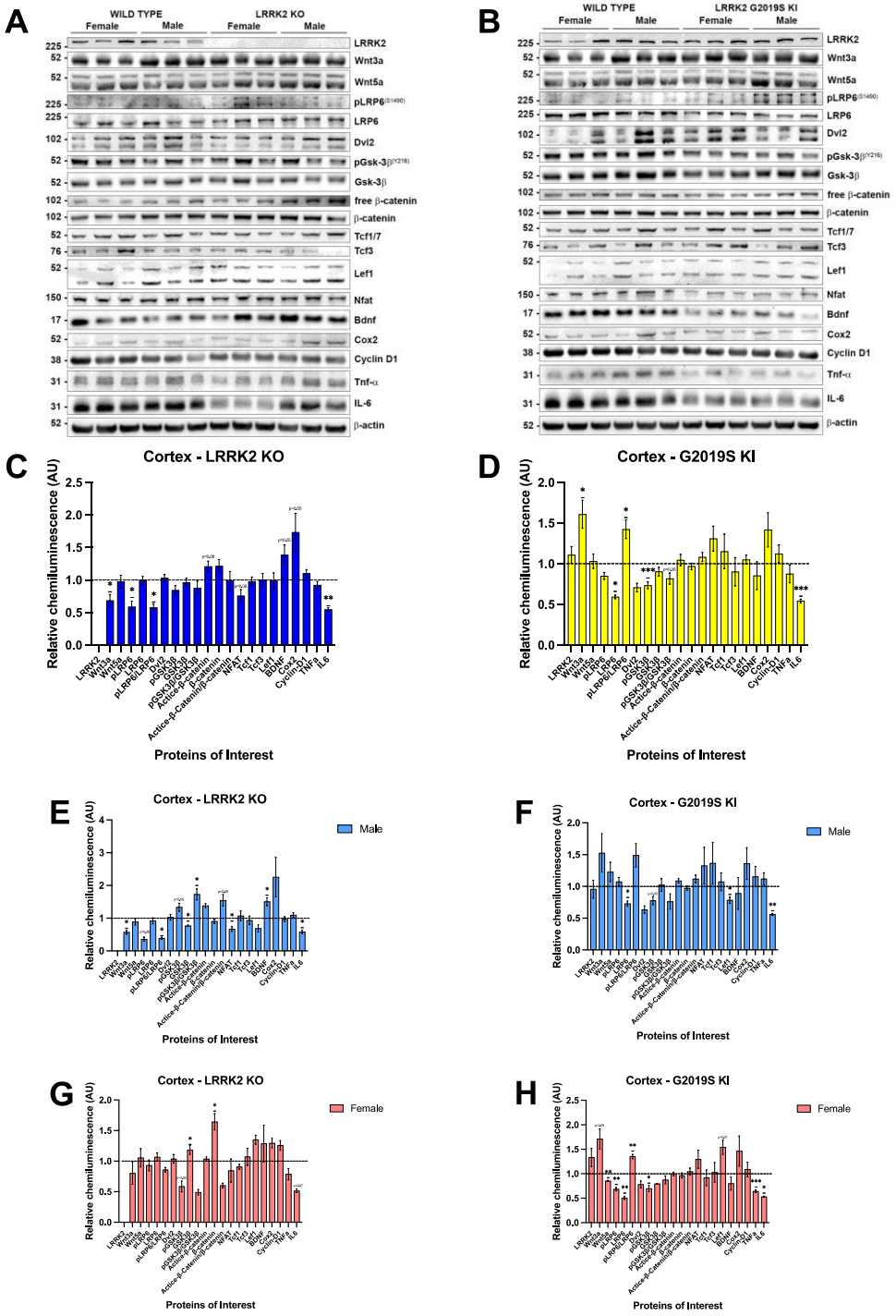


**Figure 4.10: Protein expression level analysis against wild type in cortex**

Each of the gene of interest was compared to the corresponding WT's value. WT was set as 1 and presented in a line.

**Genotype:** LRRK2; **Wnt ligands:** Wnt3a, Wnt5a; **Co-receptors**: pLRP6, LRP6; **Cytoplasmic components**: Dvl2; **β-catenin destruction complex**: pGsk3β, Gsk3β,

β-catenin, active-β-catenin; **Transcriptional factors**: NFAT, NFκB, Tc1, Tcf3, Lef1; **Downstream targets**: Cyclin-D1, BDNF, Cox2, TNFα, IL-6.

Data presented as mean ± S.E.M., compared by unpaired t-test with Welch's correction, $p<0.05$ = *, $p<0.01$ = **, $p<0.001$ = ***, $p<0.0001$ = ****; n=3 per sex per genotype.

### 4.2.4 mRNA and protein expression level differences in striatum

In the striatum, NFAT signalling pathway ligand *Wnt5a* gene expression level (p=0.07) was slightly higher in LRRK2 KO than in WT. The effect was more significant when we analysed the data by gender, *Wnt5a* mRNA level was significantly higher in male LRRK2 KO (p<0.05) and slightly higher in male G2019S KI (p=0.08) than WT (**Fig 4.11 A-B**). When we investigated the protein expression levels, Wnt5a (p<0.05) was significantly lower in LRRK2 KO compared to WT in the mixed gender group. Similar results were observed in male LRRK2 KO, Wnt5a (p<0.05) protein level was lower than WT (**Fig 4.12 C, F**). Canonical Wnt ligand Wnt3a protein level (p=0.06) was slightly higher in G2019S KI compared to WT in mixed gender analysis. NFAT signalling pathway ligand Wnt5a protein level (p=0.08), on the other hand, was slightly lower in G2019S KI when compared to WT in mixed gender group (**Fig 4.12 D**)

Co-receptor LRP6 protein level was significantly lower in G2019S KI when compared to WT in mixed gender analysis (p<0.01), and in female cohort (p<0.001), there was also a trend towards a decrease in male cohort (p=0.07) (**Fig 4.12 D, F, H**). Wnt regulator *Dvl2* mRNA level was higher (p<0.05) in male G2019S KI than WT. Dvl2 (p<0.05) protein level was significantly lower in LRRK2 KO compared to WT in mixed gender analysis. Similar results were observed in male LRRK2 KO, Dvl2 (p<0.05) protein levels were lower than WT (**Fig 4.12 C, F**). Dvl2 protein level was slightly lower

in G2019S KI than WT in the mixed gender group (p=0.06) and was significantly lower in male G2019S KI (p<0.01) (**Fig 4.12 D, F**).

Male G2019S KO had a slightly higher *Gsk3β* (p=0.09) than WT; on the other hand, it was significantly lower (p<0.05) in G2019S KI than WT in female, which again demonstrated a clear sex difference (**Fig 4.11 B-C**). When looking at GSK3β protein level in the mixed gender analysis group, it was significantly higher (p<0.05) in G2019S KI compared to WT. GSK3β protein level trended to increase in male G2019S KI, (p=0.05) compared to WT. pGSK3β in relation to total GSK3β protein level, on the other hand, was significantly lower in G2019S KI (p<0.05) than WT in the mixed gender group. pGSK3β in relation to total GSK3β protein levels showed a tendency towards decreased in male G2019S KI (p=0.06) (**Fig 4.12 D, F**).

The *β-catenin* mRNA level trended to increase in both LRRK2 KO (p=0.05) and G2019S KI (p=0.08) than WT in mixed gender group, the similar expression level was observed in male LRRK2 KO (p=0.05) and G2019S KI (p<0.05). Active-β-catenin (p=0.05) and β-catenin (p<0.01) protein levels were detected in G2019S KI when compared to WT in mixed gender. The protein expression levels for active-β-catenin (p=0.05) and β-catenin (p=0.06) were similar in male G2019S KI when compared to WT (**Fig 4.12 D, F**). As part of the β-catenin destruction complex, as well as canonical pathway target gene Axin2 mRNA level, was higher in LRRK2 KO (p<0.05) and

G2019S KI (p=0.08) than WT in the mixed gender group. *Axin2* mRNA level was also significantly higher in male LRRK2 KO (p<0.05) and G2019S KI (p<0.01) than WT (**Fig 4.11 A-B**).

Transcriptional factor *Tcf1* mRNA level was higher in male LRRK2 KO (p<0.05) and G2019S KI (p<0.05) than in the WT (**Fig 4.11 B**). Transcriptional factor Lef1 protein level was significantly lower in LRRK2 KO than WT in mixed gender group (p<0.001), as well as in male (p<0.05) and female (p<0.05) cohorts (**Fig 4.12 C, E, G**). In female G2019S KI, canonical pathway transcriptional factor Tcf1 protein level (p<0.05) was significantly higher than WT. In contrast, LEF1 protein level was significantly lower in G2019S KI than WT in the mixed gender group (p<0.01) and male cohort (p<0.01) (**Fig 4.12 D, F, H**). Transcriptional factor *Nfat* mRNA level was higher in LRRK2 KO when compared to WT (p<0.05) and G2019S KI (p=0.06) in mixed gender analysis. However, it was only slightly higher (p=0.06) in the male LRRK2 KO when compared to WT and slightly higher (p=0.05) in female LRRK2 KO than G2019S KI (**Fig 4.11 A-C**). NFAT (p=0.07) protein levels were slightly lower in male LRRK2 KO than in WT (**Fig 4.12 E**). NFAT protein level was significantly lower in G2019S KI in mixed gender analysis group (p<0.01), male cohort (p<0.05) and tendency towards decreased in the female cohort (p=0.09) when compared to WT (**Fig 4.12 D, F, H**).

Downstream target gene *Cyclin-D1*, the mRNA expression level was higher in LRRK2 KO in the mixed gender group when compared to WT (p<0.05) and G2019S KI

(p=0.07), *Cyclin-D1* mRNA level, on the other hand, was lower (p=0.08) in female G2019S KI than WT (**Fig 4.11 A, C**). The Cyclin-D1 protein expression level was significantly lower in G2019S KI when compared to WT in the mixed gender group ($p<0.05$) and male cohort ($p<0.05$) (**Fig 4.12 D, F**). Other downstream targets, such as *Cox2* mRNA level, was significantly lower in male LRRK2 KO ($p<0.05$) than in WT (**Fig 4.11 B**). Cox2 (p=0.06) and IL-6 (p=0.06) showed a trend towards decreased in LRRK2 KO when compared to WT in the mixed gender group (**Fig 4.12 C**). Male LRRK2 KO had a slightly lower Cox2 protein level (p=0.09) than WT (**Fig 4.12 F, G**). Cox2 protein level was significantly lower in G2019S KI when compared to WT in the mixed gender group ($p<0.05$) and male cohort ($p<0.05$) (**Fig 4.12 D, F**). Female LRRK2 KO had a lower IL-6 protein level ($p<0.05$) than WT (**Fig 4.12 G**)

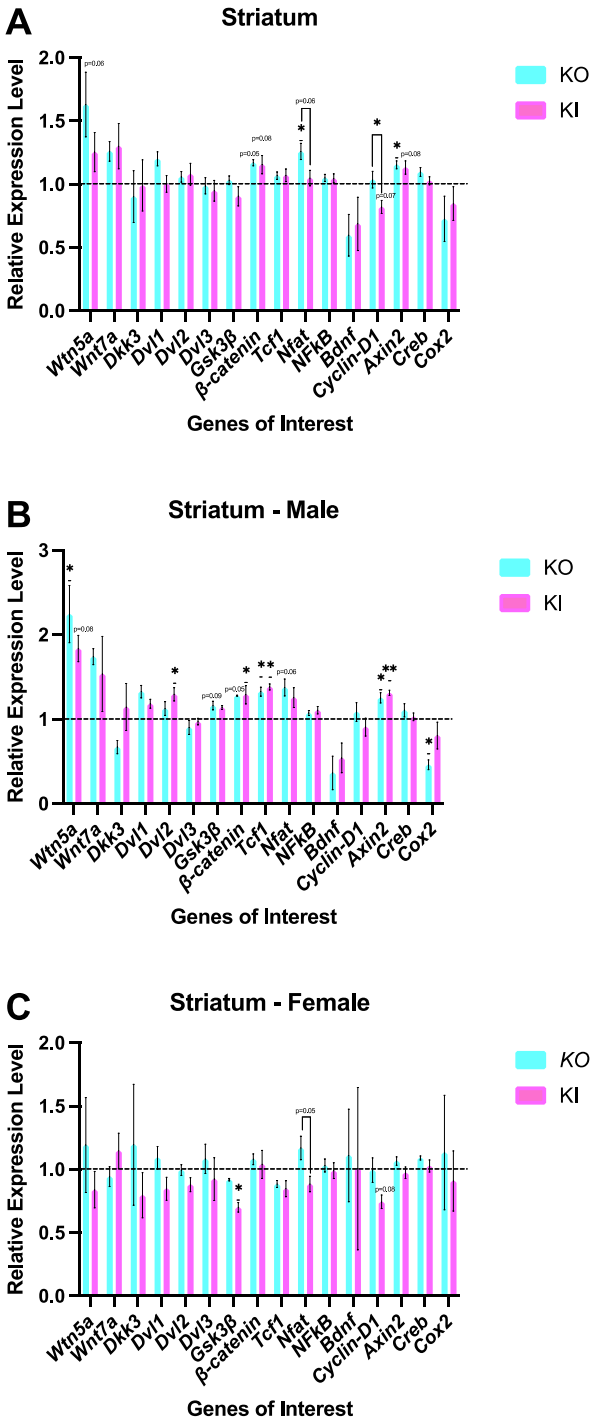


**Figure 4.11: mRNA expression level analysis against wild type in striatum**

Each of the gene of interest was compared to the corresponding WT's value. WT was set as 1 and presented in a line.

**Wnt ligands:** *Wnt5a*, *Wnt7a*; **Antagonist**: *Dkk3*; **Cytoplasmic components**: *Dvl1-3*; **β-catenin destruction complex**: *Gsk3β*, *β-catenin*, *Axin2*; **Transcriptional factors**: *Nfat*, *Nfκb*, *Tc1*; **Downstream targets**: *Cyclin-d1*, *Bdnf*, *Creb*, *Cox2*.

Data presented as mean ± S.E.M., compared by ONE-WAY ANOVA followed by Tukey's post hoc test, $p<0.05$ = *, $p<0.01$ = **, $p<0.001$ = ***, $p<0.0001$ = ****; n=3 per sex per genotype.

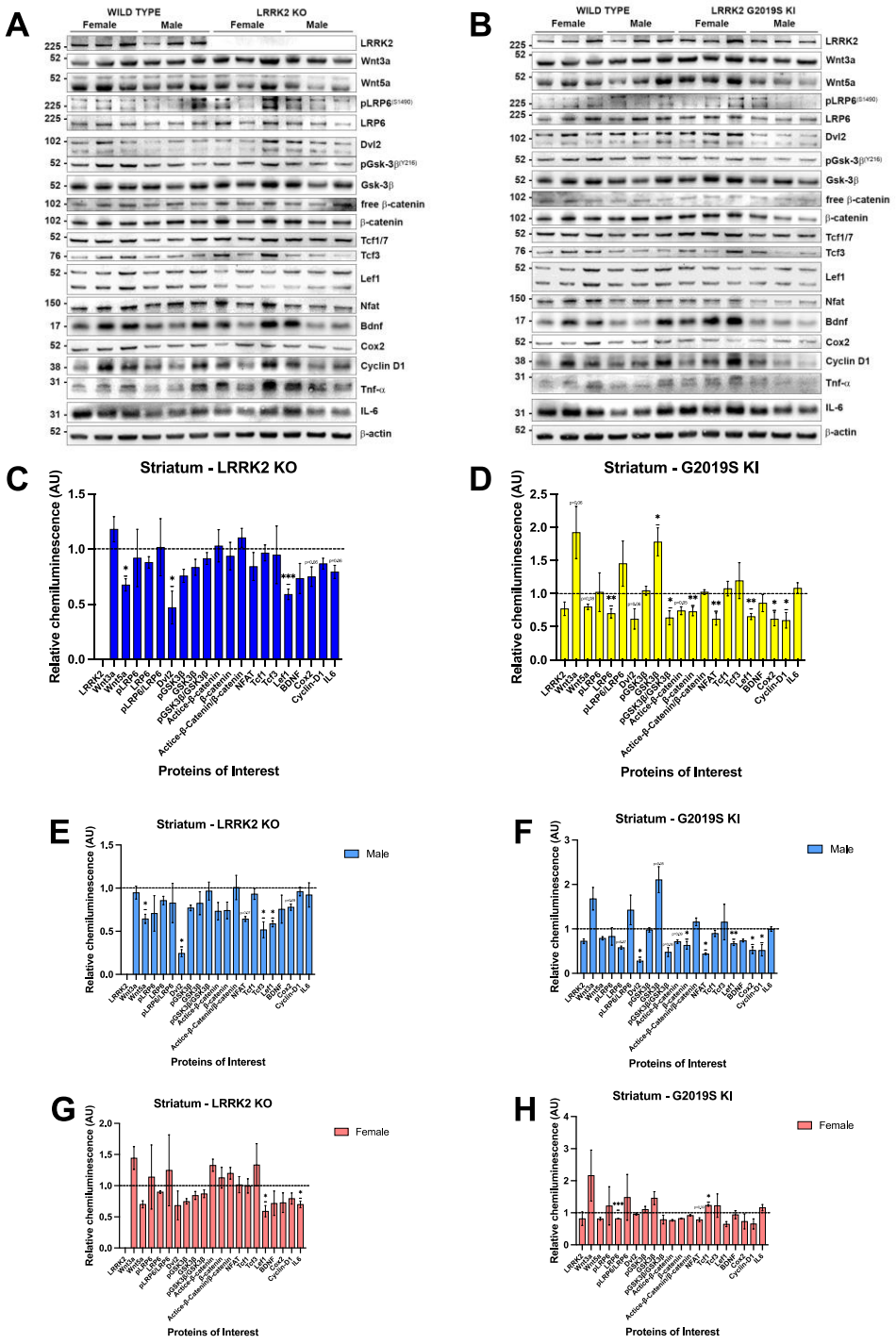


**Figure 4.12: Protein expression level analysis against wild type in striatum**

Each of the gene of interest was compared to the corresponding WT's value. WT was set as 1 and presented in a line.

**Genotype:** LRRK2; **Wnt ligands:** Wnt3a, Wnt5a; **Co-receptors**: pLRP6, LRP6; **Cytoplasmic components**: Dvl2; **β-catenin destruction complex**: pGsk3β, Gsk3β,

β-catenin, active-β-catenin; **Transcriptional factors**: NFAT, NFκB, Tc1, Tcf3, Lef1; **Downstream targets**: Cyclin-D1, BDNF, Cox2, IL-6.

Data presented as mean ± S.E.M., compared by unpaired t-test with Welch's correction, $p<0.05$ = *, $p<0.01$ = **, $p<0.001$ = ***, $p<0.0001$ = ****; n=3 per sex per genotype.

### 4.2.5 mRNA and protein expression level differences in hippocampus

Similar to what we have observed in our immunohistochemistry data, the hippocampus showed limited mRNA and protein expression differences between the genotypes. Only the Wnt antagonist *Dkk3* mRNA level showed a difference between the genotypes. It was lower in G2019S KI when compared to WT ($p<0.05$) and LRRK2 KO ($p<0.01$) in the mixed gender analysis group. In the female cohort, *Dkk3* mRNA level was higher in LRRK2 KO when compared to WT ($p<0.05$) and G2019S KI ($p<0.01$) (**Fig 4.13 A, C**).

When we compared G2019S KI to WT, LRRK2 protein level tended to be higher ($p=0.09$) in the mixed gender group (**Fig 4.14 D**). Wnt ligand Wnt3a showed a tendency to increase in female LRRK2 KO ($p=0.09$) when compared to WT (**Fig 4.14 G**). Co-receptor LRP6 protein level was slightly lower ($p=0.07$) in LRRK2 KO than in WT (**Fig 4.14 C**). The downregulation effect was more significant when we analysed male data alone, pLRP6 (S1490) ($p<0.05$) and LRP6 ($p<0.01$) protein levels were significantly lower in LRRK2 KO than WT (**Fig 4.14 C, E**). Co-receptor LRP6 protein was higher in male G2019S KI compared to WT (**Fig 4.14 F**).

Dvl2 protein level showed a trend towards decrease ($p=0.06$) in LRRK2 KO than WT in mixed gender analysis, and it was significantly lower ($p<0.05$) in male LRRK2 KO when compared to WT (**Fig 4.14 C, E**).

Active-β-catenin protein level tended to decrease (p=0.06) in LRRK2 KO compared to WT in the mixed gender analysis group. However, it was significantly lower (p<0.05) in female LRRK2 KO than WT. Total β-catenin protein level, on the other hand, was significantly higher in both mixed gender group LRRK2 KO (p<0.01) and female LRRK2 KO (p<0.01) when compared to WT. As a result, the active-β-catenin in relation to total β-catenin protein level was significantly lower in LRRK2 KO than WT in both mixed gender group (p<0.05) and female group (p<0.05) (**Fig 4.14 C, G**). β-catenin protein level (p<0.05) was significantly higher in G2019S KI when compared to WT in mixed gender analysis (**Fig 4.14 D**). Female G2019S KI showed a slightly lower active-β-catenin in relation to total β-catenin protein level (p=0.05) compared to WT (**Fig 4.14 H**).

The lower protein level of active-β-catenin indicated less Wnt signalling activity in LRRK2 KO hippocampus, which was reflected by the protein levels of transcriptional factors, Tcf1 protein level was significantly lower in LRRK2 KO than WT in the mixed gender group (p<0.01) and male cohort (p<0.05) (**Fig 4.14 C, E**). Tcf1 protein level was significantly lower (p<0.01) in G2019S KI when compared to WT in mixed gender analysis (**Fig 4.14 D**), as well as in female G2019S KI and WT comparison (p<0.05) (**Fig 4.14 H**).

In addition, NFAT protein level was also lower (p<0.05) in male LRRK2 KO than in WT. Interestingly, LEF1 protein level showed a trend towards increased (p=0.08) in

male LRRK2 KO compared to WT. Male LRRK2 KO also had a lower IL-6 protein level than WT (**Fig 4.14 C, E**).

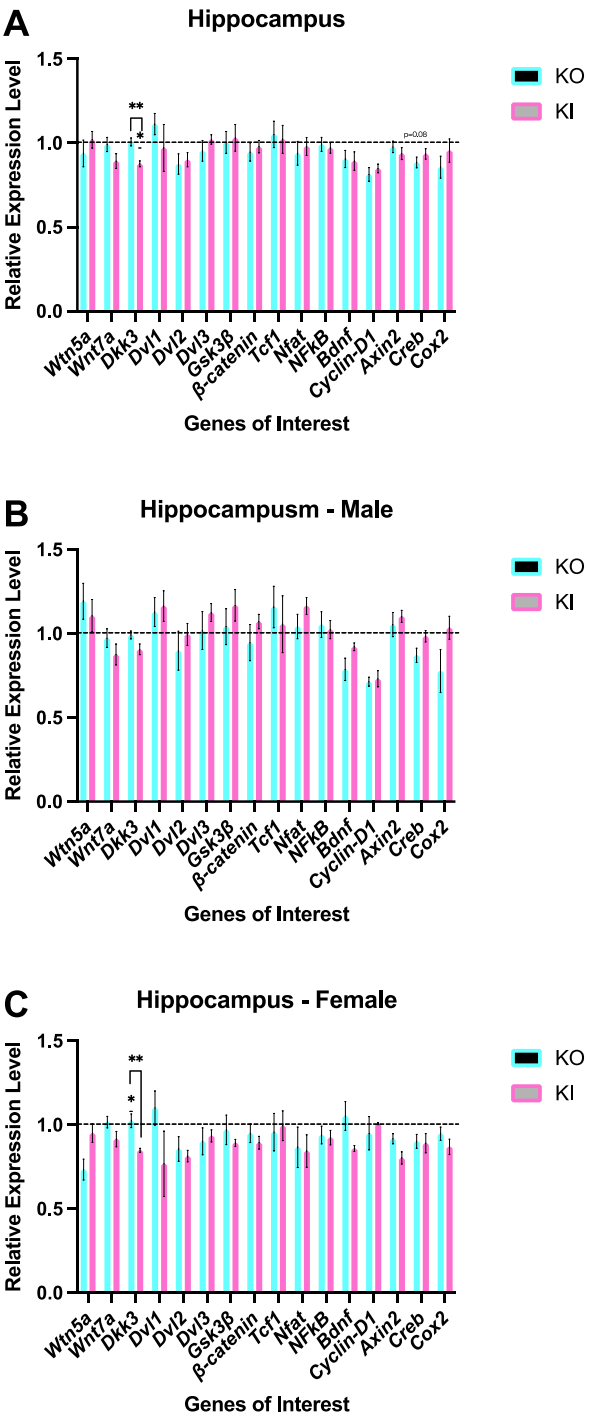


**Figure 4.13: mRNA expression level analysis against wild type in hippocampus**

Each of the gene of interest was compared to the corresponding WT's value. WT was set as 1 and presented in a line.

**Wnt ligands:** *Wnt5a*, *Wnt7a*; **Antagonist**: *Dkk3*; **Cytoplasmic components**: *Dvl1-3*; **β-catenin destruction complex**: *Gsk3β*, *β-catenin*, *Axin2*; **Transcriptional factors**: *Nfat*, *Nfκb*, *Tc1*; **Downstream targets**: *Cyclin-d1*, *Bdnf*, *Creb*, *Cox2*.

Data presented as mean ± S.E.M., compared by ONE-WAY ANAOVA followed by Tukey's post hoc test, $p<0.05$ = *, $p<0.01$ = **, $p<0.001$ = ***, $p<0.0001$ = ****; n=3 per sex per genotype.

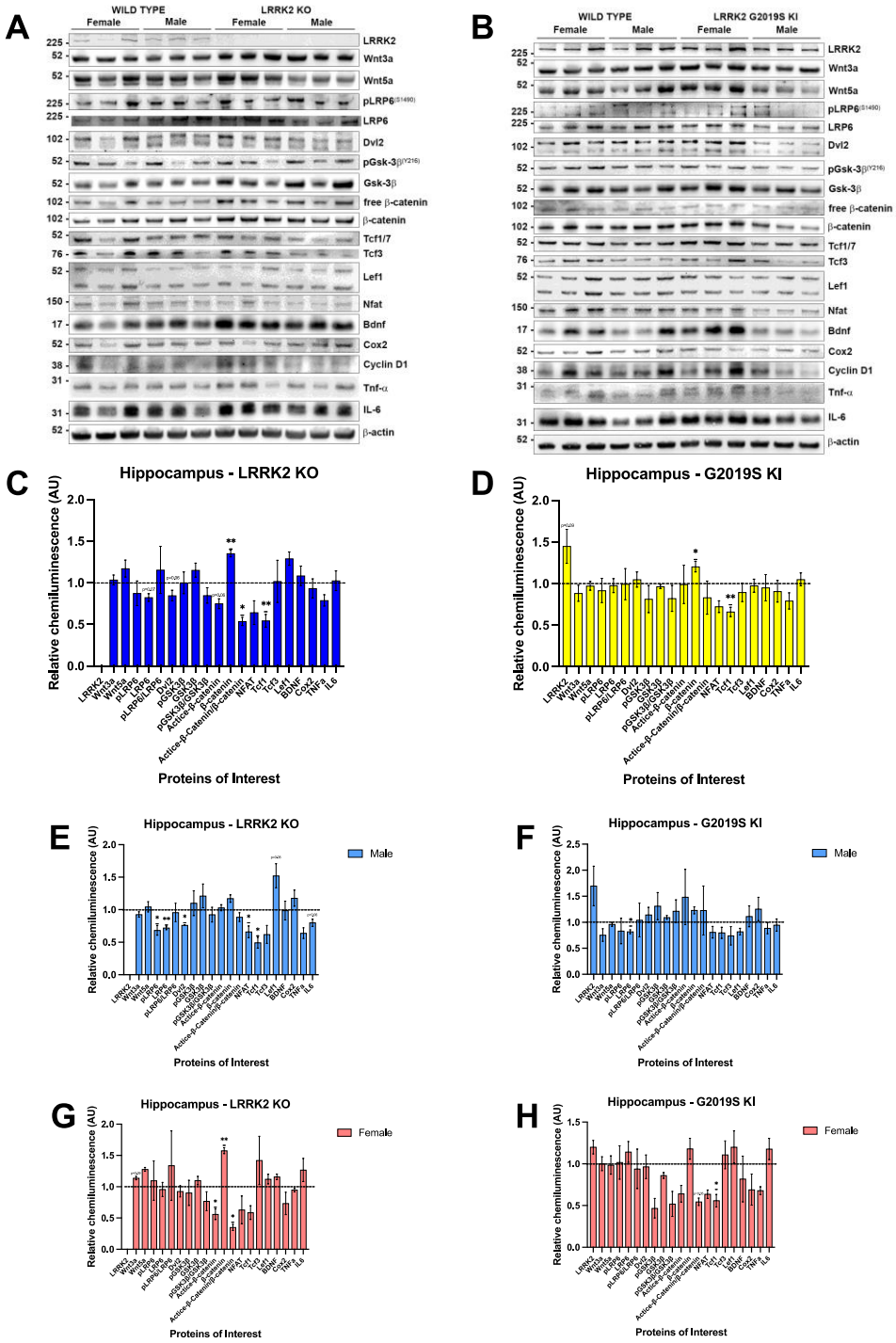


**Figure 4.14: Protein expression level analysis against wild type in hippocampus**

Each of the gene of interest was compared to the corresponding WT's value. WT was set as 1 and presented in a line.

**Genotype:** LRRK2; **Wnt ligands:** Wnt3a, Wnt5a; **Co-receptors**: pLRP6, LRP6; **Cytoplasmic components**: Dvl2; **β-catenin destruction complex**: pGsk3β, Gsk3β,

β-catenin, active-β-catenin; **Transcriptional factors**: NFAT, NFκB, Tc1, Tcf3, Lef1; **Downstream targets**: BDNF, Cox2, TNFα, IL-6.

Data presented as mean ± S.E.M., compared by unpaired t-test with Welch's correction, $p<0.05$ = *, $p<0.01$ = **, $p<0.001$ = ***, $p<0.0001$ = ****; n=3 per sex per genotype.

### 4.2.6 mRNA and protein expression level differences in olfactory bulbs

Unlike what we have observed in previous chapter, olfactory bulbs mRNA and protein levels had fewer differences between LRRK2 mutants and WT. Wnt ligands Wnt3a ($p<0.05$) and Wnt5a ($p<0.05$) protein levels were significantly higher in LRRK2 KO when compared to WT in the mixed gender analysis group, male LRRK2 KO also showed a higher Wnt5a protein level ($p<0.05$) than WT (**Fig 4.16 C, E**). Wnt3a protein level was significantly lower ($p<0.01$) in G2019S KI than WT in mixed gender analysis, male G2019S KI also showed a trend of decreased Wnt3a protein level ($p=0.05$) when compared to WT (**Fig 4.16 D, F**).

In the mixed gender analysis group, LRRK2 KO had a significantly lower phosphorylated co-receptor pLRP6 (S1490) protein level ($p<0.01$) and a trend towards increased LRP6 protein level ($p=0.07$) when compared to WT. As a result, the pLRP6 (S1490) ($p<0.01$) in relation to total LRP6 protein level was significantly lower in LRRK2 KO than in WT. Interestingly, only the pLRP6 (S1490) protein level was lower ($p<0.05$) in male LRRK2 KO when compared to WT. In female LRRK2 KO, only pLRP6 (S1490) in relation to total LRP6 showed a significantly lower protein expression level ($p<0.01$) than WT (**Fig 4.16 C, E, G**). Regulator Dvl2 protein level ($p<0.05$) was higher in LRRK2 KO than WT in the mixed gender analysis group (**Fig 4.16 C**).

The β-catenin destruction complex component *Gsk3β* mRNA level was significantly higher in male G2019S KI than in WT ($p<0.05$) (**Fig 4.15 B**). Both LRRK2 KO ($p<0.01$)

and G2019S KI ($p<0.01$) had a significantly lower *Gsk3β* mRNA level when compared to WT (**Fig 4.15 C**).

Target genes *Bdnf* mRNA level ($p<0.05$) was significantly higher in female G2019S KI than WT, *Cyclin-D1* mRNA level ($p<0.05$) was also higher in female G2019S KI when compared to LRRK2 KO (**Fig 4.15 C**). BDNF protein level trended to increase ($p=0.08$) when comparing LRRK2 KO and WT in the male cohort (**Fig 4.16 E**).

Male LRRK2 KO had a significantly higher NFAT protein level ($p<0.05$) than WT. Inflammatory cytokine Cox2 protein level showed a trend towards an increase ($p=0.06$) in G2019S KI mixed gender analysis (**Fig 4.16 E, D**).

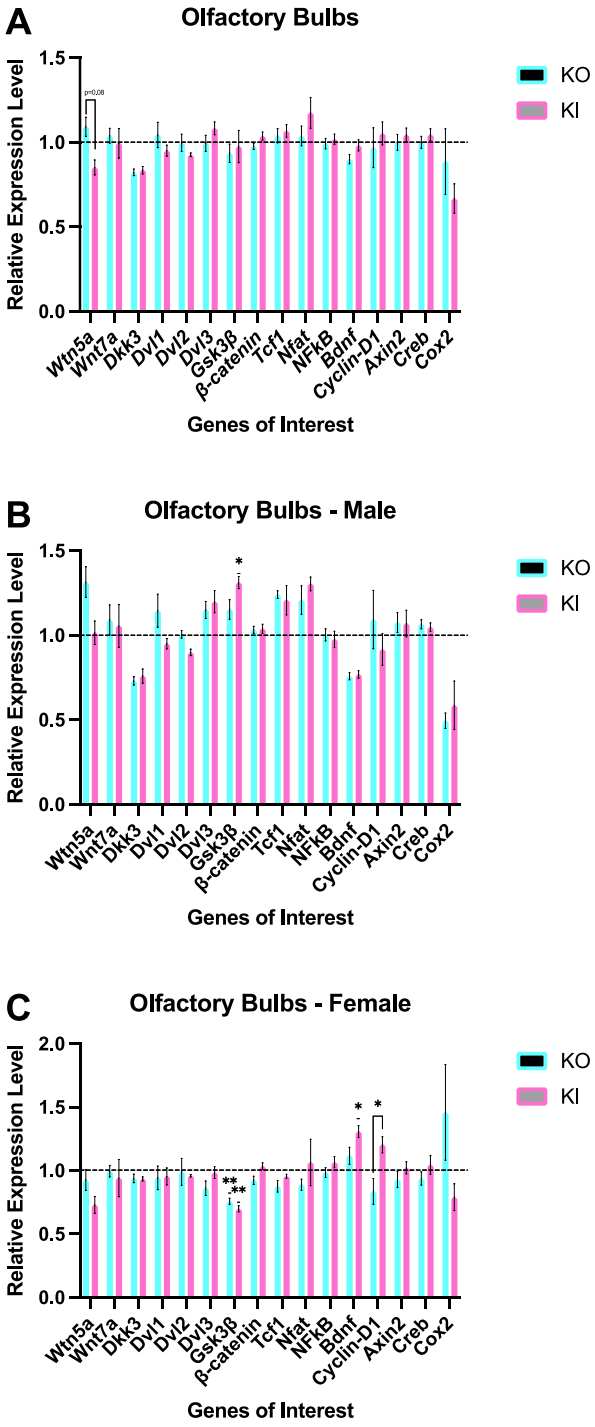


**Figure 4.15: mRNA expression level analysis against wild type in olfactory bulbs**

Each of the gene of interest was compared to the corresponding WT's value. WT was set as 1 and presented in a line.

**Wnt ligands:** *Wnt5a*, *Wnt7a*; **Antagonist**: *Dkk3*; **Cytoplasmic components**: *Dvl1-3*; **β-catenin destruction complex**: *Gsk3β*, *β-catenin*, *Axin2*; **Transcriptional factors**: *Nfat*, *Nfκb*, *Tc1*; **Downstream targets**: *Cyclin-d1*, *Bdnf*, *Creb*, *Cox2*.

Data presented as mean ± S.E.M., compared by ONE-WAY ANAOVA followed by Tukey's post hoc test, $p<0.05$ = *, $p<0.01$ = **, $p<0.001$ = ***, $p<0.0001$ = ****; n=3 per sex per genotype.

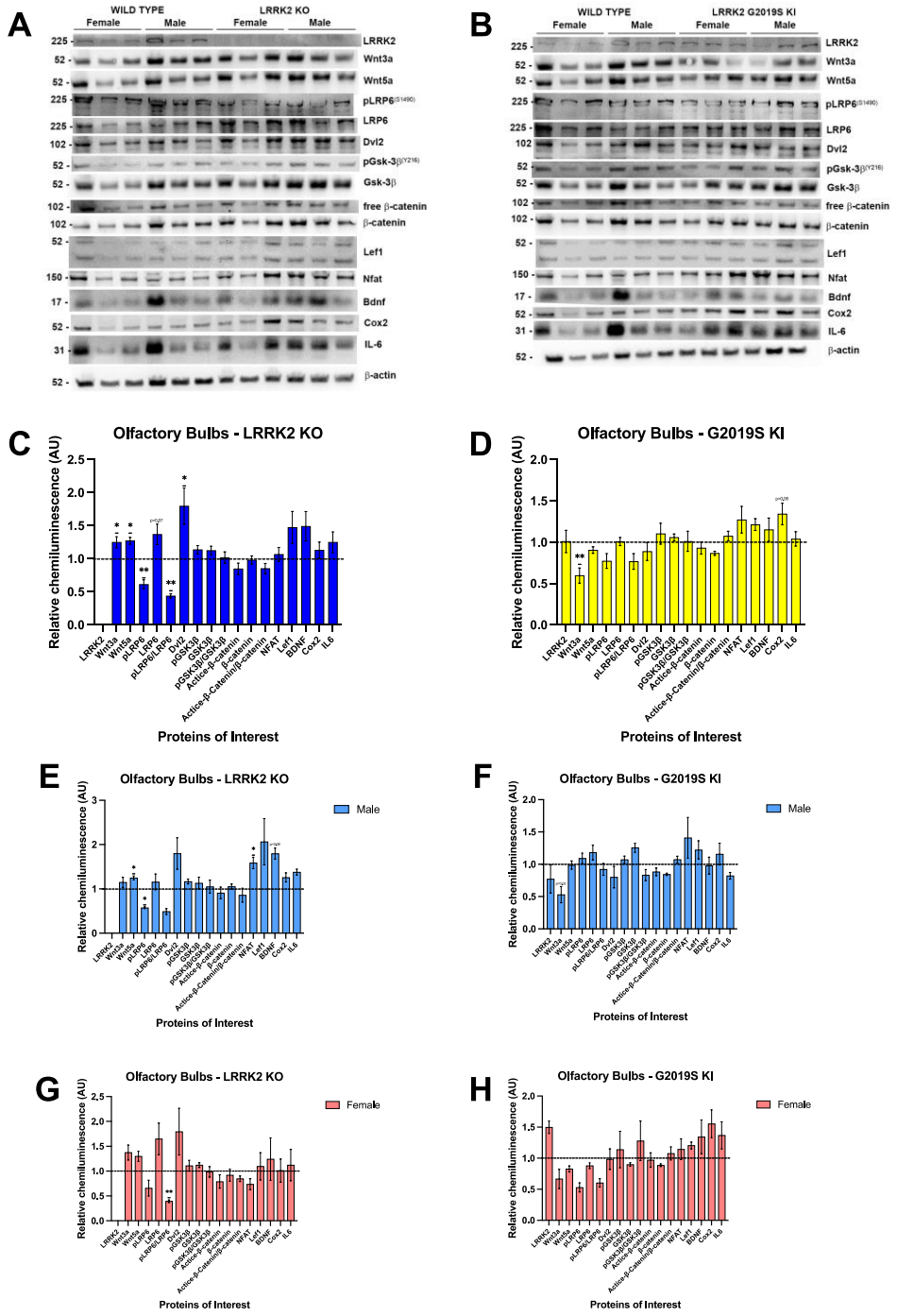


**Figure 4.16: Protein expression level analysis against wild type in olfactory bulbs**

Each of the gene of interest was compared to the corresponding WT's value. WT was set as 1 and presented in a line.

**Genotype:** LRRK2; **Wnt ligands:** Wnt3a, Wnt5a; **Co-receptors**: pLRP6, LRP6; **Cytoplasmic components**: Dvl2; **β-catenin destruction complex**: pGsk3β, Gsk3β,

β-catenin, active-β-catenin; **Transcriptional factors**: NFAT, Lef1; **Downstream targets**: BDNF, Cox2, IL-6.

Data presented as mean ± S.E.M., compared by unpaired t-test with Welch's correction, $p<0.05$ = *, $p<0.01$ = **, $p<0.001$ = ***, $p<0.0001$ = ****; n=3 per sex per genotype.

### 4.2.7 Overview

mRNA and protein expression in WT mice were used as a benchmark in comparisons to samples collected from LRRK2 KO and G2019S KI mice. There was a clear effect of sex and LRRK2 mutants having a different effect in different brain regions. WT was used as a benchmark reading to assess the expression differences in the LRRK2 mutants. A table summarised the total number of significant expression differences in LRRK2 KO and G2019S KI compared to WT.

Most significant mRNA expression level differences were found in half brain and striatum, followed by the cortex. The male G2019S KI striatum had 4 significant differences compared to half brain with 0 significance and cortex with only 1 significance. LRRK2 KO and G2019S KI hippocampus and olfactory bulbs showed the least significant differences compared to WT. Interestingly, when combining the sex, LRRK2 KO half brain showed the most significant mRNA expression level with 5 significant changes compared to the cortex and striatum, which had only 2 significant changes.

G2019S KI showed the most significant protein expression changes in the striatum and half brain in the protein expression level analysis, with 8 significant changes in both regions. More changes were observed in male G2019S KI striatum and half brain, with 6 and 7 significant changes, respectively. Again, G2019S KI hippocampus and olfactory bulbs showed the least significant changes compared to WT. Overall, GSK3β, β-catenin and LRP6 protein levels were most affected, followed by target proteins, such as BDNF and Cox2. A detailed table demonstrated all the changes in different

brain regions from LRRK2 KO and G2019S KI compared to LRRK2 WT (**Table 4.1-4.2**).

The data suggested that Wnt signalling activity is brain regions specific and LRRK2 genotype dependent.

**Table 4.1: Summary table of the LRRK2 KO and G2019S KI significant mRNA expression changes in different brain regions compared to WT mice.**

↑ indicates an upregulation compared to WT; ↓ indicates a downregulation compared to WT.

| | mRNA | Half Brain | | | Cortex | | | Striatum | | | Hippocampus | | | Olfactory bulbs | | |
|---|---|---|---|---|---|---|---|---|---|---|---|---|---|---|---|---|
| | LRRK2 KO | Male | Female | Mixed | Male | Female | Mixed | Male | Female | Mixed | Male | Female | Mixed | Male | Female | Mixed |
| Wnt ligands | *Wnt5a* | | | ↓ | | ↓ | ↓ | ↑ | | ↑ P=0.06 | | | | | | |
| | *Wnt7a* | | | | | | | | | | | | | | | |
| Wnt antagonist | *Dkk3* | | | | | | | | | | ↑ | | | | | |
| Cytoplasmic components | *Dvl1* | ↑ | | ↑ | ↑↑ | | | | | | | | | | | |
| | *Dvl2* | ↑ P=0.05 | | | | | | | | | | | | | | |
| | *Dvl3* | | | | | ↑ | | | | | | | | | | |
| β-catenin destruction complex | *Gsk3β* | ↓ | ↓ | ↓↓ | | | | ↑ P=0.09 | | | | | | | ↓↓ | |
| | *β-catenin* | | | ↓ | | | | ↑ P=0.05 | | ↑ P=0.05 | | | | | | |
| | *Axin2* | | | ↓ | | | | ↑ | | ↑ | | | | | | |
| Transcriptional factors | *Nfat* | | | | | | | ↑ P=0.06 | | ↑ | | | | | | |
| | *Nfκb* | | | | | | | | | | | | | | | |
| | *Tcf1* | ↓ P=0.05 | | | ↑ P=0.05 | | | ↑ | | | | | | | | |
| Downstream targets | *Cyclin-d* | ↑ | | | | | | | | | | | | | | |
| | *Bdnf* | | | | ↓ | ↓ P=0.05 | ↓ | | | | | | | | | |
| | *Creb* | | | | | | | | | | | | ↓ P=0.08 | | | |
| | *Cox2* | | | | ↓ P=0.07 | | | ↓ | | | | | | | | |

| | mRNA | Half Brain | | | Cortex | | | Striatum | | | Hippocampus | | | Olfactory bulbs | | |
|---|---|---|---|---|---|---|---|---|---|---|---|---|---|---|---|---|
| | G2019S KI | Male | Female | Mixed | Male | Female | Mixed | Male | Female | Mixed | Male | Female | Mixed | Male | Female | Mixed |
| Wnt ligands | *Wnt5a* | | | ↓ P=0.06 | | | | ↑ P=0.08 | | | | | | | | |
| | *Wnt7a* | | | ↑ | | | | | | | | | | | | |
| Wnt antagonist | *Dkk3* | | | | | | | | | | | | ↓ | | | |
| Cytoplasmic components | *Dvl1* | | | | | | | | | | | | | | | |
| | *Dvl2* | | | | | | | ↑ | | | | | | | | |
| | *Dvl3* | | | | | | | | | | | | | ↑ | | |
| β-catenin destruction complex | *Gsk3β* | | ↑ p=0.08 | | | | | | ↓ | | | | | | ↓↓ | |
| | *β-catenin* | | | | | | | ↑ | | ↑ P=0.08 | | | | | | |
| | *Axin2* | | | | | | | ↑↑ | | ↑ P=0.08 | | | | | | |
| Transcriptional factors | *Nfat* | | | | | | | | | | | | | | | |
| | *Nfκb* | | | | | | | | | | | | | | | |
| | *Tcf1* | | | | | | | ↑ | | | | | | | | |
| Downstream targets | *Cyclin-d* | | | | ↑↑ | | | | ↓ P=0.08 | ↓ p=0.07 | | | | | | |
| | *Bdnf* | | | | | ↓ | ↓ | | | | | | | | ↑ | |
| | *Creb* | | | | | | | | | | | | | | | |
| | *Cox2* | | | | | | | | | | | | | | | |

**Table 4.2: Summary table of the LRRK2 KO and G2019S KI significant protein expression changes in different brain regions compared to WT mice.**

↑ indicates an increased expression level; ↓ indicates a decreased expression level when compared to WT.

| | Protein | Half Brain | | | Cortex | | | Striatum | | | Hippocampus | | | Olfactory bulbs | | |
|---|---|---|---|---|---|---|---|---|---|---|---|---|---|---|---|---|
| | **LRRK2 KO** | Male | Female | Mixed | Male | Female | Mixed | Male | Female | Mixed | Male | Female | Mixed | Male | Female | Mixed |
| **Genotype** | LRRK2 | | | | | | | | | | | | | | | |
| **Wnt ligands** | Wnt3a | ↓ | | | ↓ | | ↓ | | | | | ↑ P=0.09 | | | | ↑ |
| | Wnt5a | ↓ | | ↓ P=0.07 | | | | ↓ | | ↓ | | | | ↑ | | ↑ |
| **Co-receptor** | pLRP6 | | | | ↓ P=0.06 | | ↓ | | | | ↓ | | | ↓ | | ↓↓ |
| | LRP6 | | | | | | | | | | ↓↓ | | ↓ P=0.07 | | | ↑ P=0.07 |
| | pLRP6/LRP6 | | | | ↓ | | ↓ | | | | | | | | ↓↓ | ↓↓ |
| **Cytoplasmic components** | Dvl2 | | | | | | | ↓ | | ↓ | ↓ | | ↓ | | | ↑ |
| **β-catenin destruction complex** | pGsk3β | | | ↓ P=0.09 | ↑ P=0.09 | ↓ P=0.06 | | | | | | | | | | |
| | Gsk3β | | | | ↓ | ↑ | | | | | | | | | | |
| | pGsk3β/Gsk3β | | | | ↑ | | | | | | | | | | | |
| | Active-β-catenin | | | | | | ↑ P=0.08 | | | | | ↓ | ↓ P=0.06 | | | |
| | β-catenin | | | | | ↑ | | | | | | ↑↑ | ↑↑ | | | |
| | ABC/β-catenin | | | | ↑ P=0.08 | | | | | | | ↓ | ↓ | | | |
| **Transcriptional factors** | NFAT | | ↓ | | ↓ | | ↓ p=0.06 | ↓ P=0.07 | | | ↓ | | | ↑ | | |
| | Tcf1 | | ↑ P=0.07 | ↑ P=0.05 | | | | | | | ↓ | | ↓↓ | | | |
| | Tcf3 | | | | | | | ↓ | | | | | | | | |
| | Lef1 | ↓ | | | | | | ↓ | ↓ | ↓↓↓ | ↑ P=0.08 | | | | | |
| **Downstream targets** | BDNF | ↑ | | ↑ | ↑ | | ↑ P=0.05 | | | | | | | ↑ P=0.08 | | |
| | Cox2 | | | | | | ↑ P=0.05 | ↓ P=0.09 | | ↓ P=0.06 | | | | | | |
| | Cyclin-D1 | | | ↓ P=0.07 | | | | | | | | | | | | |
| | TNFα | | | | | | | | | | | | | | | |
| | IL-6 | | | | ↓ | ↓ P=0.07 | ↓↓ | | ↓ | ↓ P=0.06 | ↓ P=0.06 | | | | | |

| | Protein | Half Brain | | | Cortex | | | Striatum | | | Hippocampus | | | Olfactory bulbs | | |
|---|---|---|---|---|---|---|---|---|---|---|---|---|---|---|---|---|
| | **G2019S KI** | Male | Female | Mixed | Male | Female | Mixed | Male | Female | Mixed | Male | Female | Mixed | Male | Female | Mixed |
| **Genotype** | LRRK2 | | | | | | | | | | | | ↑ P=0.09 | | | |
| **Wnt ligands** | Wnt3a | | | | | ↑ P=0.09 | ↑ | | | ↑ P=0.06 | | | | ↓ P=0.05 | | ↓↓ |
| | Wnt5a | | ↑ | ↑↑ | | ↓↓ | | | | ↓ P=0.08 | | | | | | |
| **Co-receptor** | pLRP6 | ↓ | ↓↓ | ↓↓↓ | | ↓↓ | | | | | | | | | | |
| | LRP6 | ↑ | | ↑ P=0.08 | ↓ | ↓↓ | ↓ | ↓ P=0.07 | ↓ | ↓↓ | ↓ | | | | | |
| | pLRP6/LRP6 | ↓ | ↓ | ↓↓↓ | | ↑↑ | ↑ | | | | | | | | | |
| **Cytoplasmic components** | Dvl2 | | | | | | | ↓ | | ↓ P=0.06 | | | | | | |
| **β-catenin destruction complex** | pGsk3β | ↓ | | | ↓ P=0.05 | ↓ | ↓↓↓ | | | | | | | | | |
| | Gsk3β | | | | | | | ↑ P=0.05 | | ↑ | | | | | | |
| | pGsk3β/Gsk3β | | | | | | ↓ P=0.06 | ↓ P=0.06 | | ↓ | | | | | | |
| | Active-β-catenin | | | | | | | ↓ P=0.09 | | ↓ P=0.05 | | | | | | |
| | β-catenin | | | | | | | ↓ | | ↓↓ | | | ↑ | | | |
| | ABC/β-catenin | | | | | | | | | | | ↓ P=0.05 | | | | |
| **Transcriptional factors** | NFAT | | | | | | | ↓ | ↓ p=0.09 | ↓↓ | | | | | | |
| | Tcf1 | | ↑↑↑ | ↑ | | | | | ↑ | | | ↓ | ↓↓ | | | |
| | Tcf3 | ↑ | | | | | | | | | | | | | | |
| | Lef1 | | | | ↓ | ↑ P=0.07 | | ↓↓ | | ↓↓ | | | | | | |
| **Downstream targets** | BDNF | ↓ | ↓ | ↓↓↓ | | | | | | | | | | | | |
| | Cox2 | ↓ | ↑ p=0.06 | ↑↑ | | | | ↓ | | ↓ | | | | | | ↑ P=0.06 |
| | Cyclin-D1 | | ↓ P=0.08 | ↓↓ | | | | ↓ | | ↓ | | | | | | |
| | TNFα | | | | | ↓↓↓ | | | | | | | | | | |
| | IL-6 | ↓ P=0.09 | | ↓ | ↓↓ | ↓ | ↓↓↓ | | | | | | | | | |

# 4.3 Discussion

In this section, we studied how LRRK2 mutants affect Wnt and NFAT signalling pathway mediators' mRNA and protein expression in selected brain areas under basal conditions. We observed differences in mRNA and protein levels between LRRK2 genotypes in all brain regions investigated. We also observed different expression levels separately when we analysed the data for male and female mice. The n of 3 for these experiments was low. We have observed an extreme expression level between 2 individual mice within the same genotype study group. Animal behaviour could significantly affect gene and protein expressions, and therefore a larger n number will be needed in future study to generate a more robust results(Eusebi et al., 2021, Kaur et al., 2019). However, despite this fact, the analysis showed that some observed expression level changes were primarily carried by one sex, whereas the other sex showed no significant change. In other examples, changes went in the same direction producing more significant results with increased confidence in the mixed sex analysis. The combined data suggested that the increased in n number would reveal more information on how sex and LRRK2 mutations affect Wnt signalling activity. As mentioned in **Chapter 3**, a power calculation will be beneficial in order to identify the right number of animals required in the study.

We observed many trends and larger non-significant changes that would have profited from an increase in the number of mice in each group. Considering the tested targets, including components from upstream components of the pathway down to the target

genes. We observed most of the significant changes in the co-receptor LRP6, BCD components and the target genes. However, the different degrees of dysregulations on different Wnt signalling mediators caused a complication in identifying which component was directly affected by LRRK2 mutations. Our findings consolidated that LRRK2 is a scaffolding protein with the Dvl proteins and within the BCD (Berwick and Harvey, 2012, Berwick et al., 2017). The loss or gain of function might have a direct effect in the Wnt signalling pathway.

The Wnt signalling activity changes in different brain region was not reflect in active-β-catenin protein expression analysis. The expression of active-β-catenin and the ratio of active-β-catenin in relation to β-catenin would directly indicate Wnt signalling pathway activation status in the studied brain regions. In the half brain samples, active-β-catenin protein level and β-catenin protein levels showed no expression difference when compared LRRK2 KO and G2019S KI to WT, which suggested Wnt signalling activity was on a similar level in all genotypes (**Fig 4.8 C, D**). However, the *β-catenin* mRNA level was downregulated in LRRK2 KO, suggesting some degree of dysregulation that might have been compensated for by changes in protein translation and/or degradation (**Fig 4.7 A**). In the striatum, downregulation of β-catenin and active-β-catenin in G2019S samples suggested a decreased in Wnt signalling activity in the striatum (**Fig 4.12 C, D**). LRRK2 KO and G2019S KI hippocampus samples showed a less active-β-catenin than β-catenin compared to WT, suggesting Wnt signalling activity was downregulated in LRRK2 mutants compared to WT (**Fig 4.14**). No changes were observed in olfactory bulbs (**Fig 4.16**). Wnt signalling activity was

reported to decline while ageing (Hofmann et al., 2014). It is important to note that our mice samples were collected at a relatively young age with a healthy physiological state. Therefore, it would be interesting to know the rate of Wnt signalling decline in different LRRK2 genotypes.

To address our data in this chapter, it is essential to discuss the roles of Wnt signalling mediators. Wnt3a is known as a canonical Wnt signalling pathway ligand. Wnt5a is important as a non-canonical Wnt signalling pathway ligand activating PCP and Wnt/Ca2+ pathways including NFAT signalling, and is crucial for DAergic neuronal morphogenesis (Andersson et al., 2008, Blakely et al., 2011). The NFAT signalling pathway is also important for immune response, with the absence of stimuli, the signalling pathway activity may be minimal. Wnt5a is also reported as an inhibitor of the canonical Wnt signalling pathway (Nemeth et al., 2007, Yuan et al., 2011). Therefore, an upregulation in Wnt5a might play a counterpart for the canonical Wnt signalling pathway ligand Wnt3a expression. Wnt7a, on the other hand, can initiate both canonical and non-canonical Wnt signalling pathways (Le Grand et al., 2009, Yoshioka et al., 2012). On the other hand, DKK3 works as an antagonist of the canonical Wnt signalling pathway (Gondkar et al., 2019). The expression of these agonists and antagonists works as a counterpart to each other, the increase of agonist expression will result in the decrease of antagonist expression, which will directly affect canonical and non-canonical Wnt signalling activities.

Overall, half brain has given us a general idea of Wnt signalling activities in LRRK2 KO and G2019S KI compared to WT at a molecular level. Both LRRK2 KO and

G2019S KI samples showed a dysregulation in mRNA and protein expression levels, however the different regulations suggested that G2019S KI is not a loss of function. G2019S samples showed the most significant changes compared to WT in all the investigated brain regions. Although male and female samples demonstrated similar signalling components patter, the unidentical regulation in different sex suggested sex could play an essential role in Wnt and NFAT signalling activities. The G2019S KI half brain showed a significant reduction of LRP6, and an increase in Wnt5a protein levels could explain the reduction in downstream targets and Cox2.

Interestingly, hyposmia indicates early PD symptoms (Braak et al., 2003). However, we observed minimal changes in olfactory bulbs and the hippocampus. It was previously reported that hyposmia is less frequent in patients with the G2019S mutation (Gaig et al., 2014). The different regulation of Wnt signalling components requires an in depth investigation into each of the individual components.

Wnt3a and Wnt5a were reported to induce phosphorylation of co-receptor LRP5/6 (Grumolato et al., 2010). We observed a decrease of pLRP6/LRP6 protein level in G2019S KI half brain and striatum (**Fig 4.8C, 4.12D**), which was caused by the significantly low protein level of pLRP6. LRP5/6 are phosphorylated upon activation of canonical and non-canonical Wnt signalling pathways. Phosphorylation of the co-receptor facilitates the binding of β-catenin destruction complex to the phosphorylated site and hence derepress phosphorylation of β-catenin. The process allows β-catenin to accumulate and translocate into the nucleus to promote gene transcriptions. Downregulation in pLRP6 would recommend a low Wnt signalling activity in the brain regions (Zeng et al., 2005, Niehrs and Shen, 2010). Our laboratory previously reported

that LRRK2 works as a scaffolding protein within the β-catenin destruction complex, the co-receptors and Dvl proteins. Therefore, LRRK2 is believed to enhance the formation of LRP6 signalosome. LRRK2 mutants and LRRK2 inhibitors negatively affected Wnt signalling activity, suggesting that the kinase domain has a curial role in Wnt signalling pathways (Berwick and Harvey, 2012, Berwick et al., 2017). We have tested Dvl mRNA expressions in different brain regions, and we observed an upregulation of *Dvl* mRNA level in male LRRK2 KO half brain and cortex (**Fig 4.7C, 4.9B**). Dvl proteins are important in both canonical and non-canonical Wnt signalling pathways. Pulvirenti *et al*. have demonstrated that Dvl2 depletion blocked proliferation and differentiation in human glioma cell line and patient derived glioma cells. The authors have also demonstrated that Wnt5a is essential for glioma cell proliferation (Pulvirenti et al., 2011). The interaction between LRRK2 and Dvl consolidates Dvl as an interesting target for Dvl2 and is important for both canonical and non-canonical Wnt signalling pathways.

Axin2, as a scaffolding protein in the destruction complex, interacts with LRP5/6 co-receptors and recruits GSK3β to facilitate the phosphorylation of β-catenin (Jho et al., 2002, Song et al., 2014). GSK3β plays a vital role to in phosphorylating β-catenin to prevent translocation into the nucleus. GSK3β has been previously reported to interact with LRRK2 in *in vitro* study. The authors reported that LRRK2 acts as an enhancer for GSK3β during the phosphorylation process of tau. The binding of G2019S mutation to GSKβ was also reported to increase GSK3β activities (Lin et al., 2010, Kawakami et al., 2014). Phosphorylation at the position tyrosine 216 of GSK3β increased the

enzymatic activities by approximately 5 folds (Krishnankutty et al., 2017). Therefore, the expression level of activated GSK3β would directly affect the expression level of β-catenin. However, in G2019S KI striatum, the inactivate GSK3β protein level was significantly higher, but the protein level of β-catenin and active-β-catenin was not reflected in that (**Fig 4.12 D**). It is also important to note that GSK3β is involved in the non-canonical Wnt signalling pathway. Downregulation of active GSK3β will result in the accumulation of NFAT and promotes transcription of inflammatory cytokines. G2019S KI half brain Cox2 protein level was largely elevated, but protein level of GSK3β remained unchanged when compared to WT (**Fig 4.8 D**). Interestingly, Cox2 has been reported by different groups that it is the target gene in both canonical and non-canonical signalling pathways (Nunez et al., 2011, Flockhart et al., 2008). Cox2 involves in inflammatory events and cancer, the elevated Cox2 protein level in half brain may suggest an early stage of inflammatory responses (**Fig 4.8 D**) (Seibert and Masferrer, 1994, Gandhi et al., 2017). The upstream components, such as Wnt ligands, β-catenin and NFAT have a dominant effect on canonical and non-canonical Wnt signalling activities. However, dysregulated transcription factor such as Tcf and Lef protein level will directly affect the Wnt signalling activities.

BDNF, a member of neurotrophin family has an important role in neurogenesis (Liu and Nusslock, 2018, Numakawa et al., 2017, Bramham and Messaoudi, 2005). BDNF was reported to have a direct correlation to the Wnt signalling pathway and is important in neuronal growth (Yang et al., 2015). High levels of BDNF and proinflammatory factors were found in idiopathic PD patients, and previous research has shown that

LRRK2 mutation carriers developed PD in a similar manner as idiopathic PD patients (Brockmann et al., 2017). Cyclin-D1, a target gene of the canonical Wnt signalling pathway, works as a cell cycle progression regulator and is required at G1 phase of cell cycle (Shtutman et al., 1999, Zhang et al., 2012).

The protein level of BDNF was predominantly downregulated in G2019S KI half brain, and the BDNF mRNA level was downregulated in both LRRK2 KO and G2019S KI cortex compared to WT (**Fig 4.8 D, 4.9 A**). Downregulation of Cyclin-D1 protein levels was observed in our G2019S KI half brain and striatum data (**Fig 4.8D, 4.12D**). The decreased of BDNF level in the brain indicated neurodegeneration in both PD and AD (Zhang et al., 2016a). Dietrich *et al* also suggested that Cyclin-D1 might play a role in mitochondria dysfunction in striatal neurodegeneration (Dietrich et al., 2022).

In this chapter, we have identified protein and mRNA expression changes in different brain regions. Our data showed mRNA and protein expressions were brain region specific, LRRK2 genotypes and sex also impact the expression levels. However, LRRK2 mutants have a larger effect than sex on the expression levels.

A higher n number is needed to test the effect of sex on Wnt signalling cascades mRNA and protein expression changes. Our next question is how LRRK2 interferes Wnt signalling pathways components when the pathway is activated under different stimuli in neurons and glia cells.

# 5 Wnt signalling activity changes in primary cell cultures under different stimulations

## 5.1 Introduction

We have identified the effect of LRRK2 genotypes and sex on Wnt signalling activities in different brain regions in mice under basal conditions described in previous chapters. In adults, Wnt signalling activity is at a delicate balance for cell maintenance and neurogenesis in the brain. As described in previous chapters, LRRK2 mutants affected the mRNA and protein expression levels differently in different brain areas. However, the effects under basal conditions were often small and/or insignificant. We are interested in knowing how LRRK2 mutants affect Wnt signalling activities when the pathway is activated. LRRK2 expression differs in different organs as well as cell types.

Previous research stated that mice have a higher LRRK2 expression in glial cells than neurons, especially in the astrocytes (Zhang et al., 2016b). Glial cells account for approximately 50% of the cells in the brain, and astrocytes are the most abundant glial cell types. There is growing evidence showing a connection between neuroinflammation in the SNc and reactive astrocytes(Verkhratsky et al., 2012, Koprich et al., 2008).

In this chapter, we performed different neuronal and astrocyte primary cell cultures from WT, LRRK2 KO and G2019S KI mice. We applied the lentivirus biosensor system onto the cells to study Wnt signalling activity under different stimulated conditions. Basal condition treated with pure culture medium was used as a control in comparison to the stimulated cohorts. The lentiviral construct contains a luciferase reporter gene downstream of the TCF/LEF or NFAT transcriptional factor. Mixed cultures with both neurons and glial cells and pure neurons and pure astrocytes were used in this study.

We studied Wnt signalling activity in different primary cultures using lentiviral biosensors. We also performed qPCR on primary astrocyte cultures to study mRNA expression changes of Wnt signalling mediators after different stimulation. The same gene list was used as in **chapter 4**, with the addition of *Wls* and *Lrp5*. We also analysed the morphological changes in astrocytes harbouring different *LRRK2* mutations after different stimulations. This chapter provides a first insight into how LRRK2 mutants affect Wnt signalling activities in astrocytes.

# 5.2 Result

## 5.2.1 Wnt and NFAT signalling activity in primary neuronal culture

We cultured primary cortical and hippocampal neurons to investigate how LRRK2 mutants affect Wnt signalling activity following activation with Wnt or inflammatory stimuli. We transduced these cultures with lentiviral biosensors for measuring canonical Wnt (TCF/LEF) or NFAT activity. When the pathway is activated, the transduced cells secrete luciferase into the culture medium. Therefore, 10ml of the culture medium was combined with luciferin substrate. Luminescence was measured with an IVIS machine. This study used two types of primary cultures: neurons with glial cells and pure neuronal cultures. Interestingly, cultures without glial cells showed a significantly lower Wnt or NFAT signalling activity compared to neuron-glial co-cultures.

The luciferase releases a luminescence signal when combined with the substrate luciferin. The amount of secreted luciferase indicates Wnt and NFAT signalling activity in the transduced cells. The TCF/LEF and NFAT signalling activity in primary hippocampal cultures was approximately 10-fold lower after cytarabine (AraC) treatment (**Fig 5.1-5.2 A, B**). The preliminary finding suggested that TCF/LEF signalling activity might be more predominant in glial cells than neurons. A control luciferase reporter gene, SFFV, was co-transduced into the cells. SFFV normalised TCF/LEF or NFAT activity to compare the signalling activities within the genotypes

under basal and stimulated conditions. Culture medium was collected at 0 hours, 6 hours and 24 hours post stimulations with either LiCl to trigger activation of TCF/LEF signalling activity or ionomycin to trigger activation of NFAT signalling activity. In our experiments, when glial cells were eliminated, pure G2019S KI hippocampal neuron cultures showed a significant increase in TCF/LEF signalling activity compared to WT by 1.5-fold under both basal ($p<0.0001$) and stimulated ($p<0.001$) conditions at 0 hours. G2019S KI also had a slightly higher TCF/LEF signalling activity than LRRK2 KO after LiCl stimulation ($p<0.05$) at 0 hours (**Fig 5.1 D**). The significant difference was about 2-fold higher in G2019S KI neurons when compared to WT ($p<0.05$) after 6 hours post LiCl treatment (**Fig 5.1 F**). Interestingly, after 24 hours post LiCl treatment, both basal and stimulated conditions showed similar results. TCF/LEF signalling activity in LRRK2 KO neurons was approximately 1.5-fold higher compared to WT ($p<0.01$). G2019S KI signalling activity level was about 2.5-fold higher than WT ($p<0.001$) (**Fig 5.1 H**). However, LiCl did not affect Wnt signalling activity in our cultured samples. The data suggested that increased Wnt signalling activity might not be caused by LiCl treatment but by other external factors.

When investigating NFAT signalling activity in hippocampal neurons, in the co-culture samples, LRRK2 KO NFAT activity level was significantly higher than WT ($p<0.05$) and G2019S KI ($p<0.01$) at the basal condition at 0-hour post treatment. The effect diminished 6 and 24 hours post treatment (**Fig 5.2 C, E, G**). All genotypes showed an increase in NFAT response after ionomycin treatment ($p<0.05$) compared to the basal condition at 6 hours (**Fig 5.2 E**). In addition, WT hippocampal neurons-glial cell co-culture NFAT signalling activity was almost 2-fold higher at 24 hours after ionomycin

treatment when compared to basal conditions ($p<0.05$) (**Fig 5.2 G**). The G2019S KI NFAT activity level in pure hippocampal neurons was, in line with the mixed cultures, significantly lower than WT at 0 hours under basal ($p<0.01$) and stimulated ($p<0.01$) conditions. G2019S neurons also showed a trend towards decrease when compared to LRRK2 KO under stimulated conditions ($p=0.08$) (**Fig 5.2 D**). At 6 hours post treatment, G2019S KI continued to show a trend towards a decrease in NFAT signalling activity when compared to WT ($p=0.06$) and LRRK2 KO ($p=0.07$) (**Fig 5.2 F**). In addition, G2019S KI pure hippocampal neuronal cultures showed a significantly lower NFAT signalling activity than LRRK2 KO ($p<0.05$) and slightly lower activity level than WT ($p=0.05$) 24 hours after ionomycin stimulation (**Fig 5.2 H**).

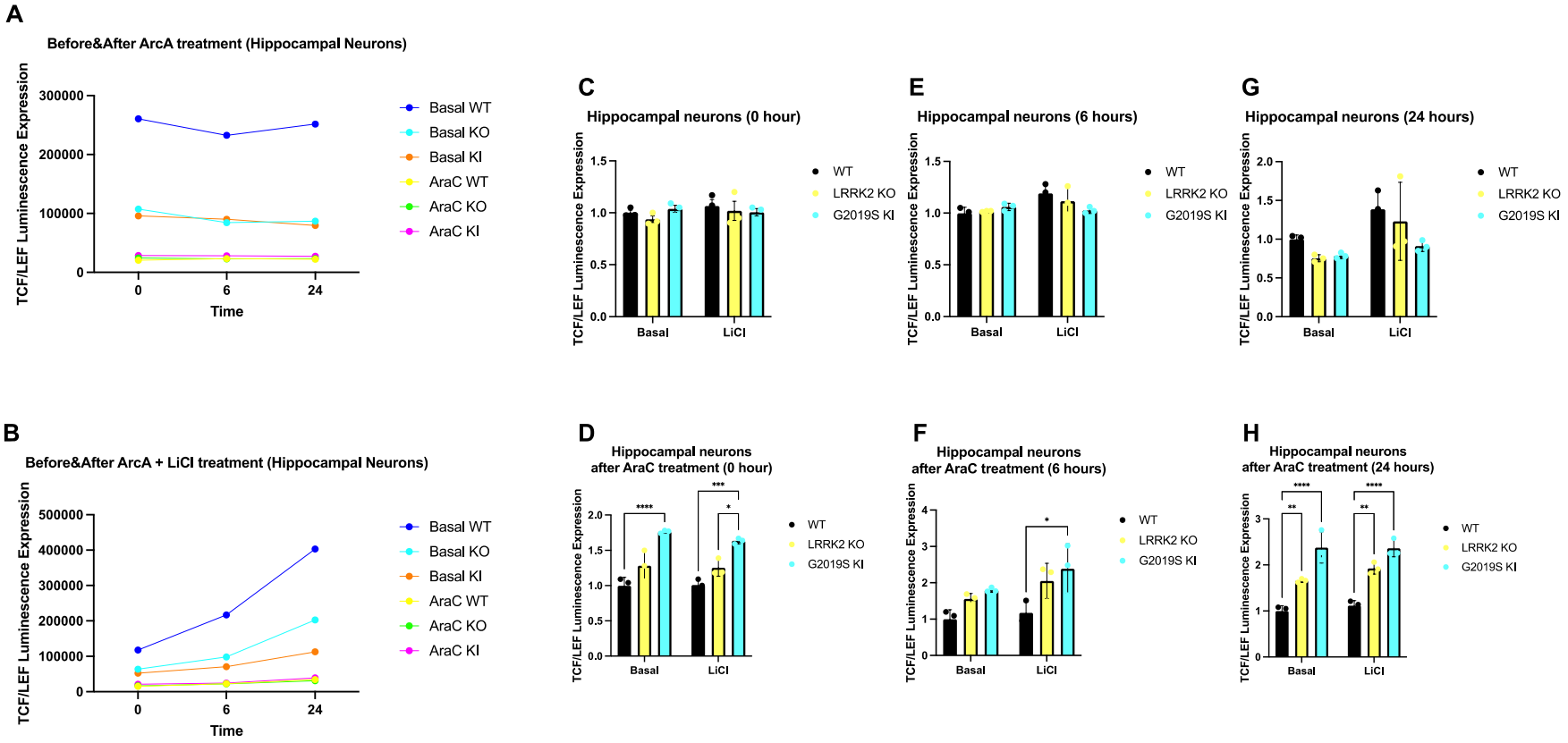


**Figure 5.1: TCF/LEF signalling activity in primary hippocampal cultures**

Primary hippocampal culture at DIV 7. AraC was used to generate pure neuronal cultures. Cells were treated with 40mM LiCl to activate TCF/LEF signalling activity. Data presented as mean ± S.E.M., compared by Two-Way-ANOVA with Tukey's post hoc test,

p<0.05 = *, p<0.01 = **, p<0.001 = ***, p<0.0001 = ****; One preparation of cell culture with 4-6 neonates per genotype. Cells plated into n=3 wells per treatment group per genotype.

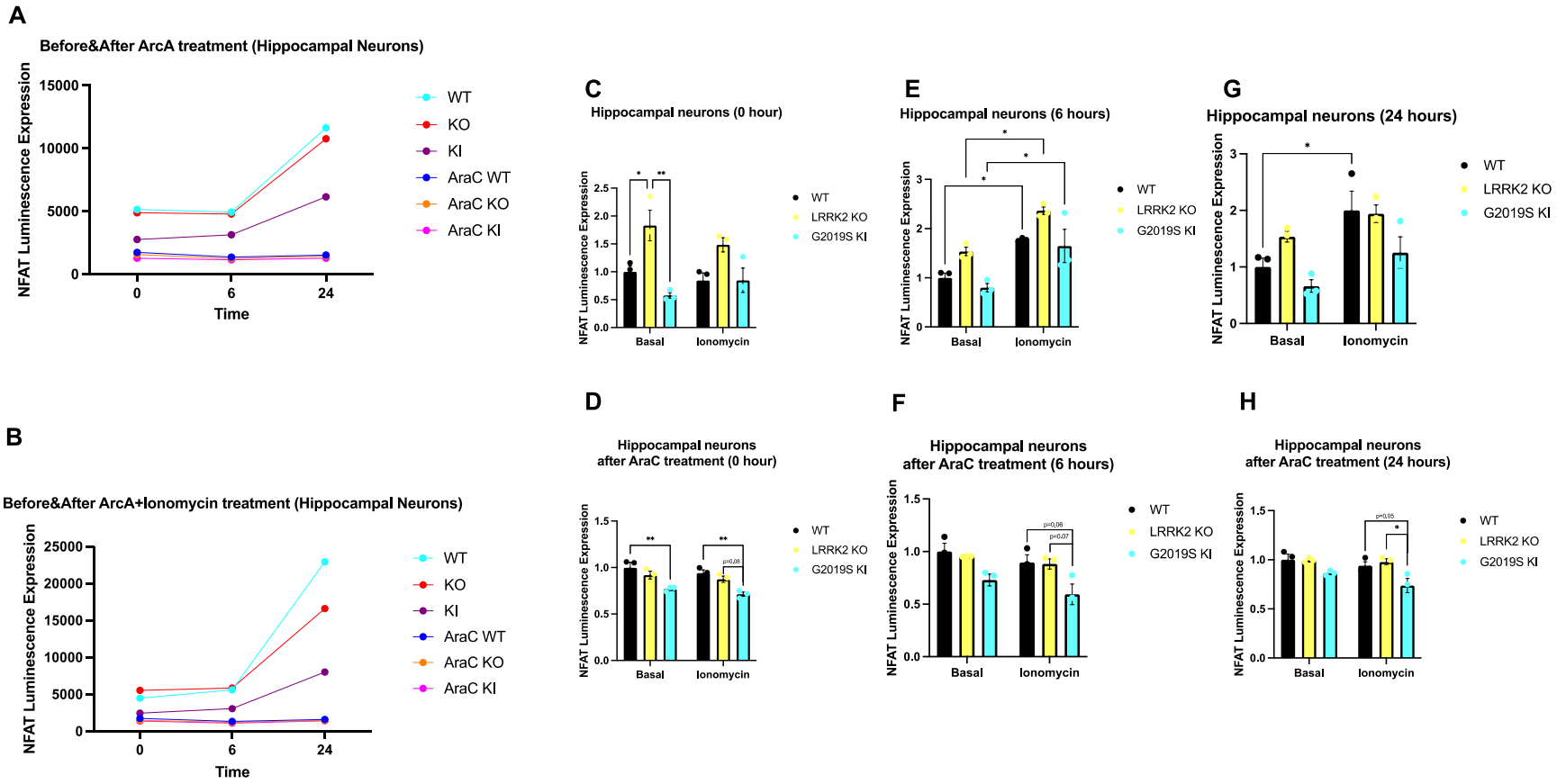
A
Before&After ArcA treatment (Hippocampal Neurons)
NFAT Luminescence Expression
15000
10000
5000
0
0
6
24
Time
WT
KO
KI
AraC WT
AraC KO
AraC KI
B
Before&After ArcA+Ionomycin treatment (Hippocampal Neurons)
NFAT Luminescence Expression
25000
20000
15000
10000
5000
0
0
6
24
Time
WT
KO
KI
AraC WT
AraC KO
AraC KI
C
Hippocampal neurons (0 hour)
NFAT Luminescence Expression
Basal
Ionomycin
WT
LRRK2 KO
G2019S KI
D
Hippocampal neurons after AraC treatment (0 hour)
NFAT Luminescence Expression
Basal
Ionomycin
WT
LRRK2 KO
G2019S KI
E
Hippocampal neurons (6 hours)
NFAT Luminescence Expression
Basal
Ionomycin
WT
LRRK2 KO
G2019S KI
F
Hippocampal neurons after AraC treatment (6 hours)
NFAT Luminescence Expression
Basal
Ionomycin
WT
LRRK2 KO
G2019S KI
G
Hippocampal neurons (24 hours)
NFAT Luminescence Expression
Basal
Ionomycin
WT
LRRK2 KO
G2019S KI
H
Hippocampal neurons after AraC treatment (24 hours)
NFAT Luminescence Expression
Basal
Ionomycin
WT
LRRK2 KO
G2019S KI

**Figure 5.2: NFAT signalling activity in primary hippocampal cultures**

Primary hippocampal culture at DIV 7. AraC was used to generate pure neuronal cultures. Cells were treated with 1μM ionomycin to activate NFAT signalling activity. Data presented as mean ± S.E.M., compared by Two-Way-ANOVA with Tukey's post hoc test, $p<0.05$ = *, $p<0.01$ = **, $p<0.001$ = ***, $p<0.0001$ = ****; One preparation of cell culture with 4-6 neonates per genotype. Cells plated into n=3 wells per treatment group per genotype.

Raw data of primary cortical culture TCF/LEF and NFAT activity levels were approximately 3-4-fold lower after cytarabine (AraC) treatment (**Fig 5.3-5.4 A, B**). Like hippocampal neuronal culture samples, TCF/LEF and NFAT signalling activity was higher in glial cells. The same procedures were performed to compare the signalling activity between each genotype under basal and stimulations conditions. The data was normalised by SFFV. Culture medium was collected at 0 hours, 6 hours and 24 hours post stimulations with either LiCl to trigger activation of TCF/LEF signalling or ionomycin to trigger activation of NFAT signalling. Like primary hippocampal neuronal cultures, glial and cortical plus glial cell co-cultures were not sensitive to LiCl treatment. LRRK2 KO co-cultured cells' TCF/LEF activity was significantly lower than WT ($p<0.05$) (**Fig 5.3 C**). G2019S KI TCF/LEF activity level showed a trend towards a lower activity level than WT ($p=0.07$) at the basal condition at 6 hours. Although G2019S KI also seemed to have a lower TCF/LEF activity level than WT by 0.5-fold, the result was not statistically significant due to a big error bar (**Fig 5.3 E)**. After treating the co-cultured cells with LiCl for 24 hours, TCF/LEF activity levels were about 1.5-fold higher in WT and G2019S KI compared to untreated samples ($p<0.05$). LRRK2 KO cortical neurons were more sensitive to LiCl treatment. The signalling activity level was increased significantly by almost 2-fold compared to the group under basal conditions. However, no significant difference was observed within the genotypes (**Fig 5.3 G**). No signalling activity differences were observed when glial cells were eliminated at the studied time points. The data suggested that TCF/LEF signalling activity might be more prominent in glial cells than cortical neurons. (**Fig 5.3 D, F, H**).

When looking at NFAT signalling activities in cortical neurons, in the co-culture samples, LRRK2 KO ($p<0.05$) and G2019S KI NFAT ($p<0.05$) activity level was significantly higher than WT at the basal condition at 0 hours post treatment. A similar NFAT activity trend was observed in the ionomycin treatment group. LRRK2 KO signalling activity was significantly lower ($p<0.01$), as well as G2019S KI ($p<0.05$) when compared to WT (**Fig 5.4 C**). Although the NFAT activity levels were similar at 6 hours post stimulations and basal condition, no statistical significance was obtained (**Fig 5.4 E**). Interestingly, after 24 hours, LRRK2 KO ($p<0.05$) and G20192S KI ($p<0.05$) NFAT signalling activity levels were significantly lower than WT under basal conditions. Ionomycin has significantly increased NFAT signalling activities by approximately 1.5-fold increased in WT ($p<0.01$), LRRK2 KO ($p<0.0001$) and G2019S KI $p<0.0001$) compared to basal condition at 24 hours post treatment. LRRK2 KO ($p=0.07$) cells tended to have a higher NFAT signalling activity level than WT under stimulated conditions (**Fig 5.4 G**). Like TCF/LEF signalling activity, NFAT signalling activity differences were diminished between the genotypes and treatment groups after glial cells were eliminated (**Fig 5.4 D, F, H**).

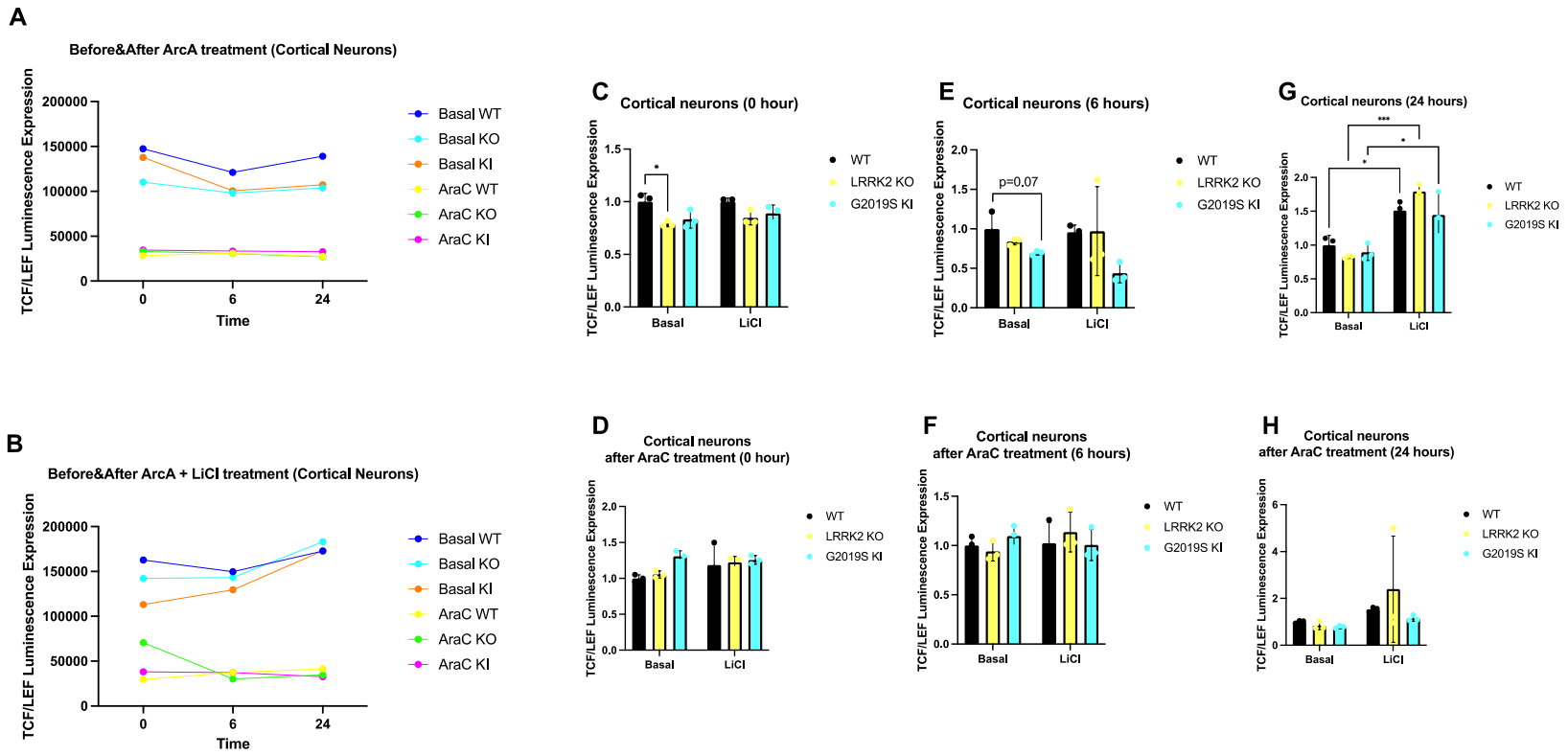


**Figure 5.3: TCF/LEF signalling activity in primary cortical cultures**

Primary cortical culture at DIV 7. AraC was used to generate pure neuronal cultures. Cells were treated with 40mM LiCl to activate TCF/LEFT signalling activity. Data presented as mean ± S.E.M., compared by Two-Way-ANOVA with Tukey's post hoc test, $p<0.05$

= *, p<0.01 = **, p<0.001 = ***, p<0.0001 = ****; One preparation of cell culture with 4-6 neonates per genotype. Cells plated into n=3 wells per treatment group per genotype.

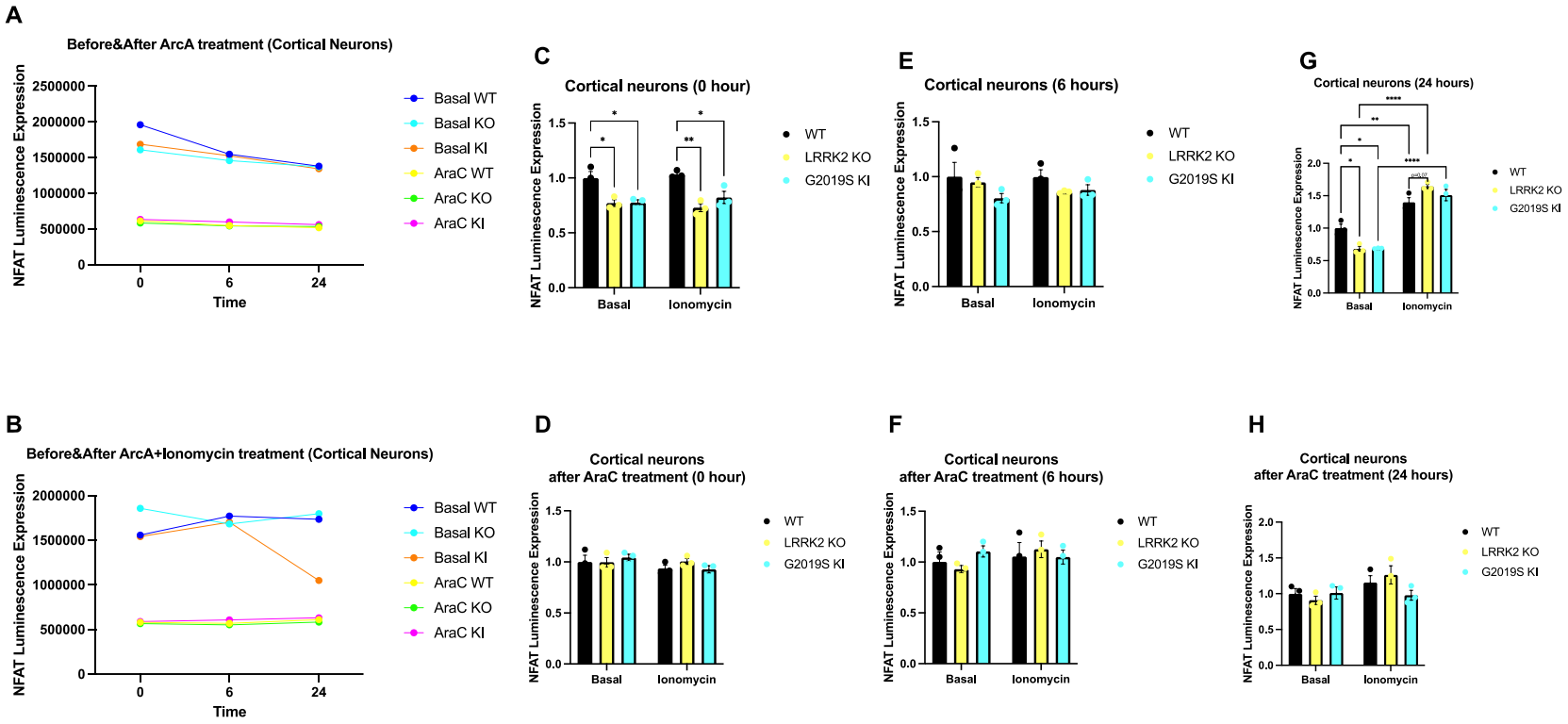


**Figure 5.4: NFAT signalling activity in primary cortical cultures**

Primary cortical culture at DIV 7. AraC was used to generate pure neuronal cultures. Cells were treated with 1μM ionomycin to activate NFAT signalling activity. Data presented as mean ± S.E.M., compared by Two-Way-ANOVA with Tukey's post hoc test,

$p<0.05$ = *, $p<0.01$ = **, $p<0.001$ = ***, $p<0.0001$ = ****; One preparation of cell culture with 4-6 neonates per genotype. Cells plated into n=3 wells per treatment group per genotype.

### 5.2.2 Canonical and NFAT Wnt signalling activity in primary astrocytes culture

We have established that Wnt and NFAT signalling activity might be more prominent in glial cells, and glial cells might be more sensitive to different stimuli than primary neuronal cell cultures. This and the fact that LRRK2 shows higher expression levels in astrocytes than neurones led to the investigation of TCF/LEF signalling pathways in astrocytes (Zhang et al., 2016b). In our primary neuronal culture study, cells were not sensitive to high dosages of LiCl and ionomycin treatments. Hence, we decided to apply other, more physiologically relevant signalling stimuli in this study. The Wnt3a ligand was chosen as an activator of the canonical Wnt signalling pathway stimulating luciferase expression downstream of TCF/LEF. The bacterial TLR4 ligand LPS was chosen to stimulate the NFAT signalling pathway. A dosage response curve was applied to find the best concentration for each stimulus. Different time points were used to find the optimal time to terminate the study. 72 hours post-treatment showed the most activity levels increase in Wnt and NFAT signalling pathways. Interestingly, the group without any treatment showed a significant increase by approximately 10-fold in NFAT signalling activity after 72 hours. We have chosen 100ng/ml of Wnt3a to stimulate the canonical Wnt signalling pathway, which increased the signalling activity level by approximately 300-400-fold. 1mg/ml of LPS was chosen to trigger NFAT signalling, which increased NFAT signalling activity by about 10-fold 72 hours after stimulations. (**Fig 5.5**).

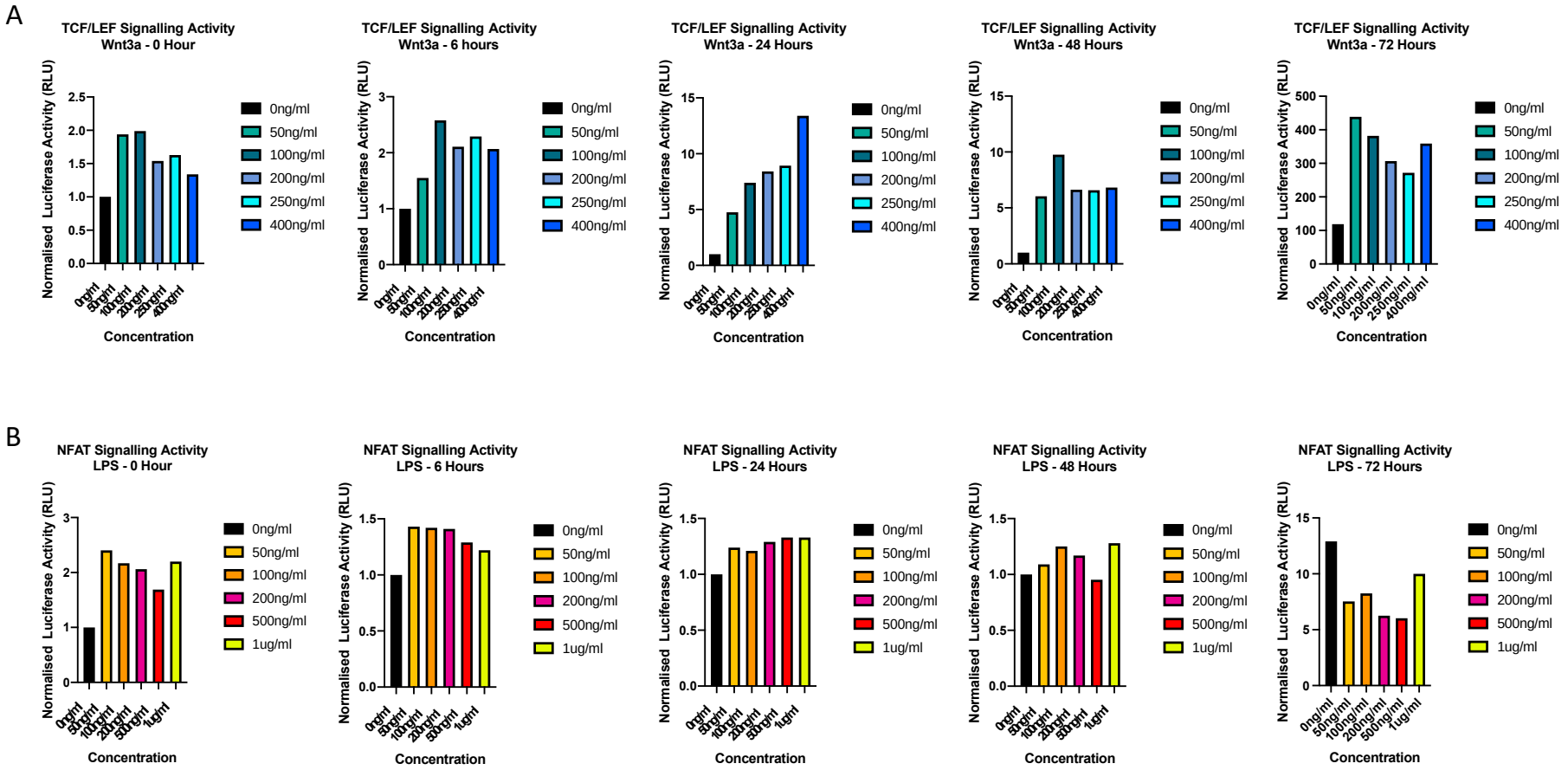


**Figure 5.5: Dosage response curve in astrocytes**

Wnt3a was used to trigger activation of TCF/LEF signalling activity; LPS was used to trigger activation of NFAT signalling activity. Both activity levels reached the peak after 72 hours post-stimulations.

After establishing the ideal stimulus concentration for our study, we focused on canonical Wnt signalling pathways. We investigated the effect of Wnt3a and LPS on different LRRK2 genotypes. Wnt3a significantly increased TCF/LEF signalling activity by about 100-fold in WT and LRRK2 KO 24 hours after stimulations ($p<0.0001$) (**Fig 5.6 A, D**). G2019S KI was not as sensitive to the stimulus as other genotypes, and statistical differences were only obtained at 48 ($p<0.05$) hours post stimulations (**Fig 5.6 G**). Both WT ($p<0.0001$), LRRK2 KO ($p<0.0001$) and G2019S KI ($p<0.01$) TCF/LEF signalling activity reached the peak at 72 hours after Wnt3a treatment (**Fig 5.6 A, D, G**). LPS was proved to trigger canonical Wnt signalling pathways, as well. Both WT ($p<0.0001$), LRRK2 KO ($p<0.0001$) and G2019S KI ($p<0.0001$) showed a significant increase of TCF/LEF activity by 10-25-fold 72 hours post treatment. LRRK2 KO was more sensitive to LPS treatment and started to show statistical differences 24 hours ($p<0.05$) and 48 hours ($p<0.05$) post-treatment when compared to basal condition (**Fig 5.6 B, E, H**). We wanted to check how Wnt3a and LPS co-treatment would affect TCF/LEF signalling activity. Under stimulated conditions, LRRK2 KO astrocyte signalling activity was significantly increased by approximately 80-fold ($p<0.0001$) at 24, 48 and 72 hours post stimulation (**Fig 5.6 F**). WT ($p<0.0001$) and G2019S KI ($p<0.01$) astrocytes also had a significantly higher TCF/LEF activity after Wnt3a/LPS co-treatments 72 hours post-stimulations compared to basal conditions (**Fig 5.6 C, I**).

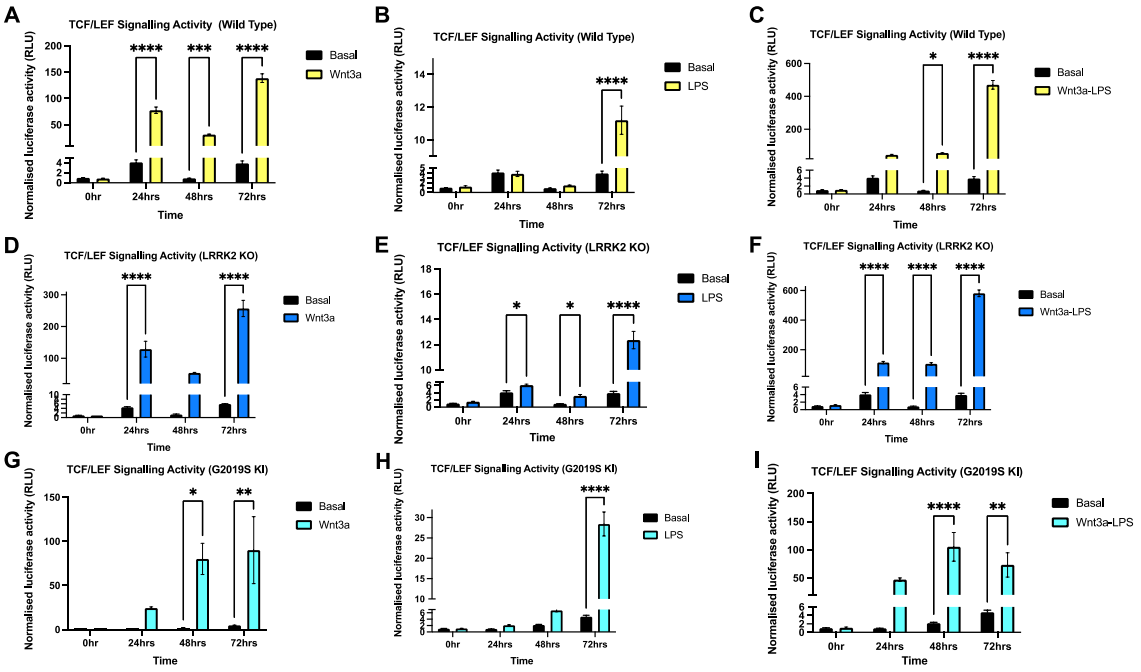


**Figure 5.6: Primary astrocytes reactivity to different stimulations**

Primary astrocytes were transduced with a lentiviral biosensor along with a TCF/LEF transcriptional factor and luciferase reporter gene. Different stimuli were applied to each of the LRRK2 genotypes. Basal condition was used as a baseline reading in comparison to stimulated conditions. Data presented as mean ± S.E.M., compared by Two-Way-ANOVA with Tukey's post hoc test, $p<0.05$ = *, $p<0.01$ = **, $p<0.001$ = ***, $p<0.0001$ = ****; One preparation of cell culture with 4-6 neonates per genotype. Cells plated into n=3 wells per treatment group per genotype.

TCF/LEF signalling activity differences were analysed between the genotypes before and after stimulations at the desired time points. LPS treatment increased TCF/LEF signalling activity, but there were no statistical differences when comparing WT to LRRK2 KO nor WT to G2019S KI. The insignificant result could be caused by the large error bars from the LPS treated samples (**Fig 5.8 A-H**). G2019S KI astrocytes had a significantly higher Wnt signalling activity after Wnt3a treatment than WT by about 5-folds after 24 hours ($p<0.0001$). Wnt signalling activity was approximately 15-fold higher ($p<0.001$) in G2019S KI astrocytes when compared to WT at 48 hours and 72 hours ($p<0.01$) post Wnt3a treatment (**Fig 5.8 D-H**). LRRK2 KO astrocytes had a slightly higher Wnt signalling activity after Wnt3a treatment compared to LRRK2 WT astrocytes; the activity level was approximately 1.4-fold higher in LRRK2 KO than WT at 48 ($p<0.01$) and 72 ($p<0.05$) hours post Wnt3a treatment (**Fig 5.8 A-D**). Wnt3a/LPS co-treatment stressed the cells and caused a significant loss of cells, which was confirmed in the next section by a confocal microscope. This could explain the dysregulation of TCF/LEF signalling activity in both LRRK2 mutants. The hypothesis was later confirmed by confocal imaging in **section 5.2.3**. G2019S KI astrocytes TCF/LEF activity level was significantly higher than WT astrocytes at 24 hours ($p<0.0001$) and 48 hours ($p<0.0001$) post stimulation by 2-fold and 10-fold, respectively (**Fig 5.8 F, G**). The activity level was significantly higher in LRRK2 KO than WT by approximately 2-fold higher at 24 hours ($p<0.01$) and 48 hours ($p<0.0001$) post Wnt3a/LPS co-treatment.

We repeated the same experiment with a lentiviral construct containing a NFAT transcriptional factor. G2019S KI astrocytes showed an increase of NFAT signalling

activity when compared to WT and LRRK2 KO at basal condition ($p<0.05$), as well as after LPS treatment ($p<0.01$) 24 hours (**Fig 5.9 B**). Interestingly, at 48 hours, LRRK2 KO astrocytes NFAT signalling activity was significantly lower than WT ($p<0.01$) and G2019S KI ($p<0.05$) by approximately 0.5-fold. LRRK2 KO ($p<0.01$) also showed a significantly lower NFAT activity level than WT 48 hours after LPS treatment. Both WT ($p<0.01$), LRRK2 KO ($p<0.001$) and G2019S KI ($p<0.0001$) astrocyte NFAT activity was significantly lower than the correspondent genotype under basal condition (**Fig 5.9 C**). 72 hours after LPS treatment, G2019S KI astrocytes NFAT activity was significantly higher than LRRK2 KO ($p<0.05$) and WT ($p<0.05$). G2019S KI NFAT signalling activity was also higher than LRRK2 KO ($p<0.05$) and WT ($p<0.01$) under basal condition, this suggested that the signalling activity differences might be due to LRRK2 genotype instead of LPS stimulation.

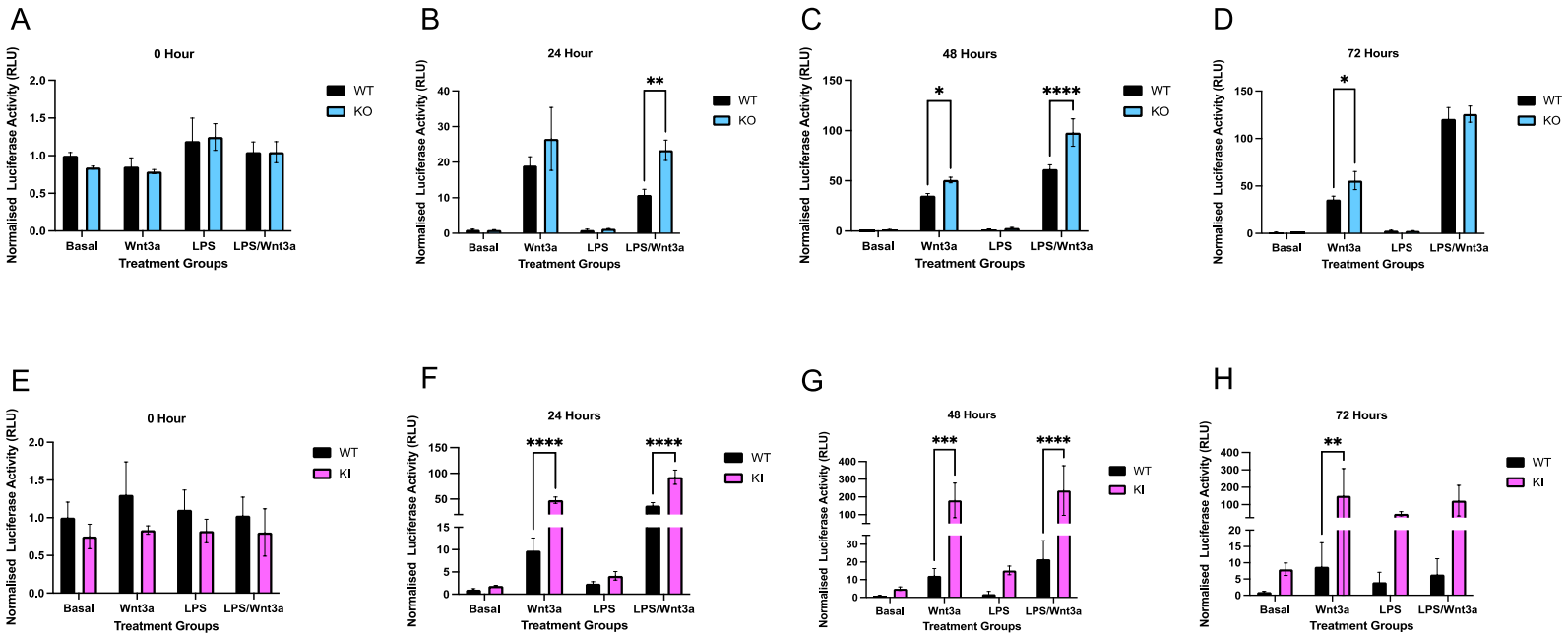


**Figure 5.8: TCF/LEF signalling activity in different LRRK2 mutants' astrocytes under basal and stimulated conditions**

Primary astrocytes were transduced with a lentiviral biosensor along with a TCF/LEF transcriptional factor and luciferase reporter gene. Wnt3a, LPS and Wnt3a/LPS were used to stimulate TCF/LEF signalling responses. At each of the timepoints, WT at basal condition was used as a baseline reading, all other samples were normalised to WT at basal condition. Data presented as mean ± S.E.M., compared by Two-Way-ANOVA with Tukey's post hoc test, $p<0.05$ = *, $p<0.01$ = **, $p<0.001$ = ***, $p<0.0001$ = ****; One preparation of cell culture with 4-6 neonates per genotype. Cells plated into n=3 wells per treatment group per genotype.

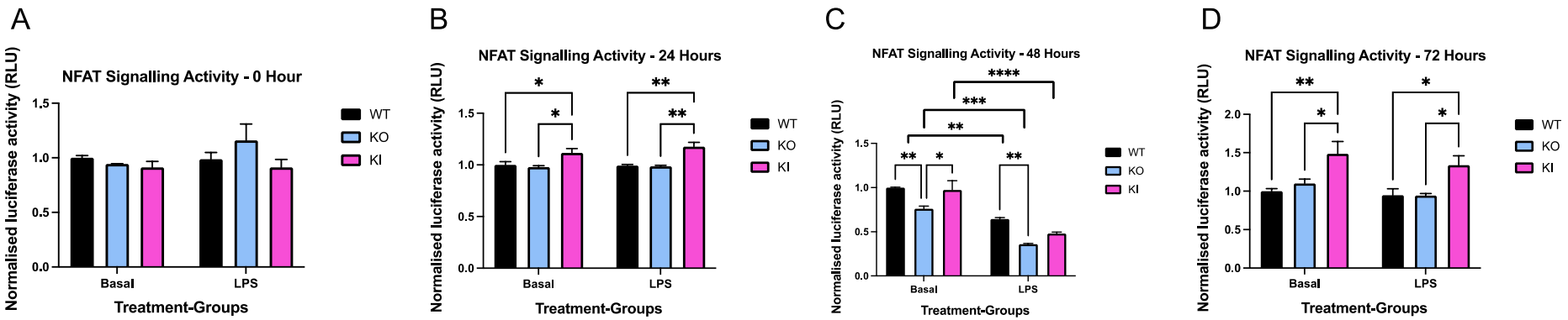


**Figure 5.9: NFAT signalling activity in different LRRK2 mutants' astrocytes after LPS stimulation**

Primary astrocytes were transduced with a lentiviral biosensor along with a NFAT transcriptional factor and luciferase reporter gene. LPS was applied to the cells to trigger immune responses. At each of the timepoint, WT at basal condition was used as a baseline reading, all other samples were normalised to WT at basal condition. Data presented as mean ± S.E.M., compared by Two-Way-ANOVA with Tukey's post hoc test, $p<0.05$ = *, $p<0.01$ = **, $p<0.001$ = ***, $p<0.0001$ = ****; One preparation of cell culture with 4-6 neonates per genotype. Cells plated into n=3 wells per treatment group per genotype.

### 5.2.3 Astrocyte morphological changes after different stimulations

LRRK2 KO and G2019S KI astrocytes demonstrated a significant increase in Wnt and NFAT signalling activity compared to WT astrocytes under different stimulations. G2019S KI astrocytes showed a much higher signalling activity than WT and LRRK2 KO astrocytes. As presented in **section 5.2.2,** cultures' Wnt and NFAT signalling activities reached the highest level at 72 hours. Therefore, we harvested the astrocytes at 72 hours and examined the morphological changes. Different shapes of astrocytes were observed in this study. Most of the astrocytes flattened out and became fibroblast-like astrocytes (**Fig 5.10 A-C**). A 2x8 tile was captured at the highest cell density position on each of the coverslips by a confocal microscope. LRRK2 KO seemed to have a higher cell density after Wnt3a and LPS stimulations (**Fig 5.12-5.13**). Wnt3a/LPS co-treatment caused a significant decrease in cell number and distorted cell morphology (**Fig 5.14**). We suspected that high cell density could be the cause of the appearance of fibroblasts like astrocytes. A standard astrocyte shape was found at the edge of the coverslip, where the cell density was relatively lower.

We first compared nuclei size within the genotype group after different stimulations. WT astrocytes nuclei size was consistent after different stimulations (**Fig 5.15 A**). LRRK2 KO astrocyte nuclei were significantly enlarged after LPS treatment when compared to basal condition ($p<0.01$) and post Wnt3a treatment ($p<0.001$). In samples treated with Wnt3a/LPS, nuclei size was significantly smaller than under basal conditions ($p<0.0001$), Wnt3a treated ($p<0.0001$), and LPS treated ($p<0.0001$)

conditions in LRRK2 KO astrocytes (**Fig 5.15 B**). G2019S KI astrocytes reacted similarly to the stimuli. After Wnt3a/LPS co-treatment, the nuclei size was significantly smaller than under LPS treated ($p<0.0001$), Wnt3a treated ($p<0.0001$) and basal conditions ($p<0.001$). Wnt3a ($p<0.001$) and LPS ($p<0.05$) treatments significantly enlarged G2019S KI nuclei size compared to G2019S KI samples under basal conditions (**Fig 5.15 C**).

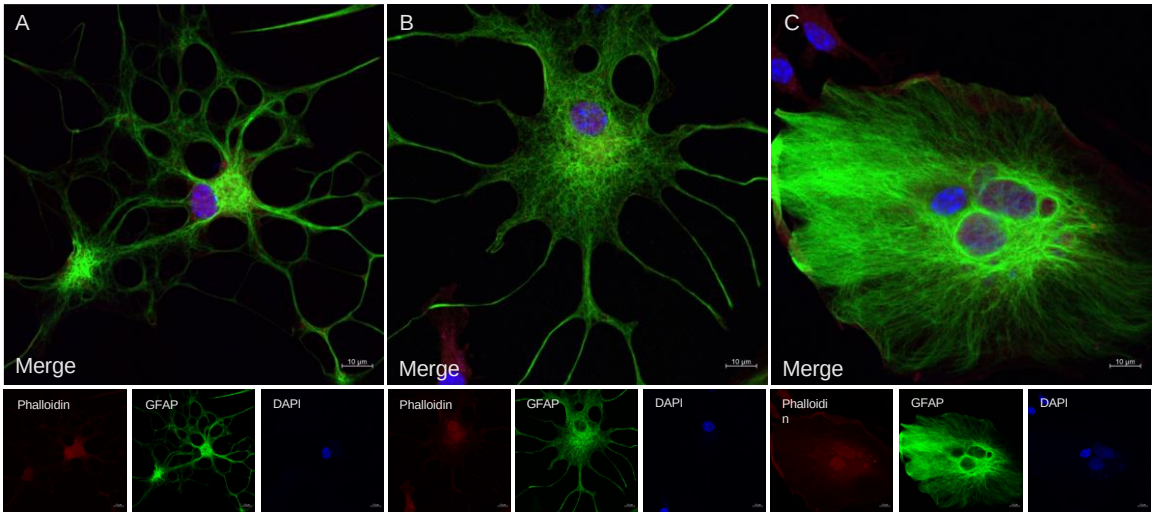


**Figure 5.10: Representative images of astrocyte isoforms**

Different isoforms of astrocytes were observed. A: Typical astrocyte shape with extended processes and branches; B: Astrocyte with flattened cell body; C: Fibroblast like astrocytes. Phalloidin was presented in red for actin staining; GFAP was presented in green for astrocyte positive cells staining; DAPI was presented in blue for nucleus staining.

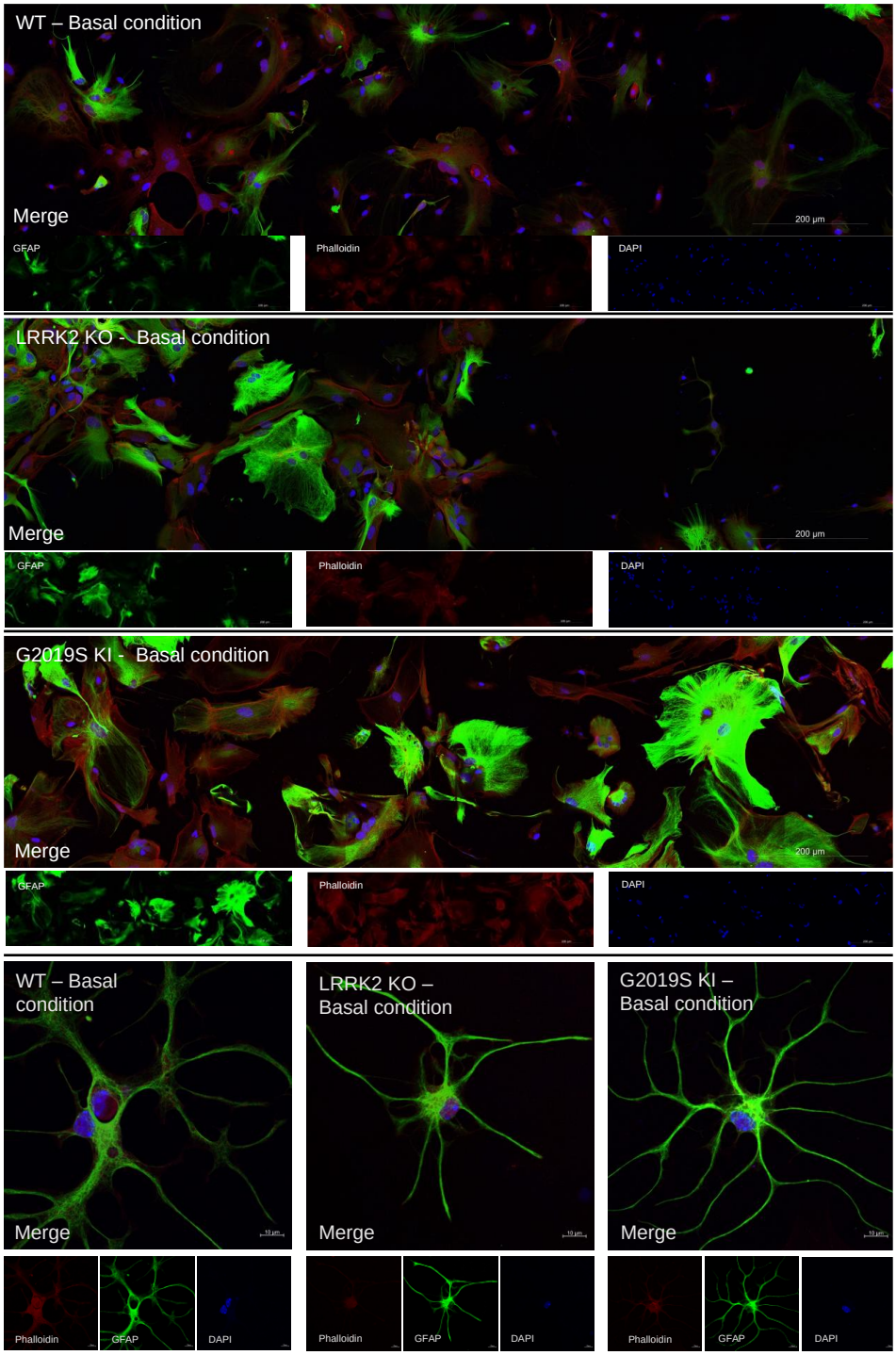


**Figure 5.11: WT, LRRK2 KO and G2019S KI astrocytes under basal conditions**

2 x 8 tiles were taken for each of the genotypes. Nuclei size was measured from the tiles. Representative single astrocyte images were presented under the tile images. Phalloidin was presented in red for actin staining; GFAP was presented in green for astrocyte positive cells staining; DAPI was presented in blue for nucleus staining. One

preparation of cell culture with 4-6 neonates per genotype. Cells plated into n=1 well per treatment group per genotype.

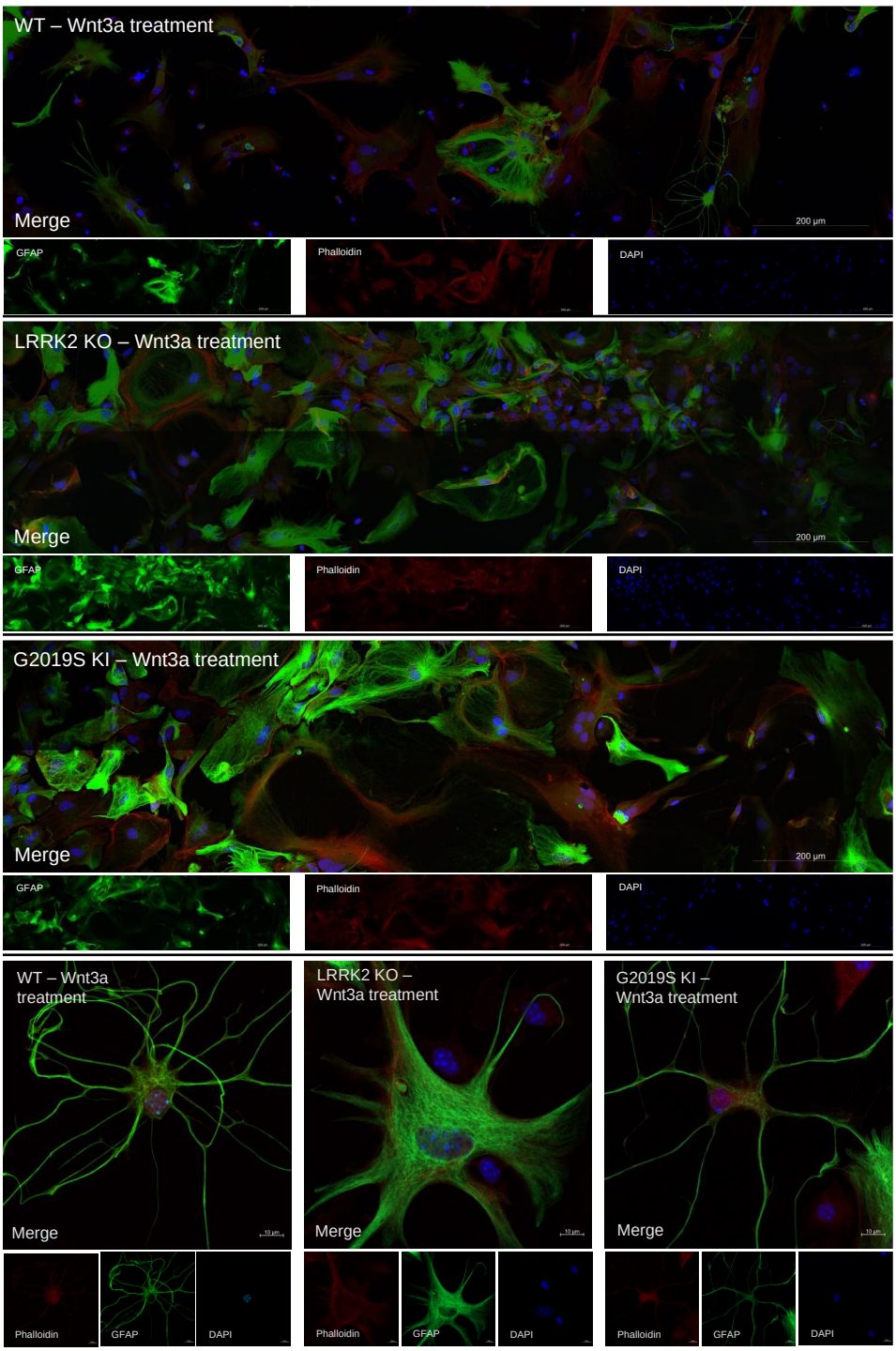


**Figure 5.12: WT, LRRK2 KO and G2019S KI astrocytes after Wnt3a stimulation**

2 x 8 tiles were taken for each of the genotypes. Nuclei size was measured from the tiles. Representative single astrocyte images were presented under the tile images. Phalloidin was presented in red for actin staining; GFAP was presented in green for astrocyte positive cells staining; DAPI was presented in blue for nucleus staining. One

preparation of cell culture with 4-6 neonates per genotype. Cells plated into n=1 well per treatment group per genotype.

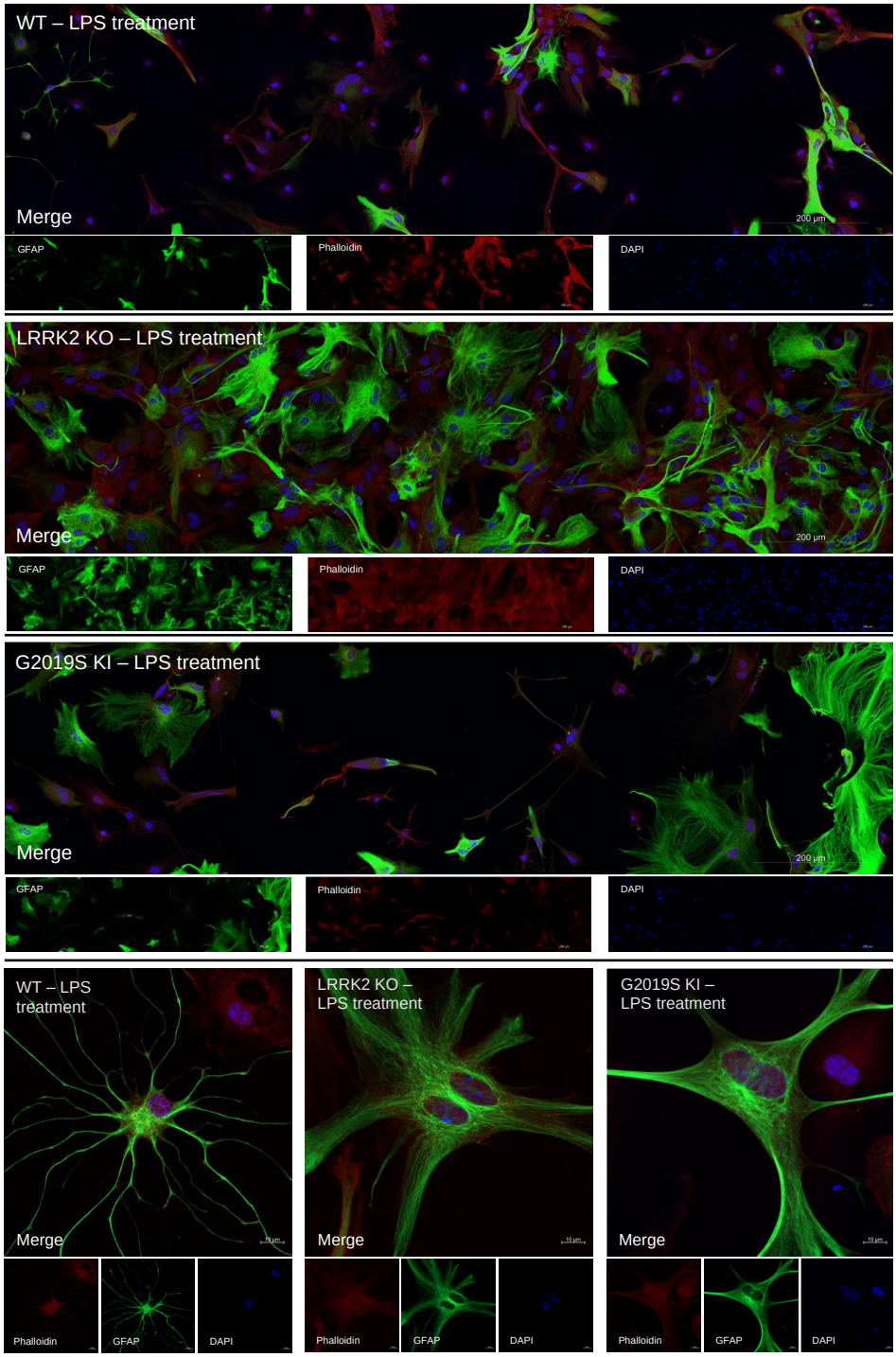


**Figure 5.13: WT, LRRK2 KO and G2019S KI astrocytes after LPS stimulation**

2 x 8 tiles were taken for each of the genotypes. Nuclei size was measured from the tiles. Representative single astrocyte images were presented under the tile images. Phalloidin was presented in red for actin staining; GFAP was presented in green for astrocyte positive cells staining; DAPI was presented in blue for nucleus staining. One

preparation of cell culture with 4-6 neonates per genotype. Cells plated into n=1 well per treatment group per genotype.

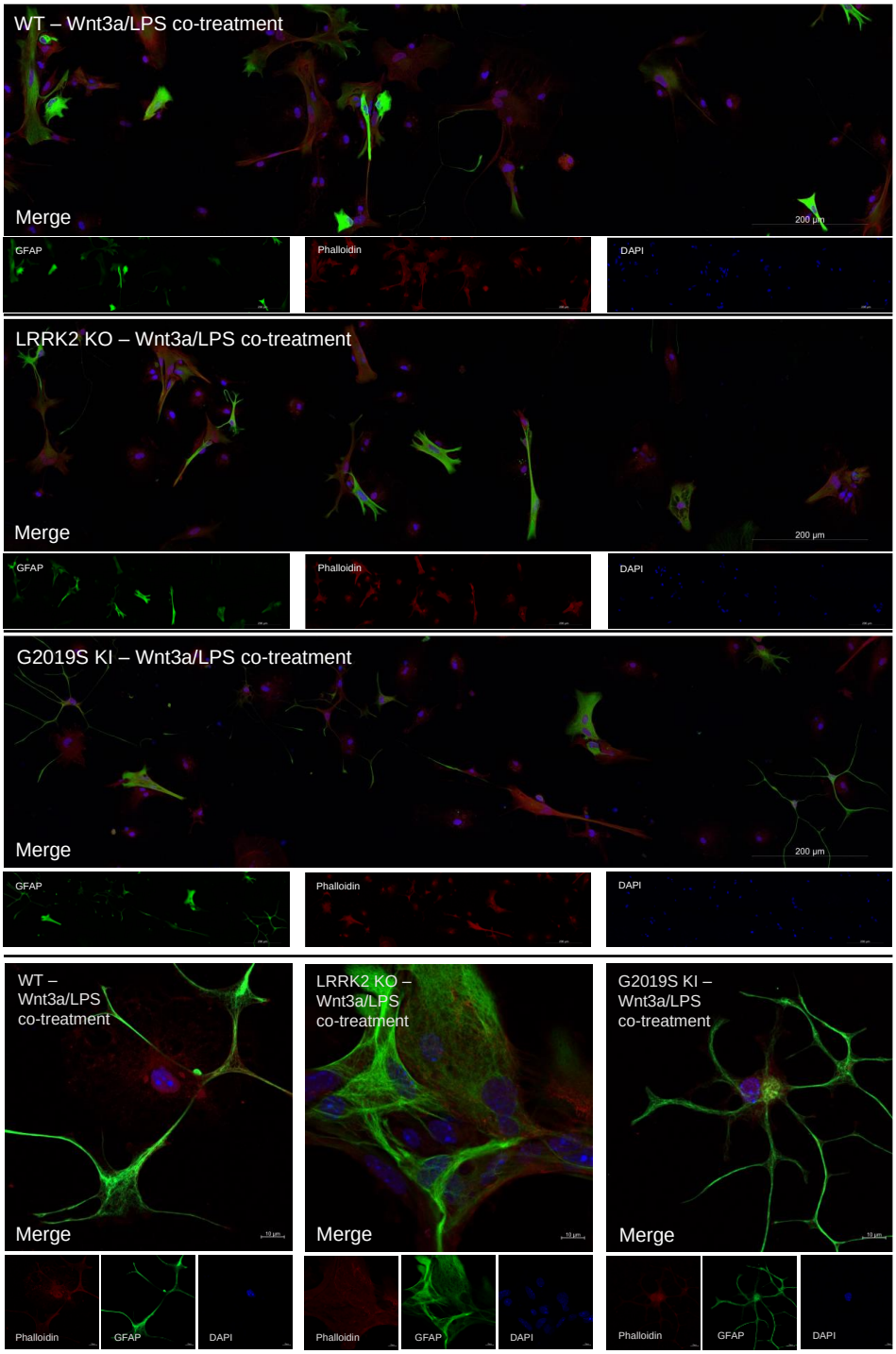


**Figure 5.14: WT, LRRK2 KO and G2019S KI astrocytes after co-stimulation**

2 x 8 tiles were taken for each of the genotypes. Nuclei size was measured from the tiles. Representative single astrocyte images were presented under the tile images. Phalloidin was presented in red for actin staining; GFAP was presented in green for astrocyte positive cells staining; DAPI was presented in blue for nucleus staining. One

preparation of cell culture with 4-6 neonates per genotype. Cells plated into n=1 well per treatment group per genotype.

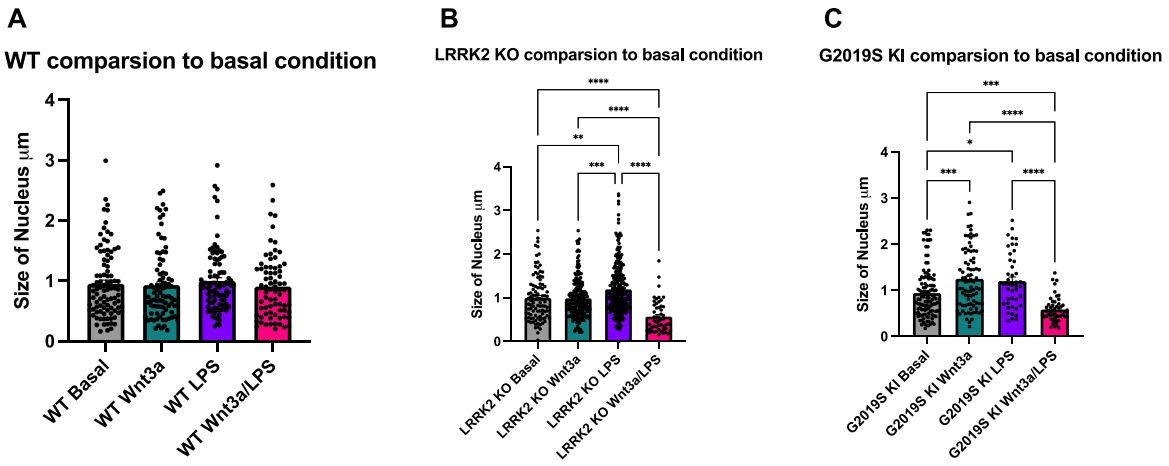


**Figure 5.15: Effect of stimuli on size of nuclei in each of the LRRK2 genotypes**

The size of nuclei was measured after different stimulation. Size of nuclei was compared within each of the genotype group after different stimulation. Data presented as mean ± S.E.M., compared by One-Way-ANOVA with Tukey's post hoc test, $p<0.05$ = *, $p<0.01$ = **, $p<0.001$ = ***, $p<0.0001$ = ****; One preparation of cell culture with 4-6 neonates per genotype. Cells plated into n=1 well per treatment group per genotype. Individual astrocyte nuclei size was measured on each of the 2x8 tiles.

WT: Basal n=95; Wnt3a n=87; LPS n=95; Wnt3a/LPS n=74

LRRK2 KO: Basal n=99; Wnt3a n=199; LPS n=267; Wnt3a/LPS n=51

G2019S KI: Basal n=119; Wnt3a n=86; LPS n=46; Wnt3a/LPS n=52

After we established the effect of the stimuli on nuclei morphology in LRRK2 genotypes, we compared the nuclei size within the genotypes under the effect of different stimuli. LRRK2 KO nuclear size tended to be larger($p=0.07$) than WT under basal conditions (**Fig 5.16 A**). When the cells were treated with Wnt3a, LRRK2 KO astrocyte nuclei were significantly bigger than WT ($p<0.05$). G2019S KI astrocyte nuclei were significantly enlarged by approximately 1.5-fold when compared to WT ($p<0.0001$) and LRRK2 KO ($p<0.0001$) (**Fig 5.16 B**). After LPS treatment, LRRK2 KO ($p<0.01$) and G2019S KI ($p<0.01$) astrocyte nuclei size was significantly bigger than WT by approximately 1.5-fold (**Fig 5.16 C**). Wnt signalling activity was significantly higher after Wnt3a/LPS co-treatment compared to basal conditions (**Fig 5.8**). However, LRRK2 KO ($p<0.01$) and G2019S KI ($p<0.05$) astrocytes nuclei size was significantly reduced compared to WT by approximately 0.5-fold (**Fig 5.16 D**). We also tried to select reactive astrocytes to measure the number of processes, the width of processors and cell volume to understand the astrocytes' activation state better. However, due to the low number of astrocytes like cells and variation in the size of processes, it was hard to measure the changes accurately. The data suggested that Wnt signalling activation significantly affects astrocyte cell morphology dependent on LRRK2 genotypes.

Overall, the data suggested that Wnt signalling activation significantly affect astrocyte cell morphology dependent on LRRK2 genotypes.

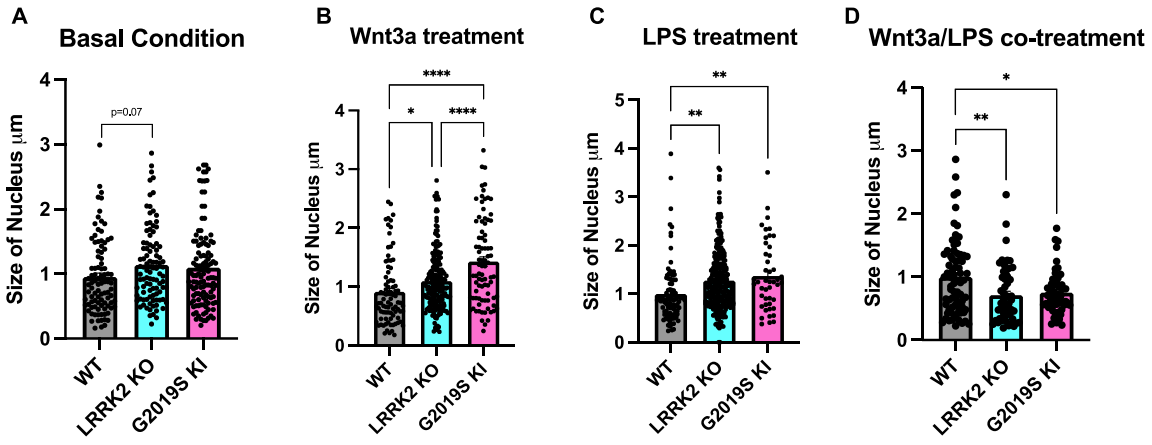


**Figure 5.16: Astrocytes morphological changes 72 hours after different stimulations**

Size of nuclei were measured and compared between WT, LRRK2 KO and G2019S KI. Cells were harvested 72 hours post stimulations. Data presented as mean ± S.E.M., compared by One-Way-ANOVA with Tukey's post hoc test, $p<0.05$ = *, $p<0.01$ = **, $p<0.001$ = ***, $p<0.0001$ = ****; One preparation of cell culture with 4-6 neonates per genotype. Cells plated into n=1 well per treatment group per genotype.

Individual astrocyte nuclei size was measured on each of the 2x8 tiles.

WT: Basal n=95; Wnt3a n=87; LPS n=95; Wnt3a/LPS n=74

LRRK2 KO: Basal n=99; Wnt3a n=199; LPS n=267; Wnt3a/LPS n=51

G2019S KI: Basal n=119; Wnt3a n=86; LPS n=46; Wnt3a/LPS n=52

## 5.2.4 *Wls* mRNA expression changes after different stimulations

Previous sections demonstrated a clear correlation between Wnt signalling activity and nuclear size in LRRK2 mutant astrocytes compared to WT. Knock-out of LRRK2 and G2019S KI might directly disrupt the scaffolds within the signalling pathways and, hence, dysregulate canonical Wnt signalling pathway mediators. Here, we examined mRNA expression changes of the signalling mediators 72 hours after Wnt3a and LPS treatments. As Wnt3a/LPS co-treatment was toxic for the cells, affecting cell survival, we did not investigate these cultures further. The mRNA expression levels of the mediators would give us a better insight into how LRRK2 interferes with Wnt signalling pathways. We observed no significant differences in canonical Wnt signalling activation at the 0-hour time point, whereas 48 hours and 72 hours post stimulation provided us with the best signalling activity levels. We investigated the mRNA expression changes within these two time points and between the genotypes under different stimulations.

Wls, a protein essential for Wnt ligand secretion, showed significantly decreased mRNA expression levels in LRRK2 KO and G2019S KI astrocytes at 48 hours after Wnt3a or LPS treatment when compared to the 72-hours timepoint but no significant differences under basal conditions (**Fig 5.17 A-C**). Interestingly, compared to the mutant, LRRK2 WT astrocytes showed a significant increase of Wls at 72 hours

compared to 48 hours under basal conditions and after Wnt3a treatment, but the opposite effect after LPS treatment underlining the difference between LRRK2 genotypes in response to different Wnt signalling activity again. It was potentially due to the high signalling activities in the cells. High Wnt ligands might result in the decreased mRNA expression level of *Wls* as a regulatory effect in the pathway. At 48 hours, there was no expression difference between the genotypes after stimulations. However, when looking at the 72 hour time point under basal condition, Wnt secretor *Wls* mRNA level was significantly reduced by about 10-20% in LRRK2 KO ($p<0.01$) and G2019S KI ($p<0.0001$) astrocytes when compared to WT. After Wnt3a stimulation *Wls* mRNA level in LRRK2 KO and G2019S KI astrocytes was approximately 50% less than WT (**Fig 5.17 D-E**).

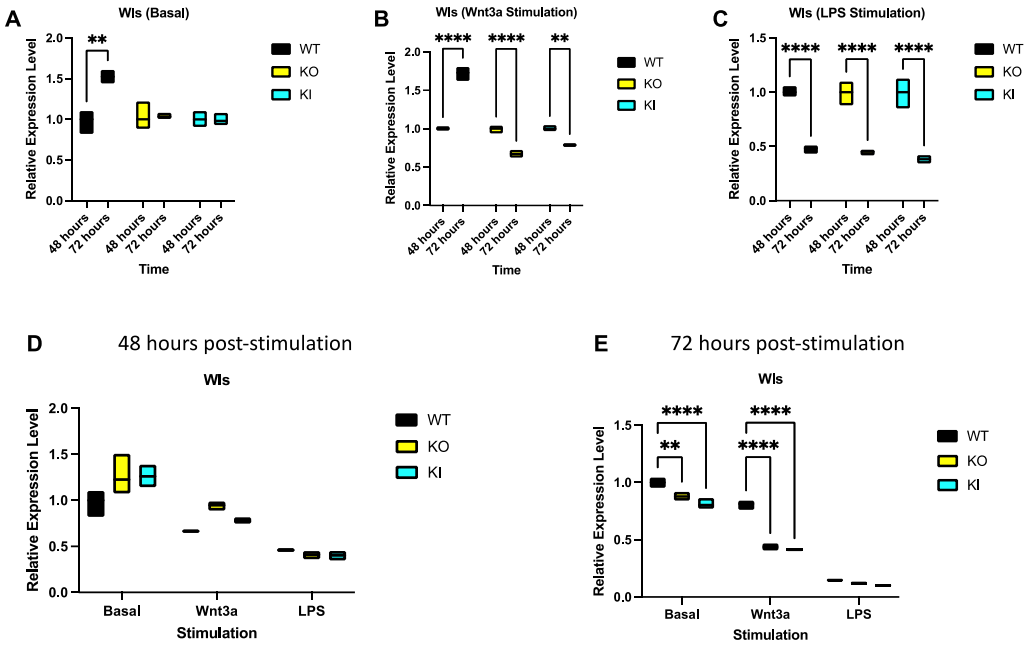


**Figure 5.17: *Wls* mRNA expression changes overtime in astrocytes after stimulations**

**A-C**: mRNA expression comparison between 48 hours and 72 hours at untreated basal condition; Wnt3a stimulation; LPS stimulation; **D-E**: Expression level comparison between different genotypes at 48 hours or 72 hours post stimulation. Data was normalised to WT under basal conditions. Data presented as mean ± S.E.M., compared by un-paired student T-test for comparison between the time points; and ONE-WAY ANOVA followed by Tukey's post hoc test for comparison between the genotypes, $p<0.05$ = *, $p<0.01$ = **, $p<0.001$ = ***, $p<0.0001$ = ****; One preparation of cell culture with 4-6 neonates per genotype. Cells plated into n=3 well per treatment group per genotype.

### 5.2.5 Wnt ligands: *Wnt5a* and *Wnt7a* mRNA expression changes after different stimulations

Under the basal condition, NFAT signalling pathway ligand *Wnt5a* mRNA level was about 50% lower ($p<0.05$) in LRRK2 KO and about 50% higher ($p<0.05$) in G2019S KI at 72 hours when compared to 48 hours. Under Wnt3a treatment, the *Wnt5a* mRNA level increased by more than 2-fold in WT and G2019S KI ($p<0.001$). LPS stimulation significantly increased *Wnt5a* mRNA level by about 20-fold in WT and G2019S KI ($p<0.0001$) when compared 72 hours and 48 hours post stimulation (**Fig 5.18 A-C**). At 48 hours, LRRK2 KO had a higher *Wnt5a* level than WT ($p<0.01$) and G2019S KI ($p<0.0001$). However, when investigating the expression level at 72 hours, *Wnt5a* mRNA level was significantly increased by 5-10-fold under LPS stimulation; LRRK2 KO ($p<0.0001$) and G2019S KI ($p<0.001$) had a significantly lower *Wnt5a* level than WT (**Fig 5.18 D-E**).

Canonical and non-canonical Wnt signalling ligand *Wnt7a* mRNA level was higher in WT ($p<0.0001$) and G2019S KI ($p<0.0001$) by about 6-fold when compared 72 hours and 48 hours post stimulation. After Wnt3a stimulation, WT ($p<0.001$) and G2019S KI ($p<0.05$) *Wnt7a* mRNA levels had about 1.5-2-fold increase after 72 hours, whereas LRRK2 KO *Wnt7a* mRNA level was decreased by about 60% ($p<0.001$) at 72 hours. LPS treatment also significantly increased *Wnt7a* mRNA level. At 72 hours, WT ($p<0.001$) and G2019S KI ($p<0.0001$) had a significantly higher *Wnt7a* mRNA level

when compared to samples collected from 48 hours. LRRK2 KO *Wnt7a* mRNA level was about 60% less ($p<0.0001$) at 72 hours when compared to 48 hours (**Fig 5.19 A-C**). By comparing the expression level between the genotypes, LRRK2 KO *Wnt7a* mRNA level was significantly higher than WT and G2019S KI under basal and Wnt3a stimulated conditions ($p<0.0001$). At 72 hours, G2019S KI *Wnt7a* mRNA level was significantly higher than WT and LRRK2 KO by about 1.5-fold ($p<0.001$) (**Fig 5.19 D**). We have observed from (**Fig 5.19 A-C**) that *the Wnt7a* mRNA level decreased over time after Wnt3a and LPS treatment. After 72 hours, Wnt3a treatment caused a significant decrease ($p<0.05$) of *Wnt7a* mRNA level in LRRK2 KO astrocytes compared to G2019S KI. *Wnt7a* mRNA level was significantly decreased in LRRK2 KO astrocytes after LPS treatment when compared to WT ($p<0.01$) and G2019S KI ($p<0.05$) (**Fig 5.19 E**).

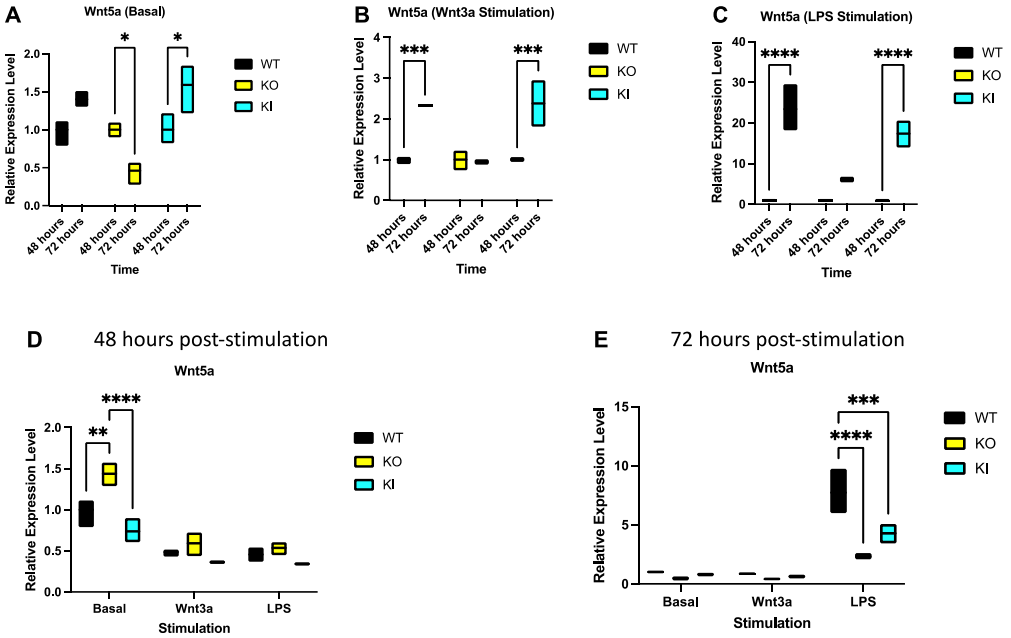


**Figure 5.18: *Wnt5a* mRNA expression changes overtime in astrocytes after stimulations**

**A-C**: mRNA expression comparison between 48 hours and 72 hours at untreated basal condition; Wnt3a stimulation; LPS stimulation; **D-E**: Expression level comparison between different genotypes at 48 hours or 72 hours post stimulation. Data was normalised to WT under basal conditions. Data presented as mean ± S.E.M., compared by un-paired student T-test for comparison between the time points; and ONE-WAY ANOVA followed by Tukey's post hoc test for comparison between the genotypes, $p<0.05$ = *, $p<0.01$ = **, $p<0.001$ = ***, $p<0.0001$ = ****; One preparation of cell culture with 4-6 neonates per genotype. Cells plated into n=3 well per treatment group per genotype.

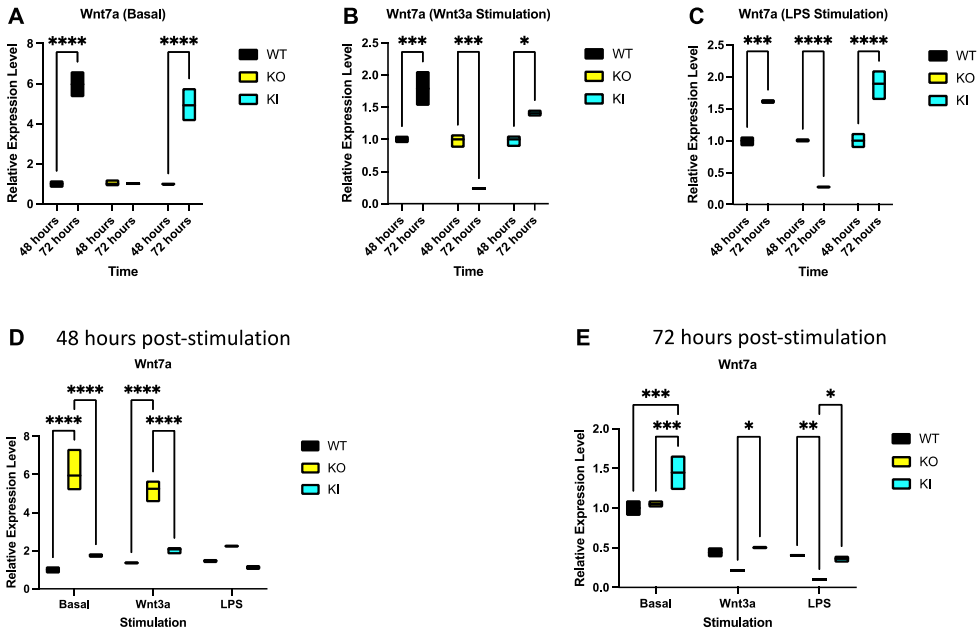


**Figure 5.19: *Wnt7a* mRNA expression changes overtime in astrocytes after stimulations**

**A-C**: mRNA expression comparison between 48 hours and 72 hours at untreated basal condition; Wnt3a stimulation; LPS stimulation; **D-E**: Expression level comparison between different genotypes at 48 hours or 72 hours post stimulation. Data was normalised to WT under basal conditions. Data presented as mean ± S.E.M., compared by un-paired student T-test for comparison between the time points; and ONE-WAY ANOVA followed by Tukey's post hoc test for comparison between the genotypes, $p<0.05$ = *, $p<0.01$ = **, $p<0.001$ = ***, $p<0.0001$ = ****; One preparation of cell culture with 4-6 neonates per genotype. Cells plated into n=3 well per treatment group per genotype.

### 5.2.5 Co-receptor and cytoplasmic component: *Lrp5* and *Dvl1-3* mRNA expression changes after different stimulations

As the pathway is activated, more Lrp5 might be required. Lrp5 mRNA expression level was significantly lower at 72 hours under the basal condition in both genotypes ($p<0.001$) compared to the expression level at 48 hours group. However, the expression level was significantly increased at 72 hours after Wnt3a and LPS stimulations in all of the genotypes by 10-15-fold ($p<0.0001$) (**Fig 5.20 A-C**). Under the basal condition, the 48 hours group LRRK2 KO astrocytes had a significantly higher *Lrp5* mRNA level ($p<0.01$) than WT, but no changes were observed under different stimulations (**Fig 5.20 D**). Wnt3a and LPS stimulation have increased *Lrp5* mRNA levels by about 5-fold compared to basal conditions. WT astrocytes had a higher *Lrp5* mRNA level than LRRK2 KO after Wnt3a ($p<0.05$) and LPS ($p<0.01$) stimulations (**Fig 5.20 E**).

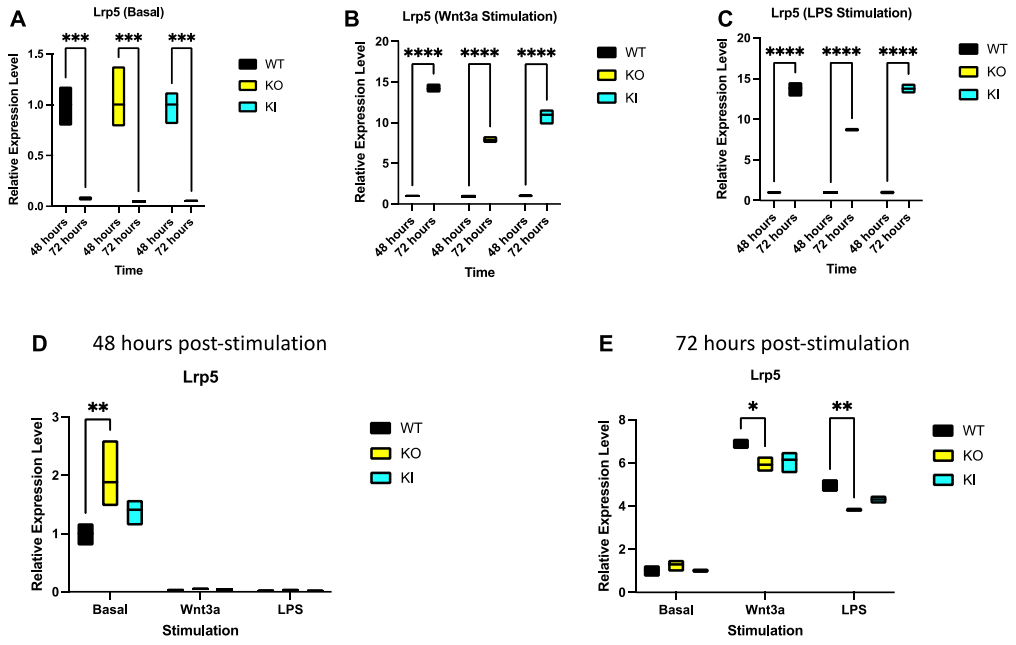


**Figure 5.20: *Lrp5* mRNA expression changes overtime in astrocytes after stimulations**

**A-C**: mRNA expression comparison between 48 hours and 72 hours at untreated basal condition; Wnt3a stimulation; LPS stimulation; **D-E**: Expression level comparison between different genotypes at 48 hours or 72 hours post stimulation. Data was normalised to WT under basal conditions. Data presented as mean ± S.E.M., compared by un-paired student T-test for comparison between the time points; and ONE-WAY ANOVA followed by Tukey's post hoc test for comparison between the genotypes, $p<0.05$ = *, $p<0.01$ = **, $p<0.001$ = ***, $p<0.0001$ = ****; One preparation of cell culture with 4-6 neonates per genotype. Cells plated into n=3 well per treatment group per genotype.

At basal condition, *Dvl1* mRNA level was significantly higher by about 3 to 4-fold in WT ($p<0.01$) and G2019S KI ($p<0.05$) in 72 hours group when compared to 48 hours group. Wnt3a did not seem to affect *the Dvl1* mRNA level in the LRRK2 mutants but caused an increase in WT ($p<0.01$). LPS, on the other hand, caused an increase in *Dvl1* mRNA level in WT and G2019S KI astrocytes at 72 hours ($p<0.001$) (**Fig 5.21 A-C**). There were no significant differences between the genotypes at 48 hours, but LRRK2 KO astrocytes showed a significant decrease in *Dvl1* mRNA level by approximately 0.5-fold when compared to WT ($p<0.01$) and G2019S KI ($p<0.05$) (**Fig 5.21 D-E**).

*Dvl2* mRNA level was higher in WT and G2019S KI under basal conditions by about 2-fold ($p<0.001$) when compared 72 hours samples with 48 hours samples. Wnt3a treatment caused an increase in the mRNA level in WT by 1.5-fold ($p<0.01$) but a decrease in LRRK2 KO by 0.5-fold ($p<0.001$) at 72 hours. LPS treatment caused a significant decrease in *Dvl2* mRNA level in all of the genotypes ($p<0.0001$) at 72 hours (**Fig 5.22 A-C**). At 48 hours, LRRK2 KO astrocytes had a significantly higher *Dvl2* mRNA level than WT and G2019S KI ($p<0.01$) by approximately 2-fold under basal conditions. The *Dvl2* mRNA expression difference in LRRK2 KO astrocytes was significantly higher after Wnt3a treatment ($p<0.0001$) when compared to WT and ($p<0.001$) when compared to G2019S KI. LPS treatment caused an increase in *Dvl2* mRNA level in LRRK2 KO when compared to WT by about 1.5-fold ($p<0.05$) and approximately 2-fold when compared to G2019S KI ($p<0.05$). *Dvl2* mRNA level was higher in WT when compared to G2019S KI ($p<0.0001$)

(**Fig 5.22 D**). Interestingly, when investigating *Dvl2* mRNA level at 72 hours, LRRK2 KO ($p<0.0001$) and G2019S KI ($p<0.01$) *Dvl2* mRNA levels were about 50% less when compared to WT after Wnt3a treatment. LPS treatment also caused a reduction in *Dvl2* mRNA level in LRRK2 KO ($p<0.0001$) and G2019S KI ($p<0.05$) when compared to WT. G2019S KI *Dvl2* mRNA level was significantly lower than LRRK2 KO ($p<0.05$) (**Fig 5.22 E**).

Under the basal condition in 72 hours, samples of WT and G2019S KI astrocytes *Dvl3* mRNA levels were significantly higher than samples collected at 48 hours ($p<0.0001$). Wnt3a ($p<0.0001$) and LPS ($p<0.001$) treatment increased *Dvl3* mRNA level in WT astrocytes by 2-fold at 72 hours (**Fig 5.23 A-C**). When comparing the expression differences between the genotypes with the 48 hours samples, LRRK2 KO had a significantly higher *Dvl3* mRNA level than WT and G2019S KI astrocytes under basal conditions ($p<0.05$). After 72 hours post stimulation, Wnt3a and LPS caused a reduction of *Dvl3* mRNA level in LRRK2 KO astrocytes, and the expression level was about 40-50% lower when compared to WT ($p<0.05$). (**Fig 5.23 D-E**).

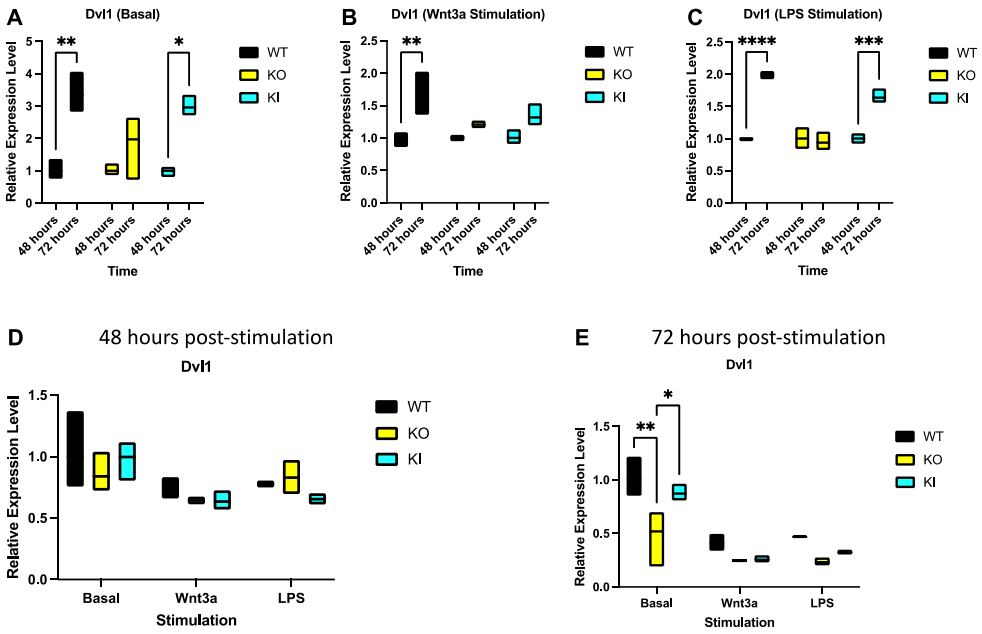


**Figure 5.21: *Dvl1* mRNA expression changes overtime in astrocytes after stimulations**

**A-C**: mRNA expression comparison between 48 hours and 72 hours at untreated basal condition; Wnt3a stimulation; LPS stimulation; **D-E**: Expression level comparison between different genotypes at 48 hours or 72 hours post stimulation. Data was normalised to WT under basal conditions. Data presented as mean ± S.E.M., compared by un-paired student T-test for comparison between the time points; and ONE-WAY ANOVA followed by Tukey's post hoc test for comparison between the genotypes, $p<0.05$ = *, $p<0.01$ = **, $p<0.001$ = ***, $p<0.0001$ = ****; One preparation of cell culture with 4-6 neonates per genotype. Cells plated into n=3 well per treatment group per genotype.

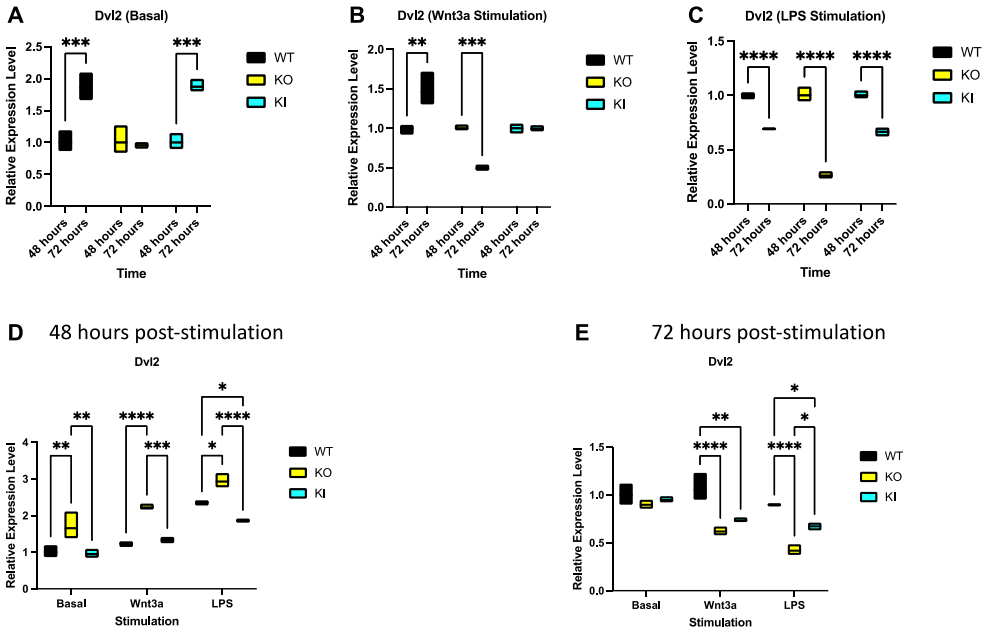


**Figure 5.22: *Dvl2* mRNA expression changes overtime in astrocytes after stimulations**

**A-C**: mRNA expression comparison between 48 hours and 72 hours at untreated basal condition; Wnt3a stimulation; LPS stimulation; **D-E**: Expression level comparison between different genotypes at 48 hours or 72 hours post stimulation. Data was normalised to WT under basal conditions. Data presented as mean ± S.E.M., compared by un-paired student T-test for comparison between the time points; and ONE-WAY ANOVA followed by Tukey's post hoc test for comparison between the genotypes, $p<0.05$ = *, $p<0.01$ = **, $p<0.001$ = ***, $p<0.0001$ = ****; One preparation of cell culture with 4-6 neonates per genotype. Cells plated into n=3 well per treatment group per genotype.

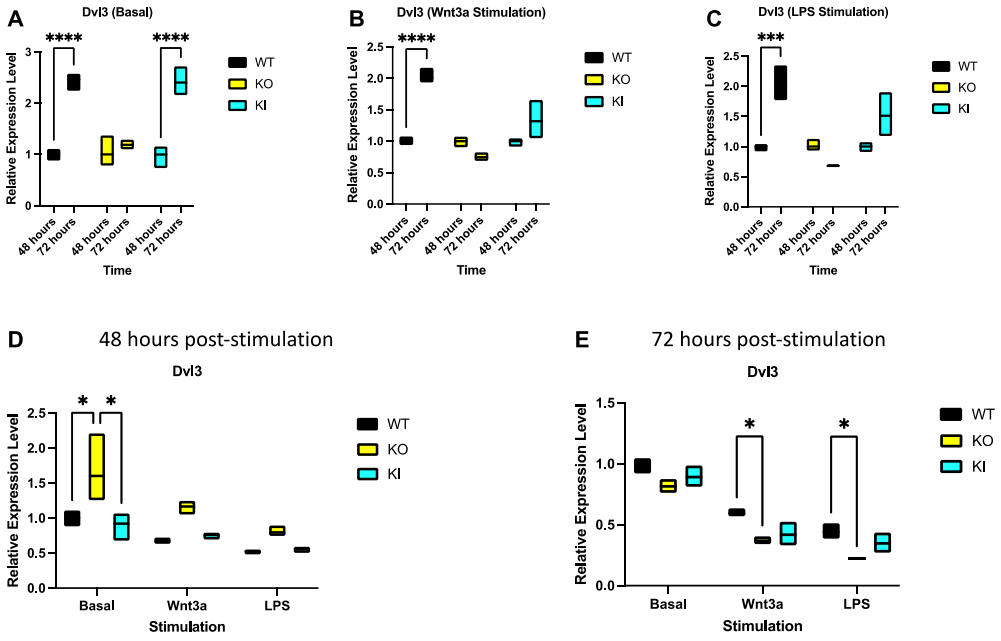


**Figure 5.23: *Dvl3* mRNA expression changes overtime in astrocytes after stimulations**

**A-C**: mRNA expression comparison between 48 hours and 72 hours at untreated basal condition; Wnt3a stimulation; LPS stimulation; **D-E**: Expression level comparison between different genotypes at 48 hours or 72 hours post stimulation. Data was normalised to WT under basal conditions. Data presented as mean ± S.E.M., compared by un-paired student T-test for comparison between the time points; and ONE-WAY ANOVA followed by Tukey's post hoc test for comparison between the genotypes, $p<0.05$ = *, $p<0.01$ = **, $p<0.001$ = ***, $p<0.0001$ = ****; One preparation of cell culture with 4-6 neonates per genotype. Cells plated into n=3 well per treatment group per genotype.

## 5.2.6 β-catenin destruction complex: *β-catenin*, *Gsk3β* and *Axin2* mRNA expression changes after different stimulations

Under basal conditions, WT and G2019S KI astrocytes had a higher *β-catenin* mRNA level by about 2.5 folds at 72 hours when compared to 48 hours samples ($p<0.0001$). Wnt3a treatment caused a significant increase of *β-catenin* mRNA level in WT at 72 hours ($p<0.001$) by almost 3-fold and a slightly decreased *b-catenin* mRNA level in LRRK2 KO ($p<0.05$). LPS caused a significant decrease of *β-catenin* mRNA levels in WT ($p<0.001$), LRRK2 KO ($p<0.0001$) and G2019S KI ($p<0.0001$) astrocytes (**Fig 5.24 A-C**). LRRK2 KO astrocytes had a significantly higher *b-catenin* mRNA level than WT and G2019S KI ($p<0.05$) by about 2-fold under the basal condition in 48 hours group. LPS treatment caused an increase in *β-catenin* mRNA level in all the genotypes, where LRRK2 KO *β-catenin* mRNA level was about 2-fold higher than WT ($p<0.001$) and G2019S KI ($p<0.01$) (**Fig 5.24 D**). At 72 hours, LRRK2 KO astrocytes showed a lower *b-catenin* mRNA level than the other genotypes ($p<0.05$). Wnt3a treatment caused a significant reduction of *β-catenin* mRNA levels in all the study groups by about 80% folds in 48 and 72 hours groups. However, no differences were observed between the genotypes. LPS also caused LRRK2 KO to have a lower *β-catenin* mRNA level than WT ($p<0.0001$) by about 0.5-fold and slightly less than G2019S KI ($p<0.05$). G2019S KI *β-catenin* mRNA level was about 0.5-fold less when compared to WT ($p<0.01$) (**Fig 5.24 E**).

*Gsk3β* mRNA level was similar when comparing the 48 hours samples to 72 hours samples under the basal condition in all genotypes. Wnt3a treatment caused a reduction of *Gsk3β* mRNA level by about 50% at 72 hours compared to 48 hours. 72 hours after LPS treatment *Gsk3β* mRNA level was increased by about 40% in WT ($p<0.05$), but a reduction of *Gsk3β* mRNA level in LRRK2 KO ($p<0.05$) astrocytes was observed when compared to 48 hours samples (**Fig 5.25 A-C**). There were no significant differences between the genotypes after different treatments at 48 hours (**Fig 5.25 D**). At 72 hours, LRRK2 KO ($p<0.01$) and G2019S KI ($p<0.05$) astrocytes *Gsk3β* mRNA levels were significantly lower than WT under basal conditions. Wnt3a treatment caused a significant reduction of *Gsk3β* mRNA level in LRRK2 KO astrocytes than WT ($p<0.01$) (**Fig 5.25 E**).

*Axin2* mRNA level was approximately 1.5-fold higher in 72 hours of collected samples than 48 hours under basal conditions ($p<0.05$). 72 hours post Wnt3a treatment caused a significant decrease of *Axin2* mRNA level in LRRK2 KO ($p<0.0001$) and G2019S KI ($p<0.01$) when compared to 48 hours samples. LPS triggered an increase in *Axin2* mRNA level in WT astrocytes ($p<0.01$) at 72 hours when compared to 48 hours samples (**Fig 5.26 A-C**). Wnt3a treatment increased *Axin2* mRNA level by approximately 3-fold than samples under basal conditions. WT had a higher *Axin2* mRNA level than LRRK2 KO ($p<0.05$) and G2019S KI ($p<0.01$) astrocytes after Wnt3a treatment (**Fig 5.26 D**). At 72 hours, WT astrocytes had higher *Axin2* mRNA levels than LRRK2 KO and G2019S samples. Under the basal condition, LRRK2 KO ($p<0.05$) and G2019S KI ($p<0.01$) astrocytes *Axin2* mRNA level was about 0.5-fold lower than WT. After Wnt3a treatment, LRRK2

mutants' *Axin2* mRNA level was about 2-fold less than WT ($p<0.0001$). LPS also caused a significantly lower *Axin2* mRNA level in LRRK2 KO ($p<0.001$) and G2019S KI ($p<0.05$) astrocytes when compared to WT (**Fig 5.26 E**).

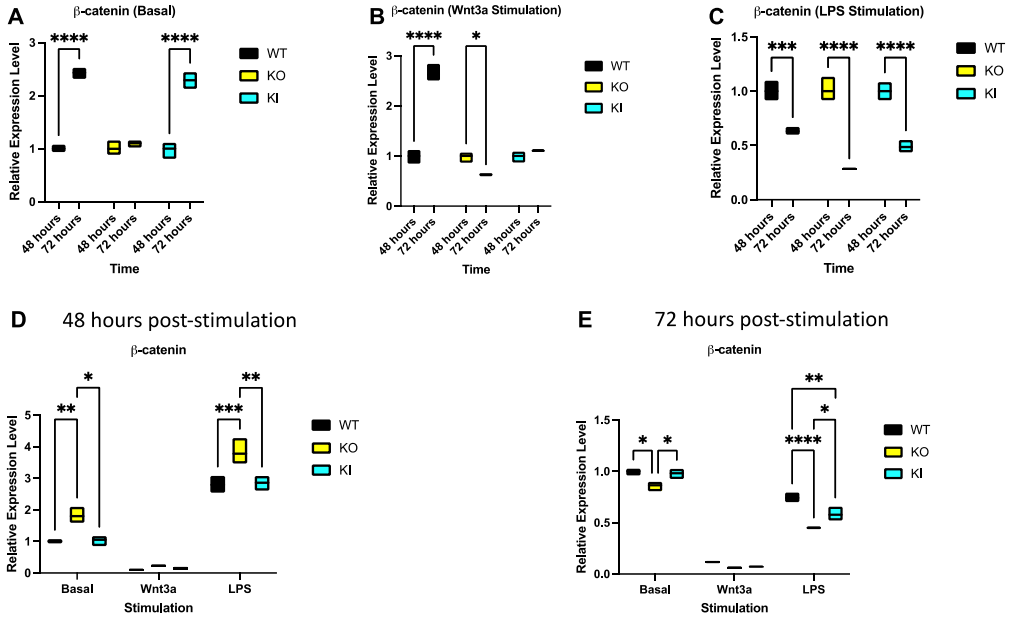


**Figure 5.24: *β-catenin* mRNA expression changes overtime in astrocytes after stimulations**

**A-C**: mRNA expression comparison between 48 hours and 72 hours at untreated basal condition; Wnt3a stimulation; LPS stimulation; **D-E**: Expression level comparison between different genotypes at 48 hours or 72 hours post stimulation. Data was normalised to WT under basal conditions. Data presented as mean ± S.E.M., compared by un-paired student T-test for comparison between the time points; and ONE-WAY ANOVA followed by Tukey's post hoc test for comparison between the genotypes, $p<0.05$ = *, $p<0.01$ = **, $p<0.001$ = ***, $p<0.0001$ = ****; One preparation of cell culture with 4-6 neonates per genotype. Cells plated into n=3 well per treatment group per genotype.

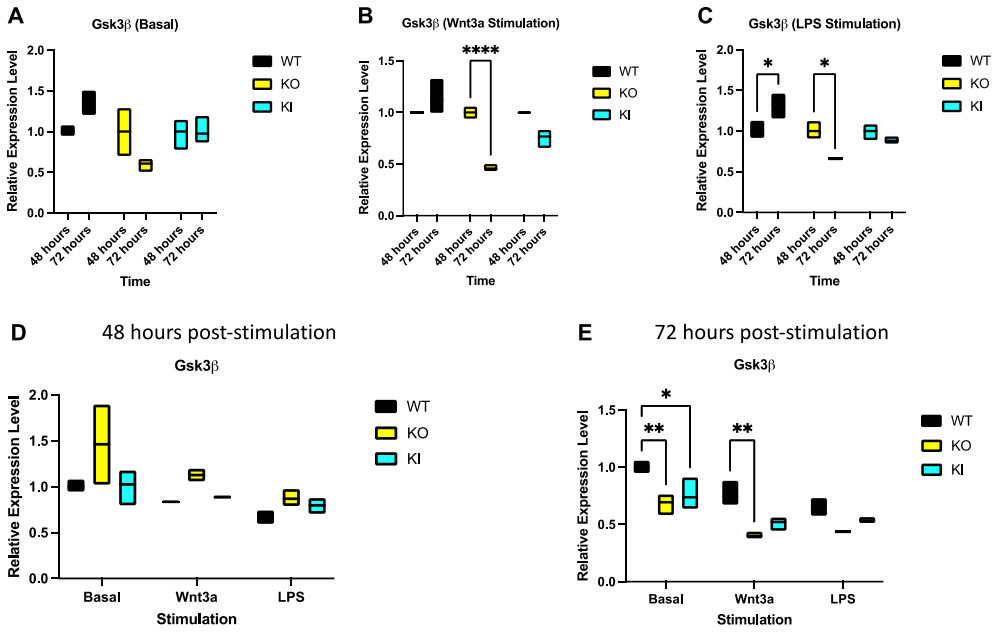


**Figure 5.25: *Gsk3β* mRNA expression changes overtime in astrocytes after stimulations**

**A-C**: mRNA expression comparison between 48 hours and 72 hours at untreated basal condition; Wnt3a stimulation; LPS stimulation; **D-E**: Expression level comparison between different genotypes at 48 hours or 72 hours post stimulation. Data was normalised to WT under basal conditions. Data presented as mean ± S.E.M., compared by un-paired student T-test for comparison between the time points; and ONE-WAY ANOVA followed by Tukey's post hoc test for comparison between the genotypes, $p<0.05$ = *, $p<0.01$ = **, $p<0.001$ = ***, $p<0.0001$ = ****; One preparation of cell culture with 4-6 neonates per genotype. Cells plated into n=3 well per treatment group per genotype.

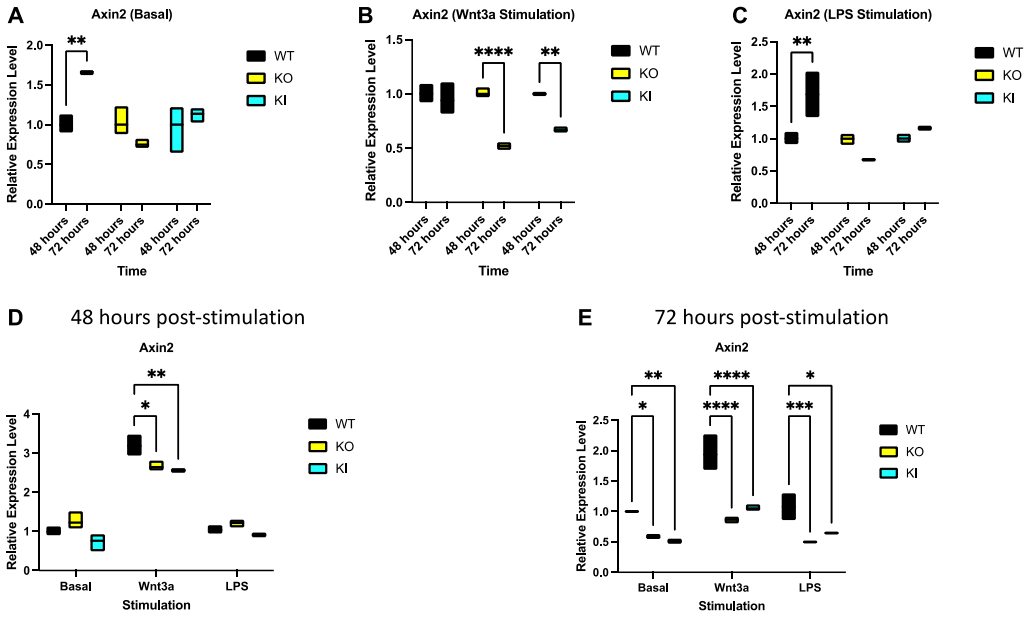


**Figure 5.26: *Axin2* mRNA expression changes overtime in astrocytes after stimulations**

**A-C**: mRNA expression comparison between 48 hours and 72 hours at untreated basal condition; Wnt3a stimulation; LPS stimulation; **D-E**: Expression level comparison between different genotypes at 48 hours or 72 hours post stimulation. Data was normalised to WT under basal conditions. Data presented as mean ± S.E.M., compared by un-paired student T-test for comparison between the time points; and ONE-WAY ANOVA followed by Tukey's post hoc test for comparison between the genotypes, $p<0.05$ = *, $p<0.01$ = **, $p<0.001$ = ***, $p<0.0001$ = ****; One preparation of cell culture with 4-6 neonates per genotype. Cells plated into n=3 well per treatment group per genotype.

## 5.2.7 Transcriptional factors: *Tcf1*, *Nfat, Nfκb* and *Creb* mRNA expression changes after different stimulations

Different transcriptional factors' mRNA expression levels were investigated. *Tcf1* mRNA level was 3-fold higher in WT ($p<0.0001$), and the expression level was also 2-fold higher ($p<0.01$) in G2019S KI astrocytes when compared 72 hours samples to 48 hours samples. Wnt3a treatment increased *Tcf1* mRNA level by 1.5-fold in WT, but approximately 0.5-fold less in LRRK2 KO astrocytes when compared 72 hours cohorts to 48 hours cohorts. LPS stimulation caused an approximately 1.5-fold incease in WT at 72 hours compared to 48 hours samples (**Fig 5.27 A-C**). Samples collected at 48 hours showed that LRRK2 KO astrocytes had a slightly higher *Tcf1* mRNA level than G2019S KI astrocytes under basal condition ($p<0.05$) and after LPS stimulation ($p<0.05$) (**Fig 5.27 D).** Interestingly, in samples collected at 72 hours, LRRK2 KO ($p<0.0001$) and G2019S KI ($p<0.001$) astrocytes had a significantly lower *Tcf1* mRNA level than WT under basal conditions. Wnt3a stimulation also significantly decreased *Tcf1* mRNA level in LRRK2 KO compared to WT ($p<0.01$). LPS stimulation caused a significant reduction of *Tcf1* mRNA level in LRRK2 KO ($p<0.001$) and G2019S KI ($p<0.05$) when compared to WT (**Fig 5.27 E**).

*The Creb* mRNA level was approximately 2-fold higher ($p<0.01$) in WT and 3-fold higher ($p<0.0001$) in G2019S KI astrocytes when comparing the samples from 72

hours to the 48 hours samples. Wnt3a treatment further increased the mRNA level to about 3.5-fold ($p<0.0001$) in WT and 3-fold ($p<0.0001$) in G2019S KI astrocytes in 72 hours samples. LPS stimulation caused an increase in *Creb* mRNA level in WT ($p<0.01$) and G2019S KI ($p<0.05$) when compared 72 hours to 48 hours samples (**Fig 5.28 A-C**). In the 48 hours samples analysis, LRRK2 KO astrocytes had a significantly higher *Creb* mRNA level than WT and G2019S KI astrocytes by approximately 1.7-fold ($p<0.0001$). *Creb* mRNA was about 1.5-fold higher in LRRK2 KO astrocytes than WT ($p<0.001$) and G2019S KI ($p<0.01$) after Wnt3a stimulations. (**Fig 5.28 D**). WT showed a significant increase in *Creb* mRNA level compared to LRRK2 KO ($p<0.001$) and G2019S KI ($p<0.05$) after 72 hours of Wnt3a treatment (**Fig 5.28 E**)

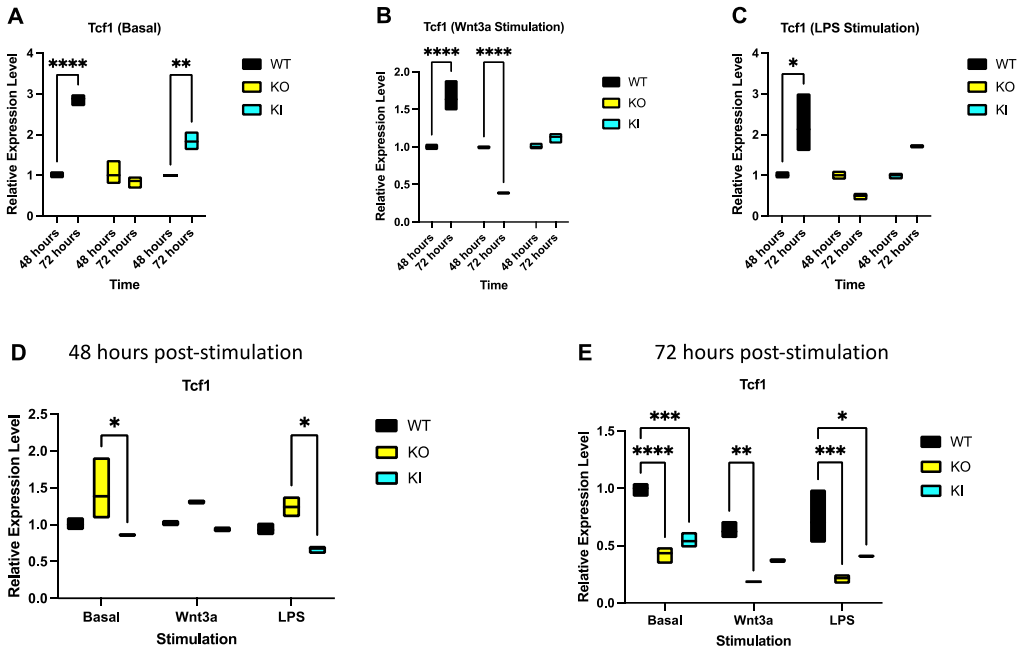


**Figure 5.27: *Tcf1* mRNA expression changes overtime in astrocytes after stimulations**

**A-C**: mRNA expression comparison between 48 hours and 72 hours at untreated basal condition; Wnt3a stimulation; LPS stimulation; **D-E**: Expression level comparison between different genotypes at 48 hours or 72 hours post stimulation. Data was normalised to WT under basal conditions. Data presented as mean ± S.E.M., compared by un-paired student T-test for comparison between the time points; and ONE-WAY ANOVA followed by Tukey's post hoc test for comparison between the genotypes, $p<0.05$ = *, $p<0.01$ = **, $p<0.001$ = ***, $p<0.0001$ = ****; One preparation of cell culture with 4-6 neonates per genotype. Cells plated into n=3 well per treatment group per genotype.

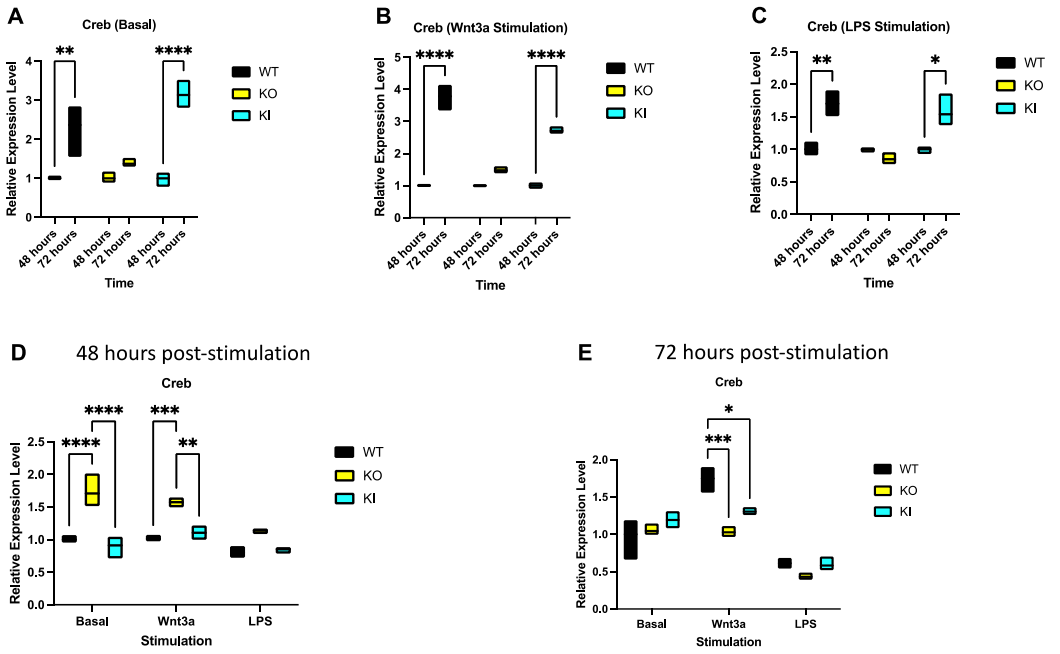


**Figure 5.28: *Creb* mRNA expression changes overtime in astrocytes after stimulations**

**A-C**: mRNA expression comparison between 48 hours and 72 hours at untreated basal condition; Wnt3a stimulation; LPS stimulation; **D-E**: Expression level comparison between different genotypes at 48 hours or 72 hours post stimulation. Data was normalised to WT under basal conditions. Data presented as mean ± S.E.M., compared by un-paired student T-test for comparison between the time points; and ONE-WAY ANOVA followed by Tukey's post hoc test for comparison between the genotypes, $p<0.05$ = *, $p<0.01$ = **, $p<0.001$ = ***, $p<0.0001$ = ****; One preparation of cell culture with 4-6 neonates per genotype. Cells plated into n=3 well per treatment group per genotype.

WT, LRRK2 KO, and G2019S KI astrocytes collected at 72 hours had a significantly lower *Nfat* mRNA level than samples collected at 48 hours by approximately 50% ($p<0.0001$). Wnt3a treatment significantly increased *Nfat* mRNA level in 72 hours WT astrocytes samples by about 1.6-fold ($p<0.0001$) and G2019S KI astrocytes by about 1.5-fold ($p<0.01$) when compared to samples collected from 48 hours. LRRK2 KO *Nfat* mRNA level was slightly decreased at 72 hours ($p<0.05$). LRRK2 KO astrocytes showed a 50% reduction of *Nfat* mRNA level 72 hours after LPS treatment compared to cells treated for 48 hours (**Fig 5.29 A-C**). LRRK2 KO astrocytes demonstrated an approximately 1.6-fold higher *Nfat* mRNA level when compared to WT and G2019S KI samples ($p<0.0001$) under the basal condition at 48 hours (**Fig 5.29 D**). Astrocytes collected at 72 hours showed different results. LRRK2 KO ($p<0.001$) and G2019S KI ($p<0.01$) *Nfat* mRNA levels were significantly higher than WT. LRRK2 KO astrocytes had a lower *Nfat* mRNA level than WT ($p<0.01$) after Wnt3a treatment. LPS treatment also caused a significant decrease in *Nfat* mRNA level in LRRK2 KO astrocytes when compared to WT ($p<0.001$) and G2019S KI ($p<0.01$) (**Fig 5.29 E**).

WT and G2019S KI astrocytes had significantly higher *Nfκb* mRNA levels at 72 hours compared to 48 hours by about 4-fold ($p<0.0001$), and LRRK2 KO also had a slightly higher *Nfκb* mRNA level at 72 hours. The expression level difference was less after Wnt3a treatment. WT and G2019S KI astrocytes *Nfκb* mRNA levels were about 2-fold ($p<0.0001$) and 1.5-fold ($p<0.05$) at 72 hours when compared to 48 hours, respectively. Wnt3a caused a significant reduction of *Nfκb* mRNA level in LRRK2 KO by approximately 50% 72 hours after stimulation compared to samples from 48 hours.

Astrocytes treated with LPS for 72 hours showed a significant decrease in *Nfκb* mRNA level in WT ($p<0.05$), G2019S KI ($p<0.01$) and LRRK2 KO ($p<0.0001$) when compared to samples collected at 48 hours (**Fig 5.30 A-C**).

Samples collected at 48 hours, LRRK2 KO astrocytes had a significantly higher *Nfκb* mRNA level than WT ($p<0.001$) and G2019S KI ($p<0.01$) at basal condition. Wnt3a significantly increased LRRK2 KO astrocytes *Nfκb* mRNA level by about 2 folds when compared to WT ($p<0.0001$) and G2019S KI (p,0.001). LRRK2 KO astrocytes treated with LPS had a slightly higher *Nfκb* mRNA level than WT and G2019S KI ($p<0.05$) (**Fig 5.30 D**). Wnt3a treatment, on the other hand, caused a reduction in *Nfκb* mRNA level in LRRK2 KO astrocytes compared to WT ($p<0.05$) (**Fig 5.30 E**).

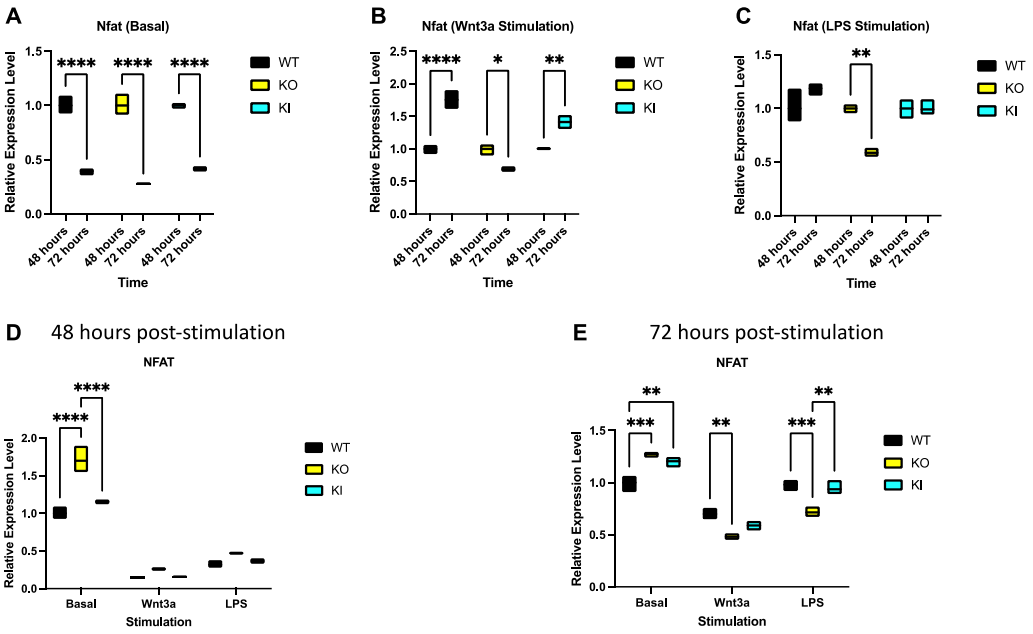


**Figure 5.29: *Nfat* mRNA expression changes overtime in astrocytes after stimulations**

**A-C**: mRNA expression comparison between 48 hours and 72 hours at untreated basal condition; Wnt3a stimulation; LPS stimulation; **D-E**: Expression level comparison between different genotypes at 48 hours or 72 hours post stimulation. Data was normalised to WT under basal conditions. Data presented as mean ± S.E.M., compared by un-paired student T-test for comparison between the time points; and ONE-WAY ANOVA followed by Tukey's post hoc test for comparison between the genotypes, $p<0.05$ = *, $p<0.01$ = **, $p<0.001$ = ***, $p<0.0001$ = ****; One preparation of cell culture with 4-6 neonates per genotype. Cells plated into n=3 well per treatment group per genotype.

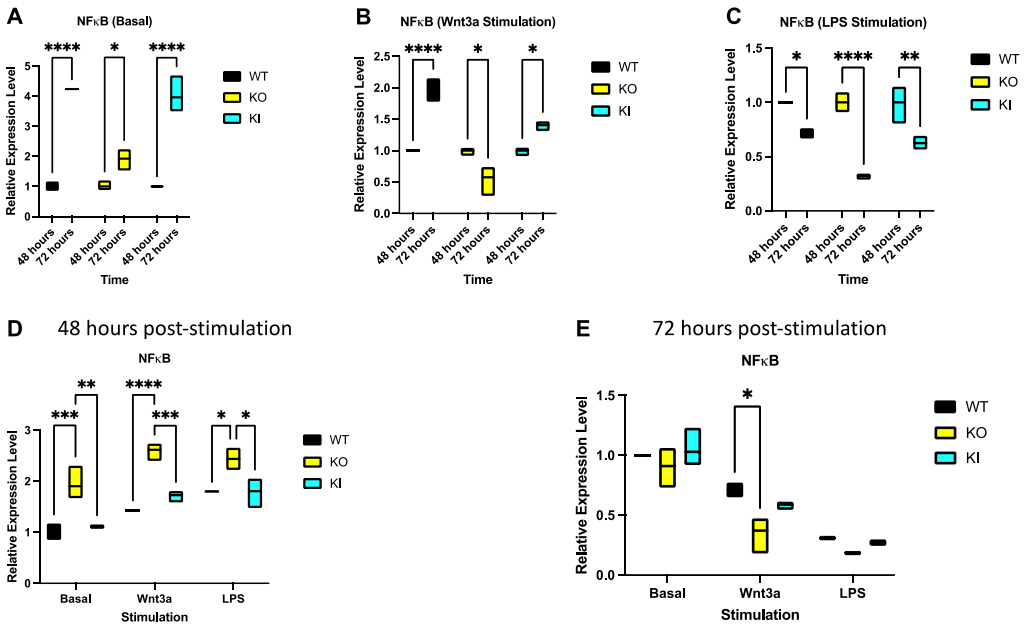


**Figure 5.30: *NFκB* mRNA expression changes overtime in astrocytes after stimulations**

**A-C**: mRNA expression comparison between 48 hours and 72 hours at untreated basal condition; Wnt3a stimulation; LPS stimulation; **D-E**: Expression level comparison between different genotypes at 48 hours or 72 hours post stimulation. Data was normalised to WT under basal conditions. Data presented as mean ± S.E.M., compared by un-paired student T-test for comparison between the time points; and ONE-WAY ANOVA followed by Tukey's post hoc test for comparison between the genotypes, $p<0.05$ = *, $p<0.01$ = **, $p<0.001$ = ***, $p<0.0001$ = ****; One preparation of cell culture with 4-6 neonates per genotype. Cells plated into n=3 well per treatment group per genotype.

## 5.2.8 Downstream targets: *Bdnf*, *Cyclin-D1, Cox2* mRNA expression changes after different stimulations

At basal conditions, the *Bdnf* mRNA level was significantly higher ($p<0.001$) in LRRK2 KO astrocytes collected at 72 hours than samples from 48 hours. After 72 hours post-Wnt3a stimulation, WT and LRRK2 KO astrocytes *Bdnf* mRNA levels were approximately 2.5-fold ($p<0.0001$) and 3-fold ($p<0.0001$) higher than samples collected from 48 hours., respectively. G2019S KI astrocytes showed a 2-fold increase ($p<0.05$) of *Bdnf* mRNA level at 72 hours compared to 48 hours samples. When G2019S KI astrocytes were treated with LPS, the *Bdnf* mRNA level was decreased by about 50% compared to samples collected at 72 hours to samples collected at 48 hours post stimulation (**Fig 5.31 A-C**). After 48 hours of Wnt3a treatment, LRRK2 KO astrocytes' *Bdnf* mRNA level was significantly reduced when compared to WT ($p<0.01$) and G2019S KI ($p<0.001$) astrocytes. LPS treatment, however, significantly increased *Bdnf* mRNA level in G2019S KI when compared to WT and LRRK2 KO samples ($p<0.05$) (**Fig 5.31 D**). 72 hours post Wnt3a treatment significantly increased *Bdnf* mRNA level in all genotypes, especially in WT when compared to LRRK2 KO ($p<0.01$) and G2019S KI ($p<0.05$) astrocytes (**Fig 5.31 E**).

Under the basal condition, WT ($p<0.0001$), LRRK2 KO ($p<0.001$) and G2019S KI ($p<0.01$) astrocytes showed a significantly higher *Cyclin-D1* mRNA level at 72 hours compared to samples collected at 48 hours. WT astrocytes' *Cyclin-D1* mRNA level

was significantly higher in 72 hours cohorts than 48 hours cohorts by more than 1.5-fold ($p<0.0001$), but LRRK2 KO astrocytes had a significantly lower *Cyclin-D1* mRNA level by about 50% 72 hours post Wnt3a treatment. 72 hours of LPS treatment significantly increased *Cyclin-D1* mRNA level in WT by about 8-fold ($p<0.0001$) and 4-fold ($p<0.0001$) in G2019S KI astrocytes compared to samples treated with LPS for 48 hours (**Fig 5.32 A-C**). At the 48-hour time point, LRRK2 KO ($p<0.0001$) and G2019S KI ($p<0.01$) astrocytes *Cyclin-D1* mRNA levels were significantly lower than WT astrocytes under basal conditions. WT astrocytes' *Bdnf* mRNA level was significantly higher than LRRK2 KO ($p<0.001$) and G2019S KI ($p<0.0001$) astrocytes by approximately 50% after Wnt3a treatment (**Fig 5.32 D**). Astrocytes collected at 72 hours showed more significant differences between the genotypes. LRRK2 KO ($p<0.0001$) and G2019S KI ($p<0.0001$) astrocytes *Cyclin-D1* mRNA levels were significantly lower than WT astrocytes by approximately 50% under basal conditions. Wnt3a treatment caused a significant reduction of *Cyclin-D1* mRNA level in all genotypes, LRRK2 KO ($p<0.0001$ and G2019S KI ($p<0.001$) astrocytes had a significant reduction of *Cyclin-D1* mRNA levels when compared to WT. LRRK2 KO ($p<0.0001$) and G2019S KI ($p<0.0001$) astrocytes *Cyclin-D1* mRNA levels were more than 50% less when compared to WT after LPS treatment (**Fig 5.32 E**).

Under the basal condition, inflammatory mediator *Cox2* mRNA was significantly higher by about 5-fold LRRK2 KO astrocytes collected at 72 hours compared to samples from 48 hours. Wnt3a treatment significantly increased *Cox2* mRNA level by approximately 40-fold in LRRK2 KO astrocytes collected at 72 hours compared to samples collected at 48 hours. However, LPS treatment decreased *Cox2* mRNA level

by more than 50% in WT ($p<0.0001$) and G2019S KI ($p<0.0001$) astrocytes 72 hours post stimulation compared to 48 hours cohort (**Fig 5.33 A-C**). After 48 hours post LPS treatment, LRRK2 KO astrocytes had a significantly lower *Cox2* mRNA level than WT ($p<0.0001$) and G2019S KI ($p<0.0001$) astrocytes, whereas G2019S KI samples had a slightly higher *Cox2* mRNA level than WT astrocytes ($p<0.01$) (**Fig 5.33 D**). However, after 72 hours post Wnt3a treatment, LRRK2 KO had a significantly higher *Cox2* mRNA level than WT ($p<0.0001$) and G2019S KI ($p<0.0001$) astrocytes by approximately 4-fold and 2-fold, respectively. G2019S KI astrocytes also demonstrated a higher *Cox2* mRNA level than WT ($p<0.01$) after Wnt3a treatment. LPS treatment significantly increased *Cox2* mRNA in LRRK2 KO astrocytes when compared to WT ($p<0.0001$) and G2019S KI ($p<0.0001$) astrocytes by approximately 2-fold and 1.5-fold, on the other hand, *Cox2* mRNA level was significantly higher in G2019S KI astrocytes than WT ($p<0.0001$) (**Fig 5.33 E**).

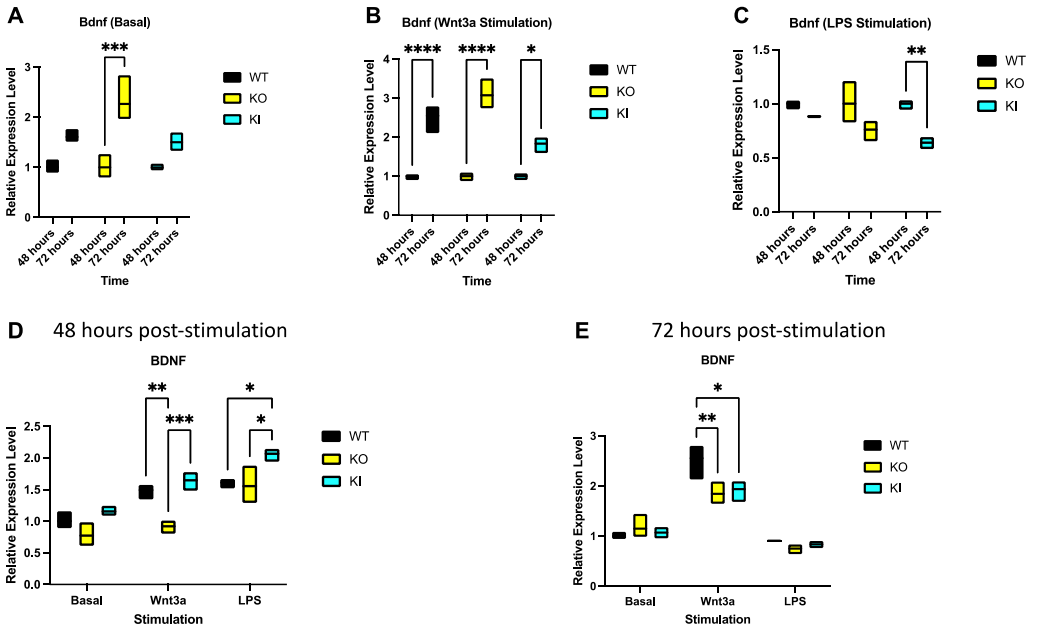


**Figure 5.31: *Bdnf* mRNA expression changes overtime in astrocytes after stimulations**

**A-C**: mRNA expression comparison between 48 hours and 72 hours at untreated basal condition; Wnt3a stimulation; LPS stimulation; **D-E**: Expression level comparison between different genotypes at 48 hours or 72 hours post stimulation. Data was normalised to WT under basal conditions. Data presented as mean ± S.E.M., compared by un-paired student T-test for comparison between the time points; and ONE-WAY ANOVA followed by Tukey's post hoc test for comparison between the genotypes, $p<0.05$ = *, $p<0.01$ = **, $p<0.001$ = ***, $p<0.0001$ = ****; One preparation of cell culture with 4-6 neonates per genotype. Cells plated into n=3 well per treatment group per genotype.

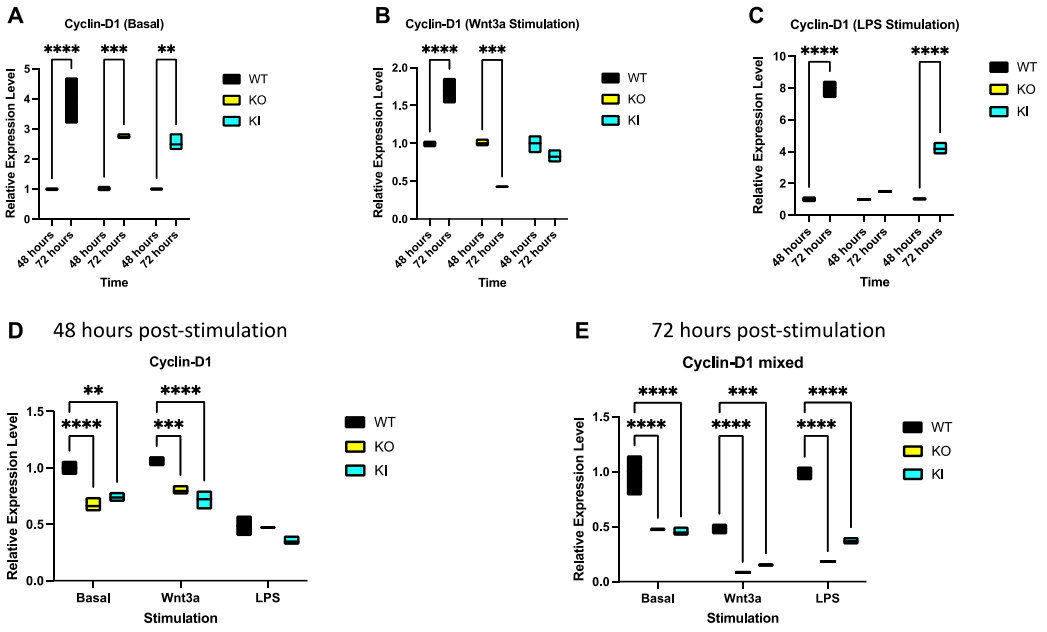


**Figure 5.32: *Cyclin-D1* mRNA expression changes overtime in astrocytes after stimulations**

**A-C**: mRNA expression comparison between 48 hours and 72 hours at untreated basal condition; Wnt3a stimulation; LPS stimulation; **D-E**: Expression level comparison between different genotypes at 48 hours or 72 hours post stimulation. Data was normalised to WT under basal conditions. Data presented as mean ± S.E.M., compared by un-paired student T-test for comparison between the time points; and ONE-WAY ANOVA followed by Tukey's post hoc test for comparison between the genotypes, $p<0.05$ = *, $p<0.01$ = **, $p<0.001$ = ***, $p<0.0001$ = ****; One preparation of cell culture with 4-6 neonates per genotype. Cells plated into n=3 well per treatment group per genotype.

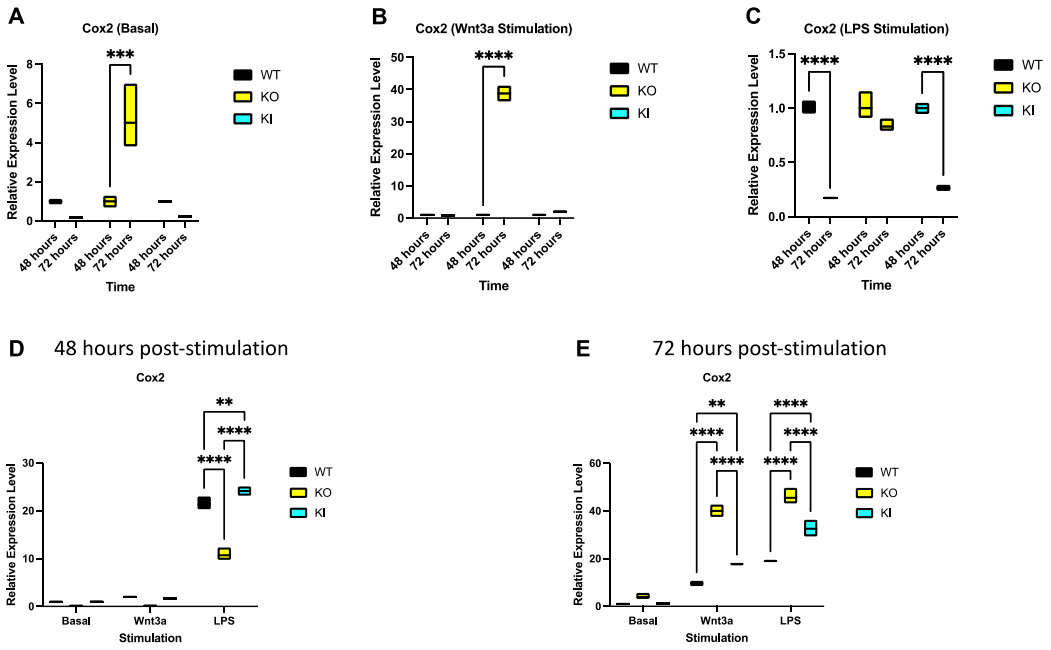


**Figure 5.33: *Cox2* mRNA expression changes overtime in astrocytes after stimulations**

**A-C**: mRNA expression comparison between 48 hours and 72 hours at untreated basal condition; Wnt3a stimulation; LPS stimulation; **D-E**: Expression level comparison between different genotypes at 48 hours or 72 hours post stimulation. Data was normalised to WT under basal conditions. Data presented as mean ± S.E.M., compared by un-paired student T-test for comparison between the time points; and ONE-WAY ANOVA followed by Tukey's post hoc test for comparison between the genotypes, $p<0.05$ = *, $p<0.01$ = **, $p<0.001$ = ***, $p<0.0001$ = ****; One preparation of cell culture with 4-6 neonates per genotype. Cells plated into n=3 well per treatment group per genotype.

### 5.2.9 Overview

mRNA expression in WT primary astrocytes under basal condition was used as a benchmark in comparisons to samples collected from LRRK2 KO and G2019S KI primary astrocytes after different stimulations. There was a clear effect LRRK2 mutants having a significant effect in Wnt signalling regulations in the primary culture. A table summarised the total number of significant expression differences in LRRK2 KO and G2019S KI compared to WT (**Table 5.1**).

Most significant mRNA expression level differences were found in LRRK2 KO and G2019S KI after either Wnt3a or LPS stimulations. Non-canonical transcriptional factor *Nfat* mRNA level was upregulated, and canonical transcriptional factor *Tcf1* mRNA level was downregulated compared to WT in both LRRK2 mutants under basal condition. However, both LRRK2 mutants dysregulated the Wnt signalling component mRNA expression in a similar manner after stimulations. Both canonical and non-canonical pathways transcriptional factors were dysregulated in the same direction in both LRRK2 mutants compared to WT. However, the different mRNA expression level between LRRK2 KO and G2019S KI astrocytes suggested the LRRK2 mutants might cause the dysregulated under different mechanisms.

**Table 5.1: Summary table of the LRRK2 KO and G2019S KI significant mRNA expression changes compared to WT mice in primary astrocytes after different stimulations.**

↑ indicates an upregulation compared to WT; ↓ indicates a downregulation compared to WT.

| Post 72 hours of treatment | | Basal condition | | | Wnt3a treated | | | LPS treated | | |
|---|---|---|---|---|---|---|---|---|---|---|
| | mRNA | WT vs LRRK2 KO | WT vs G2019S KI | LRRK2 KO vs G2019S KI | WT vs LRRP2 KO | WT vs G2019S KI | LRRK2 KO vs G2019S KI | WT vs LRRK2 KO | WT vs G2019S KI | LRRK2 KO vs G2019S KI |
| Wnt ligands secretion mediator | *Wls* | ↓↓ | ↓↓↓↓ | | ↓↓↓↓ | ↓↓↓↓ | | | | |
| Co-receptor | *Lrp5* | | | | ↓ | | | ↓↓ | | |
| Wnt ligands | *Wnt5a* | | | | | ↓ | | ↓↓↓↓ | ↓↓↓ | |
| | *Wnt7a* | ↑↑↑ | ↑↑↑ | | | | ↑ | ↓↓ | | ↑ |
| Cytoplasmic components | *Dvl1* | ↓↓ | | ↑ | | | | | | |
| | *Dvl2* | | | | ↓↓↓↓ | ↓↓ | | ↓↓↓↓ | ↓ | ↑ |
| | *Dvl3* | | | | ↓ | | | ↓ | | |
| β-catenin destruction complex | *Gsk3β* | ↓↓ | ↓ | | ↓↓ | | | | | |
| | *β-catenin* | ↓ | | ↓ | | | | ↓↓↓↓ | ↓↓ | ↑ |
| | *Axin2* | ↓ | ↓↓ | | ↓↓↓↓ | ↓↓↓↓ | | ↓↓↓ | ↓ | |
| Non-canonical pathway Transcriptional factors | *Nfat* | ↑↑↑ | ↑↑ | | ↓↓ | | | ↓↓↓ | | ↑↑ |
| | *Nfκb* | | | | ↓ | | | | | |
| Canonical pathway Transcriptional factors | *Tcf1* | ↓↓↓↓ | ↓↓↓ | | ↓↓ | | | ↓↓↓ | ↓ | |
| | *Creb* | | | | ↓↓↓ | ↓ | | | | |
| Downstream targets | *Cyclin-d1* | ↓↓↓↓ | ↓↓↓↓ | | ↓↓↓↓ | ↓↓↓ | | ↓↓↓↓ | ↓↓↓↓ | |
| | *Bdnf* | | | | ↓↓ | ↓ | | | | |
| | *Cox2* | | | | ↑↑↑↑ | ↑↑ | ↓↓↓↓ | ↑↑↑↑ | ↑↑↑↑ | ↓↓↓↓ |

# 5.3 Discussion

This chapter investigated the effect of Wnt and NFAT signalling activation in primary astrocyte and neuronal cultures. As LiCl and ionomycin treatment did not result in reliable signalling stimulation in our assays, we decided to use more physiological ligands throughout our study; Wnt3a as a canonical Wnt ligand and LPS as a ligand for the TLR4 receptor. Vehicle control was not used in this study. Each stimulus was prepared with a different solvent reagent, as the product information protocol instructed. WT under basal conditions treated with a culture medium was used as a control. Adding both solvent reagents into the culture medium as a vehicle control might affect the result's accuracy, which needs to be examined in future studies. Ideally, each treatment group should pair up with an individual group basal condition with a vehicle control treatment. However, due to stock limitation, all treated groups had to be correlated to the same control group. Therefore, no vehicle control, only the non-treated group, was used in this study.

Our findings showed that Wnt and NFAT signalling activity was depleted in pure hippocampal and cortical neuron culture compared to samples co-cultured with glial cells. This might suggest that Wnt signalling regulations differs between these cell types and activity is higher in glia cells. We therefore decided to focus on astrocytes, one of the most abundant glial cell types, contributing 20-40% of the neuroglia in the brain. Astrocytes have various functions in the brain, from development over

supporting neural networks and balancing extracellular ions to brain damage repair (Sofroniew and Vinters, 2010, Khakh and Sofroniew, 2015). Importantly, it was reported by Zhang *et al* that astrocytes have a higher LRRK2 expression than neurons and microglia in mice. It is worthwhile noting that the LRRK2 expression profile is different in humans with more LRRK2 expression in microglia and macrophages and similar LRRK2 expression levels in neurons and astrocytes (Zhang et al., 2016b). Taken together the different LRRK2 expression levels reported in mouse astrocytes and neurons and the *in vitro* Wnt signalling activity data from our primary cultures, we suggest that LRRK2 plays an essential role in Wnt and NFAT signalling regulations, and the LRRK2 expression level might be crucial. When the pathway was activated, LRRK2 KO and G2019S KI tended to increase Wnt signalling activity, and G2019S KI dysregulated Wnt signalling activity the most (**Fig 5.8**). This could potentially be caused by increased kinase activity in the G2019S mutation. As reported previously by our group, loss of LRRK2 increased Wnt signalling activity, while LRRK2 kinase inhibition decreased Wnt signalling activity in WT controls (Berwick et al., 2017). Although the underlying mechanism remains unclear, loss of LRRK2 or increased kinase activity might upregulate Wnt signalling activity and lead to abnormal cell growth. It was also reported that activation of Wnt signalling interrupts astrogliogenesis in the mouse spinal cord development (Sun et al., 2019). Therefore, LRRK2 mutants might predominantly affect Wnt signalling regulations, especially in astrocytes under a physiological state, potentially leading to neurodegenerations.

We observed the morphology of astrocytes in different LRRK2 genotype study groups. The majority of the GFAP positive cells were fibroblast like astrocytes in the higher cell

density area on the coverslips. Barbar *et al* also demonstrated that astrocytes have a variety of shapes in culture. The study has shown that serum in the growth medium causes astrocytes to expand and flatten to become a fibroblast like form (Prah et al., 2019). The results demonstrated in their study supported that the astrocytes we cultured were not fibroblast contamination, and our cells were also identified as GFAP positive. The cells displayed in our culture were likely to be reactive astrocytes with a flattened star shape (**Fig 5.11-5.14**) (Barbar et al., 2020).

Previous research states that increased mRNA or protein level in the nucleus causes an enlargement (Kume et al., 2017, Neumann and Nurse, 2007). The enlarged nucleus size in LRRK2 KO and G2019S KI samples after Wnt3a and LPS stimulations could be caused by the increased translocations of b-catenin or NFAT into the nucleus due to higher signalling activities. Nuclear dysregulation has been linked to neurodegenerations, one example is the significant increase of NFκB translocation into the nucleus in PD patients' dopaminergic neurons (Hunot et al., 1997). Abnormal nuclear changes are also linked to AD, which impacts the response to oxidative stress, the release of inflammatory mediators and DNA damage response (Iatrou et al., 2021). It has been reviewed in detail that nuclear distortion could potentially result in nuclear inclusion diseases and neurodegenerative diseases, such as PD and AD (Woulfe, 2008). Intercepting protein translocation between the cytoplasm and nucleus for signalling transduction has been proposed as an attractive therapeutic strategy. (Iatrou et al., 2021, Hachiya et al., 2021). The nuclei size is also used to diagnose specific types of cancer, such as colon cancer staging in patients. It is important to note that LRRK2 and Wnt signalling pathways were also linked to colon cancer. Dysregulated

Wnt signalling is a crucial factor in colon cancer growth (Jevtic et al., 2014, Buhmeida et al., 2006).

We observed larger astrocytes displayed in LRRK2 KO and G2019S KI cultures after Wnt3a or LPS stimulations. Hence, dysregulation of Wnt signalling activity might correlate with the size of the nucleus and the cell body. Our LRRK2 KO culture samples showed a higher number of cells when compared to WT and G2019S KI. Lebovitz *et al* demonstrated that LRRK2 reduction caused an increase in tumour initiation and tumour size (Lebovitz et al., 2021). It was demonstrated in another study that LRRK2 KO or G2019S KI caused axon growth impairment, which suggested that loss of function and gain of kinase activity in LRRK2 might have a similar effect. (Onishi et al., 2020).

The accumulating evidence of Wnt signalling dysregulation and nuclear morphology has attracted our attention to understanding the effect of Wnt signalling mediators on this matter. We examined mRNA expression of signalling mediators at two different time points with qPCR to show Wnt signalling changed over time. LRRK2 mutants were shown to affect the Wnt signalling mediators' mRNA expression level under Wnt3a or LPS stimulations compared to WT. The mRNA levels were changed accordingly to the time they were collected, corresponding to the Wnt signalling changes we observed at different time points. We have discussed the function of each of the components in **Chapter 3**. Here we will focus on these changes' potential causes and effects. Wnt signalling regulator Dvl2, transcriptional factor NFkB, and target genes Cyclin-D1 and Cox2 have drawn our attention.

*Dvl2* mRNA level was significantly lower in LRRK2 KO and G2019S KI astrocytes compared to WT post Wnt3a or LPS stimulations. Dlv2 is a key regulator in Wnt signalling pathways and plays a crucial role in colon cancer (Shen et al., 2020, Metcalfe et al., 2010). The findings consolidate the idea of the correlation between PD and bowel diseases. The downregulation of *Dvl2* mRNA level after LPS stimulation suggested that activation of non-canonical Wnt pathway via TLR4 receptor might also impact canonical Wnt signalling activity.

Our mRNA expression analysis supported the data that increased Wnt signalling promotes cell growth. The significant reduction of *Cyclin-D1* mRNA level after Wnt3a stimulation was potentially caused by the negative feedback mechanism of the Cyclin-D1 protein level in the astrocytes (**Fig 5.22 B**). Increased Wnt signalling activity promotes cells proliferation in neural stem cells. (Zhang et al., 2019) This could explain the high Wnt signalling activity and higher cell numbers in the LRRK2 KO and G2019S KI astrocytes cohorts after Wnt signalling pathway activation. Another study recently suggested that LRRK2 KO might induce parkinsonism like PD mutations. The authors knocked out LRRK2 and found that mice developed motor impairment and loss of dopaminergic neurons in the substantia nigra pars compacta at 12 months of age (Huang et al., 2022). The finding suggested that LRRK2 KO and G2019S KI might similarly cause parkinsonism.

Signalling pathway studies in astrocytes showed that Nurr1 signalling protected dopaminergic neurons from inflammation induced death. Nurr1 could suppress NFκB

and hence, prevent inflammatory responses in microglial and astrocytes. It is also important to note that aggregation of α-synuclein in astrocytes caused a reduction of Nurr1 and therefore, attenuated NFκB signalling leading to inflammatory response (Meng et al., 2020, Saijo et al., 2009). Russo *et al* demonstrated that LRRK2 regulated NFκB signalling and Cox2 transcription. The authors suggested that attenuating LRRK2 kinase activity could be a potential strategy for treating neuroinflammation in PD patients (Russo et al., 2015). Our data showed a significantly lower *NFκB* mRNA level after Wnt3a and LPS treatment, which could be due to the high protein level of NFκB. The significantly increased Cox2 mRNA level backed up the finding in LRRK2 KO and G2019S KI astrocytes samples after Wnt3a and LPS treatment (**Fig 5.22 C**). Other studies tested G2019S and R1441G mutations in LRRKS and found that LRRK2 mutations dysregulated NFκB signalling, and G2019S mutation neurons also demonstrated an increase of α-synuclein protein levels. However, silencing LRRK2 tended to decrease α-synuclein expression (Lopez de Maturana et al., 2016). This suggested that activation of the canonical Wnt pathway by Wnt3a and non-canonical Wnt pathway via TLR4 by LPS dysregulated NFκB signalling, and the effect was more significant in LRRK2 mutants. LRRK2 kinase activity might be important in balancing activity levels in these signalling pathways.

In conclusion, our data showed a dysregulation in Wnt, and NFAT signalling activity in mouse derived astrocytes. The signalling dysregulation has led to nucleus size abnormality in LRRK2 KO and G2019S KI astrocytes, which was not observed in WT astrocytes. Further analysis has shown that Wnt signalling mediators' mRNA

expression was dysregulated in the LRRK2 mutant astrocytes. Our data supported that canonical Wnt and NFAT signalling are essential for cell viability and proliferation. The significant reduction in Cyclin-D1 mRNA has suggested a negative feedback mechanism due to the excess cell growth of the LRRK2 mutant astrocytes. The dysregulations in the NFkB signalling pathway potentially lead to increased downstream activation of target genes, including Cox2. An increase in the Cox2 mRNA level might suggest an inflammatory event in the LRRK2 mutant astrocytes. Our data suggested that Wnt signalling dysregulation could lead to morphological and functional astrocyte abnormalities and PD progression.

# 6. Final discussion

## 6.1 Conclusion

Since the discovery of LRRK2 mutations in PD, research into the protein's cellular function has been one of the primary focuses. LRRK2 is also linked to other diseases, such as Chron's disease and cancer, suggesting the complex function of LRRK2. Evidence shows that LRRK2 plays an essential role in Wnt signalling pathways. Our group has identified LRRK2 being a scaffolding protein within the pathway and identified that risk and protective variants of LRRK2 affected Wnt signalling activity in opposite directions in cellular and molecular assays (Berwick and Harvey, 2012, Berwick et al., 2017, Nixon-Abell et al., 2016). Given that Wnt and NFAT signalling pathways are essential for neuronal development, differentiation, and immune responses, dysregulation in these pathways might lead to neurodegeneration and neuroinflammation. My main focus in this project was to learn how LRRK2 regulates Wnt and NFAT signalling pathways in G2019S mutant mice. LRRK2 WT and LRRK2 KO mice were used as a control for comparisons with G2019S KI mice. We aimed to gain more insights into LRRK2 and its regulatory role in signalling pathways. Our results demonstrated that Wnt signalling dysregulation is LRRK2 genotype and potentially sex dependent.

Given the LRRK2 expression level differences in different organs and brain areas (Taymans et al., 2006), we have applied a lentiviral biosensor system to examine our mice models' Wnt signalling activity in different brain areas. The biosensor was a

robust system for us to investigate the Wnt signalling pathway activation state in different brain regions in mice. Our data suggested that LRRK2 affects Wnt signalling activities in different regions in the brain in a sex and region specific manner. The LRRK2 G2019S mutation caused an increase in Wnt signalling activity in most of the studied brain areas, such as olfactory bulbs, hippocampus, and lateral ventricle under basal conditions. The increase in Wnt signalling activity in these regions could suggest enhanced levels of neurogenesis. In line with the previous publication stating that Wnt signalling activity is affected by sex (Shen et al., 2009), we observed that Wnt signalling activity differences were more significant between males and females when LRRK2 was absent in comparison to WT mice. Further suggesting the importance of LRRK2 in sex specific Wnt signalling regulation.

Thereafter, we investigated how LRRK2 dysregulates Wnt and NFAT signalling pathways at the molecular level. We performed an mRNA and protein expression analysis on mice collected under the same condition as the mice we used in the IHC study. Half brain has given us an overview of the expression changes in the brain. Although both LRRK2 KO and G2019S KI mice demonstrated a different level of mRNA and protein expression changes compared to WT, G2019S mice had the most significant changes in signalling mediators compared to WT. However, the observed dysregulation of mRNA and protein levels in LRRK2 KO and G2019S KI were different. This suggested that the LRRK2 G2019S mutation is a gain of function mutation rather than a loss of function mutation. Although the G2019S KI half brain showed no significant changes in active-β-catenin protein level compared to WT, the overall reduction in LRP6 and downstream targets suggested a reduction in Wnt signalling

activity. The G2019S KI striatum showed the most significant changes compared to WT, suggesting signalling pathway changes are most prominent in this brain area, which is highly relevant to PD. The olfactory bulb was indicated to be one of the first affected brain areas in PD patients (Braak et al., 2003). However, we did not observe significant changes in our G2019S KI samples. This was in line with a previous study showing that hyposmia is less frequent in G2019S PD patients than in idiopathic PD patients (Gaig et al., 2014).

Nevertheless, we observed the most significant differences in half brain, cortex, and striatum. Given the hypothesis that LRRK2 influences the regulation of Wnt and NFAT signalling activities, it is not surprising to observe that there were fewer mRNA and protein expression changes in the hippocampus and olfactory bulbs due to lower LRRK2 expression in these regions (Taymans et al., 2006). We observed the most significant expression changes in the GSK3β, β-catenin, co-receptor LRP6 and target genes/proteins in LRRK2 KO and G2019S KI mice. Dysregulation in LRP6 expression could directly affect Wnt signalling pathway activation. It is interesting to note that Wnt3a only activates Wnt signalling pathway via LRP6, but not LRP5. The authors have demonstrated that LRP5 and LRP6 require specific Wnt ligands for Wnt signalling activation (Singh et al., 2021). On the other hand, GSK3β has a negative correlation with β-catenin and hence, affects the transcription of target genes (MacDonald and He, 2012, MacDonald et al., 2009, Stamos and Weis, 2013). It would be in our interest to investigate the effect of G2019S KI on LRP6 and BDC in more detail.

Establishing the mRNA and protein expression differences raised another question; what happens to the signalling mediators under stimulated conditions? The hypothesis has led us to investigate primary neurons and glial cells derived from the mouse brain. I showed that mice neurons-glial co-cultures have significantly lower Wnt and NFAT signalling activity levels compared to the culture without glia cells. I suspected that the Wnt signalling differences between primary cultures could be due to LRRK2 expression differences in specific cell types. Astrocytes are the most abundant glial cell types and contribute to 20-40% of neuroglia in the brain (Khakh and Sofroniew, 2015, Sofroniew and Vinters, 2010). Unlike in humans, the LRRK2 level is higher in mouse astrocytes than in neurons, microglia, and macrophages (Zhang et al., 2016b). The finding has supported our observation of lower Wnt signalling activities in neuronal culture without glial cells.

Consequently, we chose astrocytes as the focus of our functional assays. We showed that Wnt and NFAT signalling pathways tended to have similar activity levels when comparing WT, LRRK2 KO and G2019S mutation cultures under basal conditions. However, upon stimulation with Wnt3a or LPS, LRRK2 KO and G2019S KI astrocytes showed a significantly increased Wnt signalling activity. It was interesting to observe that both LRRK2 KO and G2019S KI caused nuclear enlargement. This could be caused by the significantly increased Wnt signalling activity in LRRK2 KO and G2019S KI astrocytes. Abnormal nuclear morphology is identified as a hallmark of ageing (Pathak et al., 2021, Haithcock et al., 2005). Our finding could suggest that G2019S KI mutation may cause neurodegeneration by accelerating nuclear distortion during ageing, possibly via dysregulated Wnt signalling activity. WT astrocyte nuclei retained

a similar size under different treatments. This finding further suggested the correlation between Wnt signalling dysregulation and nuclear morphological changes (**Fig 5.15-5.16**). G2019S mutation may change LRRK2 interactions with other proteins in the signalling pathways. However, the similar dysregulation trend in LRRK2 KO and G2019S KI also suggested that loss of function or gain of function might have a similar effect. This was supported by research showing axon growth impairment in both LRRK2 KO and G2019S KI samples (Onishi et al., 2020).

I have examined the mRNA expression changes in astrocytes under basal and stimulated conditions. Wnt3a and LPS treatment caused a significant mRNA expression level difference in LRRK2 KO and G2019S KI compared to WT. Both LRRK2 mutant samples dysregulated the signalling pathway components in a similar direction. We observed significant changes in all the studied genes, which created a complication in judging which part of the signalling pathway was first affected. *Dvl2, NFκB*, *Cyclin-D1* and *Cox2* mRNA level has drawn our attention. The mRNA level of *Dvl2* was affected by both Wnt3a and LPS treatment, which suggested that activation of non-canonical Wnt pathways via TLR4 receptor also influences the canonical Wnt signalling pathway (**Fig 5.22**), suggesting the crosstalk mechanism between these two pathways. Abnormal cell proliferation could be caused by increased Wnt signalling activity in LRRK2 KO and G2019S KI astrocytes, in line with the essential role of Wnt signalling for cell proliferation (Zhang et al., 2019). But the abnormal cell growth was not reflected in the *Cyclin-D1* mRNA level, probably due to a negative feedback mechanism (**Fig 5.32**). Russo *et al* demonstrated that LRRK2 regulates the NFκB signalling pathway and Cox2 transcription (Russo et al., 2015). This was in line with

our data; we observed significant dysregulation of *NFκB* and *Cox2* mRNA levels in both LRRK2 KO and G2019S KI astrocytes (**Fig 5.30, 5.33**). This spoke for the critical role of LRRK2 in regulating canonical and non-canonical Wnt signalling pathways. Our data suggests that Wnt signalling dysregulation in LRRK2 mutant astrocytes leads to neuroinflammation and could be a main driver towards PD progression.

In summary, the work presented in this thesis investigated the role of LRRK2 in canonical and non-canonical Wnt signalling pathway regulation. LRRK2 KO and G2019S KI might affect the signalling pathways through a different mechanism, given that one is a loss of function and the other is a gain of function mutation, respectively. The level of LRRK2 could also be a direct factor affecting the signalling pathway regulation. Overall, this study shed insight into the crucial role of LRRK2 in Wnt signalling pathway regulation. Dysregulation of the signalling pathways will potentially lead to the neurodegeneration observed in PD.

## 6.2. Future directions

The accumulating evidence of the role of LRRK2 in Wnt signalling pathways and neurodegeneration has raised exciting questions on finding the exact psychological mechanism. This work's overall data showed the differences in Wnt signalling activities in healthy and disease mouse models at a young age. However, Wnt signalling declined during the ageing process in the AD mouse model (Inestrosa et al., 2020). We would be interested in investigating the change rate of Wnt signalling in our G2019S KI and LRRK2 KO mouse models compared to WT during the ageing process. In addition, identifying Wnt signalling activity differences across the brain by

coordinated injection to precisely deliver the lentiviral biosensor to targeted brain areas would be of interest (McSweeney and Mao, 2015).

The question of whether a LRRK2 mutation is a gain or loss of function has always been exciting. The gaining evidence shows that loss of function in LRRK2 does not increase the risk of PD, but the gain of kinase activity in LRRK2 has significantly increased the risk of PD (Blauwendraat et al., 2018, Whiffin et al., 2020). The increased kinase activity in LRRK2 has led to the development of LRRK2 kinase inhibitors. The pre-clinical study of LRRK2 kinase inhibitor DNL201 showed promising results by improving lysosomal function in a cellular disease model. The inhibitor was also well tolerated in the healthy group and PD patients (Jennings et al., 2022).

The question will be, can we rescue astrocytes' nucleus morphology by restoring Wnt signalling activity at a similar level to WT? The significant increase in *NFκB* and *Cox2* mRNA levels in our astrocyte data after Wnt3a treatment suggested a potential crosstalk mechanism between canonical and non-canonical Wnt signalling pathways. However, finding the balance between canonical Wnt and non-canonical Wnt signalling pathways would be challenging. It was previously shown that inhibition of RhoA kinase enhanced the phosphorylation of β-catenin by GSK3β (Pinzon-Daza et al., 2014). Therefore, excessive inhibition of Wnt signalling pathway could potentially lead to an increase in NFAT or NFκB pathway activity, which are involved in neuroinflammation.

It was reviewed that reactive astrocytes were linked to $Ca^{2+}$ dysregulation and closely related to neurodegenerative diseases such as PD and AD (Sompol and Norris, 2018, Fernandez et al., 2007). Calcineurin is activated by the increased intracellular $Ca^{2+}$ level and leads to the activation of NFAT and NFκB pathways (Kubis et al., 2003, Fernandez et al., 2007). As we have observed in **chapter 5**, an increased Wnt signalling activity might lead to the activation of astrocytes and potentially result in the activation of calcineurin. This suggested a positive correlation between Wnt signalling and neuroinflammation in G2019S mutation carrier PD patients. Inhibition of calcineurin was reported to improve symptoms in AD mice models (Cavallucci et al., 2013). It would gain insight into G2019S mutation function in patients if we could correlate Wnt signalling activities, astrocyte morphological changes, and neuroinflammation.

Targeting Wnt signalling pathway components could be a therapeutic target. However, this requires further evaluation. We observed a similar trend of Wnt signalling dysregulation in LRRK2 KO and G2019S KI astrocytes. However, G2019S has a more prominent effect on Wnt signalling dysregulation. Finding the proper adjustment of Wnt signalling activities might shed light on rescuing PD progression. Moreover, the astrocyte nuclear morphology and Wnt signalling components dysregulations indicated a possibility of a potential biomarker for PD.

Nevertheless, this study sheds light on future approaches to G2019S mutations, potential hallmarks, and therapeutic targets to tackle new PD patient treatment with LRRK2 mutations.

# Reference


LEBOVITZ, C., WRETHAM, N., OSOOLY, M., MILNE, K., DASH, T., THORNTON, S., TESSIER-CLOUTIER, B., SATHIYASEELAN, P., BORTNIK, S., GO, N. E., HALVORSEN, E., CEDERBERG, R. A., CHOW, N., DOS SANTOS, N., BENNEWITH, K. L., NELSON, B. H., BALLY, M. B., LAM, W. L. & GORSKI, S. M. 2021. Loss of Parkinson's susceptibility gene LRRK2 promotes carcinogen-induced lung tumorigenesis. *Sci Rep,* 11**,** 2097.

LOPEZ DE MATURANA, R., LANG, V., ZUBIARRAIN, A., SOUSA, A., VAZQUEZ, N., GOROSTIDI, A., AGUILA, J., LOPEZ DE MUNAIN, A., RODRIGUEZ, M. & SANCHEZ-PERNAUTE, R. 2016. Mutations in LRRK2 impair NF-kappaB pathway in iPSC-derived neurons. *J Neuroinflammation,* 13**,** 295.

MENG, Y., DING, J., LI, C., FAN, H., HE, Y. & QIU, P. 2020. Transfer of pathological alpha-synuclein from neurons to astrocytes via exosomes causes inflammatory responses after METH exposure. *Toxicol Lett,* 331**,** 188-199.

METCALFE, C., IBRAHIM, A. E., GRAEB, M., DE LA ROCHE, M., SCHWARZ-ROMOND, T., FIEDLER, M., WINTON, D. J., CORFIELD, A. & BIENZ, M. 2010. Dvl2 promotes intestinal length and neoplasia in the ApcMin mouse model for colorectal cancer. *Cancer Res,* 70**,** 6629-38.

NEUMANN, F. R. & NURSE, P. 2007. Nuclear size control in fission yeast. *J Cell Biol,* 179**,** 593-600.

ONISHI, K., TIAN, R., FENG, B., LIU, Y., WANG, J., LI, Y. & ZOU, Y. 2020. LRRK2 mediates axon development by regulating Frizzled3 phosphorylation and growth cone-growth cone communication. *Proc Natl Acad Sci U S A,* 117**,** 18037-18048.

PRAH, J., WINTERS, A., CHAUDHARI, K., HERSH, J., LIU, R. & YANG, S. H. 2019. A novel serum free primary astrocyte culture method that mimic quiescent astrocyte phenotype. *J Neurosci Methods,* 320**,** 50-63.

RUSSO, I., BERTI, G., PLOTEGHER, N., BERNARDO, G., FILOGRANA, R., BUBACCO, L. & GREGGIO, E. 2015. Leucine-rich repeat kinase 2 positively regulates inflammation and down-regulates NF-kappaB p50 signaling in cultured microglia cells. *J Neuroinflammation,* 12**,** 230.

SAIJO, K., WINNER, B., CARSON, C. T., COLLIER, J. G., BOYER, L., ROSENFELD, M. G., GAGE, F. H. & GLASS, C. K. 2009. A Nurr1/CoREST pathway in microglia and astrocytes protects dopaminergic neurons from inflammation-induced death. *Cell,* 137**,** 47-59.

SHEN, J., HU, L., YANG, L., ZHANG, M., SUN, W., LU, X., LIN, G., HUANG, C., ZHANG, X. & CHIN, Y. E. 2020. Reversible acetylation modulates dishevelled-2 puncta formation in canonical Wnt signaling activation. *Signal Transduct Target Ther,* 5**,** 115.

SOFRONIEW, M. V. & VINTERS, H. V. 2010. Astrocytes: biology and pathology. *Acta Neuropathol,* 119**,** 7-35.

SUN, S., ZHU, X. J., HUANG, H., GUO, W., TANG, T., XIE, B., XU, X., ZHANG, Z., SHEN, Y., DAI, Z. M. & QIU, M. 2019. WNT signaling represses astrogliogenesis via Ngn2-dependent direct suppression of astrocyte gene expression. *Glia,* 67**,** 1333-1343.

VERKHRATSKY, A., SOFRONIEW, M. V., MESSING, A., DELANEROLLE, N. C., REMPE, D., RODRIGUEZ, J. J. & NEDERGAARD, M. 2012. Neurological diseases as primary gliopathies: a reassessment of neurocentrism. *ASN Neuro,* 4.

WOULFE, J. 2008. Nuclear bodies in neurodegenerative disease. *Biochim Biophys Acta,* 1783**,** 2195-206.

ZHANG, J., HE, L., YANG, Z., LI, L. & CAI, W. 2019. Lithium chloride promotes proliferation of neural stem cells in vitro, possibly by triggering the Wnt signaling pathway. *Anim Cells Syst (Seoul),* 23**,** 32-41.

ZHANG, Y., SLOAN, S. A., CLARKE, L. E., CANEDA, C., PLAZA, C. A., BLUMENTHAL, P. D., VOGEL, H., STEINBERG, G. K., EDWARDS, M. S., LI, G., DUNCAN, J. A., 3RD, CHESHIER, S. H., SHUER, L. M., CHANG, E. F., GRANT, G. A., GEPHART, M. G. & BARRES, B. A. 2016. Purification and Characterization of Progenitor and Mature Human Astrocytes Reveals Transcriptional and Functional Differences with Mouse. *Neuron,* 89**,** 37-53.

AASLY, J. O., VILARINO-GUELL, C., DACHSEL, J. C., WEBBER, P. J., WEST, A. B., HAUGARVOLL, K., JOHANSEN, K. K., TOFT, M., NUTT, J. G., PAYAMI, H., KACHERGUS, J. M., LINCOLN, S. J., FELIC, A., WIDER, C., SOTO-ORTOLAZA, A. I., COBB, S. A., WHITE, L. R., ROSS, O. A. & FARRER, M. J. 2010. Novel pathogenic LRRK2 p.Asn1437His substitution in familial Parkinson's disease. *Mov Disord,* 25**,** 2156-63.

ALBANESE, F., NOVELLO, S. & MORARI, M. 2019. Autophagy and LRRK2 in the Aging Brain. *Front Neurosci,* 13**,** 1352.

ANDERSSON, E. R., PRAKASH, N., CAJANEK, L., MININA, E., BRYJA, V., BRYJOVA, L., YAMAGUCHI, T. P., HALL, A. C., WURST, W. & ARENAS, E. 2008. Wnt5a regulates ventral midbrain morphogenesis and the development of A9-A10 dopaminergic cells in vivo. *PLoS One,* 3**,** e3517.

BAMJI, S. X., SHIMAZU, K., KIMES, N., HUELSKEN, J., BIRCHMEIER, W., LU, B. & REICHARDT, L. F. 2003. Role of beta-catenin in synaptic vesicle localization and presynaptic assembly. *Neuron,* 40**,** 719-31.

BARBAR, L., JAIN, T., ZIMMER, M., KRUGLIKOV, I., SADICK, J. S., WANG, M., KALPANA, K., ROSE, I. V. L., BURSTEIN, S. R., RUSIELEWICZ, T., NIJSURE, M., GUTTENPLAN, K. A., DI DOMENICO, A., CROFT, G., ZHANG, B., NOBUTA, H., HEBERT, J. M., LIDDELOW, S. A. & FOSSATI, V. 2020. CD49f Is a Novel Marker of Functional and Reactive Human iPSC-Derived Astrocytes. *Neuron,* 107**,** 436-453 e12.

BELLOU, V., BELBASIS, L., TZOULAKI, I., EVANGELOU, E. & IOANNIDIS, J. P. 2016. Environmental risk factors and Parkinson's disease: An umbrella review of meta-analyses. *Parkinsonism Relat Disord,* 23**,** 1-9.

BENAMER, H. T. & DE SILVA, R. 2010. LRRK2 G2019S in the North African population: a review. *Eur Neurol,* 63**,** 321-5.

BERRIDGE, K. C., ROBINSON, T. E. & ALDRIDGE, J. W. 2009. Dissecting components of reward: 'liking', 'wanting', and learning. *Curr Opin Pharmacol,* 9**,** 65-73.

BERWICK, D. C. & HARVEY, K. 2011. LRRK2 signaling pathways: the key to unlocking neurodegeneration? *Trends Cell Biol,* 21**,** 257-65.

BERWICK, D. C. & HARVEY, K. 2012. LRRK2 functions as a Wnt signaling scaffold, bridging cytosolic proteins and membrane-localized LRP6. *Hum Mol Genet,* 21**,** 4966-79.

BERWICK, D. C. & HARVEY, K. 2014. The regulation and deregulation of Wnt signaling by PARK genes in health and disease. *J Mol Cell Biol,* 6**,** 3-12.

BERWICK, D. C., JAVAHERI, B., WETZEL, A., HOPKINSON, M., NIXON-ABELL, J., GRANNO, S., PITSILLIDES, A. A. & HARVEY, K. 2017. Pathogenic LRRK2 variants are gain-of-function mutations that enhance LRRK2-mediated repression of beta-catenin signaling. *Mol Neurodegener,* 12**,** 9.

BLAKELY, B. D., BYE, C. R., FERNANDO, C. V., HORNE, M. K., MACHEDA, M. L., STACKER, S. A., ARENAS, E. & PARISH, C. L. 2011. Wnt5a regulates midbrain dopaminergic axon growth and guidance. *PLoS One,* 6**,** e18373.

BLAUWENDRAAT, C., REED, X., KIA, D. A., GAN-OR, Z., LESAGE, S., PIHLSTROM, L., GUERREIRO, R., GIBBS, J. R., SABIR, M., AHMED, S., DING, J., ALCALAY, R. N., HASSIN-BAER, S., PITTMAN, A. M., BROOKS, J., EDSALL, C., HERNANDEZ, D. G., CHUNG, S. J., GOLDWURM, S., TOFT, M., SCHULTE, C., BRAS, J., WOOD, N. W., BRICE, A., MORRIS, H. R., SCHOLZ, S. W., NALLS, M. A., SINGLETON, A. B., COOKSON, M. R., COURAGE-PD CONSORTIUM, T. F. P. S. D. C. & THE INTERNATIONAL PARKINSON'S DISEASE GENOMICS, C. 2018. Frequency of Loss of Function Variants in LRRK2 in Parkinson Disease. *JAMA Neurol,* 75**,** 1416-1422.

BRAAK, H., DEL TREDICI, K., RUB, U., DE VOS, R. A., JANSEN STEUR, E. N. & BRAAK, E. 2003. Staging of brain pathology related to sporadic Parkinson's disease. *Neurobiol Aging,* 24**,** 197-211.

BRAMHAM, C. R. & MESSAOUDI, E. 2005. BDNF function in adult synaptic plasticity: the synaptic consolidation hypothesis. *Prog Neurobiol,* 76**,** 99-125.

BROCKMANN, K., SCHULTE, C., SCHNEIDERHAN-MARRA, N., APEL, A., PONT-SUNYER, C., VILAS, D., RUIZ-MARTINEZ, J., LANGKAMP, M., CORVOL, J. C., CORMIER, F., KNORPP, T., JOOS, T. O., BERNARD, A., GASSER, T., MARRAS, C., SCHULE, B., AASLY, J. O., FOROUD, T., MARTI-MASSO, J. F., BRICE, A., TOLOSA, E., BERG, D. & MAETZLER, W. 2017. Inflammatory profile discriminates clinical subtypes in LRRK2-associated Parkinson's disease. *Eur J Neurol,* 24**,** 427-e6.

BUCKLEY, S. M., DELHOVE, J. M., PEROCHEAU, D. P., KARDA, R., RAHIM, A. A., HOWE, S. J., WARD, N. J., BIRRELL, M. A., BELVISI, M. G., ARBUTHNOT, P., JOHNSON, M. R., WADDINGTON, S. N. & MCKAY, T. R. 2015. In vivo bioimaging with tissue-specific transcription factor activated luciferase reporters. *Sci Rep,* 5**,** 11842.

BUHMEIDA, A., ALGARS, A., RISTAMAKI, R., COLLAN, Y., SYRJANEN, K. & PYRHONEN, S. 2006. Nuclear size as prognostic determinant in stage II and stage III colorectal adenocarcinoma. *Anticancer Res,* 26**,** 455-62.

BUSTIN, S. & HUGGETT, J. 2017. qPCR primer design revisited. *Biomol Detect Quantif,* 14**,** 19-28.

CANTUTI-CASTELVETRI, I., KELLER-MCGANDY, C., BOUZOU, B., ASTERIS, G., CLARK, T. W., FROSCH, M. P. & STANDAERT, D. G. 2007. Effects of gender on nigral gene expression and parkinson disease. *Neurobiol Dis,* 26**,** 606-14.

CAPILLA-GONZALEZ, V., LAVELL, E., QUINONES-HINOJOSA, A. & GUERRERO-CAZARES, H. 2015. Regulation of subventricular zone-derived cells migration in the adult brain. *Adv Exp Med Biol,* 853**,** 1-21.

CARICASOLE, A., COPANI, A., CARACI, F., ARONICA, E., ROZEMULLER, A. J., CARUSO, A., STORTO, M., GAVIRAGHI, G., TERSTAPPEN, G. C. & NICOLETTI, F. 2004. Induction of Dickkopf-1, a negative modulator of the Wnt pathway, is associated with neuronal degeneration in Alzheimer's brain. *J Neurosci,* 24**,** 6021-7.

CAVALLUCCI, V., BERRETTA, N., NOBILI, A., NISTICO, R., MERCURI, N. B. & D'AMELIO, M. 2013. Calcineurin inhibition rescues early synaptic plasticity deficits in a mouse model of Alzheimer's disease. *Neuromolecular Med,* 15**,** 541-8.

CHARAN, J. & KANTHARIA, N. D. 2013. How to calculate sample size in animal studies? *J Pharmacol Pharmacother,* 4**,** 303-6.

CHEN, C. Y., WENG, Y. H., CHIEN, K. Y., LIN, K. J., YEH, T. H., CHENG, Y. P., LU, C. S. & WANG, H. L. 2012. (G2019S) LRRK2 activates MKK4-JNK pathway and causes degeneration of SN dopaminergic neurons in a transgenic mouse model of PD. *Cell Death Differ,* 19**,** 1623-33.

CHOLERTON, B., JOHNSON, C. O., FISH, B., QUINN, J. F., CHUNG, K. A., PETERSON-HILLER, A. L., ROSENTHAL, L. S., DAWSON, T. M., ALBERT, M. S., HU, S. C., MATA, I. F., LEVERENZ, J. B., POSTON, K. L., MONTINE, T. J., ZABETIAN, C. P. & EDWARDS, K. L. 2018. Sex differences in progression to mild cognitive impairment and dementia in Parkinson's disease. *Parkinsonism Relat Disord,* 50**,** 29-36.

CHUANG, C. L., LU, Y. N., WANG, H. C. & CHANG, H. Y. 2014. Genetic dissection reveals that Akt is the critical kinase downstream of LRRK2 to phosphorylate and inhibit FOXO1, and promotes neuron survival. *Hum Mol Genet,* 23**,** 5649-58.

CIVIERO, L., CIRNARU, M. D., BEILINA, A., RODELLA, U., RUSSO, I., BELLUZZI, E., LOBBESTAEL, E., REYNIERS, L., HONDHAMUNI, G., LEWIS, P. A., VAN DEN HAUTE, C., BAEKELANDT, V., BANDOPADHYAY, R., BUBACCO, L., PICCOLI, G., COOKSON, M. R., TAYMANS, J. M. & GREGGIO, E. 2015. Leucine-rich repeat kinase 2 interacts with p21-activated kinase 6 to control neurite complexity in mammalian brain. *J Neurochem,* 135**,** 1242-56.

CIVIERO, L., VANCRAENENBROECK, R., BELLUZZI, E., BEILINA, A., LOBBESTAEL, E., REYNIERS, L., GAO, F., MICETIC, I., DE MAEYER, M., BUBACCO, L., BAEKELANDT, V., COOKSON, M. R., GREGGIO, E. & TAYMANS, J. M. 2012. Biochemical characterization of highly purified leucine-rich repeat kinases 1 and 2 demonstrates formation of homodimers. *PLoS One,* 7**,** e43472.

DE LAU, L. M. & BRETELER, M. M. 2006. Epidemiology of Parkinson's disease. *Lancet Neurol,* 5**,** 525-35.

DE WIT, T., BAEKELANDT, V. & LOBBESTAEL, E. 2018. LRRK2 Phosphorylation: Behind the Scenes. *Neuroscientist,* 24**,** 486-500.

DENG, H., WANG, P. & JANKOVIC, J. 2018. The genetics of Parkinson disease. *Ageing Res Rev,* 42**,** 72-85.

DEYAERT, E., WAUTERS, L., GUAITOLI, G., KONIJNENBERG, A., LEEMANS, M., TERHEYDEN, S., PETROVIC, A., GALLARDO, R., NEDERVEEN-SCHIPPERS, L. M., ATHANASOPOULOS, P. S., POTS, H., VAN HAASTERT, P. J. M., SOBOTT, F., GLOECKNER, C. J., EFREMOV, R., KORTHOLT, A. & VERSEES, W. 2017. A homologue of the Parkinson's disease-

associated protein LRRK2 undergoes a monomer-dimer transition during GTP turnover. *Nat Commun,* 8**,** 1008.
DICK, F. D. 2006. Parkinson's disease and pesticide exposures. *Br Med Bull,* 79-80**,** 219-31.
DICK, F. D., DE PALMA, G., AHMADI, A., SCOTT, N. W., PRESCOTT, G. J., BENNETT, J., SEMPLE, S., DICK, S., COUNSELL, C., MOZZONI, P., HAITES, N., WETTINGER, S. B., MUTTI, A., OTELEA, M., SEATON, A., SODERKVIST, P., FELICE, A. & GEOPARKINSON STUDY, G. 2007. Environmental risk factors for Parkinson's disease and parkinsonism: the Geoparkinson study. *Occup Environ Med,* 64**,** 666-72.
DICKSON, D. W., UCHIKADO, H., FUJISHIRO, H. & TSUBOI, Y. 2010. Evidence in favor of Braak staging of Parkinson's disease. *Mov Disord,* 25 Suppl 1**,** S78-82.
DIETRICH, P., ALLI, S., MULLIGAN, M. K., COX, R., ASHBROOK, D. G., WILLIAMS, R. W. & DRAGATSIS, I. 2022. Identification of cyclin D1 as a major modulator of 3-nitropropionic acid-induced striatal neurodegeneration. *Neurobiol Dis,* 162**,** 105581.
ENGELHARDT, E. 2017. Lafora and Tretiakoff: the naming of the inclusion bodies discovered by Lewy. *Arq Neuropsiquiatr,* 75**,** 751-753.
ENGELHARDT, E. & GOMES, M. D. M. 2017. Lewy and his inclusion bodies: Discovery and rejection. *Dement Neuropsychol,* 11**,** 198-201.
EUSEBI, P. G., SEVANE, N., O'ROURKE, T., PIZARRO, M., BOECKX, C. & DUNNER, S. 2021. Gene expression profiles underlying aggressive behavior in the prefrontal cortex of cattle. *BMC Genomics,* 22**,** 245.
FERNANDEZ, A. M., FERNANDEZ, S., CARRERO, P., GARCIA-GARCIA, M. & TORRES-ALEMAN, I. 2007. Calcineurin in reactive astrocytes plays a key role in the interplay between proinflammatory and anti-inflammatory signals. *J Neurosci,* 27**,** 8745-56.
FESTING, M. F. & ALTMAN, D. G. 2002. Guidelines for the design and statistical analysis of experiments using laboratory animals. *ILAR J,* 43**,** 244-58.
FLOCKHART, R. J., DIFFEY, B. L., FARR, P. M., LLOYD, J. & REYNOLDS, N. J. 2008. NFAT regulates induction of COX-2 and apoptosis of keratinocytes in response to ultraviolet radiation exposure. *FASEB J,* 22**,** 4218-27.
FUNAYAMA, M., HASEGAWA, K., KOWA, H., SAITO, M., TSUJI, S. & OBATA, F. 2002. A new locus for Parkinson's disease (PARK8) maps to chromosome 12p11.2-q13.1. *Ann Neurol,* 51**,** 296-301.
FUNAYAMA, M., HASEGAWA, K., OHTA, E., KAWASHIMA, N., KOMIYAMA, M., KOWA, H., TSUJI, S. & OBATA, F. 2005. An LRRK2 mutation as a cause for the parkinsonism in the original PARK8 family. *Ann Neurol,* 57**,** 918-21.
GAIG, C., VILAS, D., INFANTE, J., SIERRA, M., GARCIA-GOROSTIAGA, I., BUONGIORNO, M., EZQUERRA, M., MARTI, M. J., VALLDEORIOLA, F., AGUILAR, M., CALOPA, M., HERNANDEZ-VARA, J. & TOLOSA, E. 2014. Nonmotor symptoms in LRRK2 G2019S associated Parkinson's disease. *PLoS One,* 9**,** e108982.
GALTER, D., WESTERLUND, M., CARMINE, A., LINDQVIST, E., SYDOW, O. & OLSON, L. 2006. LRRK2 expression linked to dopamine-innervated areas. *Ann Neurol,* 59**,** 714-9.
GAMMONS, M. V., RENKO, M., JOHNSON, C. M., RUTHERFORD, T. J. & BIENZ, M. 2016. Wnt Signalosome Assembly by DEP Domain Swapping of Dishevelled. *Mol Cell,* 64**,** 92-104.

GANDHI, J., KHERA, L., GAUR, N., PAUL, C. & KAUL, R. 2017. Role of Modulator of Inflammation Cyclooxygenase-2 in Gammaherpesvirus Mediated Tumorigenesis. *Front Microbiol,* 8**,** 538.

GANDHI, S. & WOOD, N. W. 2005. Molecular pathogenesis of Parkinson's disease. *Hum Mol Genet,* 14 Spec No. 2**,** 2749-2755.

GIASSON, B. I., COVY, J. P., BONINI, N. M., HURTIG, H. I., FARRER, M. J., TROJANOWSKI, J. Q. & VAN DEERLIN, V. M. 2006. Biochemical and pathological characterization of Lrrk2. *Ann Neurol,* 59**,** 315-22.

GILLIES, G. E., PIENAAR, I. S., VOHRA, S. & QAMHAWI, Z. 2014. Sex differences in Parkinson's disease. *Front Neuroendocrinol,* 35**,** 370-84.

GOETZ, C. G. 2011. The history of Parkinson's disease: early clinical descriptions and neurological therapies. *Cold Spring Harb Perspect Med,* 1**,** a008862.

GOLDMAN, S. M. 2014. Environmental toxins and Parkinson's disease. *Annu Rev Pharmacol Toxicol,* 54**,** 141-64.

GONDKAR, K., PATEL, K., PATIL OKALY, G. V., NAIR, B., PANDEY, A., GOWDA, H. & KUMAR, P. 2019. Dickkopf Homolog 3 (DKK3) Acts as a Potential Tumor Suppressor in Gallbladder Cancer. *Front Oncol,* 9**,** 1121.

GREGGIO, E., BUBACCO, L. & RUSSO, I. 2017. Cross-talk between LRRK2 and PKA: implication for Parkinson's disease? *Biochem Soc Trans,* 45**,** 261-267.

GREGGIO, E., JAIN, S., KINGSBURY, A., BANDOPADHYAY, R., LEWIS, P., KAGANOVICH, A., VAN DER BRUG, M. P., BEILINA, A., BLACKINTON, J., THOMAS, K. J., AHMAD, R., MILLER, D. W., KESAVAPANY, S., SINGLETON, A., LEES, A., HARVEY, R. J., HARVEY, K. & COOKSON, M. R. 2006. Kinase activity is required for the toxic effects of mutant LRRK2/dardarin. *Neurobiol Dis,* 23**,** 329-41.

GROISS, S. J., WOJTECKI, L., SUDMEYER, M. & SCHNITZLER, A. 2009. Deep brain stimulation in Parkinson's disease. *Ther Adv Neurol Disord,* 2**,** 20-8.

GRUMOLATO, L., LIU, G., MONG, P., MUDBHARY, R., BISWAS, R., ARROYAVE, R., VIJAYAKUMAR, S., ECONOMIDES, A. N. & AARONSON, S. A. 2010. Canonical and noncanonical Wnts use a common mechanism to activate completely unrelated coreceptors. *Genes Dev,* 24**,** 2517-30.

HAAXMA, C. A., BLOEM, B. R., BORM, G. F., OYEN, W. J., LEENDERS, K. L., ESHUIS, S., BOOIJ, J., DLUZEN, D. E. & HORSTINK, M. W. 2007. Gender differences in Parkinson's disease. *J Neurol Neurosurg Psychiatry,* 78**,** 819-24.

HACHIYA, N., SOCHOCKA, M., BRZECKA, A., SHIMIZU, T., GASIOROWSKI, K., SZCZECHOWIAK, K. & LESZEK, J. 2021. Nuclear Envelope and Nuclear Pore Complexes in Neurodegenerative Diseases-New Perspectives for Therapeutic Interventions. *Mol Neurobiol,* 58**,** 983-995.

HAITHCOCK, E., DAYANI, Y., NEUFELD, E., ZAHAND, A. J., FEINSTEIN, N., MATTOUT, A., GRUENBAUM, Y. & LIU, J. 2005. Age-related changes of nuclear architecture in Caenorhabditis elegans. *Proc Natl Acad Sci U S A,* 102**,** 16690-5.

HEALY, D. G., FALCHI, M., O'SULLIVAN, S. S., BONIFATI, V., DURR, A., BRESSMAN, S., BRICE, A., AASLY, J., ZABETIAN, C. P., GOLDWURM, S., FERREIRA, J. J., TOLOSA, E., KAY, D. M., KLEIN, C., WILLIAMS, D. R., MARRAS, C., LANG, A. E., WSZOLEK, Z. K., BERCIANO, J., SCHAPIRA, A. H., LYNCH, T., BHATIA, K. P., GASSER, T., LEES, A. J., WOOD, N. W. & INTERNATIONAL, L. C. 2008. Phenotype, genotype, and worldwide genetic

penetrance of LRRK2-associated Parkinson's disease: a case-control study. *Lancet Neurol,* 7**,** 583-90.
HINZ, M., STEIN, A. & UNCINI, T. 2011. Amino acid management of Parkinson's disease: a case study. *Int J Gen Med,* 4**,** 165-74.
HOFMANN, J. W., MCBRYAN, T., ADAMS, P. D. & SEDIVY, J. M. 2014. The effects of aging on the expression of Wnt pathway genes in mouse tissues. *Age (Dordr),* 36**,** 9618.
HOLDORFF, B., RODRIGUES E SILVA, A. M. & DODEL, R. 2013. Centenary of Lewy bodies (1912-2012). *J Neural Transm (Vienna),* 120**,** 509-16.
HUANG, T., XIE, Z., WANG, J., LI, M., JING, N. & LI, L. 2011. Nuclear factor of activated T cells (NFAT) proteins repress canonical Wnt signaling via its interaction with Dishevelled (Dvl) protein and participate in regulating neural progenitor cell proliferation and differentiation. *J Biol Chem,* 286**,** 37399-405.
HUANG, Y., HALLIDAY, G. M., VANDEBONA, H., MELLICK, G. D., MASTAGLIA, F., STEVENS, J., KWOK, J., GARLEPP, M., SILBURN, P. A., HORNE, M. K., KOTSCHET, K., VENN, A., ROWE, D. B., RUBIO, J. P. & SUE, C. M. 2007. Prevalence and clinical features of common LRRK2 mutations in Australians with Parkinson's disease. *Mov Disord,* 22**,** 982-9.
HUNOT, S., BRUGG, B., RICARD, D., MICHEL, P. P., MURIEL, M. P., RUBERG, M., FAUCHEUX, B. A., AGID, Y. & HIRSCH, E. C. 1997. Nuclear translocation of NF-kappaB is increased in dopaminergic neurons of patients with parkinson disease. *Proc Natl Acad Sci U S A,* 94**,** 7531-6.
IATROU, A., CLARK, E. M. & WANG, Y. 2021. Nuclear dynamics and stress responses in Alzheimer's disease. *Mol Neurodegener,* 16**,** 65.
INESTROSA, N. C. & ARENAS, E. 2010. Emerging roles of Wnts in the adult nervous system. *Nat Rev Neurosci,* 11**,** 77-86.
INESTROSA, N. C., TAPIA-ROJAS, C., LINDSAY, C. B. & ZOLEZZI, J. M. 2020. Wnt Signaling Pathway Dysregulation in the Aging Brain: Lessons From the Octodon degus. *Front Cell Dev Biol,* 8**,** 734.
JALEEL, M., NICHOLS, R. J., DEAK, M., CAMPBELL, D. G., GILLARDON, F., KNEBEL, A. & ALESSI, D. R. 2007. LRRK2 phosphorylates moesin at threonine-558: characterization of how Parkinson's disease mutants affect kinase activity. *Biochem J,* 405**,** 307-17.
JANKOVIC, J., CHEN, S. & LE, W. D. 2005. The role of Nurr1 in the development of dopaminergic neurons and Parkinson's disease. *Prog Neurobiol,* 77**,** 128-38.
JENNINGS, D., HUNTWORK-RODRIGUEZ, S., HENRY, A. G., SASAKI, J. C., MEISNER, R., DIAZ, D., SOLANOY, H., WANG, X., NEGROU, E., BONDAR, V. V., GHOSH, R., MALONEY, M. T., PROPSON, N. E., ZHU, Y., MACIUCA, R. D., HARRIS, L., KAY, A., LEWITT, P., KING, T. A., KERN, D., ELLENBOGEN, A., GOODMAN, I., SIDEROWF, A., ALDRED, J., OMIDVAR, O., MASOUD, S. T., DAVIS, S. S., ARGUELLO, A., ESTRADA, A. A., DE VICENTE, J., SWEENEY, Z. K., ASTARITA, G., BORIN, M. T., WONG, B. K., WONG, H., NGUYEN, H., SCEARCE-LEVIE, K., HO, C. & TROYER, M. D. 2022. Preclinical and clinical evaluation of the LRRK2 inhibitor DNL201 for Parkinson's disease. *Sci Transl Med,* 14**,** eabj2658.
JEVTIC, P., EDENS, L. J., VUKOVIC, L. D. & LEVY, D. L. 2014. Sizing and shaping the nucleus: mechanisms and significance. *Curr Opin Cell Biol,* 28**,** 16-27.

JHO, E. H., ZHANG, T., DOMON, C., JOO, C. K., FREUND, J. N. & COSTANTINI, F. 2002. Wnt/beta-catenin/Tcf signaling induces the transcription of Axin2, a negative regulator of the signaling pathway. *Mol Cell Biol,* 22**,** 1172-83.

JONES, S. R., CARLEY, S. & HARRISON, M. 2003. An introduction to power and sample size estimation. *Emerg Med J,* 20**,** 453-8.

KACHERGUS, J., MATA, I. F., HULIHAN, M., TAYLOR, J. P., LINCOLN, S., AASLY, J., GIBSON, J. M., ROSS, O. A., LYNCH, T., WILEY, J., PAYAMI, H., NUTT, J., MARAGANORE, D. M., CZYZEWSKI, K., STYCZYNSKA, M., WSZOLEK, Z. K., FARRER, M. J. & TOFT, M. 2005. Identification of a novel LRRK2 mutation linked to autosomal dominant parkinsonism: evidence of a common founder across European populations. *Am J Hum Genet,* 76**,** 672-80.

KAMIKAWAJI, S., ITO, G. & IWATSUBO, T. 2009. Identification of the autophosphorylation sites of LRRK2. *Biochemistry,* 48**,** 10963-75.

KANG, U. B. & MARTO, J. A. 2017. Leucine-rich repeat kinase 2 and Parkinson's disease. *Proteomics,* 17.

KATOH, M. 2005. WNT/PCP signaling pathway and human cancer (review). *Oncol Rep,* 14**,** 1583-8.

KAUR, R., STOLDT, M., JONGEPIER, E., FELDMEYER, B., MENZEL, F., BORNBERG-BAUER, E. & FOITZIK, S. 2019. Ant behaviour and brain gene expression of defending hosts depend on the ecological success of the intruding social parasite. *Philos Trans R Soc Lond B Biol Sci,* 374**,** 20180192.

KAUSHIK, S. & CUERVO, A. M. 2018. The coming of age of chaperone-mediated autophagy. *Nat Rev Mol Cell Biol,* 19**,** 365-381.

KAWAKAMI, F., SHIMADA, N., OHTA, E., KAGIYA, G., KAWASHIMA, R., MAEKAWA, T., MARUYAMA, H. & ICHIKAWA, T. 2014. Leucine-rich repeat kinase 2 regulates tau phosphorylation through direct activation of glycogen synthase kinase-3beta. *FEBS J,* 281**,** 3-13.

KETT, L. R. & DAUER, W. T. 2012. Leucine-rich repeat kinase 2 for beginners: six key questions. *Cold Spring Harb Perspect Med,* 2**,** a009407.

KHAKH, B. S. & SOFRONIEW, M. V. 2015. Diversity of astrocyte functions and phenotypes in neural circuits. *Nat Neurosci,* 18**,** 942-52.

KHAN, N. L., JAIN, S., LYNCH, J. M., PAVESE, N., ABOU-SLEIMAN, P., HOLTON, J. L., HEALY, D. G., GILKS, W. P., SWEENEY, M. G., GANGULY, M., GIBBONS, V., GANDHI, S., VAUGHAN, J., EUNSON, L. H., KATZENSCHLAGER, R., GAYTON, J., LENNOX, G., REVESZ, T., NICHOLL, D., BHATIA, K. P., QUINN, N., BROOKS, D., LEES, A. J., DAVIS, M. B., PICCINI, P., SINGLETON, A. B. & WOOD, N. W. 2005. Mutations in the gene LRRK2 encoding dardarin (PARK8) cause familial Parkinson's disease: clinical, pathological, olfactory and functional imaging and genetic data. *Brain,* 128**,** 2786-96.

KIM, B., YANG, M. S., CHOI, D., KIM, J. H., KIM, H. S., SEOL, W., CHOI, S., JOU, I., KIM, E. Y. & JOE, E. H. 2012. Impaired inflammatory responses in murine Lrrk2-knockdown brain microglia. *PLoS One,* 7**,** e34693.

KINGWELL, K. 2022. LRRK2 inhibitor progresses for Parkinson disease. *Nat Rev Drug Discov,* 21**,** 558.

KOPRICH, J. B., RESKE-NIELSEN, C., MITHAL, P. & ISACSON, O. 2008. Neuroinflammation mediated by IL-1beta increases susceptibility of dopamine neurons to degeneration in an animal model of Parkinson's disease. *J Neuroinflammation,* 5**,** 8.

KRISHNANKUTTY, A., KIMURA, T., SAITO, T., AOYAGI, K., ASADA, A., TAKAHASHI, S. I., ANDO, K., OHARA-IMAIZUMI, M., ISHIGURO, K. & HISANAGA, S. I. 2017. In vivo regulation of glycogen synthase kinase 3beta activity in neurons and brains. *Sci Rep,* 7**,** 8602.

KUBIS, H. P., HANKE, N., SCHEIBE, R. J., MEISSNER, J. D. & GROS, G. 2003. Ca2+ transients activate calcineurin/NFATc1 and initiate fast-to-slow transformation in a primary skeletal muscle culture. *Am J Physiol Cell Physiol,* 285**,** C56-63.

KUMARI, U. & TAN, E. K. 2010. Leucine-rich repeat kinase 2-linked Parkinson's disease: clinical and molecular findings. *J Mov Disord,* 3**,** 25-31.

KUME, K., CANTWELL, H., NEUMANN, F. R., JONES, A. W., SNIJDERS, A. P. & NURSE, P. 2017. A systematic genomic screen implicates nucleocytoplasmic transport and membrane growth in nuclear size control. *PLoS Genet,* 13**,** e1006767.

L'EPISCOPO, F., TIROLO, C., TESTA, N., CANIGLIA, S., MORALE, M. C., SERAPIDE, M. F., PLUCHINO, S. & MARCHETTI, B. 2014. Wnt/beta-catenin signaling is required to rescue midbrain dopaminergic progenitors and promote neurorepair in ageing mouse model of Parkinson's disease. *Stem Cells,* 32**,** 2147-63.

LANGSTON, J. W., BALLARD, P., TETRUD, J. W. & IRWIN, I. 1983. Chronic Parkinsonism in humans due to a product of meperidine-analog synthesis. *Science,* 219**,** 979-80.

LANGSTON, J. W., FORNO, L. S., REBERT, C. S. & IRWIN, I. 1984. Selective nigral toxicity after systemic administration of 1-methyl-4-phenyl-1,2,5,6-tetrahydropyrine (MPTP) in the squirrel monkey. *Brain Res,* 292**,** 390-4.

LAW, B. M., SPAIN, V. A., LEINSTER, V. H., CHIA, R., BEILINA, A., CHO, H. J., TAYMANS, J. M., URBAN, M. K., SANCHO, R. M., BLANCA RAMIREZ, M., BISKUP, S., BAEKELANDT, V., CAI, H., COOKSON, M. R., BERWICK, D. C. & HARVEY, K. 2014. A direct interaction between leucine-rich repeat kinase 2 and specific beta-tubulin isoforms regulates tubulin acetylation. *J Biol Chem,* 289**,** 895-908.

LE GRAND, F., JONES, A. E., SEALE, V., SCIME, A. & RUDNICKI, M. A. 2009. Wnt7a activates the planar cell polarity pathway to drive the symmetric expansion of satellite stem cells. *Cell Stem Cell,* 4**,** 535-47.

LEBOVITZ, C., WRETHAM, N., OSOOLY, M., MILNE, K., DASH, T., THORNTON, S., TESSIER-CLOUTIER, B., SATHIYASEELAN, P., BORTNIK, S., GO, N. E., HALVORSEN, E., CEDERBERG, R. A., CHOW, N., DOS SANTOS, N., BENNEWITH, K. L., NELSON, B. H., BALLY, M. B., LAM, W. L. & GORSKI, S. M. 2021. Loss of Parkinson's susceptibility gene LRRK2 promotes carcinogen-induced lung tumorigenesis. *Sci Rep,* 11**,** 2097.

LEE, B. D., SHIN, J. H., VANKAMPEN, J., PETRUCELLI, L., WEST, A. B., KO, H. S., LEE, Y. I., MAGUIRE-ZEISS, K. A., BOWERS, W. J., FEDEROFF, H. J., DAWSON, V. L. & DAWSON, T. M. 2010. Inhibitors of leucine-rich repeat kinase-2 protect against models of Parkinson's disease. *Nat Med,* 16**,** 998-1000.

LEE, H., JAMES, W. S. & COWLEY, S. A. 2017. LRRK2 in peripheral and central nervous system innate immunity: its link to Parkinson's disease. *Biochem Soc Trans,* 45**,** 131-139.

LEE, Y. H., CHA, J., CHUNG, S. J., YOO, H. S., SOHN, Y. H., YE, B. S. & LEE, P. H. 2019. Beneficial effect of estrogen on nigrostriatal dopaminergic neurons in drug-naive postmenopausal Parkinson's disease. *Sci Rep,* 9**,** 10531.

LESAGE, S., PATIN, E., CONDROYER, C., LEUTENEGGER, A. L., LOHMANN, E., GILADI, N., BAR-SHIRA, A., BELARBI, S., HECHAM, N., POLLAK, P., OUVRARD-HERNANDEZ, A. M., BARDIEN, S., CARR, J., BENHASSINE, T., TOMIYAMA, H., PIRKEVI, C., HAMADOUCHE, T., CAZENEUVE, C., BASAK, A. N., HATTORI, N., DURR, A., TAZIR, M., ORR-URTREGER, A., QUINTANA-MURCI, L., BRICE, A. & FRENCH PARKINSON'S DISEASE GENETICS STUDY, G. 2010. Parkinson's disease-related LRRK2 G2019S mutation results from independent mutational events in humans. *Hum Mol Genet,* 19**,** 1998-2004.

LI, W. W., LI, J. & BAO, J. K. 2012. Microautophagy: lesser-known self-eating. *Cell Mol Life Sci,* 69**,** 1125-36.

LIM, D. A. & ALVAREZ-BUYLLA, A. 2016. The Adult Ventricular-Subventricular Zone (V-SVZ) and Olfactory Bulb (OB) Neurogenesis. *Cold Spring Harb Perspect Biol,* 8.

LIN, C. H., TSAI, P. I., WU, R. M. & CHIEN, C. T. 2010. LRRK2 G2019S mutation induces dendrite degeneration through mislocalization and phosphorylation of tau by recruiting autoactivated GSK3ss. *J Neurosci,* 30**,** 13138-49.

LIN, C. H., TZEN, K. Y., YU, C. Y., TAI, C. H., FARRER, M. J. & WU, R. M. 2008. LRRK2 mutation in familial Parkinson's disease in a Taiwanese population: clinical, PET, and functional studies. *J Biomed Sci,* 15**,** 661-7.

LIPTON, J. O. & SAHIN, M. 2014. The neurology of mTOR. *Neuron,* 84**,** 275-91.

LIU, P. Z. & NUSSLOCK, R. 2018. Exercise-Mediated Neurogenesis in the Hippocampus via BDNF. *Front Neurosci,* 12**,** 52.

LIU, Z., BRYANT, N., KUMARAN, R., BEILINA, A., ABELIOVICH, A., COOKSON, M. R. & WEST, A. B. 2018. LRRK2 phosphorylates membrane-bound Rabs and is activated by GTP-bound Rab7L1 to promote recruitment to the trans-Golgi network. *Hum Mol Genet,* 27**,** 385-395.

LIU, Z., LEE, J., KRUMMEY, S., LU, W., CAI, H. & LENARDO, M. J. 2011. The kinase LRRK2 is a regulator of the transcription factor NFAT that modulates the severity of inflammatory bowel disease. *Nat Immunol,* 12**,** 1063-70.

LOBBESTAEL, E., ZHAO, J., RUDENKO, I. N., BEYLINA, A., GAO, F., WETTER, J., BEULLENS, M., BOLLEN, M., COOKSON, M. R., BAEKELANDT, V., NICHOLS, R. J. & TAYMANS, J. M. 2013. Identification of protein phosphatase 1 as a regulator of the LRRK2 phosphorylation cycle. *Biochem J,* 456**,** 119-28.

LOPEZ DE MATURANA, R., LANG, V., ZUBIARRAIN, A., SOUSA, A., VAZQUEZ, N., GOROSTIDI, A., AGUILA, J., LOPEZ DE MUNAIN, A., RODRIGUEZ, M. & SANCHEZ-PERNAUTE, R. 2016. Mutations in LRRK2 impair NF-kappaB pathway in iPSC-derived neurons. *J Neuroinflammation,* 13**,** 295.

MAAS, J. W., YANG, J. & EDWARDS, R. H. 2017. Endogenous Leucine-Rich Repeat Kinase 2 Slows Synaptic Vesicle Recycling in Striatal Neurons. *Front Synaptic Neurosci,* 9**,** 5.

MACDONALD, B. T. & HE, X. 2012. Frizzled and LRP5/6 receptors for Wnt/beta-catenin signaling. *Cold Spring Harb Perspect Biol,* 4.

MACDONALD, B. T., TAMAI, K. & HE, X. 2009. Wnt/beta-catenin signaling: components, mechanisms, and diseases. *Dev Cell,* 17**,** 9-26.

MAGUSCHAK, K. A. & RESSLER, K. J. 2012. The dynamic role of beta-catenin in synaptic plasticity. *Neuropharmacology,* 62**,** 78-88.

MARCHETTI, B., TIROLO, C., L'EPISCOPO, F., CANIGLIA, S., TESTA, N., SMITH, J. A., PLUCHINO, S. & SERAPIDE, M. F. 2020. Parkinson's disease, aging and adult neurogenesis:

Wnt/beta-catenin signalling as the key to unlock the mystery of endogenous brain repair. *Aging Cell,* 19**,** e13101.
MARTIN, I., KIM, J. W., DAWSON, V. L. & DAWSON, T. M. 2014. LRRK2 pathobiology in Parkinson's disease. *J Neurochem,* 131**,** 554-65.
MATIKAINEN-ANKNEY, B. A., KEZUNOVIC, N., MESIAS, R. E., TIAN, Y., WILLIAMS, F. M., HUNTLEY, G. W. & BENSON, D. L. 2016. Altered Development of Synapse Structure and Function in Striatum Caused by Parkinson's Disease-Linked LRRK2-G2019S Mutation. *J Neurosci,* 36**,** 7128-41.
MCSWEENEY, C. & MAO, Y. 2015. Applying stereotactic injection technique to study genetic effects on animal behaviors. *J Vis Exp***,** e52653.
MENG, Y., DING, J., LI, C., FAN, H., HE, Y. & QIU, P. 2020. Transfer of pathological alpha-synuclein from neurons to astrocytes via exosomes causes inflammatory responses after METH exposure. *Toxicol Lett,* 331**,** 188-199.
METCALFE, C., IBRAHIM, A. E., GRAEB, M., DE LA ROCHE, M., SCHWARZ-ROMOND, T., FIEDLER, M., WINTON, D. J., CORFIELD, A. & BIENZ, M. 2010. Dvl2 promotes intestinal length and neoplasia in the ApcMin mouse model for colorectal cancer. *Cancer Res,* 70**,** 6629-38.
MICHEL, P. P., HIRSCH, E. C. & HUNOT, S. 2016. Understanding Dopaminergic Cell Death Pathways in Parkinson Disease. *Neuron,* 90**,** 675-91.
MIKLOSSY, J., ARAI, T., GUO, J. P., KLEGERIS, A., YU, S., MCGEER, E. G. & MCGEER, P. L. 2006. LRRK2 expression in normal and pathologic human brain and in human cell lines. *J Neuropathol Exp Neurol,* 65**,** 953-63.
MILLS, R. D., MULHERN, T. D., LIU, F., CULVENOR, J. G. & CHENG, H. C. 2014. Prediction of the repeat domain structures and impact of parkinsonism-associated variations on structure and function of all functional domains of leucine-rich repeat kinase 2 (LRRK2). *Hum Mutat,* 35**,** 395-412.
MOISAN, F., KAB, S., MOHAMED, F., CANONICO, M., LE GUERN, M., QUINTIN, C., CARCAILLON, L., NICOLAU, J., DUPORT, N., SINGH-MANOUX, A., BOUSSAC-ZAREBSKA, M. & ELBAZ, A. 2016. Parkinson disease male-to-female ratios increase with age: French nationwide study and meta-analysis. *J Neurol Neurosurg Psychiatry,* 87**,** 952-7.
MOORE, D. L. & GOLDBERG, J. L. 2011. Multiple transcription factor families regulate axon growth and regeneration. *Dev Neurobiol,* 71**,** 1186-211.
NALLS, M. A., BLAUWENDRAAT, C., VALLERGA, C. L., HEILBRON, K., BANDRES-CIGA, S., CHANG, D., TAN, M., KIA, D. A., NOYCE, A. J., XUE, A., BRAS, J., YOUNG, E., VON COELLN, R., SIMON-SANCHEZ, J., SCHULTE, C., SHARMA, M., KROHN, L., PIHLSTROM, L., SIITONEN, A., IWAKI, H., LEONARD, H., FAGHRI, F., GIBBS, J. R., HERNANDEZ, D. G., SCHOLZ, S. W., BOTIA, J. A., MARTINEZ, M., CORVOL, J. C., LESAGE, S., JANKOVIC, J., SHULMAN, L. M., SUTHERLAND, M., TIENARI, P., MAJAMAA, K., TOFT, M., ANDREASSEN, O. A., BANGALE, T., BRICE, A., YANG, J., GAN-OR, Z., GASSER, T., HEUTINK, P., SHULMAN, J. M., WOOD, N. W., HINDS, D. A., HARDY, J. A., MORRIS, H. R., GRATTEN, J., VISSCHER, P. M., GRAHAM, R. R., SINGLETON, A. B., ANDME RESEARCH, T., SYSTEM GENOMICS OF PARKINSON'S DISEASE, C. & INTERNATIONAL PARKINSON'S DISEASE GENOMICS, C. 2019. Identification of novel risk loci, causal

insights, and heritable risk for Parkinson's disease: a meta-analysis of genome-wide association studies. *Lancet Neurol,* 18**,** 1091-1102.
NEMETH, M. J., TOPOL, L., ANDERSON, S. M., YANG, Y. & BODINE, D. M. 2007. Wnt5a inhibits canonical Wnt signaling in hematopoietic stem cells and enhances repopulation. *Proc Natl Acad Sci U S A,* 104**,** 15436-41.
NEUMANN, F. R. & NURSE, P. 2007. Nuclear size control in fission yeast. *J Cell Biol,* 179**,** 593-600.
NICHOLS, R. J., DZAMKO, N., MORRICE, N. A., CAMPBELL, D. G., DEAK, M., ORDUREAU, A., MACARTNEY, T., TONG, Y., SHEN, J., PRESCOTT, A. R. & ALESSI, D. R. 2010. 14-3-3 binding to LRRK2 is disrupted by multiple Parkinson's disease-associated mutations and regulates cytoplasmic localization. *Biochem J,* 430**,** 393-404.
NIEHRS, C. 2012. The complex world of WNT receptor signalling. *Nat Rev Mol Cell Biol,* 13**,** 767-79.
NIEHRS, C. & SHEN, J. 2010. Regulation of Lrp6 phosphorylation. *Cell Mol Life Sci,* 67**,** 2551-62.
NIXON-ABELL, J., BERWICK, D. C., GRANNO, S., SPAIN, V. A., BLACKSTONE, C. & HARVEY, K. 2016. Protective LRRK2 R1398H Variant Enhances GTPase and Wnt Signaling Activity. *Front Mol Neurosci,* 9**,** 18.
NUMAKAWA, T., ODAKA, H. & ADACHI, N. 2017. Actions of Brain-Derived Neurotrophic Factor and Glucocorticoid Stress in Neurogenesis. *Int J Mol Sci,* 18.
NUNEZ, F., BRAVO, S., CRUZAT, F., MONTECINO, M. & DE FERRARI, G. V. 2011. Wnt/beta-catenin signaling enhances cyclooxygenase-2 (COX2) transcriptional activity in gastric cancer cells. *PLoS One,* 6**,** e18562.
NUSSE, R. & VARMUS, H. E. 1982. Many tumors induced by the mouse mammary tumor virus contain a provirus integrated in the same region of the host genome. *Cell,* 31**,** 99-109.
NUSSLEIN-VOLHARD, C. & WIESCHAUS, E. 1980. Mutations affecting segment number and polarity in Drosophila. *Nature,* 287**,** 795-801.
ONISHI, K., TIAN, R., FENG, B., LIU, Y., WANG, J., LI, Y. & ZOU, Y. 2020. LRRK2 mediates axon development by regulating Frizzled3 phosphorylation and growth cone-growth cone communication. *Proc Natl Acad Sci U S A,* 117**,** 18037-18048.
ORENSTEIN, S. J., KUO, S. H., TASSET, I., ARIAS, E., KOGA, H., FERNANDEZ-CARASA, I., CORTES, E., HONIG, L. S., DAUER, W., CONSIGLIO, A., RAYA, A., SULZER, D. & CUERVO, A. M. 2013. Interplay of LRRK2 with chaperone-mediated autophagy. *Nat Neurosci,* 16**,** 394-406.
PAISAN-RUIZ, C., JAIN, S., EVANS, E. W., GILKS, W. P., SIMON, J., VAN DER BRUG, M., LOPEZ DE MUNAIN, A., APARICIO, S., GIL, A. M., KHAN, N., JOHNSON, J., MARTINEZ, J. R., NICHOLL, D., CARRERA, I. M., PENA, A. S., DE SILVA, R., LEES, A., MARTI-MASSO, J. F., PEREZ-TUR, J., WOOD, N. W. & SINGLETON, A. B. 2004. Cloning of the gene containing mutations that cause PARK8-linked Parkinson's disease. *Neuron,* 44**,** 595-600.
PAN, J., XIAO, Q., SHENG, C. Y., HONG, Z., YANG, H. Q., WANG, G., DING, J. Q. & CHEN, S. D. 2009. Blockade of the translocation and activation of c-Jun N-terminal kinase 3 (JNK3) attenuates dopaminergic neuronal damage in mouse model of Parkinson's disease. *Neurochem Int,* 54**,** 418-25.

PARKINSON, J. 2002. An essay on the shaking palsy. 1817. *J Neuropsychiatry Clin Neurosci,* 14**,** 223-36; discussion 222.
PATHAK, R. U., SOUJANYA, M. & MISHRA, R. K. 2021. Deterioration of nuclear morphology and architecture: A hallmark of senescence and aging. *Ageing Res Rev,* 67**,** 101264.
PENCEA, V., BINGAMAN, K. D., FREEDMAN, L. J. & LUSKIN, M. B. 2001. Neurogenesis in the subventricular zone and rostral migratory stream of the neonatal and adult primate forebrain. *Exp Neurol,* 172**,** 1-16.
PFAFFL, M. W. 2001. A new mathematical model for relative quantification in real-time RT-PCR. *Nucleic Acids Res,* 29**,** e45.
PINZON-DAZA, M. L., SALAROGLIO, I. C., KOPECKA, J., GARZON, R., COURAUD, P. O., GHIGO, D. & RIGANTI, C. 2014. The cross-talk between canonical and non-canonical Wnt-dependent pathways regulates P-glycoprotein expression in human blood-brain barrier cells. *J Cereb Blood Flow Metab,* 34**,** 1258-69.
POPUGAEVA, E. & BEZPROZVANNY, I. 2014. Commentary on "Synaptic function is modulated by LRRK2 and glutamate release is increased in cortical neurons of G2019S LRRK2 knock-in mice". *Front Cell Neurosci,* 8**,** 351.
PORRAS, G., DE DEURWAERDERE, P., LI, Q., MARTI, M., MORGENSTERN, R., SOHR, R., BEZARD, E., MORARI, M. & MEISSNER, W. G. 2014. L-dopa-induced dyskinesia: beyond an excessive dopamine tone in the striatum. *Sci Rep,* 4**,** 3730.
PRAH, J., WINTERS, A., CHAUDHARI, K., HERSH, J., LIU, R. & YANG, S. H. 2019. A novel serum free primary astrocyte culture method that mimic quiescent astrocyte phenotype. *J Neurosci Methods,* 320**,** 50-63.
PRZEDBORSKI, S., JACKSON-LEWIS, V., DJALDETTI, R., LIBERATORE, G., VILA, M., VUKOSAVIC, S. & ALMER, G. 2000. The parkinsonian toxin MPTP: action and mechanism. *Restor Neurol Neurosci,* 16**,** 135-142.
PULVIRENTI, T., VAN DER HEIJDEN, M., DROMS, L. A., HUSE, J. T., TABAR, V. & HALL, A. 2011. Dishevelled 2 signaling promotes self-renewal and tumorigenicity in human gliomas. *Cancer Res,* 71**,** 7280-90.
PURLYTE, E., DHEKNE, H. S., SARHAN, A. R., GOMEZ, R., LIS, P., WIGHTMAN, M., MARTINEZ, T. N., TONELLI, F., PFEFFER, S. R. & ALESSI, D. R. 2019. Rab29 activation of the Parkinson's disease-associated LRRK2 kinase. *EMBO J,* 38.
RAO, T. P. & KUHL, M. 2010. An updated overview on Wnt signaling pathways: a prelude for more. *Circ Res,* 106**,** 1798-806.
RAWAL, N., CORTI, O., SACCHETTI, P., ARDILLA-OSORIO, H., SEHAT, B., BRICE, A. & ARENAS, E. 2009. Parkin protects dopaminergic neurons from excessive Wnt/beta-catenin signaling. *Biochem Biophys Res Commun,* 388**,** 473-8.
REEKES, T. H., HIGGINSON, C. I., LEDBETTER, C. R., SATHIVADIVEL, N., ZWEIG, R. M. & DISBROW, E. A. 2020. Sex specific cognitive differences in Parkinson disease. *NPJ Parkinsons Dis,* 6**,** 7.
REEVE, A., SIMCOX, E. & TURNBULL, D. 2014. Ageing and Parkinson's disease: why is advancing age the biggest risk factor? *Ageing Res Rev,* 14**,** 19-30.
RIJSEWIJK, F., SCHUERMANN, M., WAGENAAR, E., PARREN, P., WEIGEL, D. & NUSSE, R. 1987. The Drosophila homolog of the mouse mammary oncogene int-1 is identical to the segment polarity gene wingless. *Cell,* 50**,** 649-57.

ROOSEN, D. A. & COOKSON, M. R. 2016. LRRK2 at the interface of autophagosomes, endosomes and lysosomes. *Mol Neurodegener,* 11**,** 73.

RUBIO, J. P., TOPP, S., WARREN, L., ST JEAN, P. L., WEGMANN, D., KESSNER, D., NOVEMBRE, J., SHEN, J., FRASER, D., APONTE, J., NANGLE, K., CARDON, L. R., EHM, M. G., CHISSOE, S. L., WHITTAKER, J. C., NELSON, M. R. & MOOSER, V. E. 2012. Deep sequencing of the LRRK2 gene in 14,002 individuals reveals evidence of purifying selection and independent origin of the p.Arg1628Pro mutation in Europe. *Hum Mutat,* 33**,** 1087-98.

RUSSO, I., BERTI, G., PLOTEGHER, N., BERNARDO, G., FILOGRANA, R., BUBACCO, L. & GREGGIO, E. 2015. Leucine-rich repeat kinase 2 positively regulates inflammation and down-regulates NF-kappaB p50 signaling in cultured microglia cells. *J Neuroinflammation,* 12**,** 230.

RUSSO, I., DI BENEDETTO, G., KAGANOVICH, A., DING, J., MERCATELLI, D., MORARI, M., COOKSON, M. R., BUBACCO, L. & GREGGIO, E. 2018. Leucine-rich repeat kinase 2 controls protein kinase A activation state through phosphodiesterase 4. *J Neuroinflammation,* 15**,** 297.

SAIJO, K., WINNER, B., CARSON, C. T., COLLIER, J. G., BOYER, L., ROSENFELD, M. G., GAGE, F. H. & GLASS, C. K. 2009. A Nurr1/CoREST pathway in microglia and astrocytes protects dopaminergic neurons from inflammation-induced death. *Cell,* 137**,** 47-59.

SAN LUCIANO, M., WANG, C., ORTEGA, R. A., GILADI, N., MARDER, K., BRESSMAN, S., SAUNDERS-PULLMAN, R. & MICHAEL, J. F. F. L. C. 2017. Sex differences in LRRK2 G2019S and idiopathic Parkinson's Disease. *Ann Clin Transl Neurol,* 4**,** 801-810.

SANCHO, R. M., LAW, B. M. & HARVEY, K. 2009. Mutations in the LRRK2 Roc-COR tandem domain link Parkinson's disease to Wnt signalling pathways. *Hum Mol Genet,* 18**,** 3955-68.

SATO, A., YAMAMOTO, H., SAKANE, H., KOYAMA, H. & KIKUCHI, A. 2010. Wnt5a regulates distinct signalling pathways by binding to Frizzled2. *EMBO J,* 29**,** 41-54.

SCHULTE, G., BRYJA, V., RAWAL, N., CASTELO-BRANCO, G., SOUSA, K. M. & ARENAS, E. 2005. Purified Wnt-5a increases differentiation of midbrain dopaminergic cells and dishevelled phosphorylation. *J Neurochem,* 92**,** 1550-3.

SEIBERT, K. & MASFERRER, J. L. 1994. Role of inducible cyclooxygenase (COX-2) in inflammation. *Receptor,* 4**,** 17-23.

SHARMA, S., FINDLAY, G. M., BANDUKWALA, H. S., OBERDOERFFER, S., BAUST, B., LI, Z., SCHMIDT, V., HOGAN, P. G., SACKS, D. B. & RAO, A. 2011. Dephosphorylation of the nuclear factor of activated T cells (NFAT) transcription factor is regulated by an RNA-protein scaffold complex. *Proc Natl Acad Sci U S A,* 108**,** 11381-6.

SHEN, J., HU, L., YANG, L., ZHANG, M., SUN, W., LU, X., LIN, G., HUANG, C., ZHANG, X. & CHIN, Y. E. 2020. Reversible acetylation modulates dishevelled-2 puncta formation in canonical Wnt signaling activation. *Signal Transduct Target Ther,* 5**,** 115.

SHEN, L., ZHOU, S. & GLOWACKI, J. 2009. Effects of age and gender on WNT gene expression in human bone marrow stromal cells. *J Cell Biochem,* 106**,** 337-43.

SHERER, T. B., RICHARDSON, J. R., TESTA, C. M., SEO, B. B., PANOV, A. V., YAGI, T., MATSUNO-YAGI, A., MILLER, G. W. & GREENAMYRE, J. T. 2007. Mechanism of toxicity of pesticides acting at complex I: relevance to environmental etiologies of Parkinson's disease. *J Neurochem,* 100**,** 1469-79.

SHIN, Y., HUH, Y. H., KIM, K., KIM, S., PARK, K. H., KOH, J. T., CHUN, J. S. & RYU, J. H. 2014. Low-density lipoprotein receptor-related protein 5 governs Wnt-mediated osteoarthritic cartilage destruction. *Arthritis Res Ther,* 16**,** R37.

SHTUTMAN, M., ZHURINSKY, J., SIMCHA, I., ALBANESE, C., D'AMICO, M., PESTELL, R. & BEN-ZE'EV, A. 1999. The cyclin D1 gene is a target of the beta-catenin/LEF-1 pathway. *Proc Natl Acad Sci U S A,* 96**,** 5522-7.

SHU, L., ZHANG, Y., PAN, H., XU, Q., GUO, J., TANG, B. & SUN, Q. 2018. Clinical Heterogeneity Among LRRK2 Variants in Parkinson's Disease: A Meta-Analysis. *Front Aging Neurosci,* 10**,** 283.

SIMON-SANCHEZ, J., SCHULTE, C., BRAS, J. M., SHARMA, M., GIBBS, J. R., BERG, D., PAISAN-RUIZ, C., LICHTNER, P., SCHOLZ, S. W., HERNANDEZ, D. G., KRUGER, R., FEDEROFF, M., KLEIN, C., GOATE, A., PERLMUTTER, J., BONIN, M., NALLS, M. A., ILLIG, T., GIEGER, C., HOULDEN, H., STEFFENS, M., OKUN, M. S., RACETTE, B. A., COOKSON, M. R., FOOTE, K. D., FERNANDEZ, H. H., TRAYNOR, B. J., SCHREIBER, S., AREPALLI, S., ZONOZI, R., GWINN, K., VAN DER BRUG, M., LOPEZ, G., CHANOCK, S. J., SCHATZKIN, A., PARK, Y., HOLLENBECK, A., GAO, J., HUANG, X., WOOD, N. W., LORENZ, D., DEUSCHL, G., CHEN, H., RIESS, O., HARDY, J. A., SINGLETON, A. B. & GASSER, T. 2009. Genome-wide association study reveals genetic risk underlying Parkinson's disease. *Nat Genet,* 41**,** 1308-12.

SINGH, H. D., MA, J. X. & TAKAHASHI, Y. 2021. Distinct roles of LRP5 and LRP6 in Wnt signaling regulation in the retina. *Biochem Biophys Res Commun,* 545**,** 8-13.

SOFRONIEW, M. V. & VINTERS, H. V. 2010. Astrocytes: biology and pathology. *Acta Neuropathol,* 119**,** 7-35.

SOMPOL, P. & NORRIS, C. M. 2018. Ca(2+), Astrocyte Activation and Calcineurin/NFAT Signaling in Age-Related Neurodegenerative Diseases. *Front Aging Neurosci,* 10**,** 199.

SONG, X., WANG, S. & LI, L. 2014. New insights into the regulation of Axin function in canonical Wnt signaling pathway. *Protein Cell,* 5**,** 186-93.

STAMOS, J. L. & WEIS, W. I. 2013. The beta-catenin destruction complex. *Cold Spring Harb Perspect Biol,* 5**,** a007898.

STEGER, M., DIEZ, F., DHEKNE, H. S., LIS, P., NIRUJOGI, R. S., KARAYEL, O., TONELLI, F., MARTINEZ, T. N., LORENTZEN, E., PFEFFER, S. R., ALESSI, D. R. & MANN, M. 2017. Systematic proteomic analysis of LRRK2-mediated Rab GTPase phosphorylation establishes a connection to ciliogenesis. *Elife,* 6.

STEGER, M., TONELLI, F., ITO, G., DAVIES, P., TROST, M., VETTER, M., WACHTER, S., LORENTZEN, E., DUDDY, G., WILSON, S., BAPTISTA, M. A., FISKE, B. K., FELL, M. J., MORROW, J. A., REITH, A. D., ALESSI, D. R. & MANN, M. 2016. Phosphoproteomics reveals that Parkinson's disease kinase LRRK2 regulates a subset of Rab GTPases. *Elife,* 5.

SUGIMURA, R. & LI, L. 2010. Noncanonical Wnt signaling in vertebrate development, stem cells, and diseases. *Birth Defects Res C Embryo Today,* 90**,** 243-56.

SUN, S., ZHU, X. J., HUANG, H., GUO, W., TANG, T., XIE, B., XU, X., ZHANG, Z., SHEN, Y., DAI, Z. M. & QIU, M. 2019. WNT signaling represses astrogliogenesis via Ngn2-dependent direct suppression of astrocyte gene expression. *Glia,* 67**,** 1333-1343.

SURMEIER, D. J. 2018. Determinants of dopaminergic neuron loss in Parkinson's disease. *FEBS J,* 285**,** 3657-3668.

SVEINBJORNSDOTTIR, S. 2016. The clinical symptoms of Parkinson's disease. *J Neurochem,* 139 Suppl 1**,** 318-324.
TAYMANS, J. M., VAN DEN HAUTE, C. & BAEKELANDT, V. 2006. Distribution of PINK1 and LRRK2 in rat and mouse brain. *J Neurochem,* 98**,** 951-61.
TEKIRDAG, K. & CUERVO, A. M. 2018. Chaperone-mediated autophagy and endosomal microautophagy: Joint by a chaperone. *J Biol Chem,* 293**,** 5414-5424.
THOMAS, B. & BEAL, M. F. 2007. Parkinson's disease. *Hum Mol Genet,* 16 Spec No. 2**,** R183-94.
TOZZI, A., DURANTE, V., BASTIOLI, G., MAZZOCCHETTI, P., NOVELLO, S., MECHELLI, A., MORARI, M., COSTA, C., MANCINI, A., DI FILIPPO, M. & CALABRESI, P. 2018. Dopamine D2 receptor activation potently inhibits striatal glutamatergic transmission in a G2019S LRRK2 genetic model of Parkinson's disease. *Neurobiol Dis,* 118**,** 1-8.
TYSNES, O. B. & STORSTEIN, A. 2017. Epidemiology of Parkinson's disease. *J Neural Transm (Vienna),* 124**,** 901-905.
VERKHRATSKY, A., SOFRONIEW, M. V., MESSING, A., DELANEROLLE, N. C., REMPE, D., RODRIGUEZ, J. J. & NEDERGAARD, M. 2012. Neurological diseases as primary gliopathies: a reassessment of neurocentrism. *ASN Neuro,* 4.
VOGIATZI, T., XILOURI, M., VEKRELLIS, K. & STEFANIS, L. 2008. Wild type alpha-synuclein is degraded by chaperone-mediated autophagy and macroautophagy in neuronal cells. *J Biol Chem,* 283**,** 23542-56.
WAUTERS, L., VERSEES, W. & KORTHOLT, A. 2019. Roco Proteins: GTPases with a Baroque Structure and Mechanism. *Int J Mol Sci,* 20.
WEST, A. B. 2017. Achieving neuroprotection with LRRK2 kinase inhibitors in Parkinson disease. *Exp Neurol,* 298**,** 236-245.
WEST, A. B., COWELL, R. M., DAHER, J. P., MOEHLE, M. S., HINKLE, K. M., MELROSE, H. L., STANDAERT, D. G. & VOLPICELLI-DALEY, L. A. 2014. Differential LRRK2 expression in the cortex, striatum, and substantia nigra in transgenic and nontransgenic rodents. *J Comp Neurol,* 522**,** 2465-80.
WEST, A. B., MOORE, D. J., BISKUP, S., BUGAYENKO, A., SMITH, W. W., ROSS, C. A., DAWSON, V. L. & DAWSON, T. M. 2005. Parkinson's disease-associated mutations in leucine-rich repeat kinase 2 augment kinase activity. *Proc Natl Acad Sci U S A,* 102**,** 16842-7.
WHIFFIN, N., ARMEAN, I. M., KLEINMAN, A., MARSHALL, J. L., MINIKEL, E. V., GOODRICH, J. K., QUAIFE, N. M., COLE, J. B., WANG, Q., KARCZEWSKI, K. J., CUMMINGS, B. B., FRANCIOLI, L., LARICCHIA, K., GUAN, A., ALIPANAHI, B., MORRISON, P., BAPTISTA, M. A. S., MERCHANT, K. M., GENOME AGGREGATION DATABASE PRODUCTION, T., GENOME AGGREGATION DATABASE, C., WARE, J. S., HAVULINNA, A. S., ILIADOU, B., LEE, J. J., NADKARNI, G. N., WHITEMAN, C., ANDME RESEARCH, T., DALY, M., ESKO, T., HULTMAN, C., LOOS, R. J. F., MILANI, L., PALOTIE, A., PATO, C., PATO, M., SALEHEEN, D., SULLIVAN, P. F., ALFOLDI, J., CANNON, P. & MACARTHUR, D. G. 2020. The effect of LRRK2 loss-of-function variants in humans. *Nat Med,* 26**,** 869-877.
WOLF, J. P., BOUHADDI, M., LOUISY, F., MIKEHIEV, A., MOUROT, L., CAPPELLE, S., VUILLIER, F., ANDRE, P., RUMBACH, L. & REGNARD, J. 2006. Side-effects of L-dopa on venous tone in Parkinson's disease: a leg-weighing assessment. *Clin Sci (Lond),* 110**,** 369-77.

WONG, A. Y. W., OIKONOMOU, V., PAOLICELLI, G., DE LUCA, A., PARIANO, M., FRIC, J., TAY, H. S., RICCIARDI-CASTAGNOLI, P. & ZELANTE, T. 2018. Leucine-Rich Repeat Kinase 2 Controls the Ca(2+)/Nuclear Factor of Activated T Cells/IL-2 Pathway during Aspergillus Non-Canonical Autophagy in Dendritic Cells. *Front Immunol,* 9**,** 210.

WOULFE, J. 2008. Nuclear bodies in neurodegenerative disease. *Biochim Biophys Acta,* 1783**,** 2195-206.

YANG, J. W., RU, J., MA, W., GAO, Y., LIANG, Z., LIU, J., GUO, J. H. & LI, L. Y. 2015. BDNF promotes the growth of human neurons through crosstalk with the Wnt/beta-catenin signaling pathway via GSK-3beta. *Neuropeptides,* 54**,** 35-46.

YOSHIOKA, S., KING, M. L., RAN, S., OKUDA, H., MACLEAN, J. A., 2ND, MCASEY, M. E., SUGINO, N., BRARD, L., WATABE, K. & HAYASHI, K. 2012. WNT7A regulates tumor growth and progression in ovarian cancer through the WNT/beta-catenin pathway. *Mol Cancer Res,* 10**,** 469-82.

YUAN, Y., NIU, C. C., DENG, G., LI, Z. Q., PAN, J., ZHAO, C., YANG, Z. L. & SI, W. K. 2011. The Wnt5a/Ror2 noncanonical signaling pathway inhibits canonical Wnt signaling in K562 cells. *Int J Mol Med,* 27**,** 63-9.

ZENG, X., TAMAI, K., DOBLE, B., LI, S., HUANG, H., HABAS, R., OKAMURA, H., WOODGETT, J. & HE, X. 2005. A dual-kinase mechanism for Wnt co-receptor phosphorylation and activation. *Nature,* 438**,** 873-7.

ZHANG, J., GILL, A. J., ISSACS, J. D., ATMORE, B., JOHNS, A., DELBRIDGE, L. W., LAI, R. & MCMULLEN, T. P. 2012. The Wnt/beta-catenin pathway drives increased cyclin D1 levels in lymph node metastasis in papillary thyroid cancer. *Hum Pathol,* 43**,** 1044-50.

ZHANG, J., HE, L., YANG, Z., LI, L. & CAI, W. 2019. Lithium chloride promotes proliferation of neural stem cells in vitro, possibly by triggering the Wnt signaling pathway. *Anim Cells Syst (Seoul),* 23**,** 32-41.

ZHANG, J. C., YAO, W. & HASHIMOTO, K. 2016a. Brain-derived Neurotrophic Factor (BDNF)-TrkB Signaling in Inflammation-related Depression and Potential Therapeutic Targets. *Curr Neuropharmacol,* 14**,** 721-31.

ZHANG, L., YANG, X., YANG, S. & ZHANG, J. 2011. The Wnt /beta-catenin signaling pathway in the adult neurogenesis. *Eur J Neurosci,* 33**,** 1-8.

ZHANG, Y., SLOAN, S. A., CLARKE, L. E., CANEDA, C., PLAZA, C. A., BLUMENTHAL, P. D., VOGEL, H., STEINBERG, G. K., EDWARDS, M. S., LI, G., DUNCAN, J. A., 3RD, CHESHIER, S. H., SHUER, L. M., CHANG, E. F., GRANT, G. A., GEPHART, M. G. & BARRES, B. A. 2016b. Purification and Characterization of Progenitor and Mature Human Astrocytes Reveals Transcriptional and Functional Differences with Mouse. *Neuron,* 89**,** 37-53.

ZIMPRICH, A., BISKUP, S., LEITNER, P., LICHTNER, P., FARRER, M., LINCOLN, S., KACHERGUS, J., HULIHAN, M., UITTI, R. J., CALNE, D. B., STOESSL, A. J., PFEIFFER, R. F., PATENGE, N., CARBAJAL, I. C., VIEREGGE, P., ASMUS, F., MULLER-MYHSOK, B., DICKSON, D. W., MEITINGER, T., STROM, T. M., WSZOLEK, Z. K. & GASSER, T. 2004. Mutations in LRRK2 cause autosomal-dominant parkinsonism with pleomorphic pathology. *Neuron,* 44**,** 601-7.

# Supplementary

**Supplementary Table S1: Projected incidence cases in different age groups in the UK**

Data sourced from PD UK report 2018 **(**https://www.parkinsons.org.uk/professionals/resources/incidence-and-prevalence-parkinsons-uk-report**)**

| | Estimated Number of Incidence | | | | |
|---|---|---|---|---|---|
| **Age** | 2025 | 2035 | 2045 | 2055 | 2065 |
| **45-49** | 187 | 165 | 183 | 172 | 181 |
| **50-59** | 1166 | 1218 | 1134 | 1228 | 1138 |
| **60-69** | 3331 | 3662 | 3934 | 3694 | 4026 |
| **70-79** | 7097 | 9019 | 10314 | 11144 | 10679 |
| **80+** | 5847 | 7385 | 10044 | 12784 | 14586 |
| **Aged 45+** | 31,124,564 | 33,885,980 | 35,683,759 | 36,609,021 | 37,916,280 |

**Supplementary Table S2: Projected prevalence cases in different age groups in the UK**

Data sourced from PD UK report 2018 **(**https://www.parkinsons.org.uk/professionals/resources/incidence-and-prevalence-parkinsons-uk-report)

| | Estimated Number of Prevalence | | | | |
|---|---|---|---|---|---|
| **Age** | 2025 | 2035 | 2045 | 2055 | 2065 |
| **20-29** | 142 | 157 | 155 | 152 | 157 |
| **30-39** | 407 | 371 | 410 | 404 | 398 |
| **40-49** | 1207 | 1288 | 1174 | 1299 | 1282 |
| **50-59** | 8718 | 8117 | 8798 | 8148 | 8896 |
| **60-69** | 29006 | 31204 | 29268 | 31918 | 29762 |
| **70-79** | 66141 | 75818 | 81677 | 78532 | 86096 |
| **80+** | 62962 | 85167 | 108192 | 123423 | 130020 |
| **Aged 20+** | 52,675,868 | 55,622,944 | 57,646,765 | 58,935,177 | 60,227,373 |